UNIVERSITY OF SOUTHAMPTON
FACULTY OF NATURAL AND ENVIRONMENTAL SCIENCES
Centre for Biological Sciences

FACTORS AFFECTING DNA TRIPLEX FORMATION

by Ibrahim Sayoh

Thesis for the degree of Doctor of Philosophy

June 2016

UNIVERSITY OF SOUTHAMPTON

ABSTRACT

FACULTY OF NATURAL AND ENVIRONMENTAL SCIENCES
CENTRE FOR BIOLOGICAL SCIENCES

FACTORS AFFECTING DNA TRIPLEX FORMATION

by Ibrahim Sayoh

Triplex-forming oligonucleotides (TFOs) can be used to target DNA in a sequence-specific fashion, and have a number of potential therapeutic and biotechnological applications. TFOs bind within the DNA major groove where they form sequence-specific contacts with exposed groups on the target duplex. Pyrimidine-rich TFOs bind parallel to the target purine strand forming C^+.GC and T.AT triplets and usually require conditions of low pH, which are needed for protonation of the third strand cytosines. In contrast, purine-rich TFOs bind antiparallel to the target and form triplexes containing G.GC and A.AT triplets. DNase I footprinting studies with parallel triplexes often reveal enhanced cleavage at the triplex-duplex junction at the 3'-end of the duplex purine strand. This study systematically investigated how this enhanced cleavage is affected by the nature of the base pairs that flank the TFO-binding site. For this we have used the well-characterised TFO-binding site in the *tyr*T(43-59) fragment and have changed the base at the 3'-end of the homopurine strand from cytosine to each of the other three bases in turn. In each case the footprints were accompanied by enhanced DNase I cleavage at the 3'-triplex-duplex junction on the purine strand, which is thought to be due to local structural changes that render the DNA to be more susceptible to cleavage by the enzyme. The enhancements were generally greater for flanking pyrimidines than purines. Similar experiments investigated the effect of changing the terminal triplet from T.AT to C^+.GC, again flanked by each base in turn. Although there were no significant differences in the concentration dependence of the footprints, fluorescence melting experiments showed that triplexes flanked by G and A are more stable than those flanked by C and T. We also used diethylpyrocabonate (DEPC) to probe the reactivity of adenines at the triplex-duplex junction and find that some, but not all, sequence combinations generate enhanced reactivity, suggesting that triplex formation has altered the stacking pattern of adenines on the 3'-side of the TFO binding site. For antiparallel triplex formation, DNase I enhancements were also observed at a number of bands beyond the 5'-end of each TFO's binding site. This is also attributed to the TFO-induced DNA structural changes that increase the accessibility of the enzyme to the target site. The results of concentration dependence of the footprints are similar to the parallel ones though fragment AC with 17-mer-G TFO had a much lower C_{50}.

ACKNOWLEDGEMENTS

Alhamdulillahi Rabbil Alamin; all praises due to Allah, the lord of all worlds. I would firstly like to express my gratitude to Professor Keith Fox for his kind and merciful supervision throughout my PhD research here at the University of Southampton, Dr David Rusling, Dr Scott Kimber and Dr Helen Lewis for their tuitions in the lab. Thank you to all past and present Fox lab members who have made and shared wonderful moments together. Thank you to The Royal Thai Government and The Princess of Naradhiwas University for funding and caring during the last four years. Last but not least, Thank you to my wife; Pateemoh Binlateh, my sons; Mukhlis and Munir Sayoh for their patience and support over these four years.

TABLE OF CONTENTS

ABBREVIATIONS

A	adenine
2AP	2-aminopyridine
BePI	benzo[e]pyridoindole
BgPI	benzo[g]pyridoindole
C	cytosine
DEPC	Diethyl pyrocarbonate
DMSO	dimethylsulfoxide
DNA	Deoxyribonucleic acid
DNase I	Deoxyribonuclease I
EDTA	Ethylenediaminetetraacetic acid
ENA	O2', O4'-ethylene-linked nucleic acid
Ets	E26 transformation-specific
GMF/CSF	granulocyte-macrophage colony stimulating factor
G	guanine
ICAM	intercellular adhesion molecule
$KMnO_4$	Potassium permanganate
LNA	Locked nucleic acid
MCP	monocyte chemoattractant protein
MDR	multidrug resistance
NaOAC	Sodium acetate
PCR	Polymerase chain reaction
PNA	Peptide nucleic acid
R	Purine
RNA	Ribonucleic acid
SDM	Site-directed mutagenesis
T	Thymine
TBE	Tris, Borate, EDTA buffer
TEMED	*N,N,N',N'*-Tetramethylethylenediamine
TFOs	Triplex-forming oligonucletides
TNF	Tumor necrosis factor
Y	Pyrimidine

LIST OF FIGURES

Chapter 4: The effects of base variations at the 3'-end of an antiparallel DNA triplex

LIST OF TABLES

CHAPTER 1 INTRODUCTION

Since the structure of deoxyribonucleic acid (DNA) was revealed as a double-stranded helix by Watson and Crick in 1953, using X-ray fibre diffraction techniques (Watson and Crick, 1953), interests in the study of DNA have increased dramatically. As well as considering DNA as the store of genetic information, which is transmitted from parent to daughter cells via DNA replication, a number of studies have shown that its properties can be modulated by sequence-specific binding molecules. This can be exploited as a method of treating various diseases (Leung *et al.*, 2013). Transcription factors, DNA binding ligands, DNA-binding drug molecules and triplex-forming oligonucleotides (TFOs) are among the molecules that have been found to affect its activity. TFOs bind to duplex DNA and form a three-stranded DNA structure called triplex DNA. Historically, triplex formation was first observed by Felsenfeld and Rich (1957) from an experiment that combined two polyribonucleotides (i.e., polyU and polyA) in different ratios in the presence of metal ions. This three-stranded structure was less stable than its duplex counterpart. For this reason, later studies have mostly focussed on strategies to overcome the limitations of triplex formation in physiological conditions, with the aim of using it to protect DNA sequences from transcription factors, nucleases, cross-linking and cleaving agents (Duca *et al*., 2008) and also for use as tools in molecular biology (Gowers and Fox, 1999). This introduction will describe the structure of triplex DNA, the factors affecting its stability and strategies to increase this, as well as the application of triplexes in biological contexts.

1.1. The structures of DNA

1.1.1. The structure of duplex DNA

1.1.1.1. B-form DNA

This structure is a right-handed antiparallel double-stranded helix and is thought to be the major form under physiological conditions. In this structure the bases are perpendicular to the helix axis. The number of bases per helical turn is about 10-10.5 and the number of rise per base pair is 3.4 Å. The purine residues of this structure adopt C2'-*endo* sugar pucker while the pyrimidine residues have C3'-*endo*. The glycosidic bonds of a base pair of this structure are not diametrically opposite to each other and therefore generate two grooves; major and minor grooves (Figure 1.1). The minor groove is typically narrower (6 Å versus 12 Å) and shallower (7.5 Å versus 8.5 Å) than the major one. It contains the purine N3 and pyrimidine O2 atoms of the base pair, which can serve as hydrogen acceptors and the 2- amino group of guanine which can be a hydrogen-bond donor (Berg *et al*., 2002). In the major groove the purine N7, thymine O4 and guanine O6 atoms are hydrogen bond

acceptors while the amino groups of adenine and cytosine are hydrogen bond donors. These features are crucial for the interactions to the DNA binding molecules (Zimmerman, 1982, Berg *et al*., 2002). The CD spectrum of B-form DNA shows low peak intensities as the base pairs of this structure are perpendicular to the double-helix axis which exhibits low chirality (Kypr *et al.*, 2009).

1.1.1.2. A-form DNA

This structure is also a right-handed antiparallel double-stranded helix. However it is shorter and wider than the B-form and its base pairs are tilted relative to the helix axis. The sugar conformation of this structure is C3'-*endo* resulting in a 19º tilting of the base pairs away from the helix axis. It is favoured in dehydrated conditions and was first observed in fibre diffraction studies under conditions of low humidity. The structure is also formed by double-stranded RNA and DNA-RNA hybrids as a result of the steric hindrance from the 2'-hydroxyl group (Berg *et al*., 2002). The CD spectrum of RNA-like DNA conformation (i.e. A-form) presents a large positive band at 260 nm and also a negative band at 210 nm (Kypr *et al.*, 2009).

1.1.1.3. Z-form DNA

This is left-handed antiparallel double-stranded helix with zigzagged phosphodiester backbone (Figure 1.1). Although it is mainly found in alternating GC, this can also be formed in alternating GT/AC but not alternating AT sequence. It requires condition of high salt concentrations and negative superhelical stress (Berg *et al*., 2002). The bases of this DNA structure alternate between the *anti*- and *syn*-conformations and it has only a single narrow groove similar to the minor groove of B-DNA, where the sequence-specific recognition of DNA binding molecules occurs (Herbert and Rich, 1999). Many studies suggest that the formation of this DNA conformation is linked to the transcriptional activity of the genes but not the replication (Liu and Wang, 1987, Wittig *et al.*, 1991). The CD spectrum of the left-handed Z-form DNA shows a negative band at around 290 nm and a positive band at 260 nm. This is clearly opposite to B- and A-forms as its base pairs have opposite orientation to the backbone than the two (Kypr *et al.*, 2009).

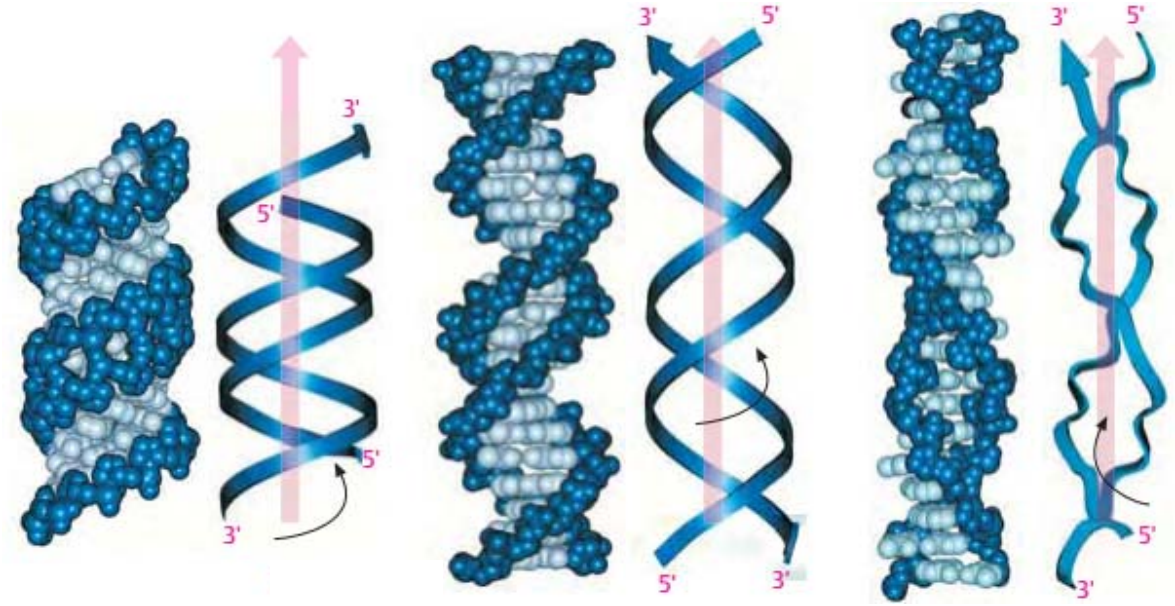

Figure 1.1 Structural forms of DNA duplex. A-DNA is a right-handed antiparallel double-stranded helix but shorter and wider than the B-form. Its base pairs are tilted relative to the helix axis. B-DNA is also a right-handed double helices in which the two strands are complementary and run antiparallel to each other. It generates two grooves; minor and major grooves as its base pairs are not diametrically opposite to each other. Z-DNA is a left-handed antiparallel double helices with zigzagged phosphodiester backbone. It has a groove that is resemble to the minor groove of B-DNA where the binding of DNA binding molecules occurs. Phosphodiester backbones are presented in dark blue whereas the base pairs are in light blue (adapted from Color Atlas of Biochemistry; Koolman J. and Rohem K.H., 2005).

1.1.2. Other DNA Structures

1.1.2.1. G-quadruplexes

A G-quadruplex is formed either by the self-association of a single stranded G-rich sequence (intramolecular) containing multiple G-tracts or the interaction of four G-rich sequences from different DNA strands (intermolecular). The structure is based on the formation of guanine tetrads and their stacking reactions to form a four-stranded structure. Monovalent cations (*e.g.* K^+, Na^+) are required to stabilise the structure, interacting with the central O6 oxygen atoms of the guanines. G-quadruplex can adopt a number of different topologies, depending on the direction of the DNA strands. In parallel G-quadruplexes all the strands are oriented in the same direction and vice versa for antiparallel quadruplexes. Sequences with the potential to form G-quadruplexes are found in the telomeric sequence of many species including human and other non-telomeric sequences throughout eukaryotic genomes, especially in gene promoters (Burge *et al.*, 2006).

1.1.2.2. The i-motif

This secondary DNA structure is formed by the self-association of single stranded cytosine-rich sequences. This structure is based on the interaction of two cytosines forming C^+.C base pairs. This requires protonation of cytosine and can therefore only occur in an acidic environment. The i-motif structure consists of intercalated hemiprotonated cytosine-cytosine base pairs and the stacking interaction of the loop region and the main cytosine core. Cations also affect the stability of this structure. In a presence of Na^+ there was no i-motif formed but only duplex DNA. Whereas in conditions containing K^+ the i-motif and G-quadruplex can be formed. All of the three structures can be observed in an environment containing both Na^+ and Mg^{2+} (Day *et al.*, 2014).

1.1.2.3. The structures of intramolecular triplex DNA or H-DNA

Although triplex DNA with synthetic polynucleotides was first suggested in 1957, Frank-Kamenetskii and colleagues first discovered that plasmid-encoded $(dR_n).(dY_n)$ sequences can form an intramolecular triple-stranded DNA structure under superhelical stress, which has since been called H-DNA (Lyamichev *et al.*, 1986, Mirkin *et al.*, 1987). The structure is formed in long mirror purine.pyrimidine sequence repeats within DNA. The first half of the sequence still forms the conventional Watson-Crick base-parings, while the bases in pyrimidine strand of the other half dissociates from their complementary strand and fold back to form Hoogsteen hydrogen bonds with the bases in purine strand of the first purine.pyrimidine duplex (Figure 1.3). These base contacts in the DNA major groove generating C^+.GC and T.AT triplets. The formation of this structure leaves the purine strand unpaired. Two isomers can be formed depending on the orientation of the third strand against its purine counterpart of the duplex; parallel or antiparallel. The parallel H-DNA is formed between pyrimidine third strand and the purine strand of the duplex. The antiparallel one on the other hand is formed between purine third strand and the purine strand of the duplex (Xodo *et al.*, 1990). H-DNA is seen in atomic force microscopy as a clear protrusion with a different thickness than DNA duplex. This is consistent with a model explaining that H-DNA leads to the formation of a kink in the duplex which gives rise to an acute angle. As a result, it brings the flanking regions in close proximity (Tiner Sr *et al.*, 2001).

1.1.2.3. The structures of intermolecular triplex DNA

TFOs are synthetic oligonucleotides that bind specifically to duplex DNA forming regions of intermolecular triple helical DNA. They are potentially useful for targeting DNA sequences and for development as gene therapeutics. The nitrogenous bases of the TFOs interact with exposed groups on the base pairs of the duplex in the major groove, via

Hoogsteen (Figure 1.2 A (right)) or reverse Hoogsteen (Figure 1.2 C (left)) base pairing and create a three stranded structure. Different triplex structures can be formed depending on the sequence of the third strand. CT-containing TFOs generate C^+.GC and T.AT triplets (Figure 1.2(A)) in a Hoogsteen arrangement in which hydrogen bonds are formed between the pyrimidine-rich TFOs and purines in the DNA target. The TFO is oriented parallel to the polypurine tract of the target sequence. Formation of the C^+.GC triplet requires low pH (< 6) conditions to promote protonation of N3 of cytosine (Gowers and Fox, 1999, Rusling *et al*., 2005, Duca *et al*., 2008)(Figure 1.2 A (left)). The crystal structure of a DNA segment containing triplexes and its triplex-duplex junction at 1.8 Å resolutions reveals that DNA triplex has unique conformation which differs from both A and B form DNA (Rhee *et al.*, 1999). The purine-rich strand of duplex and the third strand are parallel to each other. The bases of the former strand make contact with the bases of the latter strand in the major groove through Hoogsteen-type interactions and as a consequence, two additional minor grooves are formed. This also reports that the electrostatic interactions between phosphate groups and protonated cytosine change the phosphate backbone torsion angles of the purine strand. As a result, it narrows down the minor groove width of the purine-Hoogsteen strands (Rhee *et al.*, 1999). Moreover the NMR structure of an intramolecular DNA triplex linked by ethylene glycol (dsDNA: DNA triplexes) indicates that the conformations of deoxyribose sugar are of S type (i.e. as in B-DNA). However the hybrid N and S type can be seen for protonated cytosine residues in the third strand. A slightly wider minor groove can be observed (i.e. as in A-DNA) due to duplex unwinding to accommodate the third strand in the major groove and to reduce electrostatic repulsion between strands (Tarköy *et al.*, 1998).

In contrast, purine-rich TFOs bind in an antiparallel orientation relative to the purine strand of the duplex target in a reverse Hoogsteen arrangement forming G.GC, A.AT (Figure 1.2(B)) and T.AT (Figure 1.2(C)) triplets (Gowers and Fox, 1999). However, T.AT and G.GC triplets can form both antiparallel and parallel types of triplets (Figure 1.2). Although antiparallel triplex formation is pH-independent, the high G-content of these TFOs can promote the formation of competing G-quadruplex structures (Fox, 2000). One of the requirements for triplex formation is the availability of a duplex polypurine tract within the double-stranded DNA target, since the third strand usually only makes contacts with bases in the purine strand. Pyrimidine inversions within an oligopurine tract are therefore destabilizing. Although these can be targeted with G.TA and T.CG triplets, these only contain one hydrogen bond to the third strand base, and so generate triplexes with low stability. The types of triplex motif in this report are categorized according to the base composition of the TFOs and their orientation against polypurine tract of the duplex target. This includes parallel motif (CT motif) producing parallel T.AT and C^+.GC triplets, and

antiparallel motif (GA motif) generating antiparallel A.AT and G.GC and finally mixed motif (GT motif) creating either parallel or anti-parallel T.AT (Figure 1.2(D), left), parallel G.TA (Figure 1.2(D), right) and T.CG (Figure 1.2(D), middle). The last two triplets are used to target pyrimidine inversions within the polypurine tract of target duplex.

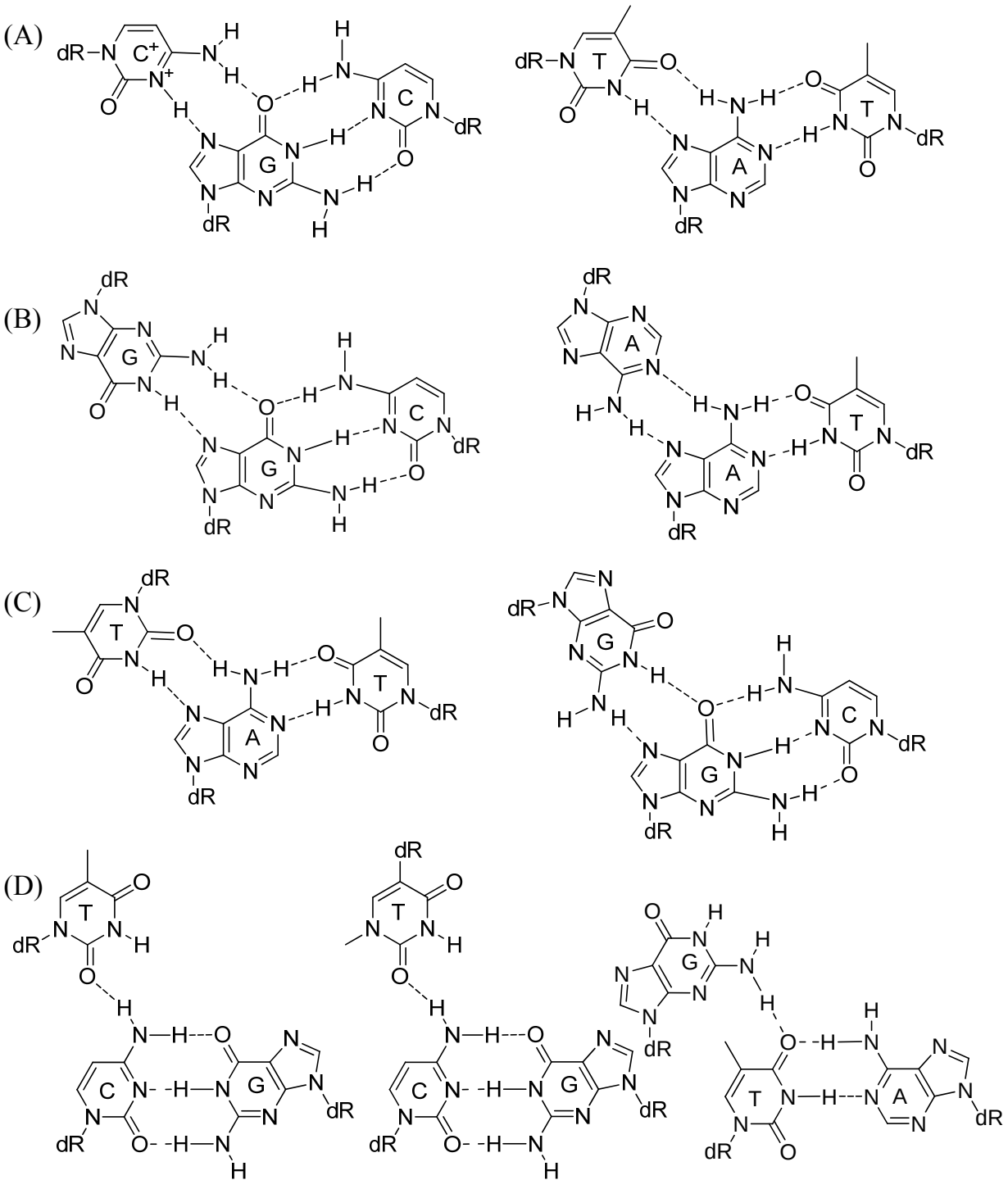

Figure 1.2 Chemical structures of the parallel C^+.GC and T.AT triplets (A), anti-parallel G.GC and A.AT triplets (B), anti-parallel T.AT (C), parallel G.GC (C), parallel T.CG (D, left), anti-parallel T.CG (D, middle) and G.TA (D, right). (Adapted from Gowers and Fox, 1999 and Rusling *et al*., 2006)

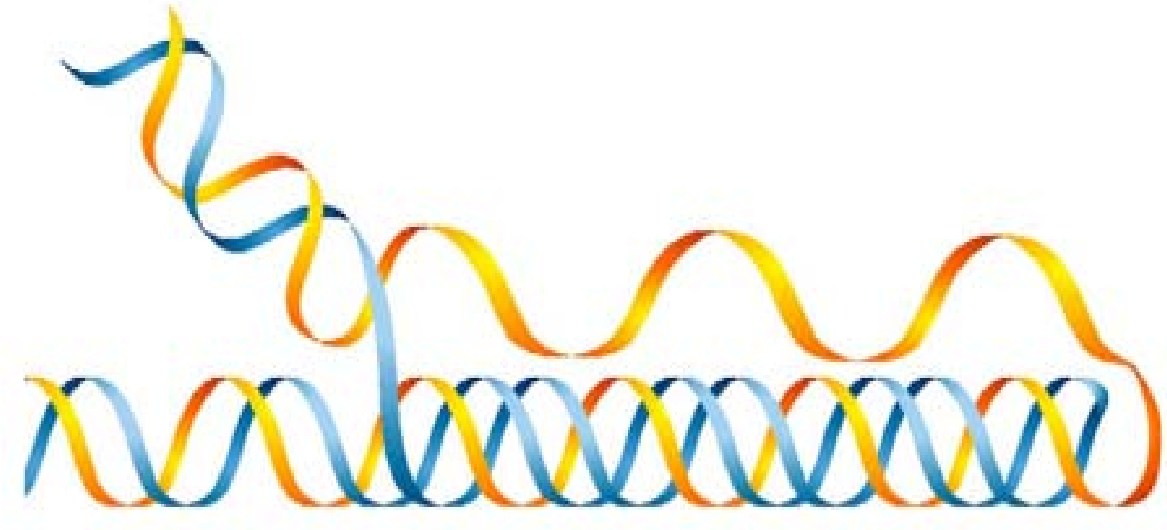

Figure 1.3. Schematic representation showing the structure of H-DNA. The blue line represents homopurine strand and the yellow line is the homopyrimidine strand of the duplex. Part of the homopyrimidine strand dissociates from the duplex and folds back to make hoogsteen hydrogen bonds with homopurine strand (adapted from Jain A. *et al*., 2008).

1.2. The factors affecting triplex stability

1.2.1. Common factors

Duplex DNA is formed by the interaction between two complementary polynucleotide sequences; the phosphate backbone gives the molecule an overall negative charge and plays a key role in the production of electrostatic repulsion between the three negatively-charged strands. This phenomenon results in the lower stability of triplexes than duplexes (Rusling *et al*., 2006). Moreover, the two patterns of sugar conformation, *N*-type (C_3-*endo*) that is found in ribose sugars of RNA, with the twist of C3' carbon up from the plane of the other four carbons, and *S*-type with C2' twisting up (C_2-*endo*) which is preferred in the deoxyribose sugar of DNA, also affect the stability of triplexes. RNA third stands generally form more stable triplexes than DNA third strands as a result of their *N*-type configuration (Rusling *et al*., 2006, Duca *et al*., 2008). Therefore, efforts to address this problem include the synthesis of compounds that can promote the *N*-type sugar conformation and reduce strand distortion. Base stacking is another factor that influences duplex and triplex DNA stability. Adding aromatic surface areas, together with hydrophobic groups (*i.e*., methyl groups) can increase triplex stability via hydrophobic stacking (Rusling *et al*., 2006, Duca *et al*., 2008).

1.2.2. Factors affecting the pyrimidine (parallel) triplex

Although the C.GC triplet can be formed within the pyrimidine motif at neutral pH, this triplet is less stable than T.AT as it contains only one hydrogen bond between N4 of cytosine and the 6-keto group of guanine. For this reason, low pH conditions (< 6.0) are required to promote cytosine protonation at N3, generating another hydrogen bond which consequently increases the stability of C^+.GC. Additionally, the presence of the positive charge within this triplet raises its stability so that isolated C^+.GC triplets are more stable than T.AT at low pH (Keppler and Fox, 1997). The arrangement of pyrimidine bases within the third strand also plays a role in stabilizing triplex formation and alternating third strand cytosine and thymine produce the highest stability. James *et al.* (2003) compared the thermodynamic and kinetic stability of four different third strands of equal length (15mer) (*i.e.* TTT, TTC, TCC and TCTC) and showed that the triplex formed by TTT is the least stable with a melting temperature of about 30 °C while TTC, TCC and TCTC produced melting temperatures of 67, 72 and 76 °C respectively. Moreover, the dissociation half-life of the triplex with alternating pyrimidine was approximately 3 days compared to only 20 minutes for the triplex formed by TCC and TTC TFOs. As DNA is a negatively charged biomolecule, it is stabilized by cations. Sugimoto and colleagues (2001) compared the thermodynamic stability of triplexes formed in the presence of various metal cations including Na^+, Mg^{2+}, Ca^{2+}, Ba^{2+}, Co^{2+} and Zn^{2+}. The results demonstrated that the highest triplex stability is observed in the presence of Mg^{2+} whereas Na^+ gives the lowest triplex stability. This is due to its smaller ionic radius and its ability to bind specifically to the phosphate group of duplex DNA (Sugimoto *et al.*, 2001).

1.2.3. Factors affecting the purine (antiparallel) triplex

The pH independent formation of this triplex has greater potential for its use in physiological conditions, but its stability remains controversial and depends on the length and base composition of the TFOs. According to Fox (1994), a reduction in the number of ApG and GpA steps in the duplex target increases the stability of this triplex, as the G.GC, A.AT and T.AT triplets are not structurally isohelical and there is therefore a distortion on moving from one triplet to the next. Among the triplets that form this motif G.GC is much more stable than A.AT, though G-rich TFOs can self-associated to form unusual structures (*i.e.* G-quartets) in the presence of monovalent metal ions (especially potassium), which compete for formation of the triplex (Fox, 2000). Although longer TFOs usually generate more stable triplexes than shorter ones, different sequence compositions can lead to different stabilities for TFOs of identical lengths. A study comparing the stability of triplexes formed by 5'-$(AGG)_4$-3' and 5'-$(GGA)_4$-3' revealed that the former triplex generated was 6-times

more stable than the latter, due to the presence of the 3'-guanine (Arimondo *et al*., 1998). Conversely, the inclusion of adenine in the same position leads to a decrease in triplex stability. The presence of Mn^{2+} favours the formation of stable antiparallel triplexes, which specifically stabilizes A.AT and T.AT triplets in GA and GT motifs respectively. DNase I footprinting of the complexes between $A_{11}(TC)_6.(GA)_6T_{11}$ and the TFO $T_{11}(AG)_6$ in the presence of Mg^{2+} showed no evidence for triplex formation even at TFO concentrations as high as 100 μM, whereas the binding between $A_{11}(TC)_6.(GA)_6T_{11}$ and $T_{11}(TG)_6$ is still evident. Substitution of Mg^{2+} by Mn^{2+} promotes triplex formation by both TFOs and the footprints persist at concentrations as low as 0.3 μM (Washbrook and Fox, 1994).

1.2.4. Factors affecting mixed sequence triplexes

Unlike other triplexes, short GT-motif third strands (12-mers) are more stable than longer ones and base modulations (*e.g*. base extension or mutation) at the 3'end have greater effects than at the 5'end (Cheng and Dyke, 1994, Fox, 2000). In addition, an increase in temperature from 4 to 37 °C results in a reduction in GT-triplex stability, while this condition promotes stable triplex formation in equivalent-length purine (GA-containing) TFOs, as it decreases the stability of the competing self-associated structures.

G.TA and T.CG triplets can be used to recognise pyrimidine inversions within polypurine tracts. These triplets each contain a single Hoogsteen hydrogen bond between the Watson-Crick base pairs and the third strand base and so have lower affinity and stability. Steric clash with the methyl group of thymine in TA base pairs also restricts the formation of the G.TA triplet (Radhakrishnan and Patel, 1994) and limits recognition of T by other synthetic nucleotides. In contrast Miller and Cushman (Miller and Cushman, 1993) reported that replacement of thymine with deoxyuridine decreased the thermal stability. This suggested that the methyl group of thymine is involved in stacking and hydrophobic interactions. Although these triplets are known to have low stability, this depends on the position of the pyrimidine inversion and the flanking regions. Destabilisation of surrounding triplets is observed when the inversion is located in a central position instead of the terminal one. The G.TA triplet is more stable when flanked by T.AT than C^+.GC (Kiessling *et al*., 1992). Like G.TA, the parallel T.CG triplet contains a single hydrogen bond between O2 of thymine and the exocyclic N4 of cytosine. The structure of these two triplets is similar and T.C and G.T have identical alignments. Moreover, the base twist of T.CG is the same as in G.TA. The G.TA triplet can be formed in parallel orientation only, while the T.CG can be either parallel or antiparallel (Gowers and Fox, 1999).

1.3. Strategies for overcoming these problems

Ideally, the third strand TFOs must be resistant to nucleases, not be affected by electrostatic repulsion between the three strands, be able to compete with other unusual DNA structures, produce a stable triplex at physiological pH and be stable for long enough to interfere with biological mechanisms.

1.3.1. Phosphate backbone modification

Despite the similarity of charge density and solubility in aqueous solutions the phosphorothioates (Figure 1.4(B)) are able to resist nuclease degradation, which is considered an ideal quality for triplex formation. The addition of phosphorothioates into the purine strand can promote triplex stability at low pH conditions, while it inhibits triplex formation when incorporated into the pyrimidine strand (Latimer *et al*., 1989, Fox, 2000). Likewise, Hacia *et al* (Hacia et al., 1994b) showed that inclusion of phosphorothioates into purine-rich TFOs results in similar triplex affinity to that of native phosphodiester linkages (Figure 1.4(A)). However this prevents triplex formation in pyrimidine-containing TFOs. In contrast, an *in vivo* study by Alunni-Fabbroni *et al.* (1996) revealed that phosphorothioate-conjugated pyrimidine TFOs can disrupt transcription of T7 polymerase. Although phosphorothioate-conjugated GT-containing TFOs prevent triplex formation, the introduction of phosphorothioates into GA-containing TFOs can promote triplex formation with low stability. Surprisingly, the triplex formed by the addition of two phosphorothioates at both ends of a GA-containing TFO retained the same affinity as the native phosphodiester, yet it is nuclease resistant and inhibits gene transcription *in vivo* (Lacoste *et al*., 1997).

Another nuclease-resistant and charge repulsion-bearing substituent is the non-ionic methylphosphonates (Figure 1.4(C)). A study by Kibler-Herzog *et al.* (Kibler-Herzog et al., 1990) showed that this substituent within a dA.dT mixture led to inhibition of triplex formation. However, another study revealed that a triplex can be formed, albeit with low stability if an alternating arrangement of phosphodiesters and methylphosphonates is present in the third strand (Kibler-Herzog *et al*., 1993). Conversely, the triplex formed from a mixture of $(CT)_8$ and $(AG)_8$ has the same stability, regardless of whether it contains methylphosphonates or a phosphodiester backbone (Callahan *et al*., 1991). Also, the complexes formed between a 2:1 mixture of methylphosphonate dA and phosphodiester dT or methylphosphonate $(AG)_8$ and phosphodiester $(CT)_8$ had higher stability than the phosphodiester third strand (Trapane *et al*., 1996). Purine-rich methylphosphonate TFOs have been used for mRNA targeting (Reynolds *et al*., 1994). The replacement of native phosphodiesters with methylphosphonates in an alternating arrangement can promote triplex

formation with a short TFO, however complete replacement by methylphosphonate leads to an unstable triplex. This phenomenon may be caused by the existence of a diastereoisomeric mixture of methylphosphonate residues. Stable triplexes can be generated by synthetic α-methylphosphonate TFOs, though these are practically hard to produce (Debart et al., 1998).

Replacement of O3' in the native phosphodiester by NH produces the new linkage called N3'-P5' amidate, which promotes more stable triplex formation than the native phosphodiester. More importantly, a sequence containing six consecutive guanines can be targeted by TFOs containing this linkage, forming a more stable triplex than those with ^{5Me}C or acridine tethered to the 5' end (Escude *et al*., 1996, Zhou-Sun *et al*., 1997); the combination of this linkage and ^{5Me}C provides even higher stability and is able to prevent *in vitro* gene transcription at pH 7.0. In contrast, the native backbone does not have this capability (Giovannangeli *et al*., 1996, Fox, 2000,). The stability of triplexes has been further increased by using RNA phosphoramidate TFOs (Figure 1.4(D)) (Gryaznov and Winter, 1998). The improvement of triplex stability by this linkage is possibly due to its preferred *N*-type sugar conformation. Moreover, it provides four-times higher association rates when combined with a cationic copolymer (Torigoe and Maruyama, 2005).

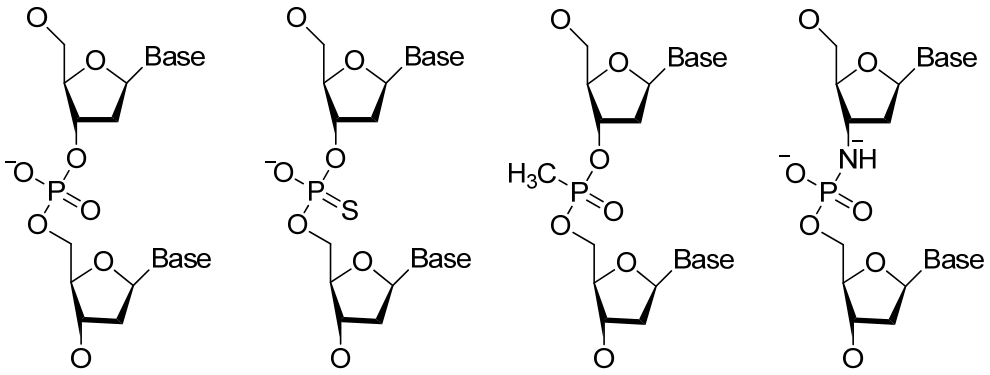

Figure 1.4 Chemical structures of Phosphodiester (A), Phosphorothioate (B), Methylphosphonate (C), Phosphoramidate (D). (Adapted from Fox, 2000 and Rusling *et al*., 2006)

1.3.2. Sugar modifications

Triplex formation was first observed with an RNA polyribonucleotide (Felsenfeld and Rich, 1957), and it is known that the *N*-type sugar conformation in RNA is more favourable for triplex formation than that of *S*-type in DNA, as this requires less target strand distortion (Asensio *et al*., 1999). Hence, sugar modifications for enabling stable triplex formation have focussed on the sugar conformation and overall charge. The *gauche* effect, obtained from the inclusion of an electronegative group at the 2'-position of the sugar as in RNA, promotes the *N*-type conformation (Bernal-Mendez and Leumann, 2001). The nuclease-resistant 2'-O-methyl substituent has been reported to promote more stable triplex formation than third strands containing deoxyribose, by stabilizing the C3'-*endo* sugar conformation. This consequently reduces the distortion of duplex target and enhances triplex rigidity (Asensio *et al*., 1999, Fox, 2000, Rusling *et al*., 2006). Other sugar modifications that restrict the C3'-*endo* conformation include Locked nucleic acid monomers (LNA or BNA) or O2', O4'-methylene-linked nucleic acids and O2', O4'-ethylene-linked nucleic acid (ENA) (Figure 1.4). The addition of LNA into TFOs can significantly increase triplex stability, though full substitution with this substituent inhibits triplex formation (Petersen and Wengel, 2003, Sun *et al*., 2004, Brunet *et al*., 2005,). ENA forms triplexes with lower thermal stability than LNA, though completely modified ENA-TFOs were able to form stable triplexes at physiological pH (Hojland *et al*., 2007). More recently, a novel LNA-TFO that contains a six-membered bridged nucleic acid formed a triplex with higher affinity than those of LNA and ENA (Rahman *et al*., 2008). Interestingly, the entirely modified version can still form a stable triplex at physiological pH.

The NMR structure of triplexes formed between duplex and LNA oligonucleotides shows that the geometry of underlying duplex is changed to an intermediate between A- and B-form structures. This occurs in order to facilitate the access of the third strand LNA to major groove and for the LNA bases to make contact with bases in purine strand of the duplex. There is also an important propeller twist between the bases of LNA and those of the purine strand of duplex which consequently allows the interactions between pyrimidines in the former strand and the 5'-flanking pyrimidines of the duplex (Sørensen *et al.*, 2004).

The development of bicyclo (Figure 1.5C) and tricyclic (Figure 1.5D) furanose is another effort to restrict sugar conformation (Tarköy and Leumann, 1993, Steffens and Leumann, 1999). The additional cyclopropane group within the 3'-O, 5'-C ethylene bridge, which typically restricts the sugar in an *S*-type conformation, showed an ability to form an *N*-type sugar. A study of Renneberg and Leumann found that TFOs containing this modification increased the T_m by 2 °C for each modification at pH 7 (Renneberg and

Leumann, 2004). Another analogue, morpholino (Figure 1.5E), replaces the ribose sugar with a six-membered morpholine ring, and the phosphodiester with phosphorodiamidate. At a high concentration of cations, the triplex formed by this analogue was less stable than TFOs containing N3'-P5' amidate. However, it produced more stable triplexes at low ionic strength (Lacroix *et al*., 2000, Basye *et al*., 2001). Besides, this analogue was reported to stabilize a TC triplex and was used in combination with α-oligonucleotides to improve triplex stability (Lacroix *et al*., 2000, Michel *et al*., 2003).

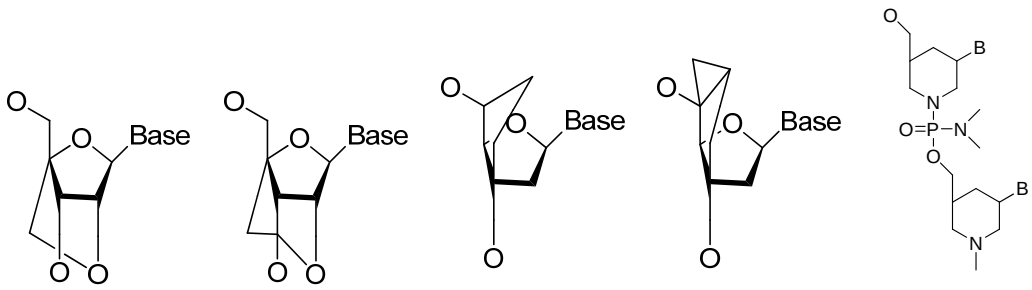

(A) **(B)** **(C)** **(D)** **(E)**

Figure 1.5 Chemical structures of LNA (A), ENA (B), bicyclo-DNA (C), tricyclo-DNA (D), morpholino (E).

1.3.3. Base modifications

The development of base analogues has been aimed to address a number of problems including pH dependency, charge repulsion, base stacking and pyrimidine inversion. There are two main types of analogue namely pyrimidine and purine base analogues (Fox, 2000). 5-Methyl cytosine (^{5Me}C), pseudoisocytosine, 6-oxocytosine and 2-aminopyridine (2AP) are pyrimidine analogues (Figure 1.6) while 8-oxoadenine and its derivatives, N7-G, P1 and N7-inosine are purine ones (Figure 1.7). Even though ^{5Me}C does not promote triplex formation at physiological pH (Koh and Dervan, 1992), the additional methyl group raises the pK value compared to the natural cytosine base (Povsic and Dervan, 1989, Xodo *et al.*, 1991) which encourages the formation of triplex at higher pHs. This improved stability is also caused by the release of water molecules, the improved base stacking or the increase in hydrophobic interaction in the major groove. This eventually leads to an improvement in the pH profile and increases triplex affinity (Xodo *et al*., 1991, Singleton and Dervan, 1992, Rusling *et al*., 2006). Due to the difficulty in synthesis and availability, the non-charged pseudoisocytosine has received limited use for triplex formation. Potentially, this analogue can be used to overcome the pK problem, especially the charge interaction between protonated cytosines in contiguous C^+.GC triplets. This analogue is able to form a stable triplex with a duplex

target containing six contiguous guanines (Fox, 2000). The hydrogen at the N3 position causes this base to resemble a protonated cytosine, which is able to form a Hoogsteen hydrogen bond with guanine; its N1 hydrogen provides a stable hydrogen bond with guanine (Ono *et al*., 1992). A number of other derivatives have been prepared, which successfully form stable triplexes including the 2'-O-methyl substituent of pseudoisocytosine, which gives stability at pH 7, 2-aminopyridine that can be used to target a run of consecutive GC base pairs and a pyrrolidino derivative which generates a triplex with 2.5-3 °C increase in T_m per modification and also targets contiguous guanines (Ono *et al*., 1991, Ono *et al*., 1992,). Another cytosine analogue that can recognize guanine is 6-oxocytosine, which is able to form triplexes in a pH independent manner, though it produces less stable triplexes than cytosine and ^{5Me}C at lower pHs. This observation suggests the importance of the positive charge in protonated cytosine for forming triplexes with high stability (Fox, 2000). The alternating arrangement of this analogue with ^{5Me}C and replacement of deoxyribose with a flexible acyclic linker in 6-oxocytosine-containing TFOs however can promote stable triplex formation (Xiang *et al*., 1996, Xiang and McLaughlin, 1998). Further derivatives of 6-oxocytosine (e.g. 2'-O-methyl, ribo derivatives and 2'-aminoethoxy) were designed but these still generate triplexes with low stability and do not increase affinity (Rusling *et al*., 2006). The 2-aminopyridine analogue (2AP) was found to promote more stable triplexes than C or ^{5Me}C, both at high and low pH in which it suggested that the triplex is intrinsically more stable (Cassidy *et al*., 1997, Fox, 2000). Similarly, a footprinting study on the interaction between $(2AP)_6T_6$ and the target sequence $G_6A_6.T_6C_6$ revealed that this can form a triplex with high stability at pH 7.0 while $^{5Me}C_6T_6$ and C_6T_6 formed complexes that were only stable at pH 5.0 (Cassidy *et al*., 1997). These properties are due to the 2-aminopyridine's pK of 6.86 which is close to physiological pH. The conjugation of psoralen into TFOs containing this analogue has been used to target the aromatase gene, (Bates *et al*., 1996).

8-oxoadenine, its N6-methyl and 7, 8-dihydro derivatives are purine analogues, which form a stable triplet with GC in a pH independent manner (Jetter and Hobbs, 1993, Miller and Cushman, 1993, Fox, 2000, Rusling *et al*., 2006). Moreover, it is able to recognize a target site containing a run of guanines. However, when used in isolation these analogues produce low affinity triplexes as the triplets formed are not isomorphous with T.AT (Rusling *et al*., 2006). Another two analogues that form triplexes in a pH independent manner are N7-G and P1. At an alternating GA-containing target sequence they showed a 6-fold lower triplex affinity than ^{5Me}C, though the triplex was 4-times more stable than ^{5Me}C at a target site containing six contiguous guanines. This can be explained since alternating N7-G.GC and T.AT or P1.GC and T.AT triplets are not structurally isomorphic (Koh and Dervan,

1992, Radhakrishnan *et al*., 1993, Hunziker *et al*., 1995, Brunar and Dervan, 1996, Fox, 2000). P2, which is derived by moving the glycosidic linkage from N7 in P1 to N8, showed no triplex formation. This emphasises the significance of the position of the phosphodiester backbone for these analogues (Fox, 2000). In addition, an amino group-depleted N7G (i.e. N7-Inosine) was able form a stable triplex in a pH-independent manner at targets contains alternating GA and at runs of Gs. This occurred due to the formation of a single hydrogen bond between N1H of inosine and N7 of guanine (Fox, 2000). On the other hand, Rusling *et al*. suggested that an additional hydrogen bond might form between the carbonyl group of inosine and the CH group of guanine, and that this could provide stability because of its slightly positive-electrostatic properties (Marfurt and Leumann, 1998, Rusling *et al*., 2006). Further efforts to overcome the sequence constraints, which occur within alternating GA targets, include the development of acyclic glycerol derivatives, positively charged substituents and 2'aminoethoxy derivatives (St. Clair *et al.*, 1998). However, their properties have still not overcome all the problems with forming stable triplexes and further new analogues, with isomorphic triplex structures are vital to alleviate the sequence dependency.

Other analogues have been developed in an attempt to overcome pyrimidine interruptions within the ideal oligopurine tract. Pyridine-2-one and pyridine-4-one (Figure 1.8 (A and B respectively)), are both thymine analogues, that lack either the 4-carbonyl or 3-NH group from the native thymine. These provide increased selectivity for CG over other base pairs, compare to T (which forms an unstable T.CG triplet) as these analogues cannot bind to adenine and they use their carbonyl group to recognize the exocyclic amino group of cytosine (Durland *et al*., 1994, Rusling *et al*., 2006). Elimination of the 4-carbonyl group of thymine produces 5-methyl-pyrimidine-2-one, which disrupts recognition of adenine as the hydrogen is missing from N3. However, its remaining 2-carbonyl group can still hydrogen bond with cytosine and produces a triplet that is as stable as its T.CG counterpart (Marfurt and Leumann, 1998, Prevot-Halter and Leumann, 1999). Its pyrrolopyrimidine-2-one derivative, featuring the addition of an aromatic ring and the same hydrogen bonding pattern can still recognize CG and forms a triplet with CG that is more stable than native thymine at pH 6.0 (Ranasinghe *et al*., 2005, Rusling *et al*., 2005). Another analogue, that remains unprotonated at all pHs is 2-aminopyrimidine (d2APm, pK = 3.3, Figure 1.8(C)). This analogue contains a nitrogen atom that can interact with the exocyclic amino group of cytosine and creates a triplex with 4 °C higher T_m than cytosine (Chen and McLaughlin, 2000). Instead of using a single analogue to target pyrimidine inversions, the combination of those analogues with modified sugars and/or backbones has also been tested. The LNA-containing 2-pyridine base increased the T_m by 9 °C per single substitution which is higher than that attached with deoxyribose (Obika *et al*., 2001). Other compounds, such as 1-

isoquinolone and imidazole and its derivatives, have also been attached to LNA for recognition of CG interruptions, though these produced triplexes which are less stable than T.AT and C^{+}.GC (Hari *et al*., 2003, Hari *et al.*, 2005). Unlike the CG interruption, there are fewer approaches for overcoming TA interruption because of problems due to steric hindrance by the methyl group at the 5-position. The attachment of 3-oxo-2, 3-dihydropyridazine to a PNA backbone (Figure 1.8D), using a β-alanine linker, increased the T_m at an isolated TA interruption by 5 °C. In this case the linker avoids the interaction with the thymine methyl group and the analogue is able to form a hydrogen bond with the 4-oxo group of T (Eldrup et al., 1997). An attempt by Fox's group to modify guanine by introducing an aminoethoxy into its 2'-position or adding a propargylamino group at the 7-position of 7-deazaG did not enhance the affinity of the G.TA triplet, but instead increased the affinity for GC rather than the TA interruption (Rusling *et al*., 2006).

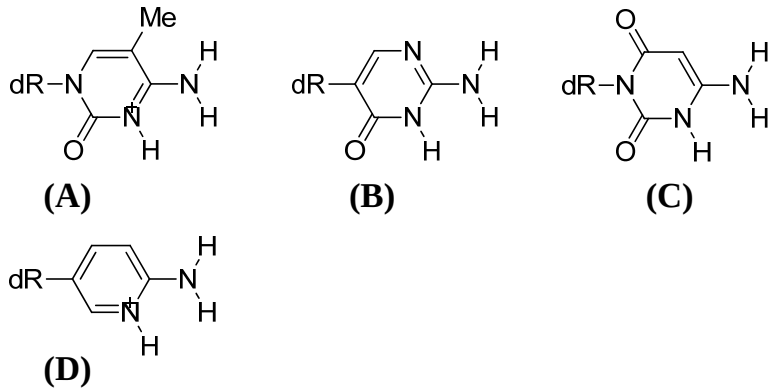

Figure 1.6 Chemical structures represent pyrimidine base analogues; 5-Methyl cytosine (^{5Me}C) (A), Pseudoisocytosine (B), 6-oxocytosine (C) and 2-aminopyridine (2AP) (D). (Adapted from Fox, 2000 and Rusling *et al*., 2006)

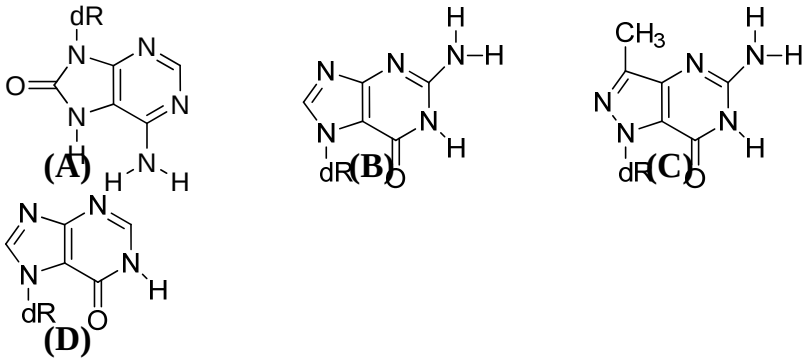

Figure 1.7 Chemical structures represent purine base analogues; 8-oxoadenine (A), N7-G (B), P1 (C) and N7-inosine (D). (Adapted from Fox, 2000 and Rusling *et al*., 2006)

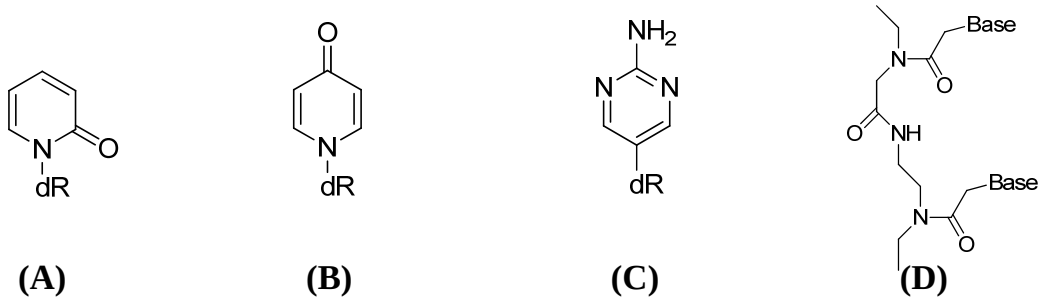

Figure 1.8 Chemical structures of Pyridine-2-one (A), Pyridine-4-one (B), 2-aminopyrimidine (C) and PNA (D)

1.3.4. Binding agents

1.3.4.1. Triplex binding ligands

Another way to stabilise triplexes is to use ligands that selectively bind to triplexes, but not duplexes, thereby drawing the equilibrium towards triplex formation. Polycyclic compounds, with large aromatic surface areas, are considered to possess the capability to bind selectively to triplexes. One of the first of these to be studied was benzo[*e*]pyridoindole (BePI) (Figure 1.9 (A)), which is a cationic compound, which uses its massive ring structure to overlap and stack (intercalate) between adjacent triplets, but is too large to bind to duplex base pairs. This compound preferentially stabilizes triplexes containing T.AT triplets rather than C^+.GC due to the unfavourable electrostatic repulsion with the positive charges of C^+.GC (Mergny *et al*., 1992, Fox, 2000). BePI is thought to bind with its side chain within the major groove, between the duplex pyrimidine strand and the third strand. In contrast benzo[*g*]pyridoindole (BgPI) (Figure 1.9 (B)), which binds with equal affinity to BePI is positioned with its side chain between the duplex pyrimidine strand and the third strand within the major groove (Escude *et al.,* 1995). Additional attempts to fuse aromatic rings onto compounds led the synthesis of benzo[*f*]pyridoquinoxaline (Figure 1.9(C)), benzo[*f*]quinoquinoxaline (Figure 1.9(D)) and dibenzophenanthrolines (Figure 1.9(E)) which all stabilize triplexes, though the dibenzophenanthrolines seems to be the most effective (Marchand *et al*., 1996, Baudoin *et al*., 1998, Escude *et al*., 1998,). By using calorimetric and spectrophotometric techniques, the binding selectivity and thermodynamic parameters of 2,6 disubstituted amidoanthraquinones (Figure 1.9(F)) and their 1,4 counterparts have been determined. These demonstrated that the 2,6 analogues preferentially bind and stabilize triplexes while their 1,4 counterparts promote third strand dissociation and result in the disruption of triplex stability (Haq *et al*., 1996). 2,7-disubstituted anthraquinone sulphonamides showed greater triple stabilizing potential than their 2,6 counterparts (Kan *et al.*, 1997). Fox's group compared the affinity of four di-substituted and two monosubstituted amidoanthraquinone to address the effect of substitution position. This showed that the

decrease in triplex affinity is in the order 2,7>1,8=1,5>2,6 (Keppler *et al*., 1999, Fox, 2000,). Naphthylquinoline (Figure 1.9(G)) derivatives that have aromatic rings to stack with the three bases in a triplet are also successful triplex binding ligands, though these also selectively bind to T.AT over C^+.GC triplets. Their unfused aromatic rings have torsional flexibility and are therefore able to stack better on the three bases in a triplet, which may not be coplanar. This compound works well with both parallel and anti-parallel triplexes (Chandler *et al*., 1995, Cassidy *et al*., 1996, Strekowski *et al*., 1996).

1.3.4.2. Ligand-conjugated TFOs

DNA binding ligands can also be covalently attached to TFOs, and act as non-specific anchors holding the TFO in place. Acridines (Figure 1.9(H)) are DNA intercalators that have been attached to the end of TFOs and increase triplex stability (Sun *et al*., 1989, Birg *et al*., 1990, Sun *et al*., 1991, Grigoriev *et al*., 1992, Stonehouse and Fox, 1994). This ligand is thought to intercalate at the triplex-duplex junction and is mostly used with parallel, pyrimidine-containing TFOs, though it can also stabilize antiparallel GA- and GT-containing TFOs in both the parallel and anti-parallel orientations (Fox, 1994, Gamper *et al*., 1997, Klysik *et al.*, 1997, Orson *et al*., 1999). The attachment of this ligand to the 3'-end of a TFO generates a less stable triplex than when it is attached at the 5'-end (Sun *et al*., 1989, Birg *et al.*, 1990, Stonehouse and Fox, 1994,). This can be explained since intercalators are known to bind better to YpR steps, which will be present at the 5'-end of the TFO, than to RpY which will be present at the 3'-end (Collier *et al*., 1991, Mouscadet *et al.*, 1994).

A number of cross linking agents (*e.g*., azidoproflavin, azidophenacyl) have also been employed to stabilize triplex formation. The most studied is psoralen in which it is conjugated to the TFOs. A psoralen-TFOs conjugate targets the homopurine strand of the duplex and induces triplex formation. It then photoinduces a cross-link between the two strands of duplex at TpA steps. The covalent attachment of psoralen (Figure 1.9(I)) at the 5'-end of a pyrimidine TFO promoted triplex formation with the HIV proviral sequence, containing a 16 base oligopurine tract at pH 6.0, despite the presence of contiguous GC base pairs. However, at high concentrations the psoralen-conjugated TFOs formed a complex with a secondary site that contained only 8 base pairs (Takasugi *et al*., 1991, Giovannangeli *et al*., 1992). Further studies have reported that psoralen-conjugated TFOs can target a 20 base pair tract within the aromatase gene, even though this contained three CG interruptions within the polypurine tract, which were recognised using T.CG triplets (Macaulay *et al.*, 1995, Bates *et al.*, 1995). Moreover, the replacement of cytosine by guanine to form a G.GC triplet increased the binding (Bates *et al*., 1995, Macaulay *et al*., 1995). The potential of cross-linking agents is not only limited to gene inactivation but they can be used for site-

specific mutagenesis. Psoralen-conjugated GA-containing TFOs produced mostly TA to AT transversions at the psoralen intercalation site, which is thought to occur via transcription-coupled repair alone or in combination with nucleotide excision repair mechanisms (Gasparro *et al*., 1994, Wang *et al*., 1995, Wang *et al*., 1996, Barre *et al*., 1999,). However, some studies suggested that this mechanism is dependent on the sequence characteristics and experimental conditions (Fox, 2000).

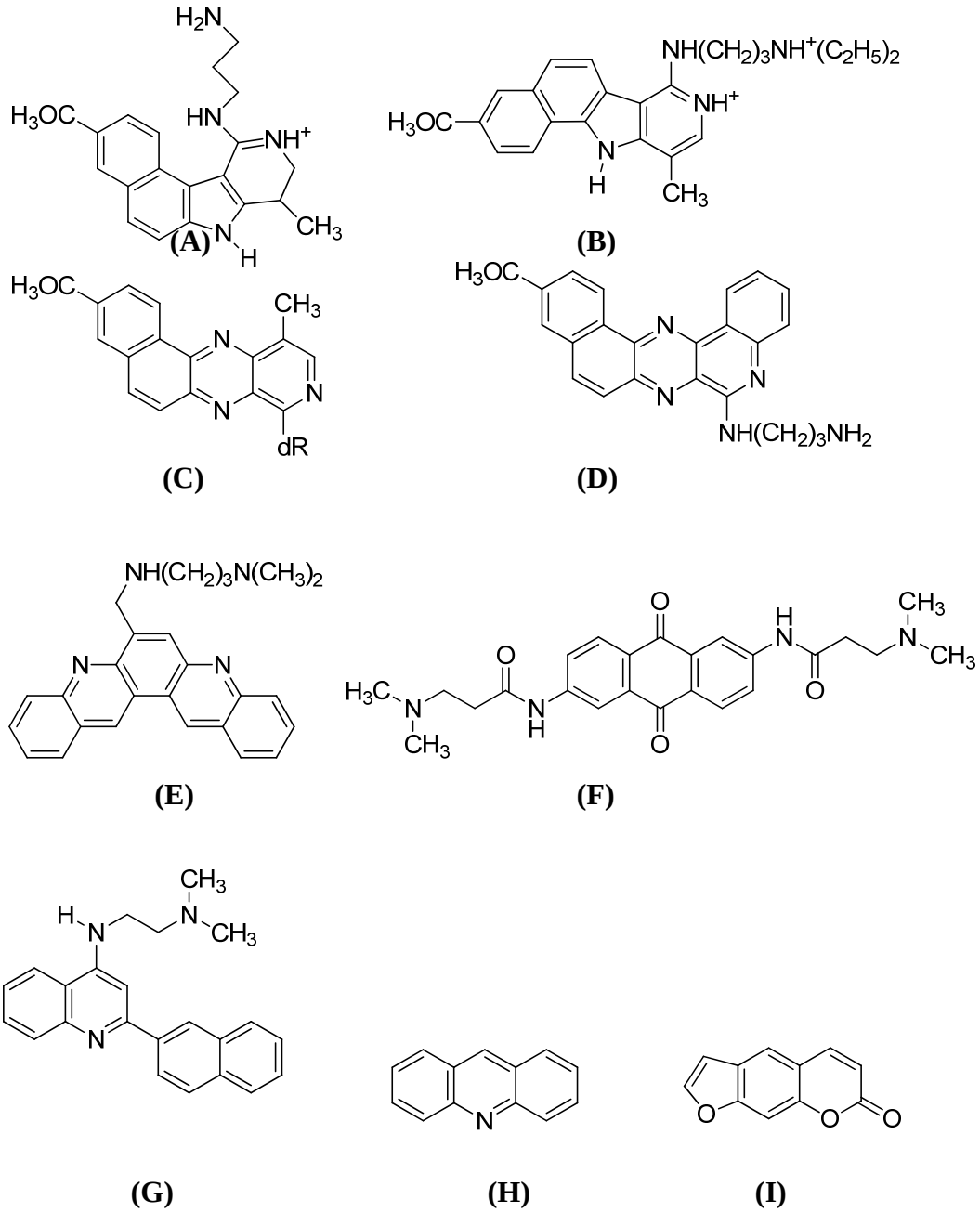

Figure 1.9 Chemical structures of benzo[*e*]pyridoindole (A), benzo[*g*]pyridoindole (B), benzo[*f*]pyridoquinoxaline (C), benzo[*f*]quinoquinoxaline (D),dibenzophenanthrolines (E), 2,6 disubstituted amidoanthraquinones (F), naphthylquinoline (G), acridines (H) and psoralen (I)

1.4. Biological applications of triplexes

1.4.1. DNA transcription and replication

The formation of a triplex within the major groove of DNA prevents the binding of specific proteins to the DNA and eventually its functionality (Duca et al., 2008, Boer et al., 2009). A number of studies have reported that triplex formation can inhibit the transcription of several genes including the cancer-related c-*myc* gene (Hacia *et al.*, 1994a, Napoli *et al*., 2006), inflammatory-related TNF-α gene (Aggarwal *et al*., 1996), ets2 (Carbone *et al.*, 2003), MCP-1 (Marchand *et al*., 2000), cell adhesion molecule ICAM-1 (Besch *et al*., 2002), GMF/CSF (Kochetkova *et al*., 1997), tie1 (Hewett *et al*., 2006), HER2/neu (Ebbinghaus *et al*., 1999), bcr/abl (Rapozzi *et al.*, 2002). The mechanisms of these inhibitions can be through interfering with the binding of transcription factors or the formation of the initiation complex (Svinarchuk *et al*., 1997, Karympalis *et al*., 2004, Hewett *et al*., 2006). The elongation step of transcription can be inhibited either by TFOs alone or in combination with psoralen (Giovannangeli *et al*., 1996, Ebbinghaus *et al*., 1999,).

A study with psoralen-conjugated TFOs showed that they can be used as a tool to deliver a gene enhancer to the target gene in order to promote transcription factor recruitment and eventually activate transcription. This strategy was shown to increase gene expression by 4-fold (Song *et al.*, 2004). These TFOs were also found to increase a γ-globin gene expression by 4-fold via introduction of a single mutation at the -280 region of the gene, which is known to negatively regulate the gene. The mutation at this site therefore increases the gene expression (Xu *et al*., 2000). Moreover, it is also found to be due to the formation of a triplex within the suppressor sequence of the gene (Song *et al*., 2004). Some studies have also suggested that the interaction of TFOs with replication initiation sites can disrupt the function of DNA polymerase and thus inhibit replication (Guieysse *et al.*, 1995, Diviacco *et al*., 2001). Additionally, the use of an acridine-conjugated oligothymidine to target the viral initiation site of SV40 showed the capability to reduce its replication, in which it is believed that the triplex works by inhibiting the function of a helicase in the replication complex (Birg *et al.*, 1990).

1.4.2. Gene mutagenesis and recombination

The conjugation of site-specific DNA damaging agents, such as photoactivatable agents, metal complexes, orthophenanthroline or metalloporphyrins and enzymes, with TFOs can increase gene mutation (Majumdar *et al.*, 1998, Barre *et al.*, 2000, Christensen *et al.*, 2004) and recombination (Faruqi *et al*., 2000, Datta *et al*., 2001, Vasquez *et al*., 2001). Among those agents, psoralen is commonly attached to the TFOs and it is believed it

produces base pair specific adducts in the duplex target and eventually leads to mutation (Rogers *et al*., 2005, Duca *et al*., 2008). However, using psoralen-conjugated TFOs presents a problem as the requirement for an adjacent TpA step reduces the target options (Duca *et al*., 2008). In addition, a number of compounds have been conjugated to TFOs that have the capability to modify the gene itself or its promoter, such as a 2-amino-6-vinylpurine derivative and chlorambucil, (Ziemba *et al*., 2001, Nagatsugi *et al*., 2002). The combination of modified TFOs, such as PNAs and bis-PNAs, with other damaging agents such as psoralen, benzophenone and anthraquinone molecules was reported to produce a 6.5-fold increase in mutation (Faruqi *et al*., 1998, Rogers *et al*., 2002, Rogers *et al*., 2004, Cheng *et al*., 2006, Miller *et al*., 2007).

1.4.3. Anti-gene and therapeutics

Although triplex formation has proved to have promising capability to modulate a number of biological processes, its implementation in cellular contexts still has many limitations including nuclear and cellular membrane penetration, target sequence accessibility and its instability in both nuclear and cytoplasmic environments. Therefore, there have been many strategies to overcome those limitations. Cholesterol-conjugated TFOs were able to gain access to rat liver cells, especially hepatocytes and stellate cells, indicating that this compound can successfully penetrate through cellular and nuclear membranes and inhibit gene transcription (Cheng *et al*., 2006). Despite attempts to use viral delivery systems and cationic complexes to overcome the polyanionic property of TFOs, the immune response against viral proteins and the difficulty of use *in vivo* are the major concern of these strategies (Hermiston and Kuhn, 2002, Dobbelstein, 2003). A study to address the problem of TFO delivery used highly branched 3D molecules, namely dendrimers, which effectively uptake the TFOs both in vitro and *in vivo* (Santhakumaran *et al*., 2004). However, the accessibility of TFOs to the specific target sequences within the context of chromatin, and its effective concentration in a cellular context are some of the major concerns for using TFOs as future therapeutics. Since the use of TFOs alone still poses many problems, the conjugation with existing anti-cancer drugs (*i.e*. daunomycin) have been tested to increase the affinity or cytotoxicity of the drugs. This conjugation also increases triplex stability via intercalating mechanisms and has been used to inhibit c-*myc* and MDR1 gene transcription (Carbone *et al.*, 2004, Stierle *et al*., 2008).

1.5. Footprinting techniques for studying triplexes

Since development of footprinting technique in 1978 for studying DNA-protein interactions (Galas and Schmitz, 1978) the technique has been used to identify and

characterize the binding sites for DNA-binding proteins, small molecules and TFOs (Hampshire *et al.*, 2007). The agents used in this technique, such as chemicals or enzymes, cleave a radioactively-labelled duplex DNA, in the absence and presence of any DNA-binding ligands. In the ideal situation the cleavage agent is not sequence selective and produces an even ladder of cleavage products, which are then resolved using denaturing polyacrylamide gel electrophoresis (Hampshire *et al*., 2007). In the presence of a sequence-selective DNA binding ligand, the cleavage agents are unable to cleave and the DNA is protected. As a consequence, a "footprint" appears as a gap in the ladder of bands (Figure 1.10). The binding site of the ligand is identified by comparing the cleavage pattern to those in the absence of ligand. The concentration dependence of footprints and cleavage enhancements are quantified and fitted to a simple binding curve. The C_{50} values are calculated which is the concentration of ligand at which the binding site is 50% occupied (Hampshire *et al*., 2007). In most footprinting experiments, the concentration of target DNA (nanomolar) is relatively lower than the ligand (micromolar) therefore the binding of ligand is not determined by stoichiometric ratio of ligand to DNA but rather by the equilibrium binding constant. The calculated C_{50} values obtained from footprinting experiments under this condition are therefore equivalent to the equilibrium dissociation constant (K_d) (Fox, 1997). These are used to estimate the binding strength (affinity) of ligand to its binding site on DNA (Hampshire *et al.*, 2007)

TFOs bind sequence-selectively to the major groove of duplex DNA while the DNase I cuts from the minor groove. In this case the inhibition of cleavage is therefore not due to direct steric blockage of the DNase I, but must be due to TFO-induced DNA structural changes or changes in its flexibility. It has also been noticed by several studies that there is often enhanced DNase I cleavage at the 3'end of the oligopurine tract of the TFO binding site at the duplex-triplex junction (Bijapur *et al.*, 1999, Brown *et al*., 1996, Cardew *et al*., 2012). This may be because the binding of TFOs in the major groove induces changes in DNA local structure and makes the minor groove of the duplex-triplex junction more susceptible to DNase I cleavage at this point. The formation of triplexes between various target sites (*i.e.* $A_8GA_8.T_8CT_8$, $T_8AT_8.A_8TA_8$ and $T_8GT_8.A_8CA_8$) and various TFOs (*i.e.* A_8NA_8 and T_8NT_8 where N is each bases in turn) revealed that the footprints are mostly followed by enhanced DNase I cleavage at the 3'-end of the TFOs' binding sites even in weak interactions (i.e. faint footprints) (Chandler and Fox, 1993). This enhanced cleavage was also evident in the binding reactions between other TFOs (*i.e.* G_5T_5, T_5G_5, T_5C_5 and C_5T_5) and their targets (*i.e.* $G_6A_6.T_6C_6$ and $A_6G_6.C_6T_6$) in the conditions with triplex-binding ligand and without (Cassidy *et al.*, 1994). Similar enhancements were also observed with 139 base-pair fragments in the presence of actinomycin D which the author suggested that it

could arise from two possible origins; the structural changes in DNA or the mass-action effects. The former can be described as that mentioned in the case of TFOs though this antibiotics approaches DNA in the same direction as DNase I (*i.e.* sterically block DNase I cleavage through DNA minor groove). The latter (*i.e.* mass-action effects) is due to the displacement of enzyme from antibiotics binding sites therefore increasing the enzyme concentration somewhere else (Goodisman and Dabrowiak, 1992). Low and colleagues also observed large enhancements at a number of sites on 160 base-pair fragments that bound to echinomycin. In addition to the DNA structural alteration mechanism, they proposed that the origin of enhancements could also arise from an attractive interaction between cleaving agents (*i.e.* DNase I and DNase II) and antibiotics however their results had led them to reject the latter mechanism (Low *et al.*, 1984). The observed enhancements were also seen around AT-rich region of 160 base-pair fragments bound to anti-cancer drug mitoxanthrone and other anthraquinone-based drugs suggesting that the location of the drugs' side chain in the DNA major groove induces DNA structural alterations (Fox *et al.*, 1986). This effect will be explored in the results chapters 3 and 4.

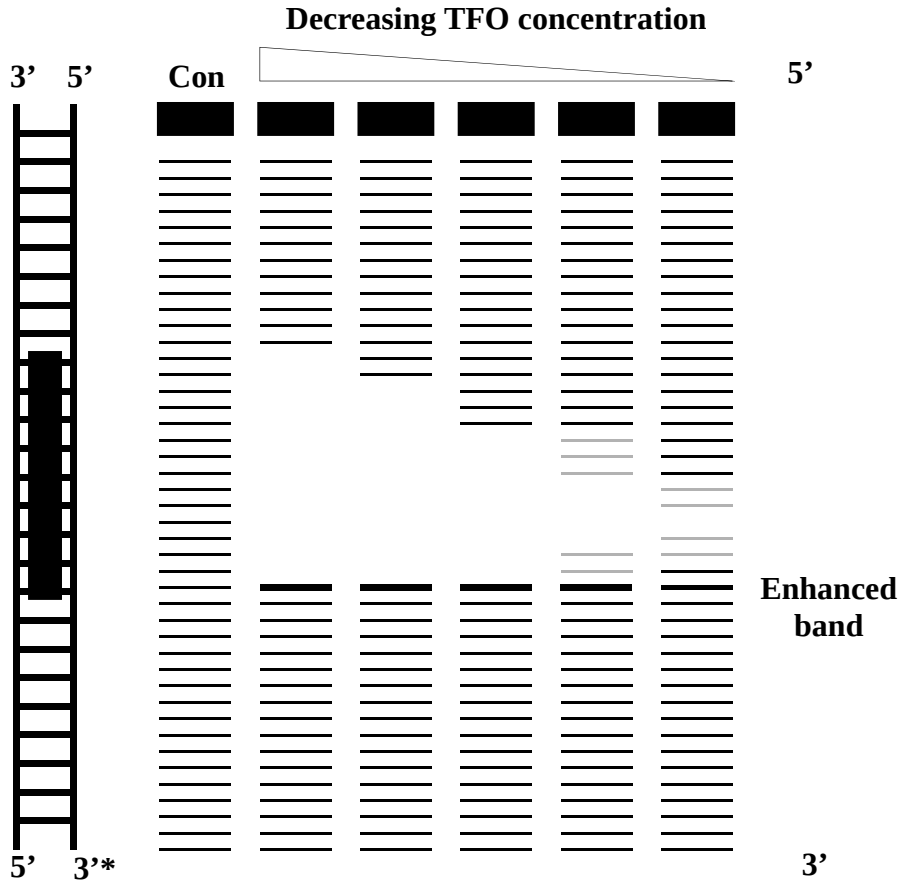

Figure 1.10 Schematic representation of the footprinting technique. On the left represents a duplex DNA which was radioactively labelled at the 3'-end (asterisk) and bound to the TFO (filled box). On the right is a footprinting gel in which the "Con" is a cleavage pattern in the absence of TFO and the rest of the lanes are the patterns in the presence of the decreasing TFO concentrations.

1.5.1. Enzymatic footprinting probes

1.5.1.1. DNase I endonuclease

The DNase I endonuclease is a glycoprotein enzyme with a molecular mass of 30,400. This enzyme recognizes double-stranded DNA, binds within the minor groove and cleaves O3'-P bond of the phosphodiester backbone producing single strand nicks (Suck and Oefner, 1986). Divalent cations (*e.g.* magnesium and calcium) are required and it has been shown that the cleavage activity in the presence of magnesium is more efficient than in the presence of calcium (Hampshire *et al*., 2007). The proposed mechanism for DNase I cleavage is that it uses the amino acid sequence within its exposed loop, containing arginine 70, asparagine 71, serine 72, tyrosine 73 and lysine 74, to bind the minor groove of the duplex (Figure 1.11). The enzyme-DNA complex is then stabilized by electrostatic interaction between the positively charged amino acid, arginine or lysine, and the negatively charged phosphodiester backbone (Suck and Oefner, 1986). The enzymatic activity starts as the histidine 131 receives a pair of electrons from the carboxylate ion of glutamate 75. This then attacks water molecule 390, which attack phosphorus in the phosphodiester backbone. As a result, the O3'-P bond is cleaved (Suck and Oefner, 1986). The cleavage reaction can be stopped by modification of histidine 131 (Suck and Oefner, 1986) or using EDTA to chelate divalent cations. Although DNase I is not sequence-dependent, it generates an uneven ladder of cleavage products (Fox *et al.*, 1984). This is due to the fact that DNA sequence affects its local structure (*i.e*. variations in the minor groove width and bending properties) which restricts the interaction between amino acid residues in the exposed loop of DNase I and duplex DNA. The A_nT_n tracts for example have a narrow minor groove (Liepinsh *et al.*, 1994) which restricts access of the exposed loop and reduces the cleavage frequency (Suck and Oefner, 1986). In contrast $G_n.C_n$ tracts have a wider minor groove, but are less flexible and are cut poorly, as DNA bending is an integral part of the cleavage reaction. Despite the extended area of interaction between the enzyme and DNA, which results in considerable ambiguity in determining the exact ligand binding sites, it is still widely used as a footprinting cleavage agent because of its ability to function at a wide range of pHs (pH5.0-pH9.0) and temperatures and its simple preparation for use in the experiments (Hampshire *et al*., 2007, Jain *et al*., 2008, Suck and Oefner, 1986). DNase I has been used to study sequence selectivity of eukaryotic transcription factor Sp1 on murine MT-I promoter and the inhibitory effect of pyrimidine oligonucleotides on the function of this promoter through triplex formation (Maher *et al.*, 1989). It was also adopted to determine sequence specificity and affinity of transcription factor IID (TFIID) on TATA elements within adenovirus major late promoter (MLP) (Hahn *et al.*, 1989). The use of this enzyme

in combination with other cleavage agents (*i.e.* $KMnO_4$, Phenylphenanthroline, hydroxyl radicals and Methidiumpropyl-EDTA) revealed the modified conformation of bacterial mercuric ion resistance operon (mer) upon the binding of Hg-activated MerR protein (Frantz and O'Halloran, 1990). Fox and Waring (1986) have used this enzyme to locate the binding site of noglamycin antibiotics on DNA fragments *tyr*T, *ptyr*2, *pUC*13 and *Xbs*1 and found that the preferred binding sequences of this antibiotics are TpG (CpA) and GpT (ApC) steps. They also found DNase I cleavage enhancements at the region flanking the antibiotics binding site which could arise from local DNA conformational changes induced by the binding of this antibiotics. The enzyme has also been adopted to study the interaction of DNA with other small molecules such as distamycin, netropsin, Hoechst 33258 and berenil (Abu-daya *et al.*, 1995). In addition, this was also used to examine the sequence selectivity, specificity and affinity of TFOs on DNA target duplex through DNA triplex formation (Gowers and Fox, 1998, Gowers and Fox, 1999, Gowers and Fox, 1997). Not only those quantitative footprinting with this enzyme obtained both association and dissociation constants of TFOs which are an estimate of the TFO binding strength (Hampshire *et al.*, 2007).

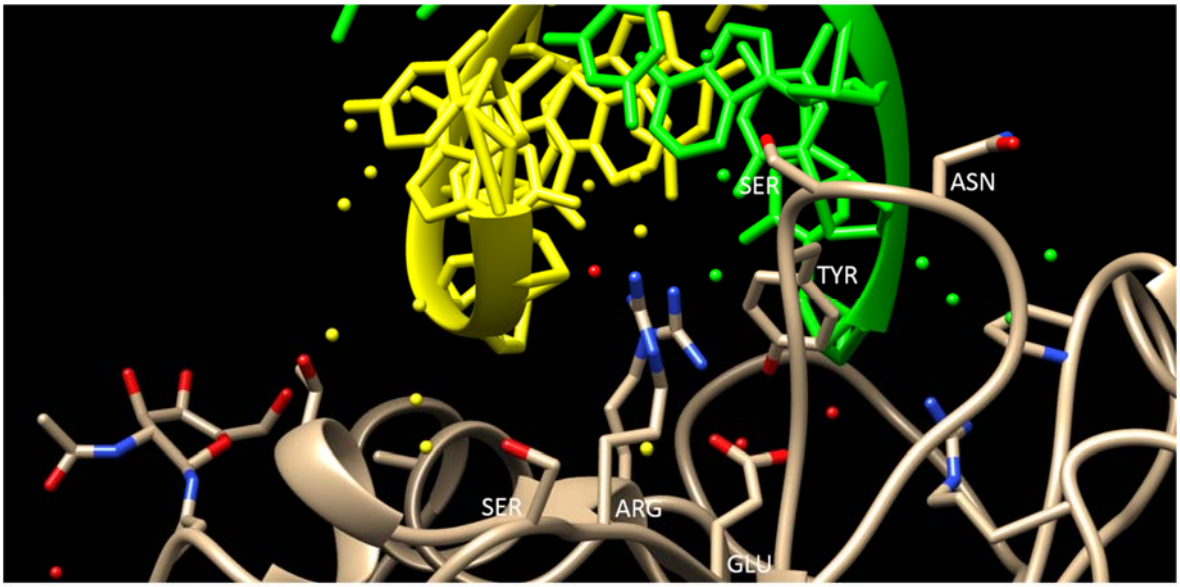

Figure 1.11. Structure of DNase I-DNA complex at 2 Å resolution. Amino acid residues (*i.e.* arginine, asparagine, serine, tyrosine and lysine) that interact directly with DNA molecule are labelled (adapted from Suck and Oefner, 1986 and Lahm and Suck, 1991, PDB number = 2DNJ).

1.5.1.2. Micrococcal nuclease

Micrococcal nuclease is an enzyme with a molecular weight of 16,800 Da. It requires Ca^{2+} ions as a cofactor for its catalytic activity and it cleaves DNA at the O-5'-P bond. Its long and narrow binding pocket preferentially interacts with single stranded rather than double stranded DNA, and it therefore cuts a loop or hairpin structure much more efficient than a duplex. It cleaves duplex DNA only in some circumstances such as strands breathing. The polarity and hydrophobicity of its side chains can make contact with DNA phosphates and act as thymine base binding site respectively. This explains sequence selectivity of the enzyme, which cleaves exclusively at pT and pA (Drew, 1984). Micrococcal nuclease has been reported to use for the determination of the binding sites of DNA-binding drugs especially those containing AT-rich sequences (Fox and Waring, 1987). It was also used to study the differences of chromatin structure during active and inactive X chromosome (Pfeifer and Riggs, 1991).

1.5.1.3. DNase II endonuclease

DNase II has a molecular weight of 40,000 and requires no metal ion cofactor for its catalytic function. It cleaves DNA at O-5'-P bond at a low pH, which is required nucleophilic attack by the active site histidine residue (Drew, 1984). The preferentially cleaves purine-rich (or pyrimidine-rich) regions of duplex DNA, though its precise binding requirement are not known. It is also reported to cleave purine-rich sequences with lower efficiency than corresponding pyrimidine-rich region, which may be explained as the purine-rich loop remains stacked but the pyrimidine one is not (Drew, 1984). Cons and Fox (1990) reported to use this cleavage agent for the detection of the conformational changes of the $(AT)_n$ sequence that flanks the binding site of GC-selective ligand mithramycin. Other researchers had used this enzyme to identify the sequence selectivity and the structural relationship of *Xenopus* transcription factor IIIA (TFIIIA), the histone octamer and Xenopus somatic gene for 5S RNA though the data from DNase II footprinting are not as informative as that with DNase I (Rhodes, 1985).

1.5.1.4. S_1 nuclease

S_1 nuclease is an enzyme with a molecular weight of 32,000. It cleaves DNA at the O-3'-P bond at low pHs and requires Zn^{2+} as cofactor. This enzyme is not sequence specific but exclusively cuts single stranded DNA substrates. These can include the nucleotides at the tips of cruciforms and right-left junctions in supercoiled plasmids (Drew, 1984). The enzyme cleaves a 5'-end phosphate better than 5'-OH. This can be explained as S_1 nuclease requires several phosphates in succession to perform its nucleophilic attack. In duplex DNA,

the two sugar-phosphate strands are in close proximity therefore they are protected from S1 nuclease attack. On the other hand, a loop region and a helix terminus become more susceptible to this enzyme (Drew, 1984). S_1 nuclease has been reported for the detection of unpaired bases at the loop region of cruciform DNA (Lilley, 1983) and at the region adjacent to the left and right junctions in supercoiled plasmid DNAs (Singleton *et al.*, 1983).

1.5.2. Chemical footprinting probes

1.5.2.1. Diethyl pyrocarbonate (DEPC)

DEPC reacts most exclusively with adenine and to some extent with guanine residues by modifying their N7 atom. It is less reactive with double-stranded B-DNA due to close stacking of the neighbouring bases. However, it shows high reactivity to the N7 of exposed purines within single stranded DNA and unusual DNA structures *e.g*. Z-DNA and cruciform loops. Since it only modifies the bases, treatment with alkali (*e.g* hot piperidine) is necessary to obtain ring opening of modified N7 and cleavage of phosphodiester backbone at the modified bases (Jeppesen and Nielsen, 1988, Kahl and Paule, 2009). DEPC has been reported for the detection of DNA structural changes induced by the interaction with intercalator (Jeppesen and Nielsen, 1988) and those with anti-tumour antibiotics bleomycin and phleomycin (Fox and Grigg, 1988). This also used to probe secondary DNA structures formed as a result of DNA negative supercoiling (Herr, 1985) and loops structure of cruciform DNA (Furlong and Lilley, 1986).

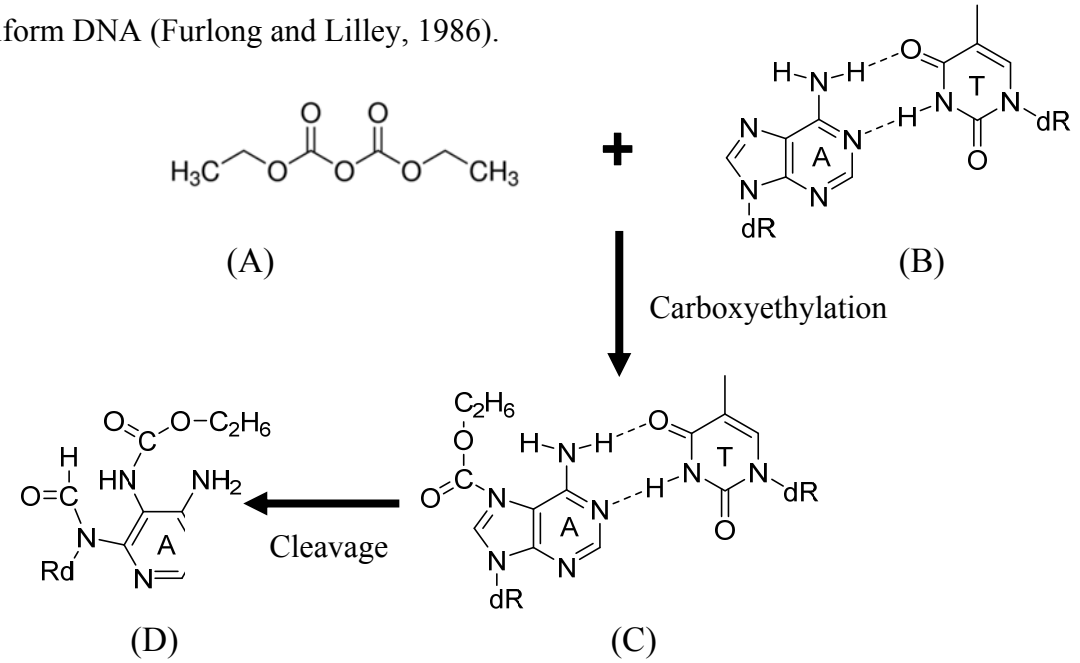

Figure 1.12. Chemical reaction between DEPC and adenine. DEPC (A) reacts with N7 atom of adenine (B) and gives rise to N7 carboxyethyl adenosine (C). The ring of N7 carboxyethyl adenosine then cut open (D) by hot peperidine (adapted from Sinden, 1994).

1.5.2.2. Potassium permanganate ($KMnO_4$)

$KMnO_4$ reacts with double bonds of pyrimidine residues in single stranded DNA and preferentially oxidize thymine residues over cytosines. This is due to the out-of-plane attack on the 5, 6-double bond of the pyrimidine . This oxidation transforms double bonds to vicinal diols which leads to the loss of aromaticity. Since it only modifies the bases, treatment with alkali (*e.g.* hot piperidine) is necessary to obtain ring opening of vicinal diols and cleavage of phosphodiester backbone at the the modified bases (Kahl and Paule, 2009). This reagent has been reported to use for the detection of DNA distortion and mechanisms in lac promoter sequence during transcription (Sasse-Dwight and Gralla, 1989). It has also been used to probe the structural changes to DNA around elongation complexes during DNA transcription (Kainz and Roberts, 1992). Fox and Grigg (1988) have used this reagent to study DNA structural deformation induced by anti-tumour antibiotics; bleomycin and phleomycin. In addition $KMnO_4$ has also been used to detect structural variations within DNA molecule such as B-Z transition and Z-Z junction (Jiang *et al.*, 1991). Interestingly this can be used both in *in vivo* and *in vitro* experiments (Ohlsen and Gralla, 1992).

1.5.2.3. Hydroxyl radicals

Hydroxyl radicals are small (approximately the size of a water molecule) highly reactive and non-sequence specific footprinting reagents. They are generated in the Fenton reaction between Fe(II)-EDTA and hydrogen peroxide.

$$[Fe(II)EDTA]^{2-} + H_2O_2 \longrightarrow \text{-}OH + OH^- + [Fe(III)EDTA]^{1-}$$

A reducing agent, such as sodium ascorbate, is needed to reverse the Fe(III) product of this reaction back to Fe(II) which can be reused as a substrate until the hydrogen peroxide is depleted. This radical attacks DNA on the deoxyribose moiety in the minor groove and displaces 3'-phosphoryl leading to strand break (Tullius and Dombroski, 1986, Prigodich and Martin, 1990, Hampshire *et al.*, 2007). Hydroxyl radicals have been reported for the detection of sequence selectivity of DNA gyrase and the conformational changes of DNA in DNA gyrase-DNA complex (Orphanides and Maxwell, 1994). This has also been used to locate the binding site of ribosomal protein on a 16S rRNA and the helical features of this RNA on the binding mechanisms (Powers and Noller, 1995).

1.5.2.4. Dimethyl sulfate (DMS)

DMS is a highly reactive and widely used chemical for determining sequence selectivity of DNA binding molecules. It can be employed both *in vitro* and *in vivo* experiments as it reacts quickly with DNA and can effectively penetrate intact cells. DMS

chemically modifies DNA by methylating the N7 atom of guanine and N3 of cytosine. As this only modifies the bases, a piperidine treatment is needed to produce strand breaks at the methylated bases. Since guanine N7 is located in the DNA major groove it is useful for examining the interaction with major groove binding ligands, such as triplex forming oligonucleotides. It can also be used to detect local DNA conformational changes such as unwinding, in which the DNA may become reactive to DMS (Shaw and Stewart, 2001, Tijerina *et al.*, 2007). More recently, DMS has also been employed to identify *in vivo* RNA structure profiling (Ding *et al*., 2015).

1.6. Melting studies for determining the stability of triplexes

1.6.1. UV thermal melting study

UV melting is a simple method for determining the stability of nucleic acids. It is based on the measurement of changes in absorbance that arise from changes in nucleic acid structures. The nucleobases become unstacked and more exposed to solvent as the structures dissociate. This results in a temperature-dependence increase in absorbance, which is usually measured at 260 nm. The results acquired from this technique are easy to interpret and lead to ligand-induced increases in the melting temperature. However they are usually only low throughput (most spectrophotometers can only measure a maximum four samples at a time while fluorescence melting study can run thirty-two samples) and require relatively large sample volumes (1-3 ml) with an OD_{260} of at least 0.2. The changes in absorbance measured by this technique are usually small (typically about 25%) therefore it may not be suitable for examining the secondary structures of nucleic acids such as triplexes and quadruplexes as these contain multiple, overlapping melting transitions (Darby *et al.*, 2002). Figure 1.13 shows UV absorbance at 260 nm of DNA triple helices as it dissociates to the underlying duplex following gradual temperature increase. The curve represents two melting transitions; the first transition derives from the dissociation of the third strand from the duplex whereas the second one derives from the denaturation of the two duplex complimentary strands. The temperature at the mid-point of the transitions, at which half of the molecules melt is the melting temperature (T_m). Therefore T_m1 is triplex melting temperature and T_m2 belongs to duplex. The T_m of duplex is typically higher than that of the triplex as it is a much more stable complex by nature.

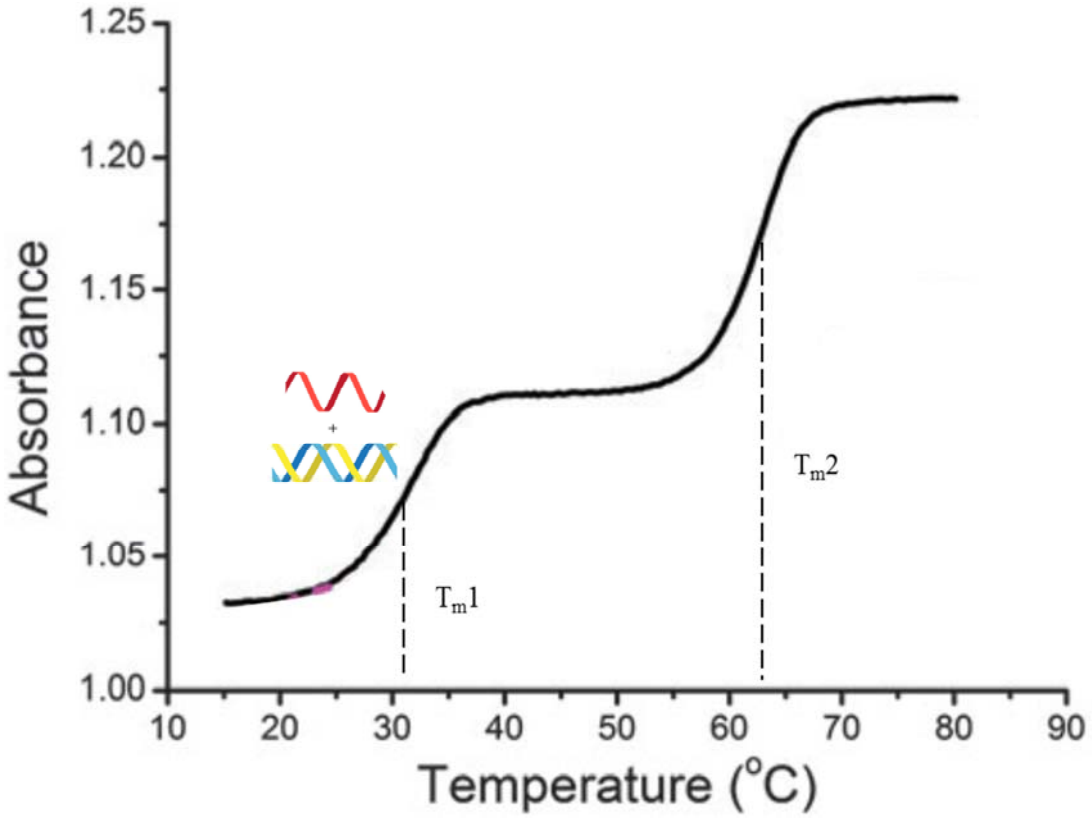

Figure 1.13. UV absorbance of DNA triple helices at 260 nm (arbitrary unit) as a function of temperature (˚C). The curve represents two melting transitions from the two complexes; triplex melting (T_m1) and duplex melting (T_m2) (adapted from Brown *et al.*, 2014).

1.6.2. Fluorescence melting study

Fluorescence melting is a variation of the UV melting method, which has been used to measure the stability of nucleic acids, their interaction with ligands and the formation of secondary structures. These include hairpin, triplexes, G-quadruplexes and their binding ligands (Ellouze *et al.*, 1997, Antony *et al.*, 2001, Darby *et al.*, 2002). The technique uses oligonucleotides containing appropriately attached fluorophores, such that the fluorescence is quenched when the structure is folded, but shows a large increase in fluorescence when the DNA is denatured and the fluorescent groups are separated. For the measurement of intermolecular triplex stability, the fluorophore and quencher are placed on the purine strand of the duplex and the third strand respectively. This therefore enable the measurement of the third strand dissociation rather than the duplex. The third strand can be added in excess to the reaction mixture without hampering the melting results. Upon the formation of triplex, the fluorophore is in close proximity to the quencher resulting in quenching of the fluorescence signal. When the third strand dissociates from the duplex the fluorophore and quencher are separated, leading to a marked increase of fluorescence. The T_m corresponds to the mid-point of the transition, at which half of the molecules will have melted is the

melting temperature (T_m) (Figure 1.14) which is usually assessed by determining the maximum of the first derivative (Figure 1.15). This determines the stability of triplexes and a high T_m value represents a high triplex stability. Fluorescence melting is a high throughput technique which in the work described in this thesis used a Roche Light-Cycler. It only requires a small amount of sample (20 µl) and is able to measure 32 melting profiles in parallel (Darby *et al*., 2002).

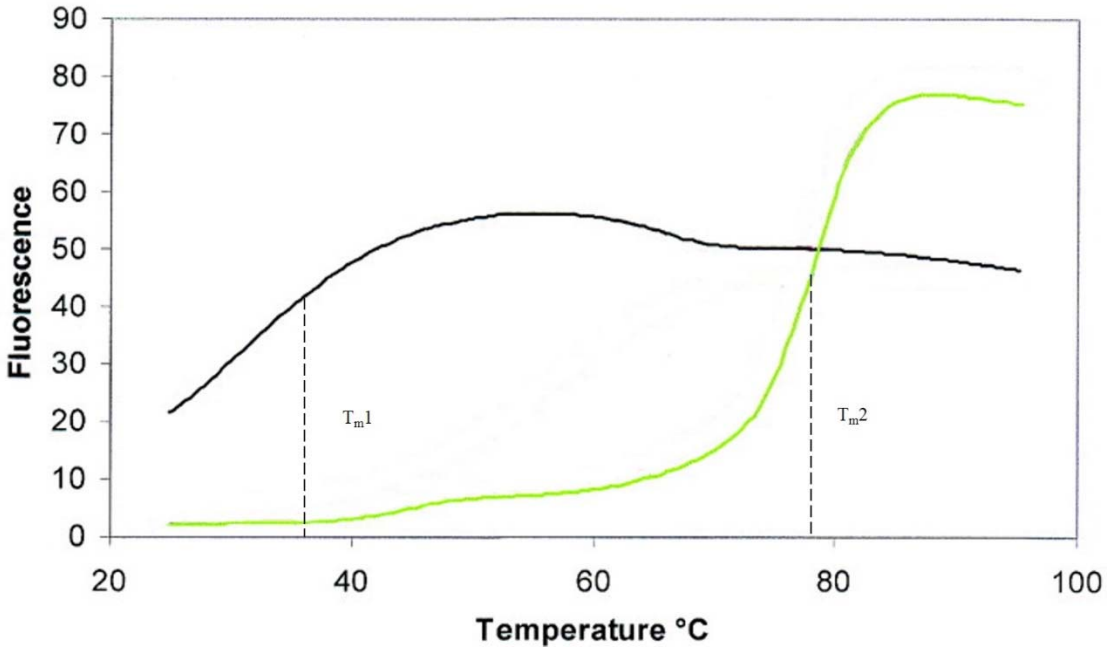

Figure 1.14. Fluorescence melting profiles for triplex (black) and duplex (green) DNA. Melting temperatures of triplex (T_m1) and duplex (T_m2) correspond to the temperatures at which half of the molecules that have melted (adapted from Darby *et al*., 2002).

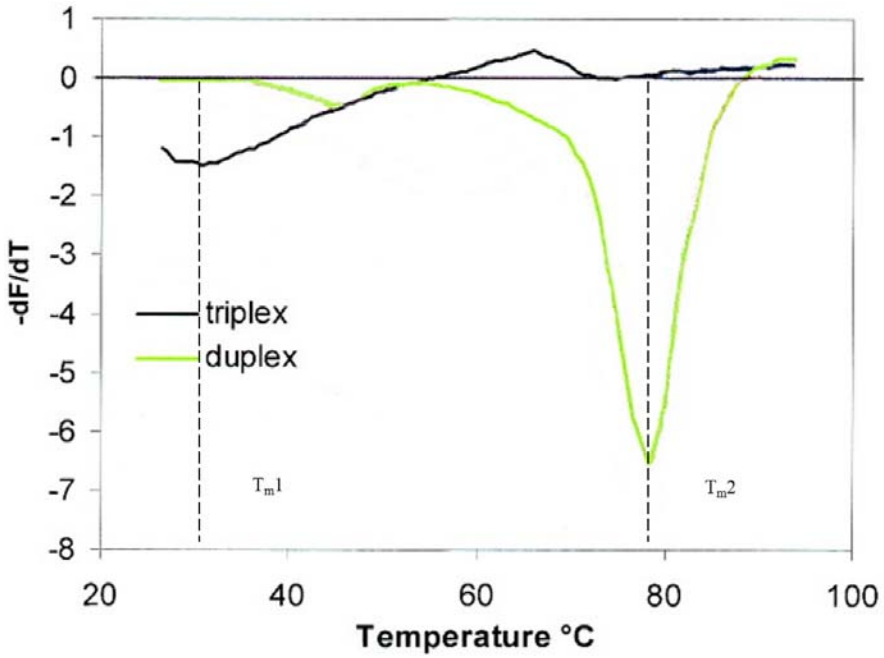

Figure 1.15. The first derivatives of the melting profiles of triplex (black) and duplex (green) DNA. The maxima of this derivatives is usually determined as accurate T_ms (adapted from Darby *et al.*, 2002).

1.7. Purpose of this study

As described above, DNase I enhancements are frequently observed at the triplex-duplex junction. Although the reason for this enhancement is not clear, it is thought to be due to a local change in DNA structure. This effect has only been observed at the 3'-end of the target purine strand. The aim of this study is to examine how the flanking base pairs in the *tyr*T(43-59) fragment affect this enhanced cleavage. The triplex affinity at these sites was assessed by quantitative DNase footprinting and fluorescence melting studies. The effect of these base pair changes is also examined with a range of other enzymic and chemical footprinting agents.

CHAPTER 2 MATERIALS AND METHODS

2.1. Triplex-forming oligonucleotides (TFOs)

The following triplex-forming oligonucleotides (TFOs) were provided by ATDBio and were synthesized using an Applied Biosystems ABI 394 automated DNA/RNA synthesizer using a solid phase DNA phosphoramidite synthesis cycles. The oligonucleotides were then purified by gel filtration, dissolved in water and kept at -20 °C until required.

pyrimidine TFOs	purine TFOs
5'-CTCTTTTTTCTT (12-mer-T)	5'-AAGAAAAAAGAGAAGGA (17-mer-A)
5'-CTCTTTTTTCTC(12-mer-C)	5'-GAGAAAAAAGAGAAGGA (17-mer-G)
5'-CTCTTTTTTCT (11-mer)	5'-AAGAAAAAAGAG (12-mer-A)
	5'-GAGAAAAAAGAG (12-mer-G)

Table 2.1 Oligonucleotide sequences used in parallel (left) and antiparallel (right) triplex formation. The pyrimidine TFOs shown in left column are different in length and base compositions; the 12-mer-C has a 3'-cytosine as the last base instead of thymine in the 12-mer-T whereas an 11-mer has one base shorter. The 17-mer-A purine TFO has a 5'-adenine as the last base instead of guanine in the 17-mer-G; these have five bases at the 3'-end longer than the 12-mers otherwise contain identical sequences (i.e 17-mer-A is identical to 12-mer-A and 17-mer-G is identical to 12-mer-G).

2.2. DNA fragments

The 160-base-pair promoter sequence of the *E. coli* tyrosine tRNA gene (*tyr*T) (Appendix 1) has been used to study the functionality of the promoter (Drew and Travers, 1984) as a model for examining the structure of DNA (Travers *et al*., 1983), and as a fragment for footprinting experiments (Fox and Waring, 1984). This has been modified so as to produce a fragment containing a 17-mer homopurine stretch (5'-AGGAAGAGAAAAAAGAA-3') between positions 43 to 59 (Fox *et al.*, 2001) that has been widely used in triplex footprinting experiments (Cardew and Fox, 2010). It represents an ideal template for examining TFO-induced footprints. The *tyr*T sequence was cloned into the pUC18 plasmid between the EcoRI and AvaI sites (Brown and Fox, 1999). This was transformed into competent *E. coli* TG2 cells and the plasmid was purified using Qiagen miniprep kit before isolating the fragment and radiolabelling at the 3'-end with α-^{32}P[dATP]. Several variants of this sequence (Appendix 2-9) have been prepared in this work to study the effects of flanking sequence on triplex formation.

2.3. Competent TG2 cells and transformation

2.3.1. Preparation of competent TG2 cells

Competent E.coli TG2 cells were prepared by plating out stocks of the cells onto 2YT agar medium (16 g tryptone, 10 g yeast extract, 5 g NaCl/L) and incubating overnight at 37 °C. A single colony was then picked and inoculated into 5 ml of 2YT broth medium and incubated overnight at 37 °C in a shaking incubator. 1 ml of the overnight culture was transferred into 100 ml of 2YT broth medium and grown at 37 °C until the OD_{600} value was between 0.5-0.8 (typically 2 hours). 20 ml of this culture was transferred to a Sterilin tube and centrifuged at 3,000 rpm for 10 minutes before removing the supernatant. The pellet was then resuspended in 20 ml of cold transformation buffer containing 50 mM $CaCl_2$ and 10 mM Tris-HCl pH 7.4 and centrifuged again at 3,000 rpm for 10 minutes. After removing the supernatant, the pellet was resuspended in 5 ml of transformation buffer and kept in the fridge at 4 °C for up to 2 weeks.

2.3.2. Transformation into competent TG2 cells

One µl of the plasmid (approximately 0.4 µg) was added into 200 µl of competent TG2 cells and the mixture was immediately placed on ice for 30 minutes. It was then heat shocked at 42 °C for 1 minute before placing on ice again for another 2 minutes. The transformed cells were then plated out onto 2YT agar media containing 100 µg/ml carbenicillin and grown overnight at 37 °C. The plates were stored in the fridge at 4 °C for further use.

2.4. Plasmid DNA purification by Qiagen miniprep kit

A single TG2 colony was picked and inoculated into 5 ml of 2YT broth medium containing 100 µg/ml carbenicillin and incubated overnight at 37 °C in a shaking incubator. It was then divided into Eppendorf tubes and centrifuged at 3000 rpm for 3 minutes to pellet the cells; the medium was discarded. Plasmid DNA was then extracted using as Qiagen miniprep kit according to the manufacturer's instructions. The pellet was resuspended in 250 µl of resuspension buffer containing RNase to degrade the existing RNAs. The cells were then lysed using 250 µl of lysis buffer (containing 1% SDS and 200 mM sodium hydroxide) and the cellular contents were precipitated by adding 350 µl of N3 buffer pH 4.8 (containing 4.2 M guanidine hydrochloride and 0.9 M potassium acetate) and mixed until a clear solution was obtained. This was centrifuged at 13,000 rpm for 10 minutes and the supernatant was transferred to a Qiagen miniprep column. The supernatant was spun through the column at 13,000 rpm for 1 minute and the flow-through was discarded. The column, containing bound

plasmid, was then washed with 500 µl of PB buffer (containing 5 M guanidine hydrochloride and 30% isopropanol) and spun at 13,000 rpm for 1 minute and the flow-through was discarded. It then was washed by adding 750 µl of PE buffer and spun again to remove flow-through. The plasmid was eluted from the column by adding 50 µl of elution buffer EB (or water) and left at room temperature for 5 minutes before eluting the DNA by centrifuging at 13,000 rpm for 1 minute. The concentration of plasmid was measured at 260 nm using a nanodrop spectrophotometer and the fresh plasmid was used for 3'-end α-^{32}P radioactive labelling of the required DNA fragment. The typical concentration was 300 ng/µl.

2.5. 3'-end labelling

Forty µl of plasmid DNA (approximately 16 µg) was digested with EcoRI (12 units) and AvaI (10 units) with 4 µl of 10x NEB Multicore® buffer. This reaction was performed at 37 °C for 2 hours. The digested products were then labelled at the 3'-end of the EcoRI site in a reaction containing 1 µl of α-^{32}P dATP (10µCi), 0.5 µl (20 units/µl) of enhanced-AMV Reverse Transcriptase and 4 µl of 10x buffer for enhanced-AMV Reverse Transcriptase. This mixture was incubated at 37 °C for 1 hour before adding 20 µL of loading dye (20% ficoll containing 10 mM EDTA and 0.01% bromophenol blue) and the fragments were separated by electrophoresis on a 6% nondenaturing polyacrylamide gel (20 cm long) at 400 Volts and 20 Watts, until the bromophenol blue approached the bottom of the plate (typically about 50 minutes). The plates were separated and the gel was exposed to X-ray film for about 5 minutes to identify the position of the radioactive bands. The band corresponding to the 110-base-pair DNA *tyr*T fragment was excised and transferred to a sealed P1000 tip containing a glass wool plug and covered with 400 µL of 10mM Tris-HCl pH 7.5 containing 1mM EDTA. This was gently shaken overnight at room temperature to elute the DNA from the gel. The pipette tip was inserted into a pipette the DNA was eluted, leaving the gel slice, which was trapped above the glass wool. The DNA solution was precipitated by adding 1000 µl of absolute ethanol and placed on dry ice for 10 minutes. It was then centrifuged at 13,000 rpm for 10 minutes and the supernatant was removed, checking that the radioactivity remained in the pellet. The pellet was then washed with 200 µl of 70% ethanol and spun at 13,000 rpm for another 2 minutes. The supernatant was discarded and the pellet was dried in a vacuum centrifuge to remove the remaining alcohol. The pellet was resuspended in 10mM Tris-HCl pH 7.5 containing 0.1mM EDTA to obtain a concentration of about 10 c.p.s/µl as determined on a hand held Geiger counter. This was stored at -20 °C for footprinting experiments.

2.6. DNaseI footprinting

The pyrimidine-containing TFOs for parallel triplex formation were serially diluted in 50 mM sodium acetate (NaOAc) pH 5.0 in the presence of 1 mM $MgCl_2$ to make the desired initial concentrations. Three µl of each TFOs dilutions was then mixed with 1.5 µl of radioactively-labelled DNA making final TFO concentrations of 3.0, 1, 0.6, 0.3, 0.1, 0.03, 0.01 µM and these were incubated at room temperature for 2 hours. DNase I cleavage was performed by adding 2 µl of 0.14 units/ml of DNaseI (diluted in 20 mM NaCl, 2 mM $MgCl_2$ and 2 mM $MnCl_2$) and digested for 2 minutes. The cleavage reactions were then stopped by adding 5 µl of DNaseI stop solution containing 80% formamide, 10 mM EDTA and 0.1% bromophenol blue. The cleavage products were heated at 100 °C for 3 minutes and then crash cooled on ice before subjecting to polyacrylamide gel electrophoresis. A control experiment without adding TFO was performed simultaneously. A GA sequencing marker was prepared by adding 1.5 µl of radioactively-labelled DNA into 20 µl of water and 5 µl of DNaseI stop solution, heated at 100 °C for 30 minutes (with the cap open) and loaded onto the gel alongside the cleavage products as a GA marker lane. The similar procedures as above were also performed with purine-containing TFOs (for antiparallel triplex formation) though these were diluted in 10 mM Tris-HCl pH 7.0 in the presence of 50 mM NaCl and 10 mM $MnCl_2$.

2.7. Micrococcal nuclease footprinting

The pyrimidine and purine TFOs were diluted as described in the procedures for DNase I footprinting. Three µl of each concentration of the TFOs was mixed with 1.5 µl of radioactively-labelled DNA making final concentrations of 20, 10, 5 and 1 µM, and incubated at room temperature for 2 hours. The mixtures were cleaved by adding 2 µl of 5 units/ml of Micrococcal nuclease (diluted in 50 mM Tris-HCl pH 7.6 containing 2 mM $CaCl_2$) and digested for 2 minutes. The cleavage reactions were then stopped by adding 5 µl of DNaseI stop solution. The cleavage products were heated at 100 °C for 3 minutes and then crash cooled on ice before subjecting to polyacrylamide gel electrophoresis. A control experiments and GA sequencing marker were prepared as mention above and loaded onto the gel alongside the cleavage products.

2.8. Hydroxyl radical footprinting

The pyrimidine and purine TFOs were diluted as described above for DNase I footprinting. 6 µl of each concentration of the TFOs was mixed with 3 µl of radioactively-labelled DNA making final concentrations of 20, 10, 5, and 1 µM, and incubated at room temperature for 2 hours. The mixtures were cleaved by adding 10 µl of hydroxyl radical mix

containing 1:1:2:2 ratio of 0.4 mM $(NH_4)_2Fe(SO_4)_2.6H_2O$, 2.5 mM EDTA, 10 mM Ascorbic acid and 0.3% H_2O_2 respectively. These were digested for 30 minutes and stopped by adding 2 µl of 3M NaOAc pH 5.0. The cleavage products were precipitated by adding 100 µl of absolute ethanol and left on dry ice for 10 minutes. They were then spun at 13,000 rpm (17,922xg) in an Eppendorf centrifuge for 10 minutes using table top centrifuge and the supernatant was discarded. The pellet was washed with 100 µl of 70% ethanol, spun at 13,000 rpm for 30 seconds and the supernatant was removed again. It was then dried in a vacuum centrifuge for 10 minutes and dissolved in 8 µl of DNaseI stop solution. This was then heated at 100 °C for 3 minutes and crashed cooled on ice before subjecting to polyacrylamide gel electrophoresis. A similar procedure without adding TFOs was also performed as a control. The GA sequencing marker was prepared as described above and loaded onto the gel alongside the cleavage products.

2.9. DEPC footprinting

Three µl of absolute DEPC was added to the mixtures and the reaction was left for 30 minutes with occasional mixing. The reaction was stopped by adding 2 µl of 3M NaOAc pH 5.0 and the DEPC-modified products were precipitated, washed and dried as described for the hydroxyl radical footprinting. The modified DNA was then cleaved by adding 50 µl of 10% (v/v) piperidine and heated at 100 °C for 30 minutes and dried in vacuum centrifuge for 10 minutes. The pellets were washed with H_2O and dried again. They were then dissolved in 8 µl of DNaseI stop solution and heated at 100 °C for 3 minutes. The solutions were crash cooled on ice before subjecting to polyacrylamide gel electrophoresis. A similar procedure without adding TFOs was also performed as a control. GA sequencing markers were prepared as described above and loaded onto the gel alongside the cleavage products.

2.10. $KMnO_4$ footprinting

Oligonucleotide-DNA complexes were prepared as described above. Two µl of 50 mM $KMnO_4$ was added to the mixtures. The reaction was stopped after 2 minutes by adding 0.5 µl of mercaptoethanol and the $KMnO_4$-modified products were precipitated, washed and dried as described for hydroxyl radical footprinting. The modified products were cleaved by adding 50 µl of 10% piperidine, heated at 100 ° for 30 minutes and then dried in a vacuum centrifuge for 10 minutes. The pellets were washed with H_2O and dried again. They were then dissolved in 8 µl of DNaseI stop solution and heated at 100 °C for 3 minutes. These were crashed cooled on ice before subjecting to polyacrylamide gel electrophoresis. A similar procedure without adding TFOs was also performed as a control. GA sequencing

markers were prepared as described above and loaded onto the gel alongside the cleavage products.

2.11. Polyacrylamide gel electrophoresis (PAGE)

The 8.5% denaturing polyacrylamide gels were prepared with 17 ml of 19:1 of Acrylamide: Bis-acrylamide (UreaGel), 5 ml of 10 x TBE buffer containing 8M urea, and 28 ml of diluent (50% (w/v) urea). 200 µl of 20% (w/v) of ammonium persulphate and 40 µl of TEMED were then added to initiate polymerization. A metal plate was clamped to the gels to ensure even temperature distribution. Gels were run at 1,500 Volts and 44 Watts, and were pre-heated for 30 minutes before loading the samples. The samples were subjected to electrophoresis for about 1 hour and 30 minutes (until the blue dye reached the bottom of the plates). The plates were separated and the gels were soaked in 10% (v/v) acetic acid for 10 minutes. They were then transferred onto 3MM paper, covered with Saran wrap and dried under vacuum at 80 °C for 1 hour and 30 minutes. The dried gels were exposed to a phosphorimage screen overnight and recorded using a Typhoon Phosphorimager.

2.12. Footprint analysis

The footprinting gels were examined to identify the area where the DNA was protected from DNase I cleavage. The sequence of the protected region was identified by comparing with the GA marker lane. Bands with enhanced cleavage and in the footprints were identified and then quantified by measuring the intensities for each gel lanes (i.e. for the highest TFO concentration down to control) using ImageQuant TL software. These were then divided by the intensities of bands outside the footprints within the same lane which were not affected by the TFOs. The data (arbitrary units) were used to generate footprinting plots of TFO concentrations (µM) against relative intensity using the following binding equations; the first equation is used for enhanced bands and the second one is for footprints:

$$B/B_{max} = [TFO]/([TFO] + C_{50})$$

$$B/B_{max} = C_{50}/(C_{50}+[TFO])$$

Where B is band intensity, B_{max} is maximum band intensity, [TFO] is TFO concentration and C_{50} is the TFO concentration which reduces the band intensity by 50%. From these plots, the C_{50} values were obtained; these are used to estimate the affinity of the target-TFOs binding in a condition where the target DNA is much lower than the dissociation constant. Similar analyses were performed with the other cleavage agents (i.e. micrococcal nuclease, DEPC and $KMnO_4$).

For hydroxyl radical footprinting gels, the bands within and around the TFO binding site (i.e. 5'-AAAGTGTTAGGAAGAGAAAAAAGAXXTG-3') at 10 μM TFO concentration were quantified using ImageQuant TL software. The intensity of each bands was normalised by subtracting the value with the lowest intensity and later divided with the substraction value between the highest and the lowest intensities. These normalised values were then plotted against the above sequence generating densitometer plot. An identical analysis was also performed with the bands in the absence of the TFO as a control experiment.

2.13. Site-directed mutagenesis (SDM)

In order to study the effects of flanking bases on TFO binding affinity the base at position 42, flanking the 3'-end of polypurine tract, was mutated from wild-type cytosine to each base in turn by site-directed mutagenesis. This was achieved by QuickChange PCR using the following three pairs of forward and reverse primers:

5'GAAGAGAAAAAAGAAGTGGTTGCGTAATTTTC-3' and
5'GAAAATTACGCAACCACTTCTTTTTTCTCTTC-3' to introduce guanine,

5'GAAGAGAAAAAAGAAATGGTTGCGTAATTTTC-3' and
5'GAAAATTACGCAACCATTTCTTTTTTCTCTTC-3' to introduce adenine and

5'GAAGAGAAAAAAGAATTGGTTGCGTAATTTTC-3' and
5'GAAAATTACGCAACCAATTCTTTTTTCTCTTC-3' to introduce thymine.

A 0.5 μl of each pair of primers (150 ng/μl) was added to a reaction mixture containing 0.1 μl of wild-type *tyr*T (159 ng/μl) as a DNA template, 1 μl of 10 mM dNTPs as a source of nucleotide triphosphates, 1.5 μl of DMSO, 5 μl of 10 x reaction buffer, 1 μl of *Pfu* DNA polymerase (2-3 units/μl) and water to make up the 50 μl reaction volume. The mixture was then subjected to PCR with the following temperature cycles; template denaturing at 95 °C for 30 seconds, primer annealing at 50 °C for 1 minute, and primer extension at 68 °C for 4 minutes and 30 seconds. This was repeated for 18 cycles and the PCR products were then digested by adding 0.5 μl of DpnI endonuclease and incubated at 37 °C for 5 hours in order to degrade the original methylated DNA templates. The digested products were transformed into TG2 cells as described above.

Identical experiments were also carried out to mutate the base at position 43 within the polypurine stretch of wild-type *tyr*T from adenine to guanine and the base at position 42 flanking the 3'-end of polypurine stretch was mutated from wild-type cytosine to either

guanine, adenine or thymine. Using the following four pairs of primers produced the GC-mutant, GG-mutant, GA-mutant and GT-mutant respectively.

5’-GAAGAGAAAAAAGAGCTGGTTGCGTAATTTTC-3’

5’GAAAATTACGCAACCAGCTCTTTTTTCTCTTC-3’

5’-GAAGAGAAAAAAGAGGTGGTTGCGTAATTTTC-3’

5’GAAAATTACGCAACCACCTCTTTTTTCTCTTC-3’

5’-GAAGAGAAAAAAGAGATGGTTGCGTAATTTTC-

3’5’GAAAATTACGCAACCATCTCTTTTTTCTCTTC-3’

5’-GAAGAGAAAAAAGAGTTGGTTGCGTAATTTTC-3’

5’GAAAATTACGCAACCAACTCTTTTTTCTCTTC-3’

The sequences of polypurine binding site (underlined) and flanking region (highlighted) of the eight mutant fragments obtained from these experiments are presented in the following table.

Fragments	Sequences
AC	5′-ACCA**G**TTCTTTTTTCTCTTCCTAACAC-3′ 3′-TGGT**C**AAGAAAAAAGAGAAGGATTGTG-5′
AG	5′-ACCA**C**TTCTTTTTTCTCTTCCTAACAC-3′ 3′-TGGT**G**AAGAAAAAAGAGAAGGATTGTG-5′
AA	5′-ACCA**T**TTCTTTTTTCTCTTCCTAACAC-3′ 3′-TGGT**A**AAGAAAAAAGAGAAGGATTGTG-5′
AT	5′-ACCA**A**TTCTTTTTTCTCTTCCTAACAC-3′ 3′-TGGT**T**AAGAAAAAAGAGAAGGATTGTG-5′
GC	5′-ACCA**G**CTCTTTTTTCTCTTCCTAACAC-3′ 3′-TGGT**C**GAGAAAAAAGAGAAGGATTGTG-5′
GG	5′-ACCA**C**CTCTTTTTTCTCTTCCTAACAC-3′ 3′-TGGT**G**GAGAAAAAAGAGAAGGATTGTG-5′
GA	5′-ACCA**T**CTCTTTTTTCTCTTCCTAACAC-3′ 3′-TGGT**A**GAGAAAAAAGAGAAGGATTGTG-5′
GT	5′-ACCA**A**CTCTTTTTTCTCTTCCTAACAC-3′ 3′-TGGT**T**GAGAAAAAAGAGAAGGATTGTG-5′

Table 2.2 The sequences of polypurine binding site (underlined) and flanking region (highlighted) used in triplex formation.

2.14. DNA sequencing

The eight plasmids obtained from the previous sections (3.2.1 and 3.2.2) were transformed into *E. coli* TG2 cells for propagation. After growing the cells overnight plasmids were prepared using the QIAGEN plasmid miniprep kit; the DNA concentrations were determined using a Nanodrop. The plasmids were diluted to a concentration of 50 ng/µl and sent for sequencing by MWG Eurofins. The sequencing electropherograms were manually analysed to locate and confirm the inserted polypurine tract.

2.15. Fluorescence melting studies

To examine the thermal stability of triplexes, the following Dabcyl-labelled TFOs and the 5'-end fluorophore-labelled oligonucleotides were synthesized by ATDBio. These were prepared using an Applied Biosystems ABI 394 automated DNA/RNA synthesizer using solid phase DNA phosphoramidite synthesis cycles. The oligonucleotides were then purified either by HPLC or gel filtration, dissolved in water and kept at -20 °C until required.

TFOs used in this study	
Dabcyl-labelled pyrimidine TFOs	Dabcyl-labelled purine TFOs
5′-**Q**-CTCTTTTTTCTT-3′	5′-AAGAAAAAAGAGAAGGA-**Q**-3′
5′-**Q**-CTCTTTTTTCTC-3′	5′-GAGAAAAAAGAGAAGGA-**Q**-3′
5′-**Q**-CTCTTTTTTCT-3′	5′-AAGAAAAAAGAG-**Q**-3′
	5′-GAGAAAAAAGAG-**Q**-3′

A

Target duplex used to form 12-mer and 11-mer triplexes	
Unlabelled pyrimidine-rich strands	5'-fluorophore-labelled purine-rich strands
5′-CAACCAGTTCTTTTTTCTC-3′	5′-**F**-GAGAAAAAAGAA**C**TGGTTG -3′
5′-CAACCACTTCTTTTTTCTC-3′	5′-**F**-GAGAAAAAAGAA**G**TGGTTG -3′
5′-CAACCATTTCTTTTTTCTC-3′	5′-**F**-GAGAAAAAAGAA**A**TGGTTG -3′
5′-CAACCAATTCTTTTTTCTC-3′	5′-**F**-GAGAAAAAAGAA**T**TGGTTG -3′
5′-CAACCAGCTCTTTTTTCTC-3′	5′-**F**-GAGAAAAAAGAG**C**TGGTTG -3′
5′-CAACCACCTCTTTTTTCTC-3′	5′-**F**-GAGAAAAAAGAG**G**TGGTTG -3′
5′-CAACCATCTCTTTTTTCTC-3′	5′-**F**-GAGAAAAAAGAG**A**TGGTTG -3′
5′-CAACCAACTCTTTTTTCTC-3′	5′-**F**-GAGAAAAAAGAG**T**TGGTTG -3′
Target duplex used to form 17-mer antiparallel triplex	
Unlabelled pyrimidine-rich strands	5'-fluorophore-labelled purine-rich strands
5′-CAACCAGTTCTTTTTTCTCTTCCT-3′	5′-**F**-AGGAAGAGAAAAAAGAA**C**TGGTTG-3′

5′-CAACCACTTCTTTTTTCTCTTCCT-3′	5′-**F**-AGGAAGAGAAAAAAGAA**G**TGGTTG-3′
5′-CAACCAGCTCTTTTTTCTCTTCCT-3′	5′-**F**-AGGAAGAGAAAAAAGAG**C**TGGTTG-3′
5′-CAACCACCTCTTTTTTCTCTTCCT-3′	5′-**F**-AGGAAGAGAAAAAAGAG**G**TGGTTG-3′

B

Table 2.3 The sequences of TFOs (A) and polypurine binding site (underlined) and flanking region (highlighted) (B) used in melting studies of parallel and antiparallel triplexes.

To determine the melting profiles of parallel triplexes, the Dabcyl-labelled pyrimidine TFOs were serially diluted in 50 mM sodium acetate (NaOAc) pH 5.0 containing 200 mM NaCl in the absence or presence of $MgCl_2$ to make the desired initial concentrations. Each of the duplex strands, *i.e.* unlabelled pyrimidine-rich strand and 5'-fluorophore-labelled purine-rich strand, was also diluted in the same buffer to make initial concentration of 1 µM. Five µl of each of the three oligonucleotides was mixed in a 20 µl total reaction volume generating final TFO concentrations of 9.0, 5.0, 3.0, 1.0 and 0.25 µM respectively. The final concentration of each of the duplex strands was 0.25 µM for all experiments. The mixtures were then heated and cooled in a Roche LightCycler with the following cycles of melting and annealing.

The temperature cycles were set as the following;

1. Initial Denaturation at 98 ºC for 5 minutes

2. Annealing from 98 ºC to 35 ºC at 0.1 ºC/second rate

3. Temperature remains at 35 ºC for 5 minutes

4. Denaturation from 35 ºC to 98 ºC at 0.1 ºC/second rate

The fluorescence signal was measured and each of the values were normalised by substracting with the value at the lowest temperature and then divided with the substraction value between the fluorescence at the highest and the lowest temperature. The normalised values were then plotted as a function of the temperature and the melting and annealing curves were obtained. Melting temperatures (T_m) were estimated from the maxima in the first derivatives of the melting profile. Similar experiments were performed to assess antiparallel triplex stability, using 50 mM sodium phosphate (NaH_2PO_4) pH 7.0 containing 200 mM NaCl in the presence or absence of $MnCl_2$.

CHAPTER 3 THE EFFECTS OF BASE VARIATIONS AT THE 3'-END OF A PARALLEL DNA TRIPLEX

3.1. Introduction

Intermolecular DNA triplexes can be formed between CT-rich TFOs and purines in the DNA target, resulting in the generation of T.AT and C^+.GC triplets. This requires low pH conditions to promote protonation of N3 of cytosine in the C^+.GC triplet. The TFO is oriented parallel to the polypurine tract of the target sequence (Moser and Dervan, 1987, Gowers and Fox, 1999, Rusling *et al.*, 2005). DNase I cleavage patterns of a parallel triplex formed at the polypurine sequence of *tyr*T (43-59), with the 12-mer (5'-CTCTTTTTTCTT) , revealed that the footprints were always accompanied by the enhanced cleavage at the 3'duplex-end of the TFO's binding site (Brown *et al.*, 1996, Bijapur *et al.*, 1999, Cardew *et al.*, 2012). This was thought to be due to TFO-induced structural changes within the duplex at the triplex-duplex junction, which rendered this position more susceptible to cleavage by the enzyme. Since nucleotide sequence determines the geometry, flexibility and rigidity of duplex DNA (El Hassan and Calladine, 1997, Hunter et al., 2005,Frank-Kamenetskii, 2014), we were interested to discover how this enhancement was affected by the nature of the flanking sequence and to discover whether it was sequence- or structure-specific.

Our rationale was to change the 3'-flanking nucleotide from cytosine to each of the other three bases in turn within the *tyr*T (43-59) fragment to provide information on the enhancement and triplex affinity at single-base resolution. These mutations created AC, AG, AT and AA dinucleotide steps at the triplex-duplex junction, which were firstly examined with the original and 12-mer-C TFO (5'-CTCTTTTTTCTC-3'). The formation of triplex between these variant *tyr*T fragments and a shorter 11-mer TFO (5'-CTCTTTTTTCT-3') can provide additional information on whether DNase I enhancements were only observed at the specific position reported previously, or if they can also be observed at other triplex-duplex junctions. Several other cleavage agents were also used in this work as they have different mechanisms of recognition and cleavage and may detect other aspects of triplex-induced changes in DNA structure. These included Micrococcal nuclease, hydroxyl radicals, DEPC and $KMnO_4$ (Drew, 1984, Jeppesen and Nielsen, 1988, Kahl and Paule, 2009, Hampshire et al., 2007). The combination of cleavage patterns from different cleavage agents was expected to give the details of the duplex structural changes induced by TFOs.

Melting experiments with fluorescently-labelled molecular beacon oligonucleotides and a LightCycler were also used in a high throughput method to measure triplex stability, as described by Darby and colleagues (Darby *et al.*, 2002). These synthetic oligonucleotides

were designed to have fluorophore (fluorescein) attached to the 5'-end of the polypurine strand and with a quencher (dabcyl) attached to the 5'-end of the TFO. The formation of a triplex quenches the fluorescence signal and the dissociation of the TFO on melting is accompanied by a large enhancement in the signal. In addition to the four variants mentioned above, the base at the 3'-end of the polypurine strand was also mutated from adenine to guanine, while retaining the different bases flanking the 3'-end of polypurine tract. This generated triplex target sites containing GC, GG, GT and GA dinucleotide steps at the triplex-duplex junction. The replacement of the 3'-T.AT triplet with C^+.GC in these four variants and 12-mer-C TFO increased the stability of the triplex as C^+.GC is more stable than T.AT. This will therefore provide insights on the effects of increased affinity on cleavage enhancement at the triplex-duplex junction. The effects of the third strand mismatches and the effects with shorter (11-mer) TFOs were also examined with these four variants.

3.2. Experimental design

3.2.1. Mutagenesis of the 3'-end base flanking the TFO binding site

To examine the effects of a single nucleotide changes on triplex formation and its effect on the cleavage enhancement, the base flanking the 3'-end of the TFO binding site was mutated from cytosine to the other three bases (*i.e*. thymine, guanine and adenine). This was carried out by site directed mutagenesis using the primers described in Chapter 2. As a result of these experiments, four variants of the target duplex containing either cytosine, guanine, adenine or thymine as the 3'-end base flanking the TFO binding site were obtained. These were called AC, AG, AA and AT where the first base corresponds to the 3'-end of the target site and the second base to the first base outside.

3.2.2. Mutagenesis of the last base at the 3'-end of the TFO binding site

To examine the effects of changing the 3'-base from adenine to guanine on triplex formation and DNase I enhancements, the base at the 3'-end of the TFO binding site was mutated from adenine to guanine, while the flanking bases at the 3'-end of polypurine strand remain the same as mentioned above. This was carried out by site directed mutagenesis using AC, AG, AA and AT as templates and the corresponding primers described in Chapter 2. As a result four additional variants of the target duplex containing guanine as the last base at the 3'-end of the TFO binding site, flanked by each base in turn were obtained. These were called GC, GG, GA and GT.

3.2.3. Footprinting assays of parallel triplex formation

The radiolabelled fragments AC, AG, AA and AT were incubated with different concentrations of 5'-CTCTTTTTTCTT (12-mer-T), 5'-CTCTTTTTTCT (11-mer) and 5'-CTCTTTTTTCTC (12-mer-C) to form 12-mer, 11-mer and the 12-mer with 3'-end triplet mismatch (i.e. C.AT), parallel triplexes respectively. These binding reactions were performed at pH 5.0 in the absence or presence of $MgCl_2$. The complexes were cleaved by different cleavage agents as described in Chapter 2. The cleavage products were resolved on denaturing polyacrylamide gels and the gels were dried and exposed to the phosphorimager screens. The images were taken and analysed using ImageQuant TL software. Identical experiments were also performed with GC, GG, GA and GT. Again they were targeted with 5'-CTCTTTTTTCTC (12-mer-C), 5'-CTCTTTTTTCT (11-mer) and 5'-CTCTTTTTTCTT (12-mer-T) to form 12-mer, 11-mer and the 12-mer with 3'-end triplet mismatch (T.GC), parallel triplexes respectively.

3.2.4. Fluorescence melting studies with parallel triplexes

For the determination of triplex thermal stability, the following 5'-dabcyl-labelled TFOs and 5'-fluorescein-labelled target duplex strands were designed and synthesized. In a typical reaction, each of the duplex strands (*i.e.* the unlabelled pyrimidine-rich strand and the 5'-fluorophore-labelled purine-rich strand) was mixed to obtain a final duplex concentration of 0.25 µM. The TFO was then added to generate the final concentrations of 9, 5, 3, 1 and 0.25 µM. The mixtures were subjected to melting and annealing cycles and the fluorescence signals were measured. The melting curves were plotted and the T_ms were obtained.

TFOs used in this study
Dabcyl-labelled pyrimidine TFOs
5’-**Q**-CTCTTTTTTCTT-3’ (12-mer-T)
5’-**Q**-CTCTTTTTTCTC-3’ (12-mer-C)
5’-**Q**-CTCTTTTTTCT---3’ (11-mer)

A

Target duplexes used to form 12-mer triplexes with a 3’-T.AT triplet	
Unlabelled pyrimidine-rich strands	**5’-fluorophore-labelled purine-rich strands**
5’-CAACCAGTTCTTTTTTCTC-3’	5’-**F**-GAGAAAAAAGA**AC**TGGTTG-3’
5’-CAACCACTTCTTTTTTCTC-3’	5’-**F**-GAGAAAAAAGA**AG**TGGTTG-3’
5’-CAACCATTTCTTTTTTCTC-3’	5’-**F**-GAGAAAAAAGA**AA**TGGTTG-3’
5’-CAACCAATTCTTTTTTCTC-3’	5’-**F**-GAGAAAAAAGA**AT**TGGTTG-3’

B

Target duplexes used to form 12-mer triplexes with a 3’-C^+.GC triplet	
Unlabelled pyrimidine-rich strands	**5’-fluorophore-labelled purine-rich strands**
5’-CAACCAGCTCTTTTTTCTC-3’	5’-**F**-GAGAAAAAAGA**GC**TGGTTG-3’
5’-CAACCACCTCTTTTTTCTC-3’	5’-**F**-GAGAAAAAAGA**GG**TGGTTG-3’
5’-CAACCATCTCTTTTTTCTC-3’	5’-**F**-GAGAAAAAAGA**GA**TGGTTG-3’
5’-CAACCAACTCTTTTTTCTC-3’	5’-**F**-GAGAAAAAAGA**GT**TGGTTG-3’

C

Table 3.1 Oligonucleotide sequences used in parallel triplex melting studies. The TFOs shown in **(A)** are different in length and base compositions; the 12-mer-C has a 3’-cytosine as the last base instead of thymine in the 12-mer-T whereas an 11-mer has one base shorter. All are labelled with dabcyl at their 5’-end. Sequences shown in **(B)** are used to form target duplexes that end with 3’-AC, AG, AA and AT dinucleotides (underlined). The purine-rich strands with different 3’-end flanking bases (in red) are on the right panel; their unlabelled complementary strands presented on the left. Sequences shown in **(C)** are used to form target duplexes with 3’-end GC, GG, GA and GT dinucleotides (underlined). The purine-rich strands with different 3’-end flanking bases (in red) are on the right panel; their unlabelled complementary strands presented on the left. These purine strands are all labelled with fluorophore at their 5’-end.

3.3. Results

3.3.1. The effects of flanking base changes at the 3'-end of the target site

3.3.1.1. The 12-mer triplex formed with 12-mer-T TFO

The DNase I cleavage patterns of triplexes, formed between the eight variant *tyr*T sequences and the 12-mer-T TFO (5'-CTCTTTTTTCTT-3') in 50 mM sodium acetate pH 5.0 (no $MgCl_2$) are shown in Figure 3.1. Footprints are evident with 10 μM oligonucleotide for all the fragments. However, these are not clear, and some cleavage products can still be seen within them. Faint 3'-end cleavage enhancements are observed with AA, AT and AG, though these are not as strong as those with the original sequences AC. We therefore optimized the binding conditions for triplex formation by including 5 mM or 1 mM of $MgCl_2$ in the reaction buffer (Figure 3.2). Clear footprints and intense enhancements can be seen at TFO concentrations as low as 0.1 μM in the presence of 5 mM $MgCl_2$, whereas these typically require 3 μM TFO in the presence of only 1 mM $MgCl_2$. However, we chose to include 1 mM $MgCl_2$ in the reaction buffer for the rest of our experiments as this provides a measurable graded decrease in intensity of the enhanced bands; inclusion of 5 mM $MgCl_2$ generates triplexes that are too stable to measure accurately.

These graded changes in intensity are very important for constructing footprinting plots to obtain C_{50} values. In contrast the footprints in the absence of $MgCl_2$ (Figure 3.1), require high concentrations of TFO and are not clear enough for further analysis. DNase I footprinting experiments with all four fragments, in the presence of 1 mM $MgCl_2$ are shown in Figure 3.3. All of these show clear footprints, which are accompanied by clear enhancements of the bands at the triplex-duplex junction (indicated on the gels). In each case clear footprints are noticed at 3 μM TFO (3 μM) and gradually disappear at lower concentrations. With fragments AC and AG (Figure 3.3) three bands with decreased intensity are also evident below (3'-) the TFO's binding site; the footprint also extends above (5'-) the TFO binding site. In contrast, the footprints with fragments AA and AT (Figure 3.3) only extend in the upper (5'-) direction. All the fragments show enhanced DNase I cleavage at the 3'-end (below) the TFO's binding site, at the triplex-duplex junction. This is concentration dependent. Visual inspection of these gels suggests that the enhancement is strongest with AC and is weakest with AA. This corresponds with relative intensities of the enhanced bands measured at the highest TFO concentration (Table 3.2). DNase I cleavage of the target duplex in the absence of TFO is typically poor, especially in the region containing consecutive adenines. However there are sufficient clear bands to be able to identify the TFO footprints. Quantitative analysis of the concentration dependence of these

enhancements is presented in Figures 3.4 and the calculated C_{50} values are presented in Table 3.2. These reveal that there is no significant difference in the C_{50} values for each of the target duplexes.

```
5′-…CAACCAXTTCTTTTTTCTCTTCCTAACACTT…-3′
3′-…GTTGGTXAAGAAAAAAGAGAAGGATTGTGAA…-5′
        3′-TTCTTTTTTCTC-5′ (12-mer-T TFO)
```

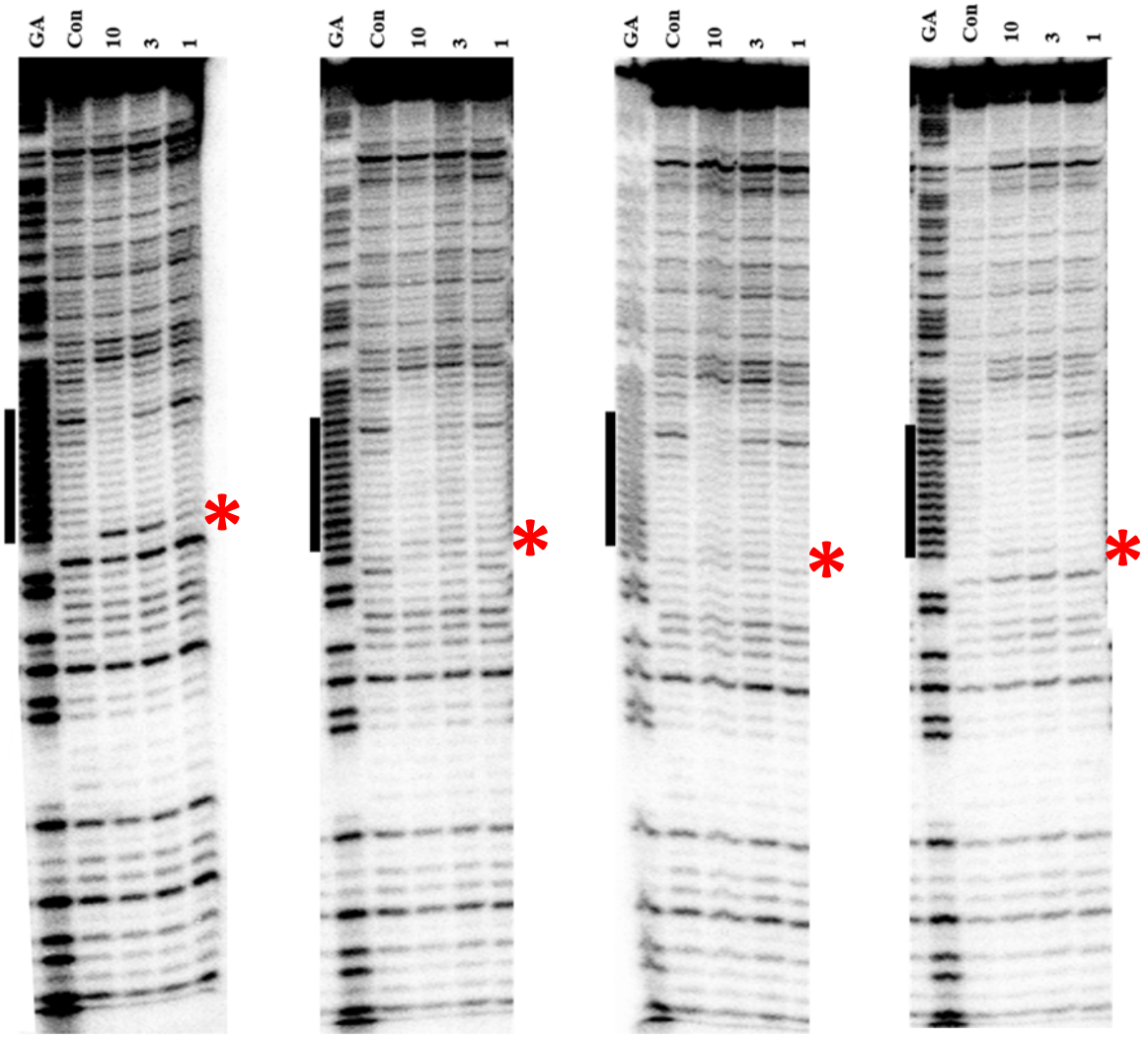

Figure 3.1 DNase I cleavage patterns of the four DNA fragments (AC, AG, AA and AT) containing different bases (X) at the 3'-end of the homopurine stretch (underlined) in the presence of different concentration of the 12-mer-T TFO. These experiments were performed in 50 mM NaOAc at pH 5.0 and were equilibrated for 2 hours at room temperature before digesting with DNase I. TFO concentrations (μM) are shown at the top of each gel lane. The tracks labelled "GA" and "con" are Maxam-Gilbert markers specific for purines and the cleavage pattern in the absence of TFOs respectively. The filled box indicates the location of the triplex target site and the red asterisk shows the position of enhanced DNase I cleavage.

5′-…CAACCAGTTCTTTTTTCTCTTCCTAACACTT…-3′
3′-…GTTGGTCAAGAAAAAAGAGAAGGATTGTGAA…-5′
3′-TTCTTTTTTCTC-5′ (12-mer-T TFO)

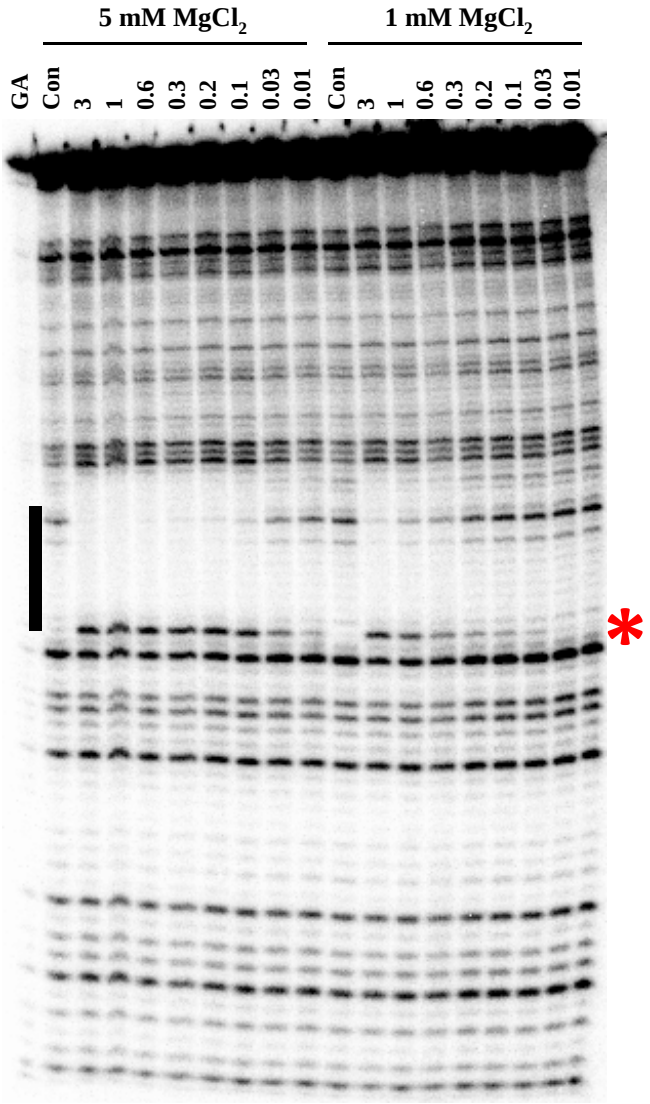

AC

Figure 3.2 DNase I cleavage patterns of *tyr*T (43-59) (sequence AC) in the presence of varying concentrations of the 12-mer-T TFO. These experiments were performed in 50 mM NaOAc at pH 5.0 in the presence of either 5 mM $MgCl_2$ (left) or 1 mM $MgCl_2$ (right) and equilibrated for 2 hours at room temperature before digesting with DNase I. The TFO concentrations (μM) are shown at the top of each gel lane and the tracks labelled "GA" and "con" are Maxam-Gilbert markers specific for purines and the cleavage pattern in the absence of TFOs respectively. The filled box indicates the location of the triplex target site and the red asterisk shows the position of enhanced DNase I cleavage at the triplex-duplex junction.

5′-…CAACCAXTTCTTTTTTCTCTTCCTAACACTT…-3′
3′-…GTTGGTXAAGAAAAAAGAGAAGGATTGTGAA…-5′
3′-TTCTTTTTTCTC-5′ (12-mer-T TFO)

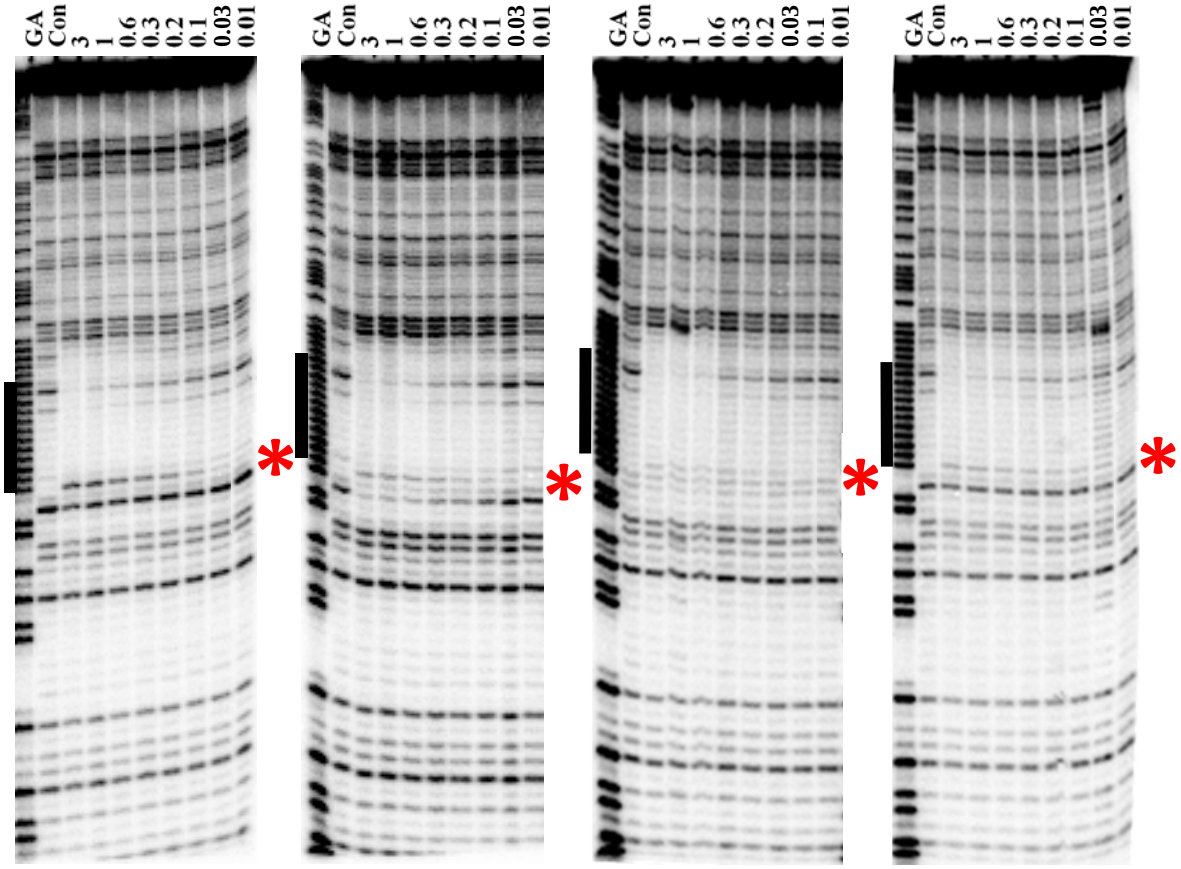

Figure 3.3 DNase I cleavage patterns of the four *tyr*T fragments in the presence of the 12-mer-T TFO. X is C, G, A and T in turn. These experiments were performed in 50 mM NaOAc at pH 5.0 in the presence of 1 mM $MgCl_2$ and equilibrated for 2 hours at room temperature before digesting with DNase I. TFO concentrations (μM) are shown at the top of each gel lane. Tracks labelled "GA" and "con" are Maxam-Gilbert markers specific for purines and the cleavage patterns in the absence of TFO respectively. The filled boxes indicate the location of the triplex target sites and the red asterisks show the position of enhanced DNase I cleavage at the triplex-duplex junction.

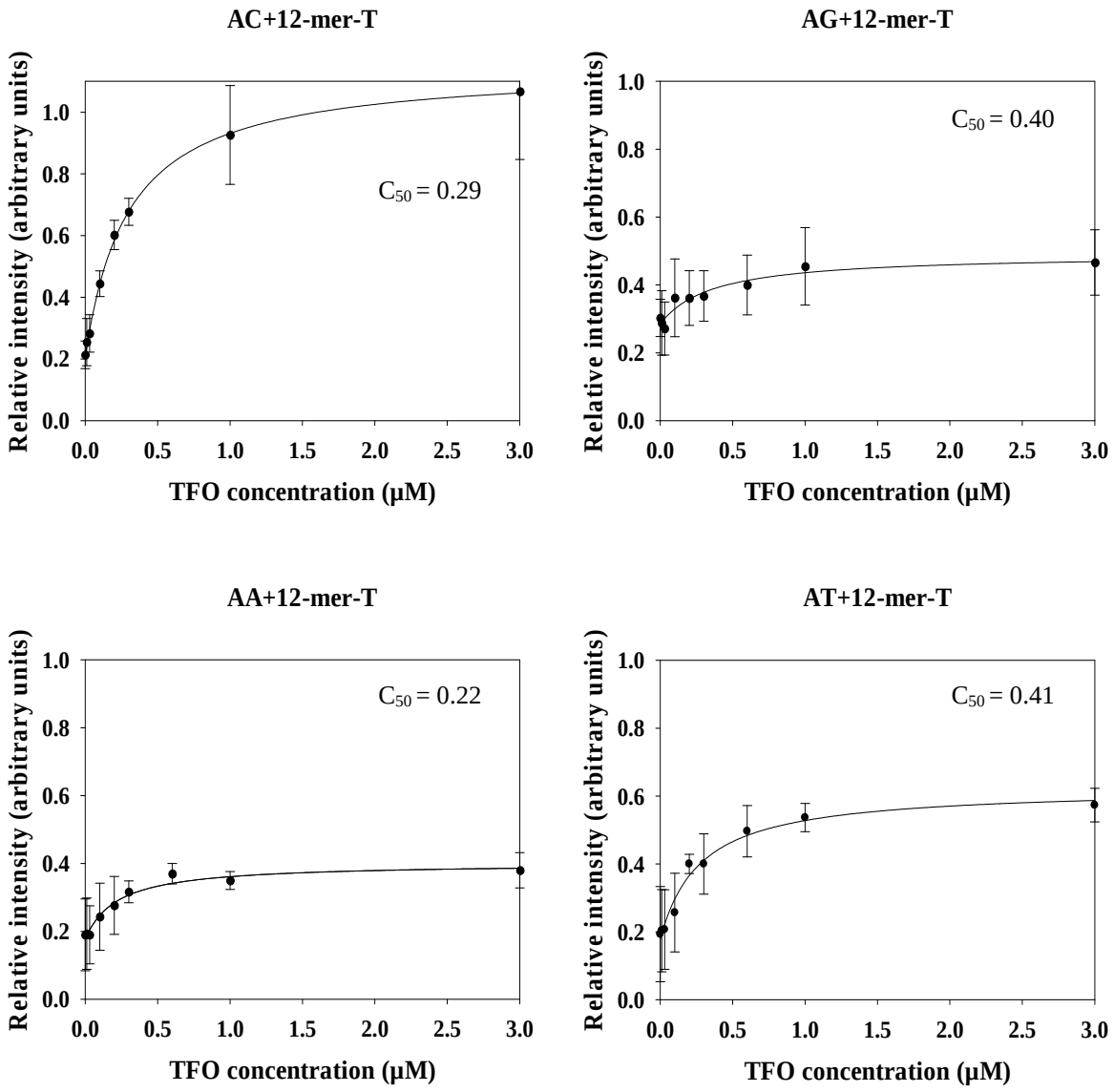

Figure 3.4 Footprinting plots showing the intensities of the enhanced band (arbitrary units) as a function of TFO concentration (μM). These were obtained from the DNase I footprinting gels of the triplex formed between 12-mer-T TFO and the four *tyr*T sequences as shown in Figure 3.3. The C_{50} values, which correspond to the TFO concentration at which the relative intensity is half the maximum, are shown in table 3.2. The curves correspond to a simple binding equation that was fitted to the data.

*tyr*T derivatives	12-mer-T TFO	
	Enhanced band intensities (Relative arbitrary unit)	**C_{50} values (μM)**
AC	0.92±0.01	0.29±0.09
AG	0.50±0.04	0.40±0.18
AA	0.35±0.01	0.22±0.03
AT	0.57±0.05	0.41±0.21

Table 3.2 The intensities of enhanced bands at the highest TFO concentration (relative arbitrary unit) and C_{50} values (μM) obtained from the DNase I footprinting plots of triplex formed between 12-mer-T and the four *tyr*T fragments (AC, AG, AA and AT).

To examine the triplexes in further details these complexes were subjected to cleavage by a range of cleavage agents including DEPC, $KMnO_4$, Micrococcal nuclease and Hydroxyl radicals.

Figure 3.5 shows the result of footprinting experiments with DEPC. This reagent reacts mainly with adenines, though cleavage is generally poor in duplex DNA and it has mainly been used for detecting changes in DNA structure (Jeppesen and Nielsen, 1988, Kahl and Paule, 2009,). The control lanes of these footprints show some reaction at the As within the oligopurine tracts (especially in six consecutive As) and at the 3'-end of the oligopurine tract in AA and AT (but not AG and AC). DEPC cleavage at these sites in the oligopurine tract is attenuated by interaction with the TFO in a concentration dependent manner. However, there is no TFO-induced enhanced cleavage at any position in all the fragments.

Figure 3.6 shows the results of similar experiments for $KMnO_4$ cleavage of the four variant fragments in the presence of the TFO. $KMnO_4$ reacts exclusively at thymines, especially at the TT dinucleotide at the 5'-end (above) of TFO's binding site, and so does not cleave within the TFO binding site in the oligopurine tract. No TFO-induced changes in $KMnO_4$ reaction are evident. Most notably there is no enhanced cleavage at the 3'-end of sequence AT.

Similarly footprinting experiments with micrococcal nuclease are shown in Figure 3.7. This enzyme cuts exclusively at A and T residues, and shows very little cleavage within the oligopurine tract, though there is a good cleavage site just above (5'-) this tract in all the fragments. Once again no TFO-induced changes in the cleavage pattern are observed. This

is especially noteworthy for fragments AA and AT, which contain extra A/T residues. Note that micrococcal nuclease cuts the O-5'-P bond, and so generates radiolabelled DNA fragments that have a 5'-hydroxyl, which do not exactly co-migrate with the GA marker lanes (which have a 5'-terminal phosphate).

Figure 3.8 shows the results of hydroxyl radical footprinting reactions with these four DNA fragments. Hydroxyl radicals, which produce a very even ladder of cleavage products, are thought to attack DNA primarily at C4', from the minor groove. Although the footprints are hardly seen with these fragments, the reduction of band intensities in a presence of TFO compared to the control is evident within their binding sites (Figure 3.9). Again no significant changes in the cleavage pattern and band intensity at the triplex-duplex junction.

5′-…CAACCAXTTCTTTTTTCTCTTCCTAACACTT…-3′
3′-…GTTGGTXAAGAAAAAAGAGAAGGATTGTGAA…-5′
3′-TTCTTTTTTCTC-5′ (12-mer-T TFO)

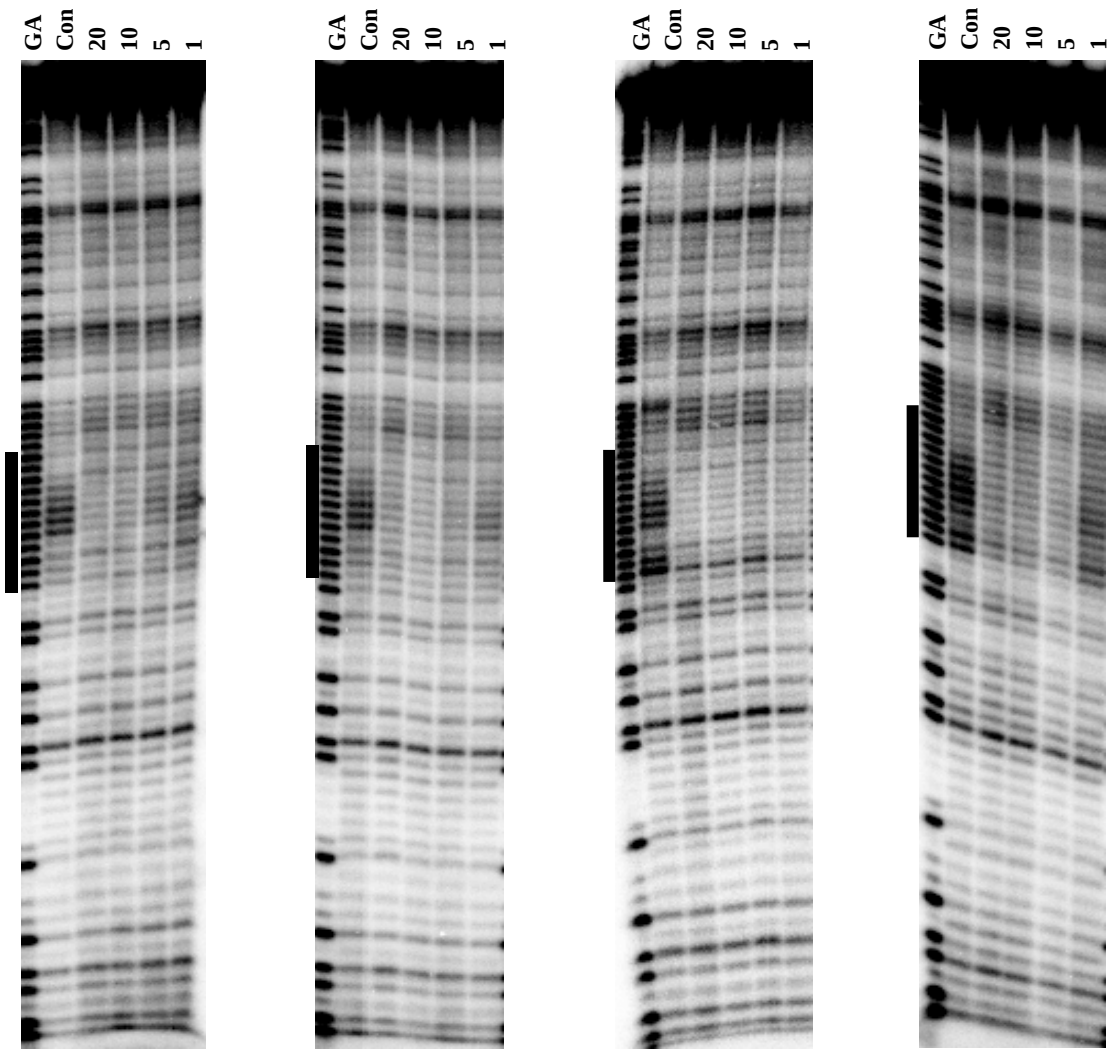

Figure 3.5 DEPC cleavage patterns of the four *tyr*T fragments in the presence of the 12-mer-T TFO. X is C, G, A and T in turn. These experiments were performed in 50 mM NaOAc at pH 5.0 in the presence of 1 mM $MgCl_2$ and equilibrated for 2 hours at room temperature before reacting with DEPC. TFO concentrations (μM) are shown at the top of each gel lane and the tracks labelled "GA" and "con" are Maxam-Gilbert markers specific for purines and the cleavage patterns in the absence of TFO respectively. The filled boxes indicate the location of the triplex target sites.

5′-…CAACCAXTTCTTTTTTCTCTTCCTAACACTT…-3′
3′-…GTTGGTXAAGAAAAAAGAGAAGGATTGTGAA…-5′
3′-TTCTTTTTTCTC-5′ (12-mer-T TFO)

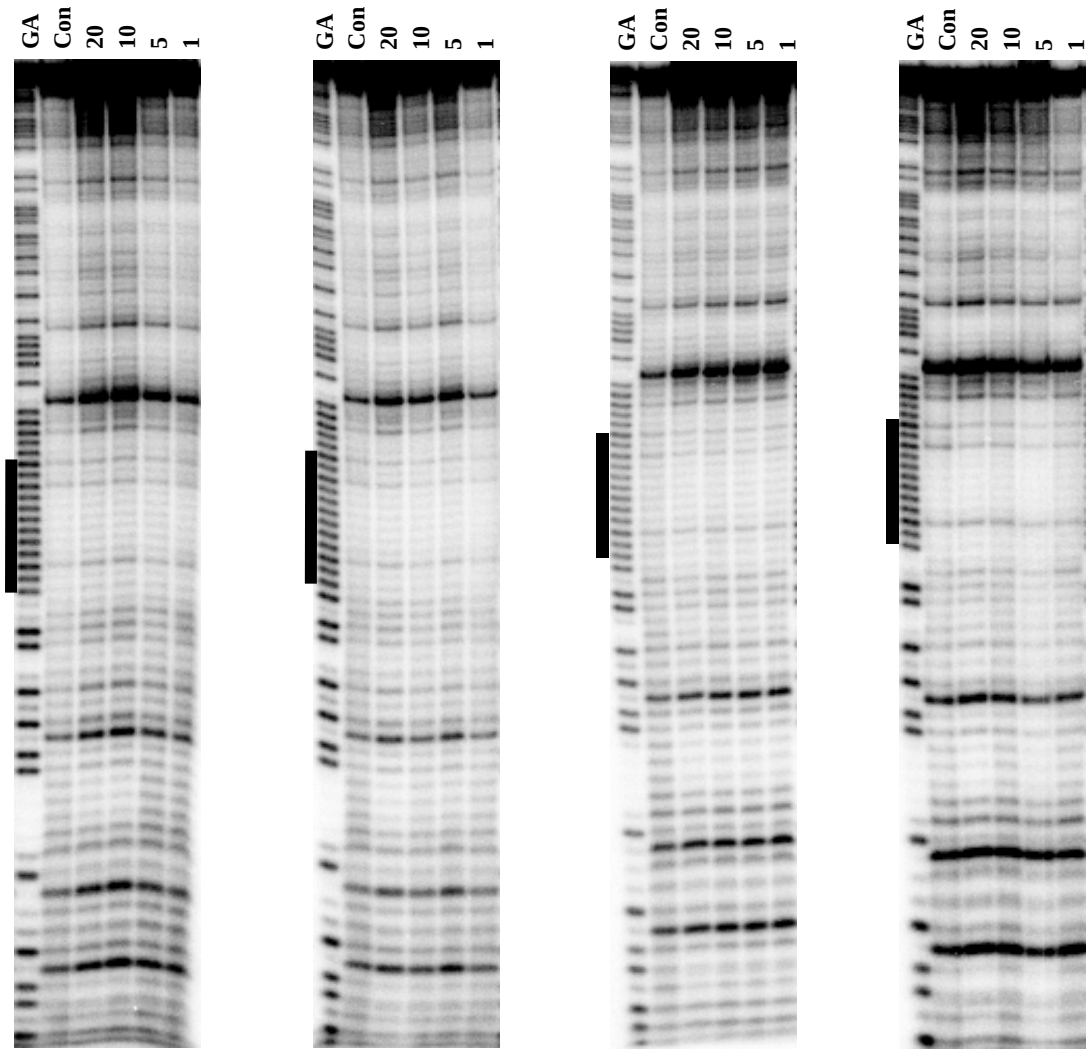

Figure 3.6 $KMnO_4$ cleavage patterns of the four *tyr*T DNA fragments in the presence of the 12-mer-T TFO. X is C, G, A and T in turn. These experiments were performed in 50 mM NaOAc at pH 5.0 in the presence of 1 mM $MgCl_2$ and equilibrated for 2 hours at room temperature before reacting with $KMnO_4$. TFO concentrations (μM) are shown at the top of each gel lane. Tracks labelled "GA" and "con" are Maxam-Gilbert markers for specific for purines and the cleavage pattern in the absence of TFOs respectively. The filled boxes indicate the location of the triplex target sites.

5′-…CAACCAXTTCTTTTTTCTCTTCCTAACACTT…-3′
3′-…GTTGGTXAAGAAAAAAGAGAAGGATTGTGAA…-5′
3′-TTCTTTTTTCTC-5′ (12-mer-T TFO)

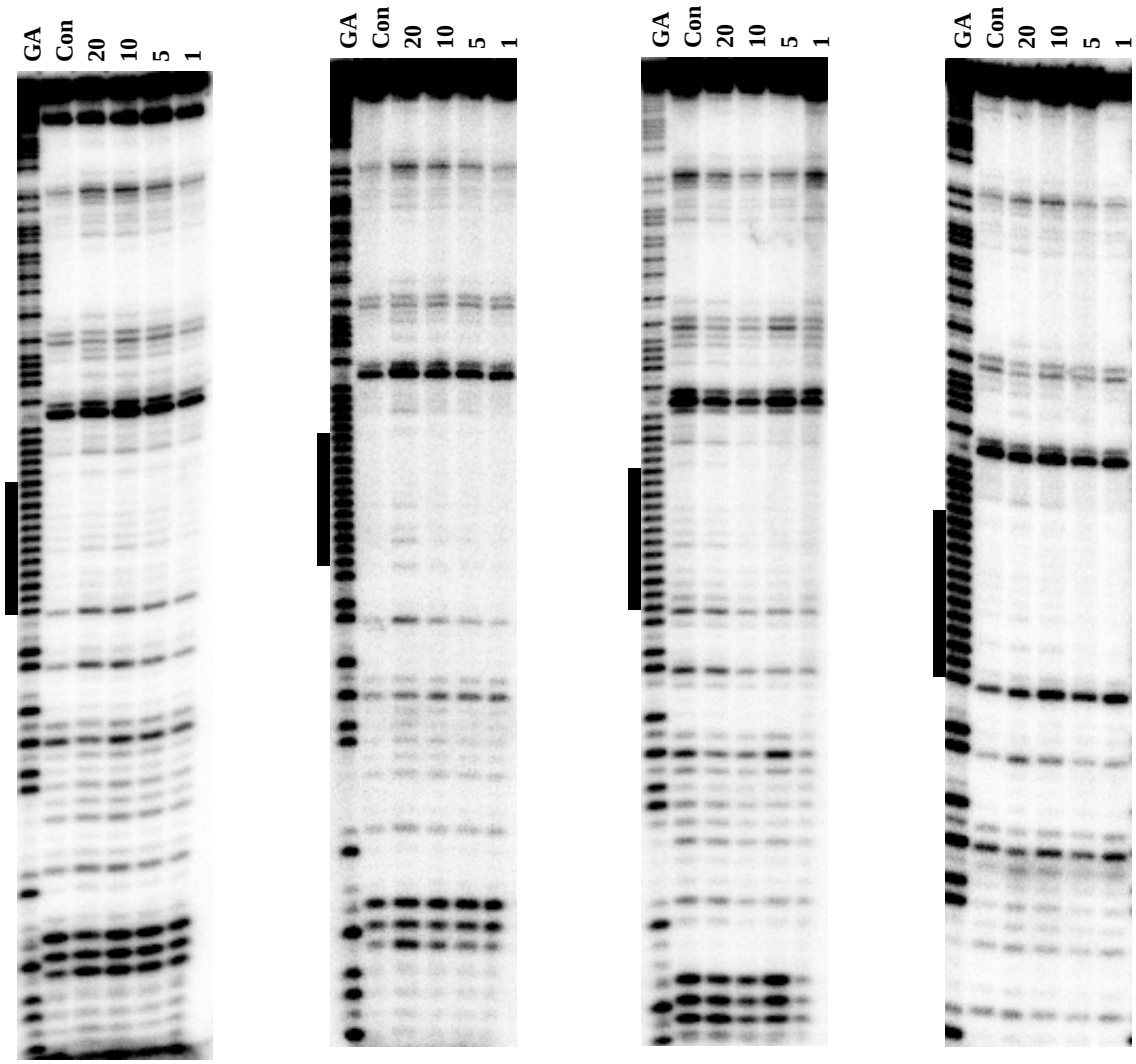

Figure 3.7 Micrococcal nuclease of the four *tyr*T fragments in the presence of the 12-mer-T TFO. X is a C, G, A and T in turn. These experiments were performed in 50 mM NaOAc at pH 5.0 in the presence of 1mM $MgCl_2$ and equilibrated for 2 hours at room temperature before digesting with the enzyme. TFO concentrations (μM) are shown at the top of each gel lane. The tracks labelled "GA" and "con" are Maxam-Gilbert markers specific for purines and the cleavage patterns in the absence of TFOs respectively. The filled boxes indicate the location of the triplex target sites.

5′-…CAACCAXTTCTTTTTTCTCTTCCTAACACTT…-3′
3′-…GTTGGTXAAGAAAAAAGAGAAGGATTGTGAA…-5′
3′-TTCTTTTTTCTC-5′ (12-mer-T TFO)

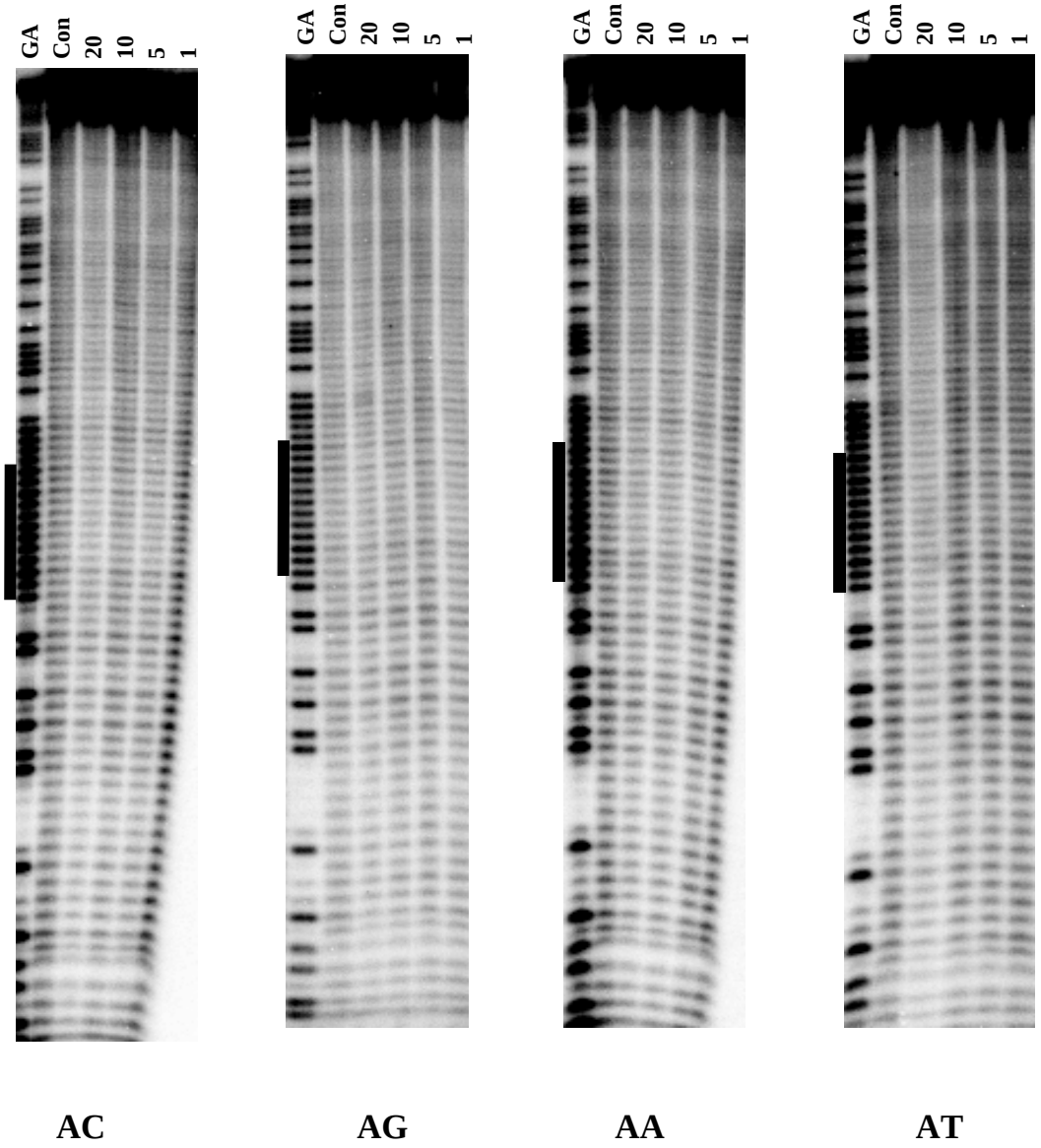

Figure 3.8 Hydroxyl radical cleavage of the four *tyr*T fragments in the presence of the 12-mer-T TFO. X is C, G, A and T in turn. These experiments were performed in 50 mM NaOAc at pH 5.0 in the presence of 1mM $MgCl_2$ and equilibrated for 2 hours at room temperature before digesting with the hydroxyl radical mixture. TFO concentrations (μM) are shown at the top of each gel lane. The tracks labelled "GA" and "con" are Maxam-Gilbert markers specific for purines and the cleavage patterns in the absence of TFOs respectively. The filled boxes indicate the location of the triplex target sites.

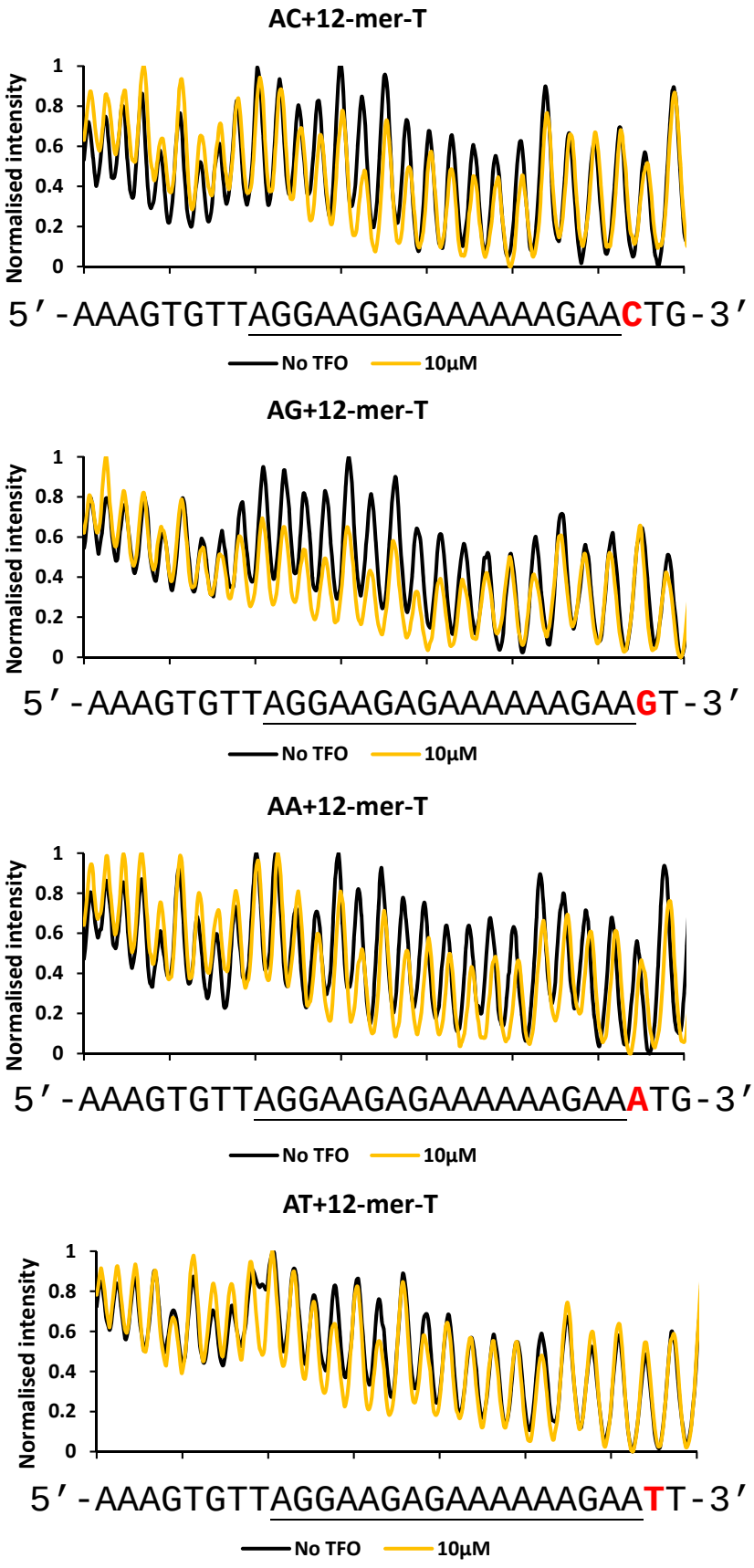

Figure 3.9 Densitometer plots of hydroxyl radical cleavage of the four fragments in the absence (black) and presence (yellow) of 10 μM of the 12-mer-T TFO (taken from the gels shown Figure in 3.8).

3.3.1.2. The formation of an 11-mer triplex

These experiments were extended by examining the interaction of an 11-mer TFO, which lacks the 3'-terminal nucleotide that was present in the two 12-mer oligonucleotides, but otherwise binds to the same target sequence. We would expect the affinity to be lower, and for any enhancements to be one base higher. The target site for this TFO was flanked by the same base (A) in four of the variant *tyr*T sequences, but they differ in the identity of the next base.

DNase I footprints for the interaction of the 11-mer TFO with the four *tyr*T variants are presented in Figures 3.10. It can be seen that, as for the 12-mer, the footprints extend above the target site by about three base pairs, and that, unlike the results with the 12-mer-T triplexes, protection can be seen below the binding site in all four of the variant sequences (below the single enhanced band at the triplex-duplex junction) (Figure 3.10). Enhanced DNase I cleavage (indicated by the red asterisks) is evident at the triplex-duplex junctions for all four sequences though, as expected, this is one base higher in the gel than with the 12-mer-T TFOs. The intensity of the enhanced band is most pronounced in sequence AC and weakest in AA (Table 3.3). Quantitative analysis of the concentration dependence of these enhancements is presented in Figures 3.11 and the calculated C_{50} values are presented in Table 3.1. These reveal no significant differences in the values for the various target duplexes. As expected, these are higher than the C_{50} values for the triplexes formed by 12-mer-T TFO.

5′-…CAACCAXTTCTTTTTTCTCTTCCTAACACTT…-3′
3′-…GTTGGTXAAGAAAAAAGAGAAGGATTGTGAA…-5′
3′-TCTTTTTTCTC-5′ (11-mer TFO)

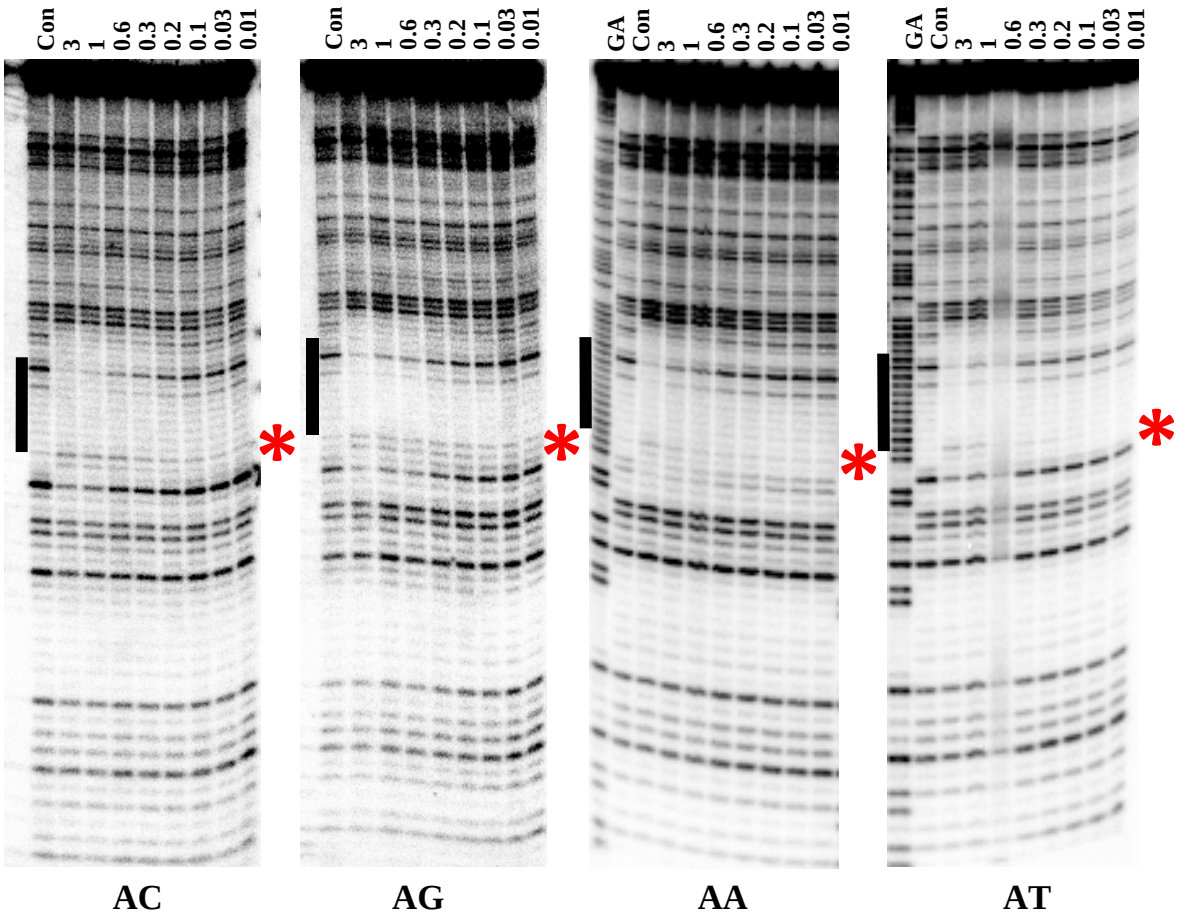

Figure 3.10 DNase I cleavage patterns of the four *tyr*T fragments in the presence of the 11-mer TFO. X is C, G, A and T in turn. These experiments were performed in 50 mM NaOAc at pH 5.0 in the presence of 1 mM $MgCl_2$ and equilibrated for 2 hours at room temperature before digesting with the enzyme. TFO concentrations (μM) are shown at the top of each gel lane and the tracks labelled "con" show the cleavage patterns in the absence of TFO. The filled boxes indicate the location of the triplex target sites and the red asterisks show the positions of enhanced DNase I cleavage.

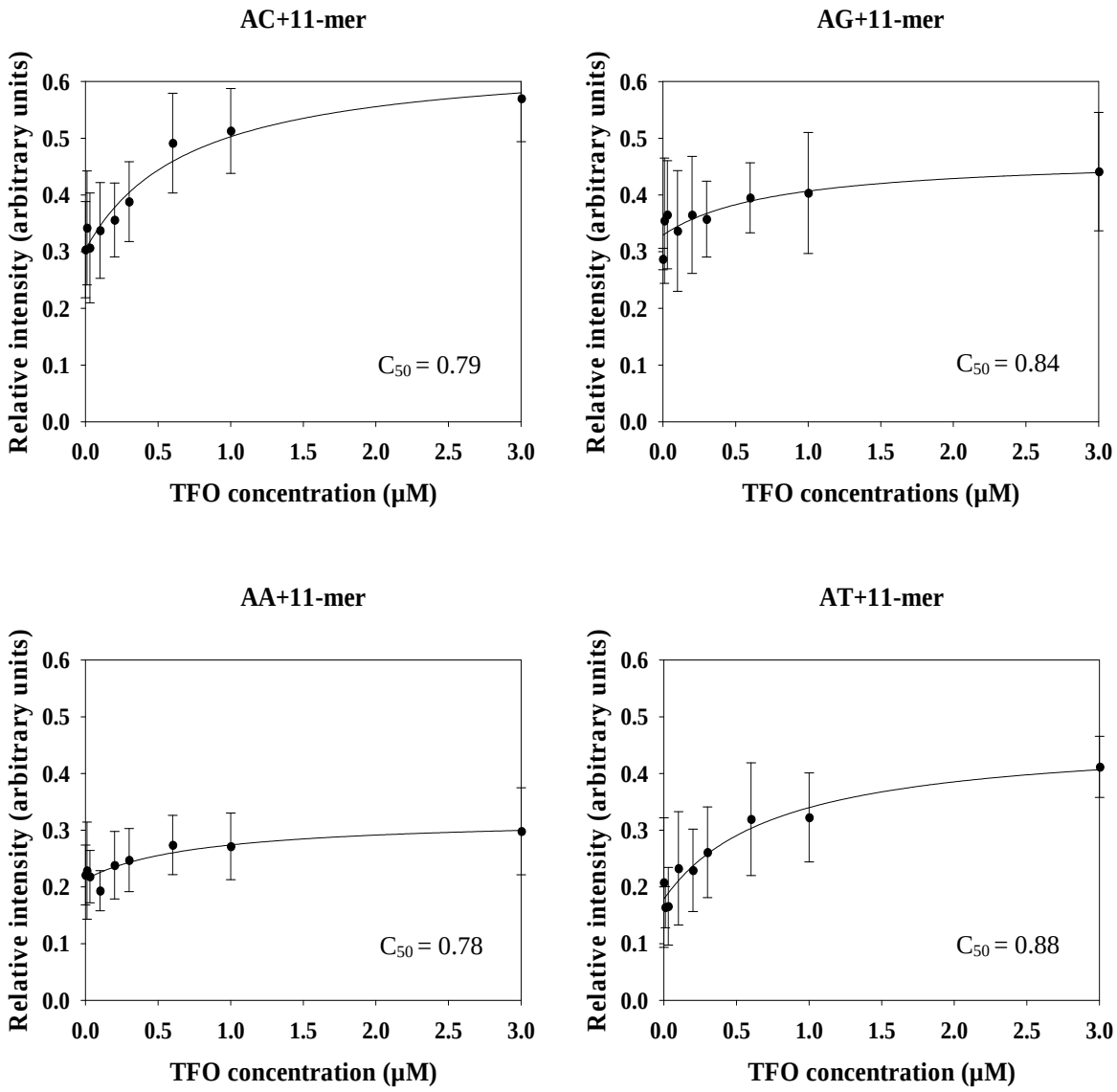

Figure 3.11 Footprinting plots showing the intensities of the enhanced band (arbitrary units) as a function of TFO concentration (μM). These were obtained from the DNase I footprinting gels of the 11-mer triplex formed between the 11-mer TFO and the four *tyr*T sequences as shown in Figures 3.10. The C_{50} values derived from these data, which correspond to the TFO concentration at which the relative intensity is half the maximum, are shown in table 3.3. The curves correspond to a simple binding equation that was fitted to the data.

*tyr*T derivative	11-mer TFO	
	Enhanced band intensities (relative arbitrary unit)	**C_{50} values (μM)**
AC	0.57±0.08	0.79±0.39
AG	0.40±0.08	0.84±0.24
AA	0.30±0.08	0.78±0.41
AT	0.40±0.07	0.88±0.46

Table 3.3 The intensities of enhanced bands at the highest TFO concentration (relative arbitrary unit) and C_{50} values (μM) obtained from the DNase I footprinting plots of triplex formed between 11-mer TFOs and the four *tyr*T fragments (AC, AG, AA and AT).

The results of DEPC modification reactions for the four duplex variants in the presence of the 11-mer TFO are presented in Figure 3.12. In contrast to the results with the 12-mer-T TFO, enhanced reaction to DEPC is seen at the 3'-end of these TFO binding sites in sequences AC, AG and AA, though not in AT. In each instance these enhancements are located at the A after the 11-mer binding site (i.e. at A<u>A</u>C, A<u>A</u>G, and A<u>A</u>A, with sequences AC, AG and AA respectively), as indicated by the red asterisk. This enhanced reaction is strongest for sequence AA, while AC and AG produce enhancements of similar intensity.

The reaction of $KMnO_4$ with each of these sequences is shown in Figure 3.13 and, as noted with 12-mer-T TFOs, there are no TFO-induced changes in the modification pattern. Similarly the 11-mer TFO produces no significant changes in either the micrococcal nuclease cleavage pattern (Figure 3.14) or the hydroxyl radical footprinting gels (Figure 3.15). However, the reduction of band intensities in a presence of TFO compared to the control is seen within the binding sites, especially, of the AC and AG (Figure 3.16).

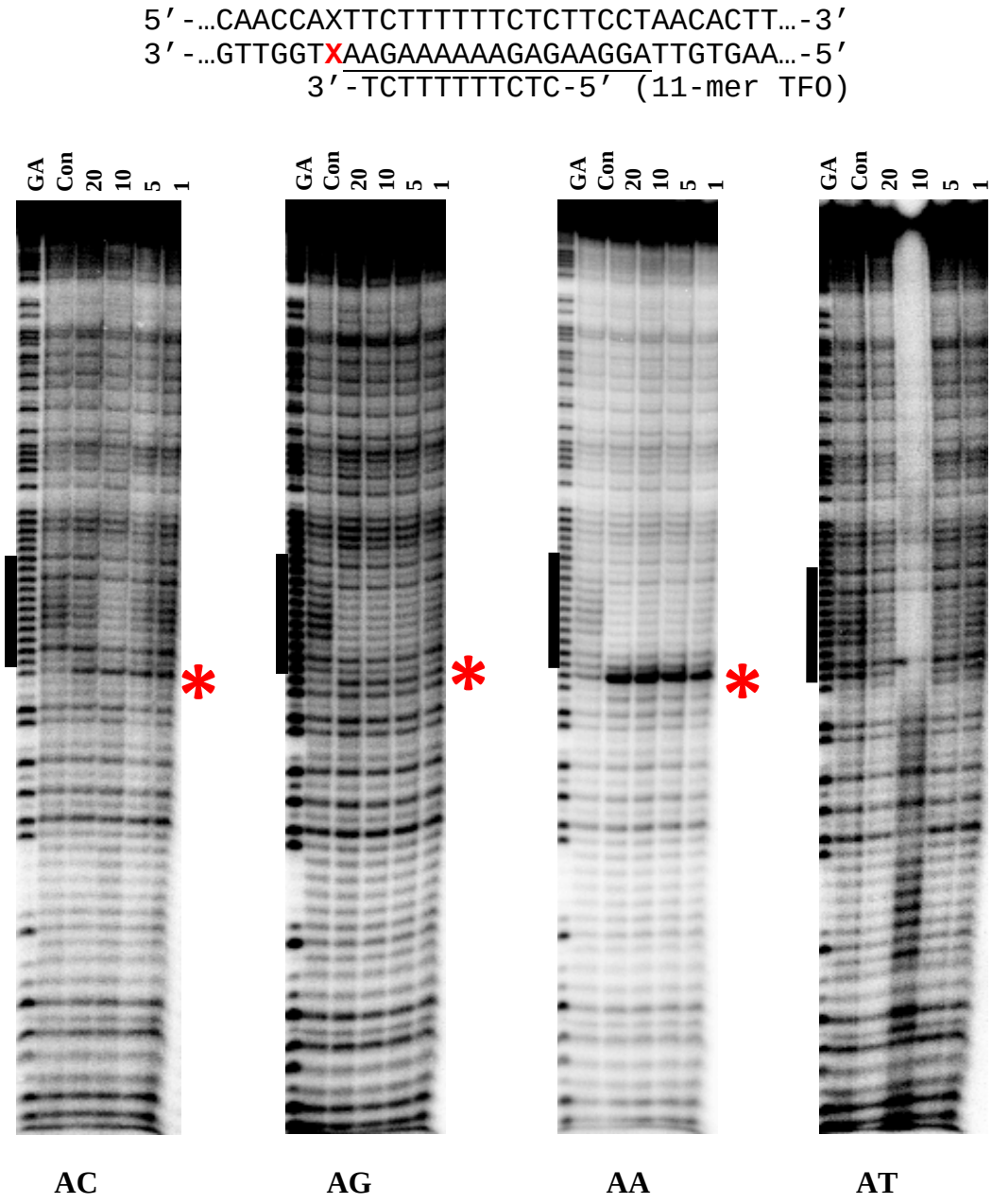

Figure 3.12 DEPC cleavage patterns of the four *tyr*T sequences in the presence of the 11-mer TFO. These experiments were performed in 50 mM NaOAc at pH 5.0 in the presence of 1mM $MgCl_2$ and equilibrated for 2 hours at room temperature before addition of DEPC. TFO concentrations (μM) are shown at the top of each gel lane. The tracks labelled "GA" and "con" are Maxam-Gilbert markers specific for purines and the cleavage patterns in the absence of TFOs respectively. The filled boxes indicate the location of the triplex target sites and the red asterisks show the position of enhanced DNase I cleavage.

```
5′-…CAACCAXTTCTTTTTTCTCTTCCTAACACTT…-3′
3′-…GTTGGTXAAGAAAAAAGAGAAGGATTGTGAA…-5′
          3′-TCTTTTTTCTC-5′ (11-mer TFO)
```

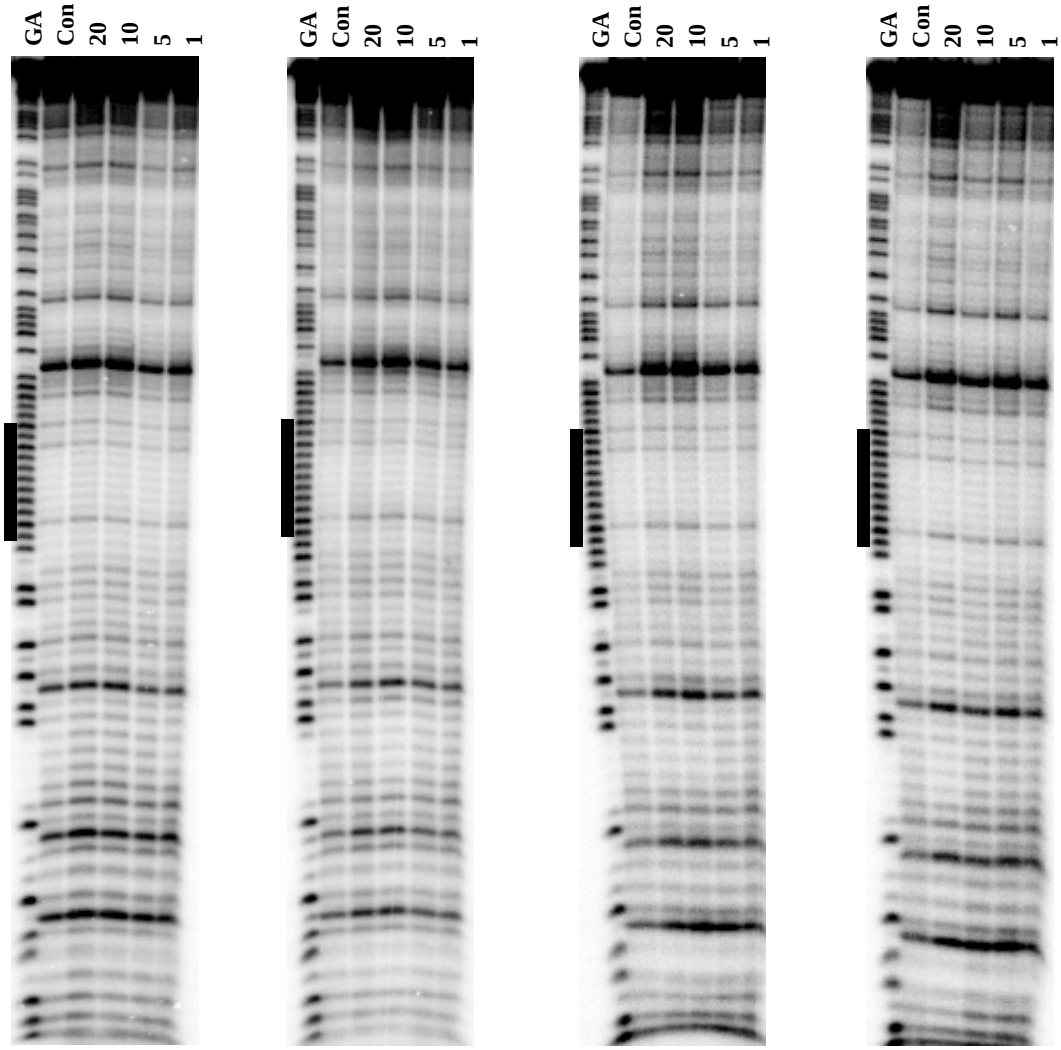

Figure 3.13 $KMnO_4$ cleavage patterns of the four *tyr*T fragments in the presence of the 11-mer TFO. These experiments were performed in 50 mM NaOAc at pH 5.0 in the presence of 1mM $MgCl_2$ and equilibrated for 2 hours at room temperature before the addition of $KMnO_4$. TFO concentrations (μM) are shown at the top of each gel lane. Tracks labelled "GA" and "con" are Maxam-Gilbert markers specific for purines and the cleavage patterns in the absence of TFOs respectively. The filled boxes indicate the position of the triplex target sites.

5′-…CAACCAXTTCTTTTTTCTCTTCCTAACACTT…-3′
3′-…GTTGGTXAAGAAAAAAGAGAAGGATTGTGAA…-5′
3′-TCTTTTTTCTC-5′ (11-mer TFO)

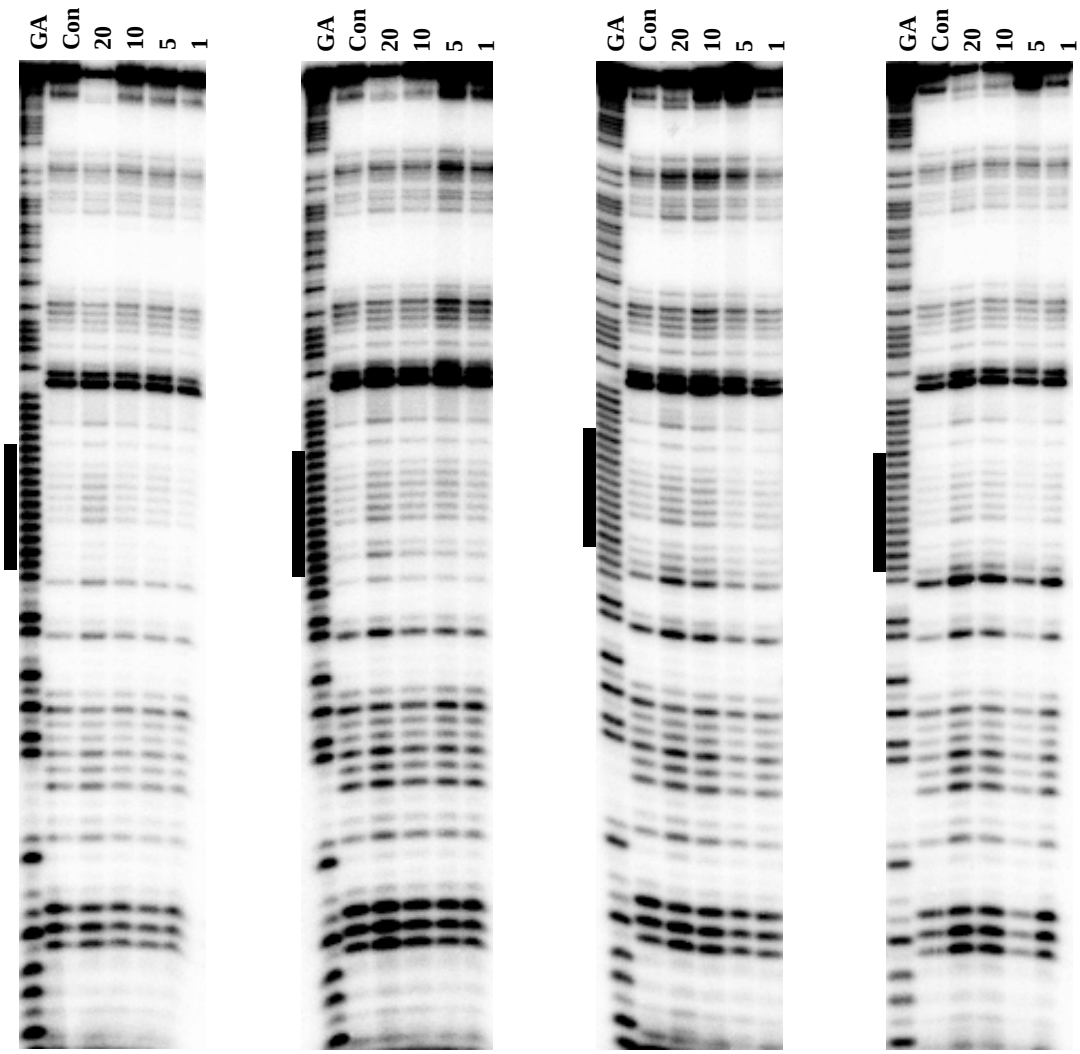

Figure 3.14 Micrococcal nuclease cleavage patterns of the four *tyr*T fragments in the presence of the 11-mer TFO. These experiments were performed in 50 mM NaOAc at pH 5.0 in the presence of 1mM $MgCl_2$ and equilibrated for 2 hours at room temperature before digesting by the enzyme. TFO concentrations (μM) are shown at the top of each gel lane and the tracks labelled "GA" and "con" are Maxam-Gilbert markers specific for purines and the cleavage patterns in the absence of TFOs respectively. The filled boxes indicate the triplex target sites.

5′-…CAACCAXTTCTTTTTTCTCTTCCTAACACTT…-3′
3′-…GTTGGTXAAGAAAAAAAGAGAAGGATTGTGAA…-5′
3′-TCTTTTTTCTC-5′ (11-mer TFO)

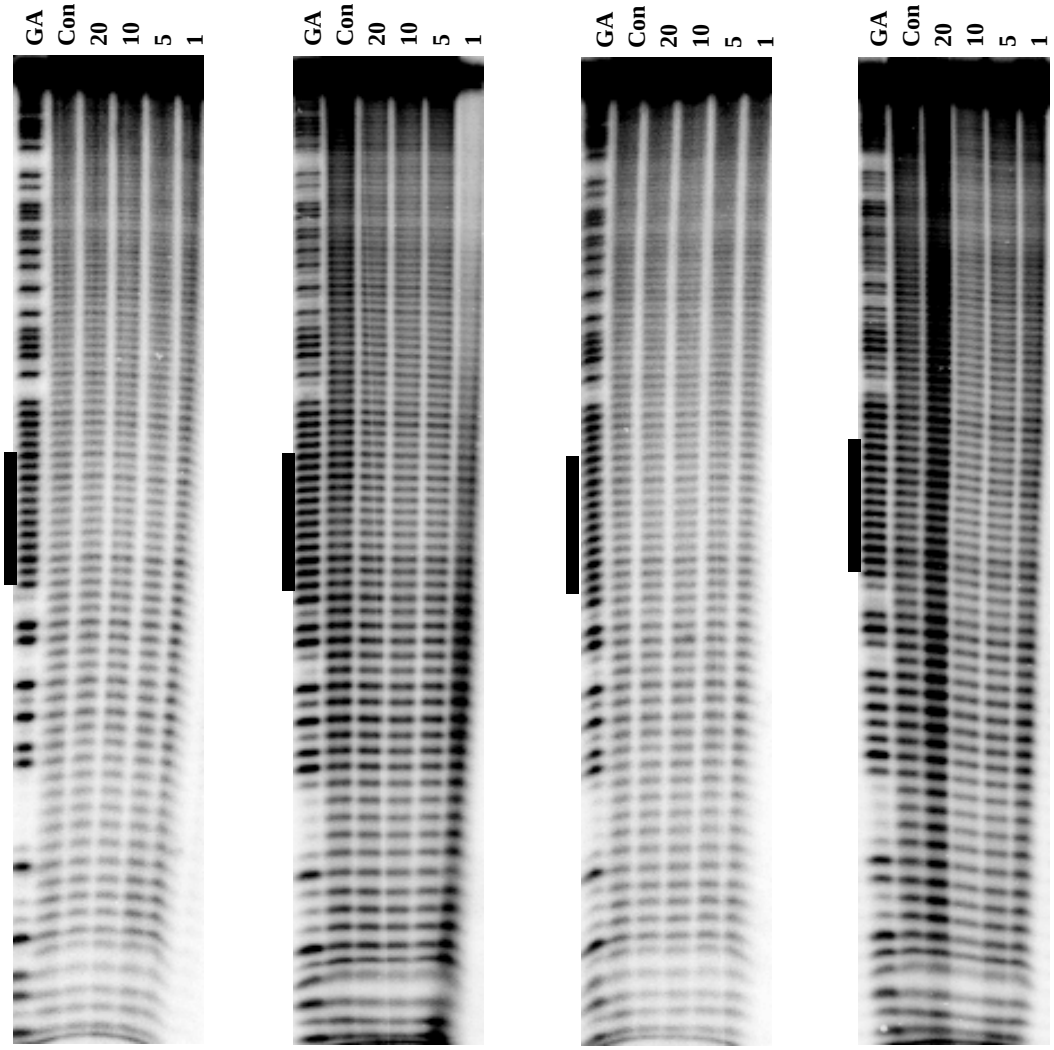

AC **AG** **AA** **AT**

Figure 3.15 Hydroxyl radical cleavage patterns of the four *tyr*T fragments in the presence of the 11-mer TFO. These experiments were performed in 50 mM NaOAc at pH 5.0 in the presence of 1 mM $MgCl_2$ and equilibrated for 2 hours at room temperature before addition of the hydroxyl radical mixture. TFO concentrations (μM) are shown at the top of each gel lane. Tracks labelled "GA" and "con" are Maxam-Gilbert markers specific for purines and the cleavage patterns in the absence of TFOs respectively. The filled boxes indicate the location of the triplex target sites.

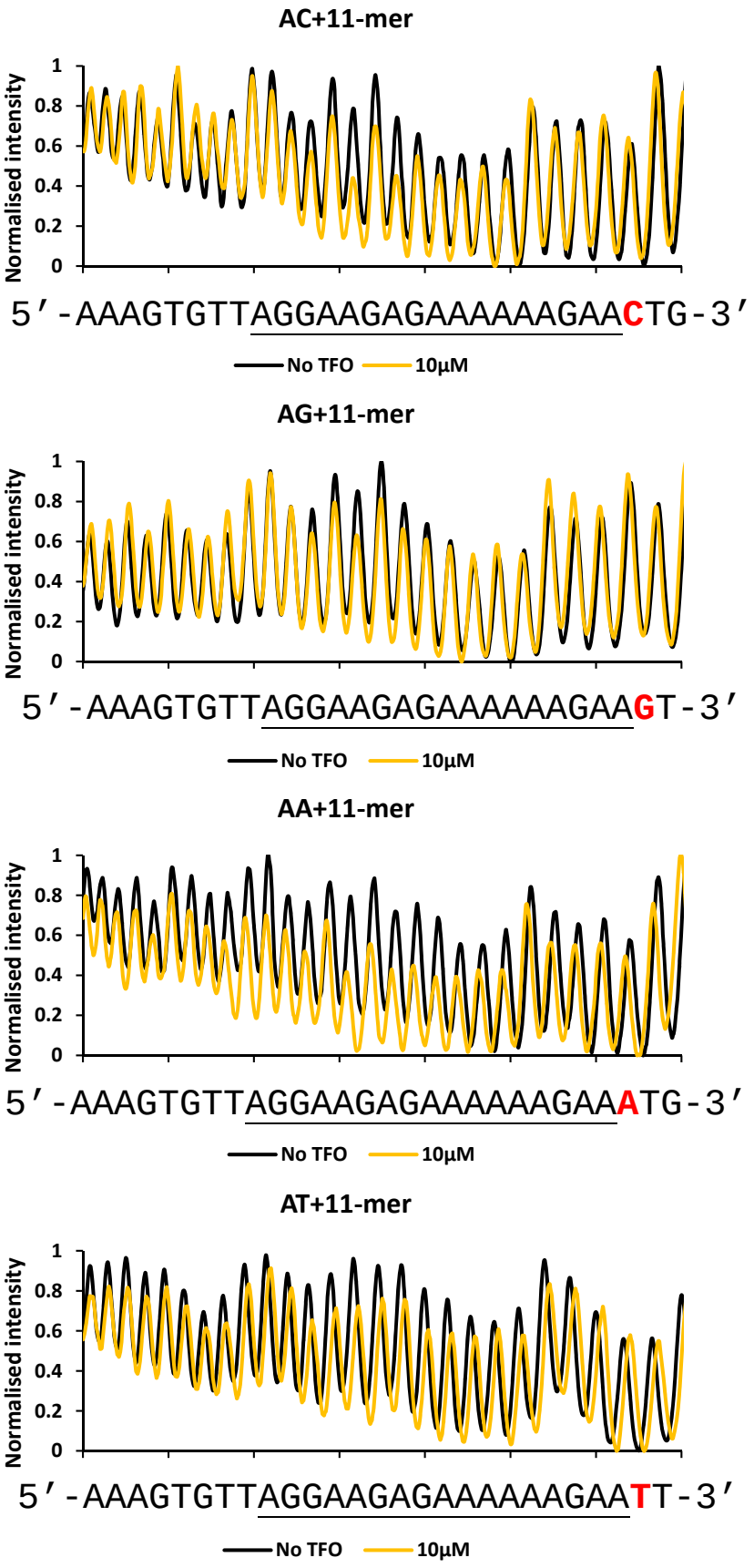

Figure 3.16 Densitometer plots of hydroxyl radical cleavage of the four fragments in the absence (black) and presence (yellow) of 10 μM of the 11-mer TFO (taken from the gels shown Figure in 3.15).

3.3.1.3. The 12-mer triplex formed with 12-mer-C TFO, generating a 3'-end mismatch

Similar experiments were performed with the 12-mer-C TFO, which differs from 12-mer-T by replacement of the 3'-T with C, and so generates an 11-mer triplex with a 3'-terminal C.AT triplet mismatch. We were interested to examine this combination to determine the location of the enhancements; would these occur at the end of the 11-mer canonical triplex, or at the end of the mismatched 12-mer triplex. Previous studies (Cardew *et al.,* 2011) suggested that some triplexes with terminal mismatches could produce enhanced DNase I cleavage in both locations. DNase I footprinting experiments with this TFO are presented in Figures 3.17. As expected, higher concentrations of this TFO are required to generate clear footprints as it generates fewer canonical triplets. The enhancements at the 3'- (lower) end of the binding site are generally weaker than those seen with the full 12-mer-T TFO. Interestingly, with sequences AT and AC, these can be seen at two positions at the 3'-end of the binding site. One of these is at the mismatched triplet (red asterisk in Figure 3.17), in the same position as the enhanced cleavage with the 12-mer-T triplexes. Another enhancement appears one base above this, in the same position as the enhancement seen with the 11-mer triplexes (see above). There is no enhanced bands evident with AG and AA. Again sequence AC produces the strongest DNase I enhancement (Table 3.4).

5′-…CAACCAXTTCTTTTTTCTCTTCCTAACACTT…-3′
3′-…GTTGGTXAAGAAAAAAGAGAAGGATTGTGAA…-5′
3′-CTCTTTTTTCTC-5′ (12-mer-C TFO)

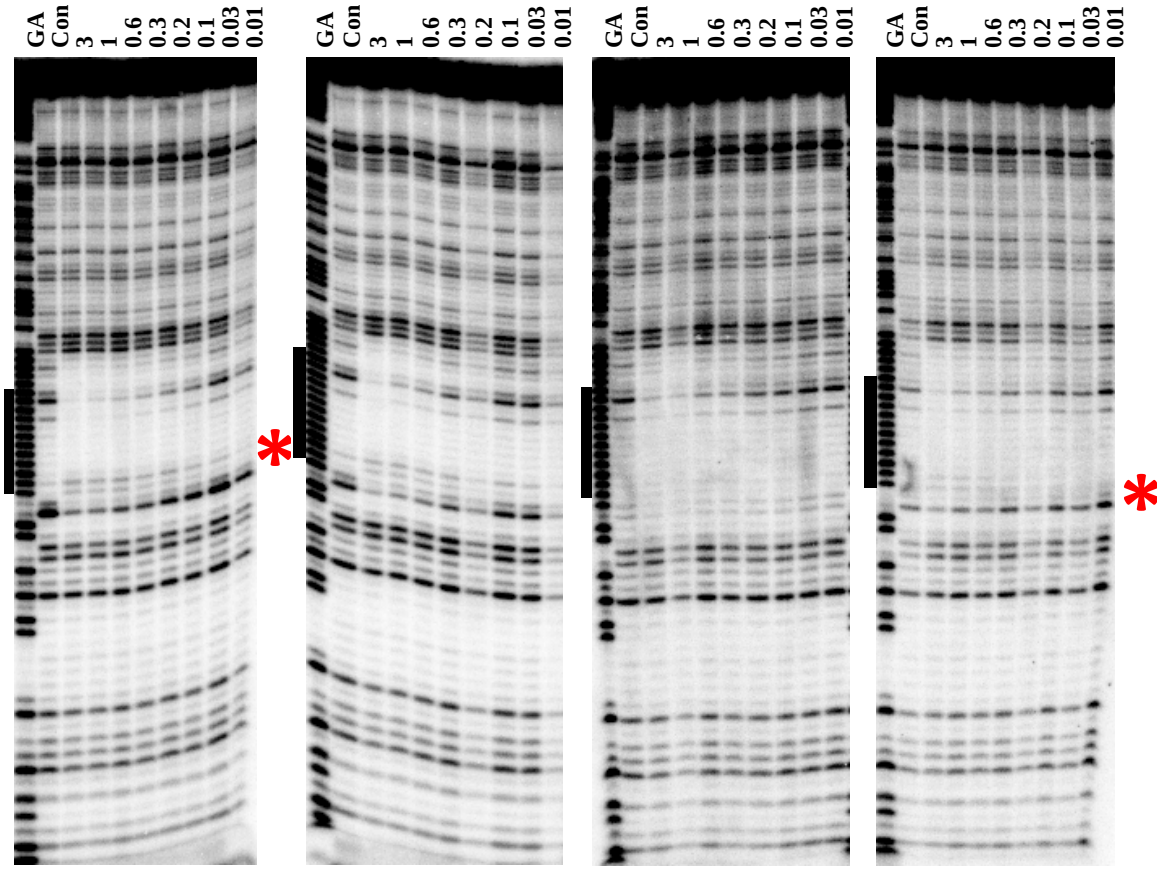

Figure 3.17 DNase I cleavage patterns of the four *tyr*T fragments in the presence of the 12-mer-C TFO. X is C, G, A and T in turn. These experiments were performed in 50 mM NaOAc at pH 5.0 in the presence of 1 mM $MgCl_2$ and equilibrated for 2 hours at room temperature before digestion by the enzyme. TFO concentrations (μM) are shown at the top of each gel lane. Tracks labelled "GA" and "con" are Maxam-Gilbert markers specific for purines and the cleavage patterns in the absence of TFO respectively. The filled boxes indicate the location of the triplex target sites and the red asterisks show the position of enhanced DNase I cleavage. The mismatched triplet is highlighted in yellow.

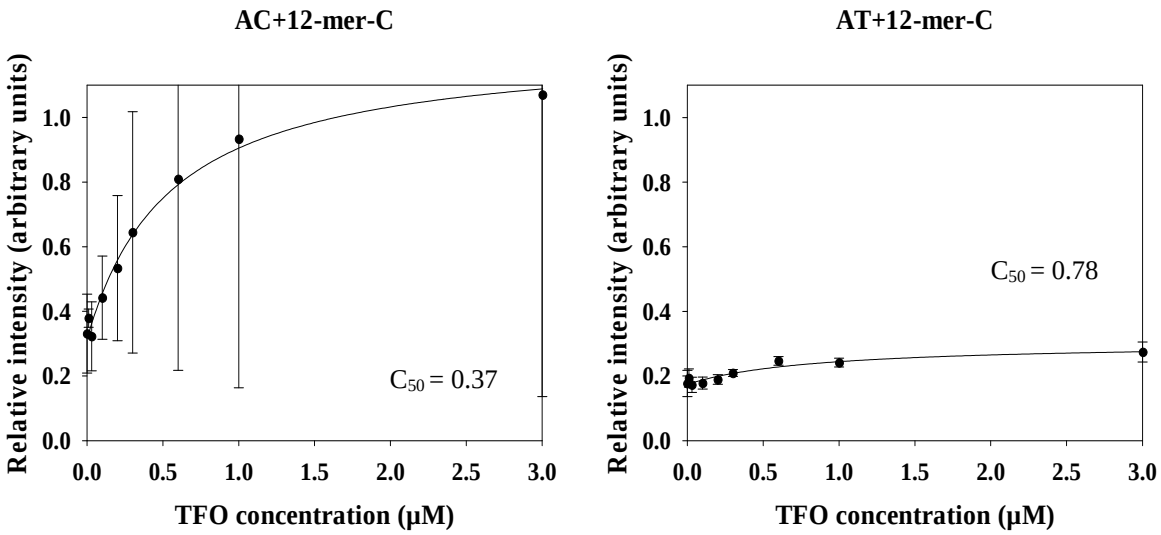

Figure 3.18 Footprinting plots showing the intensities of the enhanced band (arbitrary units) as a function of TFO concentration (μM). These were obtained from the DNase I footprinting gels of the 12-mer triplex formed between the 12-mer-C TFO and the AC and AT sequences as shown in Figures 3.17. The C_{50} values derived from these data, which correspond to the TFO concentration at which the relative intensity is half the maximum, are shown in table 3.4. The curves correspond to a simple binding equation that was fitted to the data.

***tyr*T derivative**	**12-mer-C TFO**	
	Enhanced band intensities (relative band intensity)	**C_{50} values (μM)**
AC	1.07±0.93	0.37±0.37
AG	N/A	N/A
AA	N/A	N/A
AT	0.27±0.03	0.78±0.58

Table 3.4 The intensities of enhanced bands at the highest TFO concentration (relative arbitrary unit) and C_{50} values (μM) obtained from the DNase I footprinting plots of triplex formed between 12-mer-C and the AC and AT.

Similar footprinting experiments with DEPC are shown in Figure 3.19. The cleavage patterns are similar to those formed with 12-mer-T, though there are remarkable DEPC cleavage enhancements at the 3'-end of the triplex-duplex junction in sequences AC, AA and AT (strongest for AA). These are located at the position of enhanced DNase I cleavage with 12-mer-T and enhanced DEPC reaction with 11-mer. No enhanced DEPC cleavage is seen with sequences AG.

The reaction of $KMnO_4$ with the triplexes formed with 12-mer-C is shown in Figure 3.20. These show very similar patterns to those with 12-mer-T and 11-mer, with no TFO-induced changes in the cleavage pattern. Again this is most noteworthy for AT, which contains a T adjacent to the TFO binding site.

Micrococcal nuclease footprinting patterns with TFO 12-mer-C are shown in Figure 3.21. These are similar to those seen with 12-mer-T and 11-mer TFO and show no significant TFO-induced changes in the cleavage pattern.

Similar hydroxyl radical footprinting reactions with these sequences in the presence of 12-mer-C TFO are shown in Figure 3.22 and 3.23. Once again there are no significant TFO-induced changes in the cleavage pattern.

5′-…CAACCAXTTCTTTTTTCTCTTCCTAACACTT…-3′
3′-…GTTGGTXAAGAAAAAAGAGAAGGATTGTGAA…-5′
3′-CTCTTTTTTCTC-5′ (12-mer-C TFO)

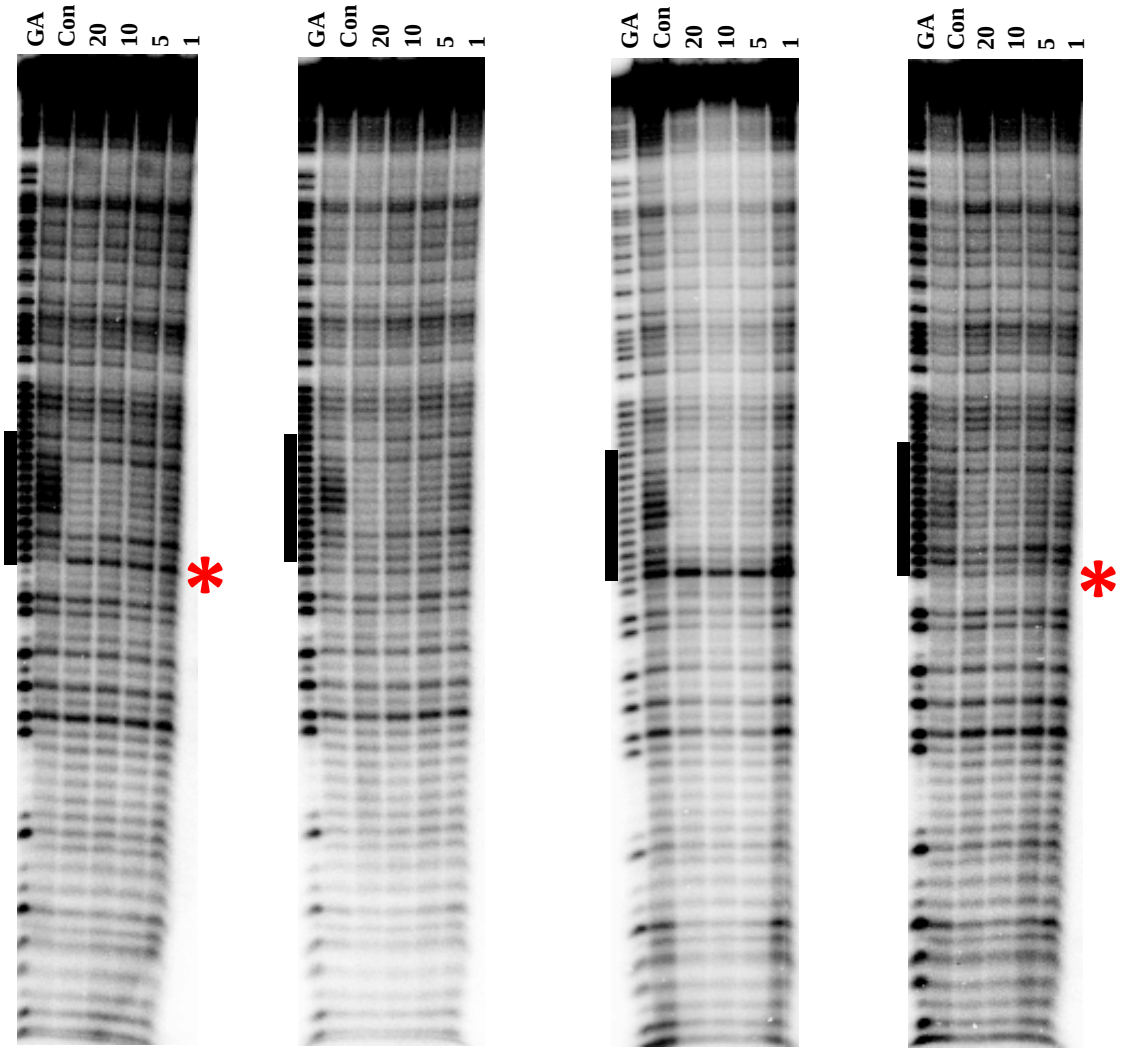

AC **AG** **AA** **AT**

Figure 3.19 DEPC cleavage patterns of the four *tyr*T sequences in the presence of the 12-mer-C TFO. These experiments were performed in 50 mM NaOAc at pH 5.0 in the presence of 1mM $MgCl_2$ and equilibrated for 2 hours at room temperature before reacting with DEPC. TFO concentrations (μM) are shown at the top of each gel lane. Tracks labelled “GA” and “con” are Maxam-Gilbert markers specific for purines and the cleavage patterns in the absence of TFOs respectively. The filled boxes indicate the location of the triplex target sites and the red asterisks show the positions of enhanced DNase I cleavage. The mismatched triplet is highlighted in yellow.

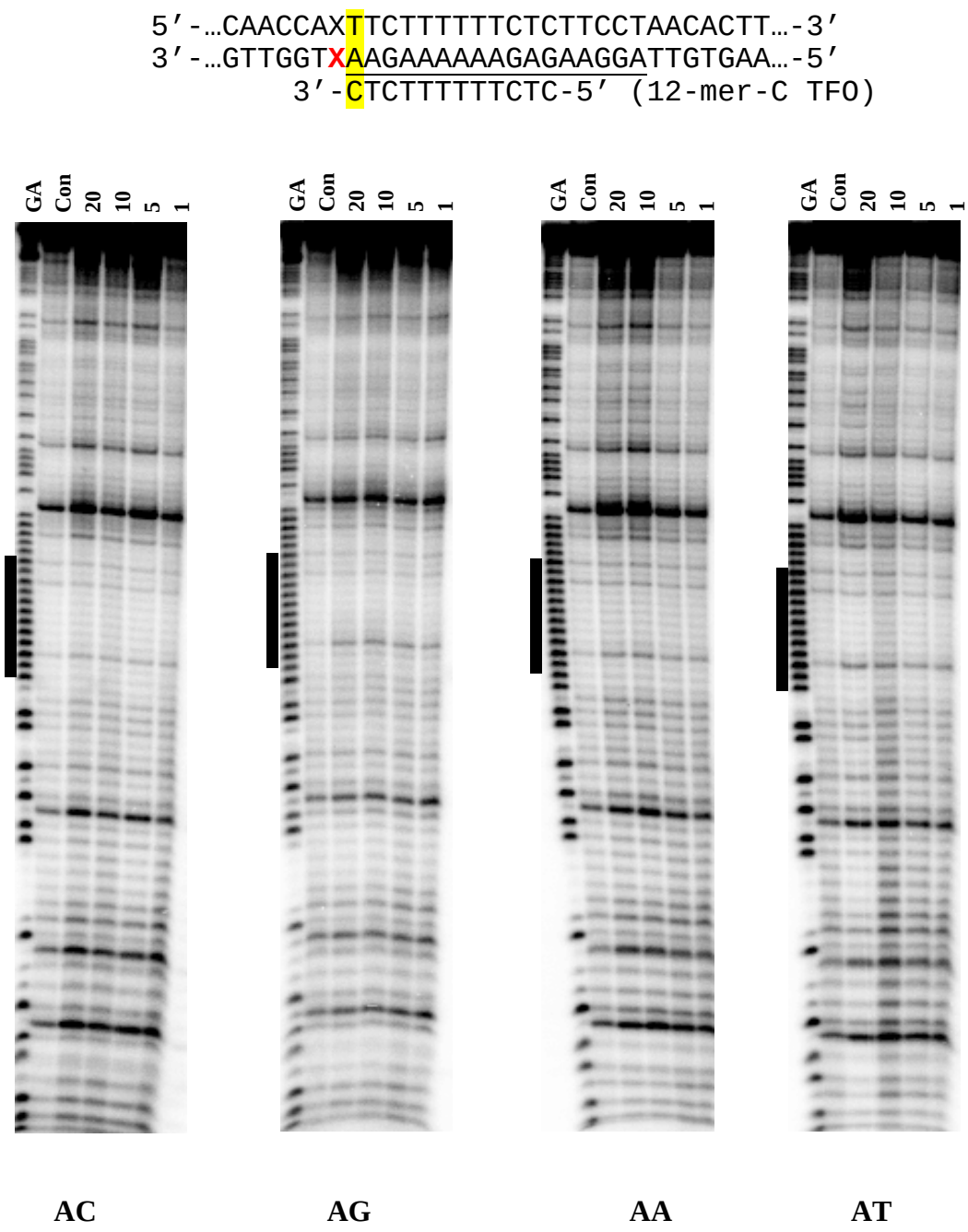

Figure 3.20 $KMnO_4$ cleavage patterns of the four *tyr*T sequences in the presence of the 12-mer-C TFO. These experiments were performed in 50 mM NaOAc at pH 5.0 in the presence of 1mM $MgCl_2$ and equilibrated for 2 hours at room temperature before addition of $KMnO_4$. TFO concentrations (μM) are shown at the top of each gel lane. Tracks labelled "GA" and "con" are Maxam-Gilbert markers specific for purines and the cleavage patterns in the absence of TFOs respectively. The filled boxes indicate the location of the triplex target sites and the mismatched triplet is highlighted in yellow.

```
5′-…CAACCAXTTCTTTTTTCTCTTCCTAACACTT…-3′
3′-…GTTGGTXAAGAAAAAAGAGAAGGATTGTGAA…-5′
        3′-CTCTTTTTTCTC-5′ (12-mer-C TFO)
```

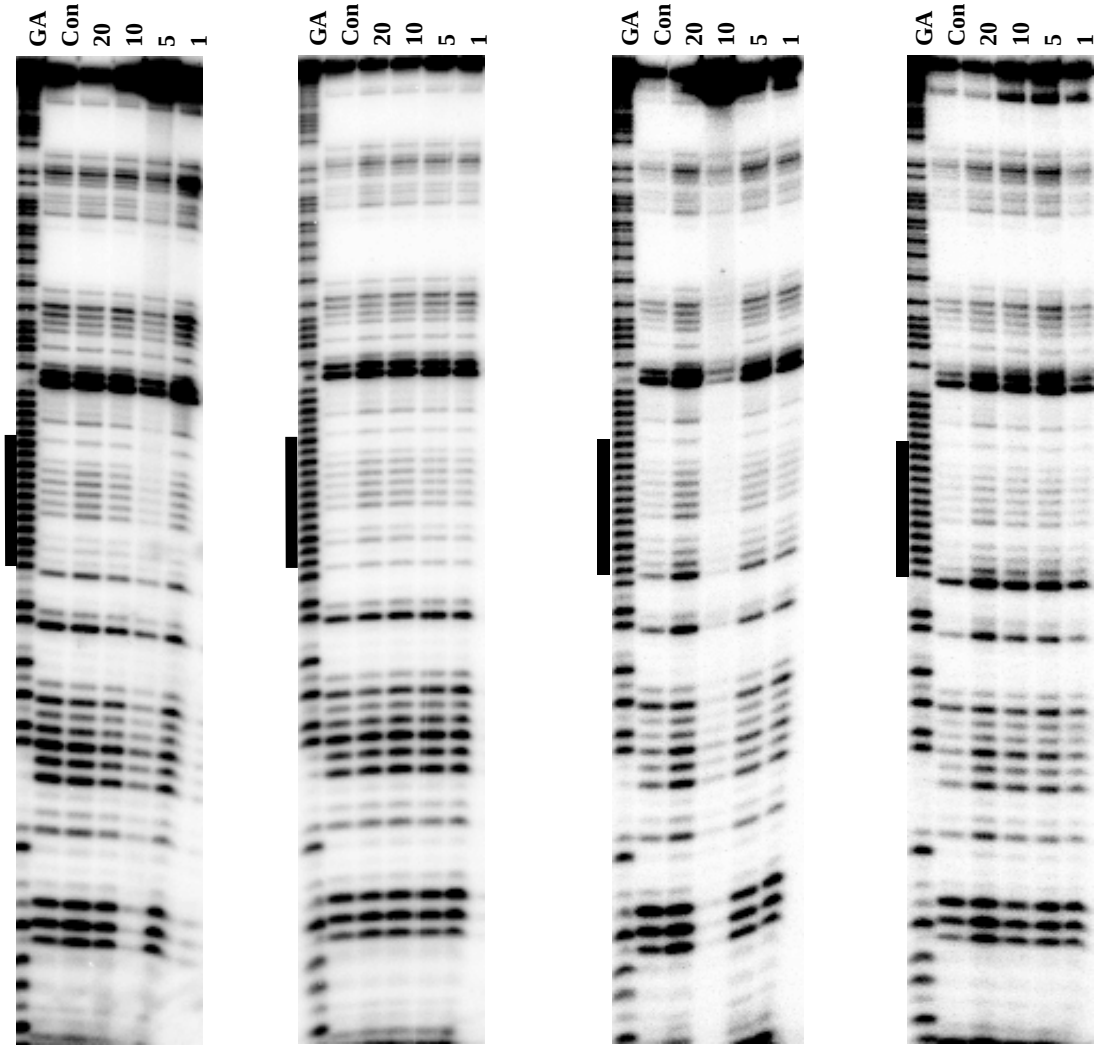

Figure 3.21 Micrococcal nuclease cleavage patterns of the four *tyr*T sequences in the presence of the 12-mer-C TFO. These experiments were performed in 50 mM NaOAc at pH 5.0 in the presence of 1mM $MgCl_2$ and equilibrated for 2 hours at room temperature before adding the enzyme. TFO concentrations (μM) are shown at the top of each gel lane. Tracks labelled "GA" and "con" are Maxam-Gilbert markers specific for purines and the cleavage patterns in the absence of TFOs respectively. The filled boxes indicate the location of the triplex target sites and the mismatched triplet is highlighted in yellow.

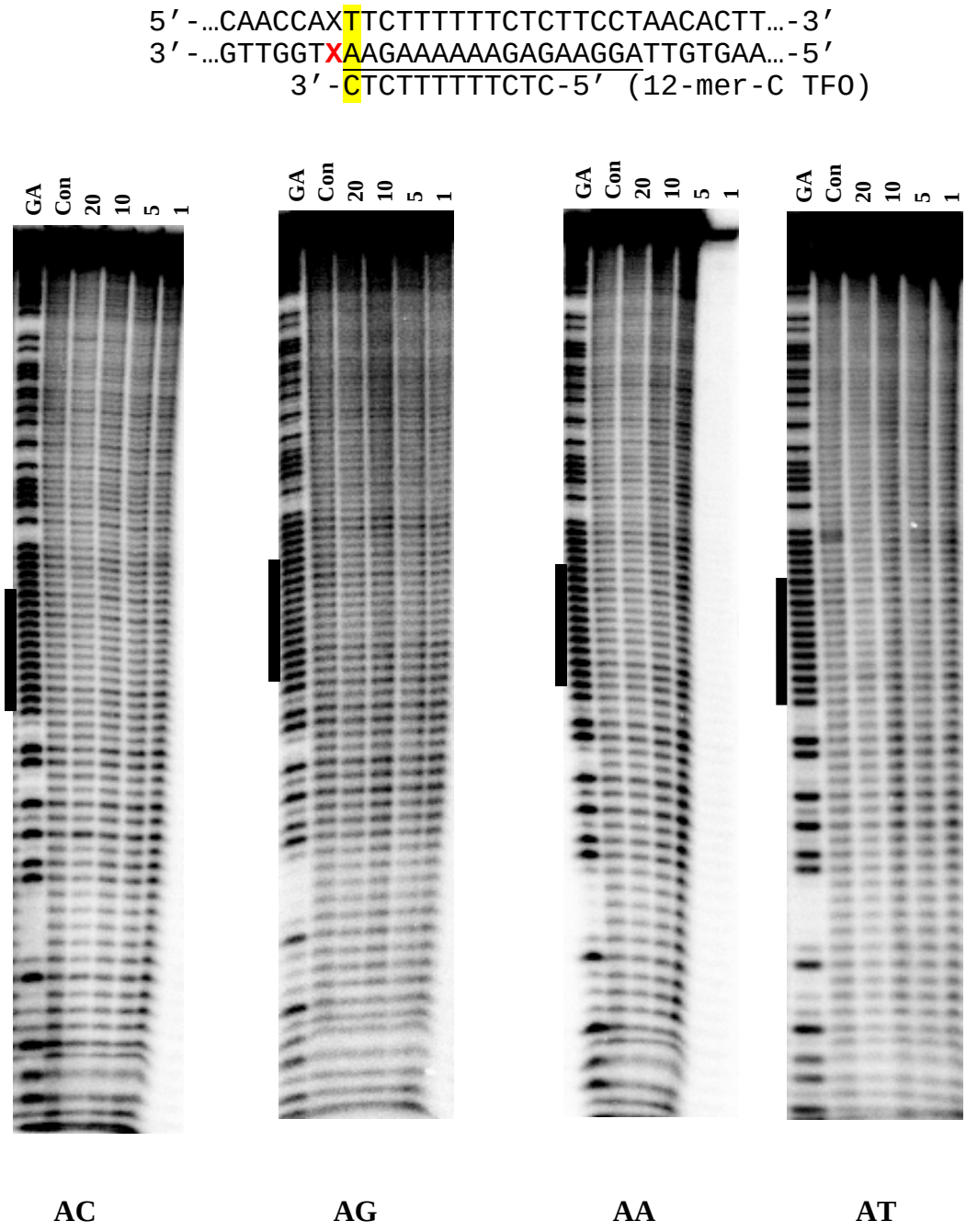

Figure 3.22 Hydroxyl radical cleavage patterns of the four *tyr*T fragments in the presence of the 12-mer-C TFO. These experiments were performed in 50 mM NaOAc at pH 5.0 in the presence of 1mM $MgCl_2$ and equilibrated for 2 hours at room temperature before adding the hydroxyl radical mixture. TFO concentrations (μM) are shown at the top of each gel lane and the tracks labelled "GA" and "con" are Maxam-Gilbert markers specific for purines and the cleavage patterns in the absence of TFOs respectively. The filled boxes indicate the location of the triplex target sites and the mismatched triplet is highlighted in yellow.

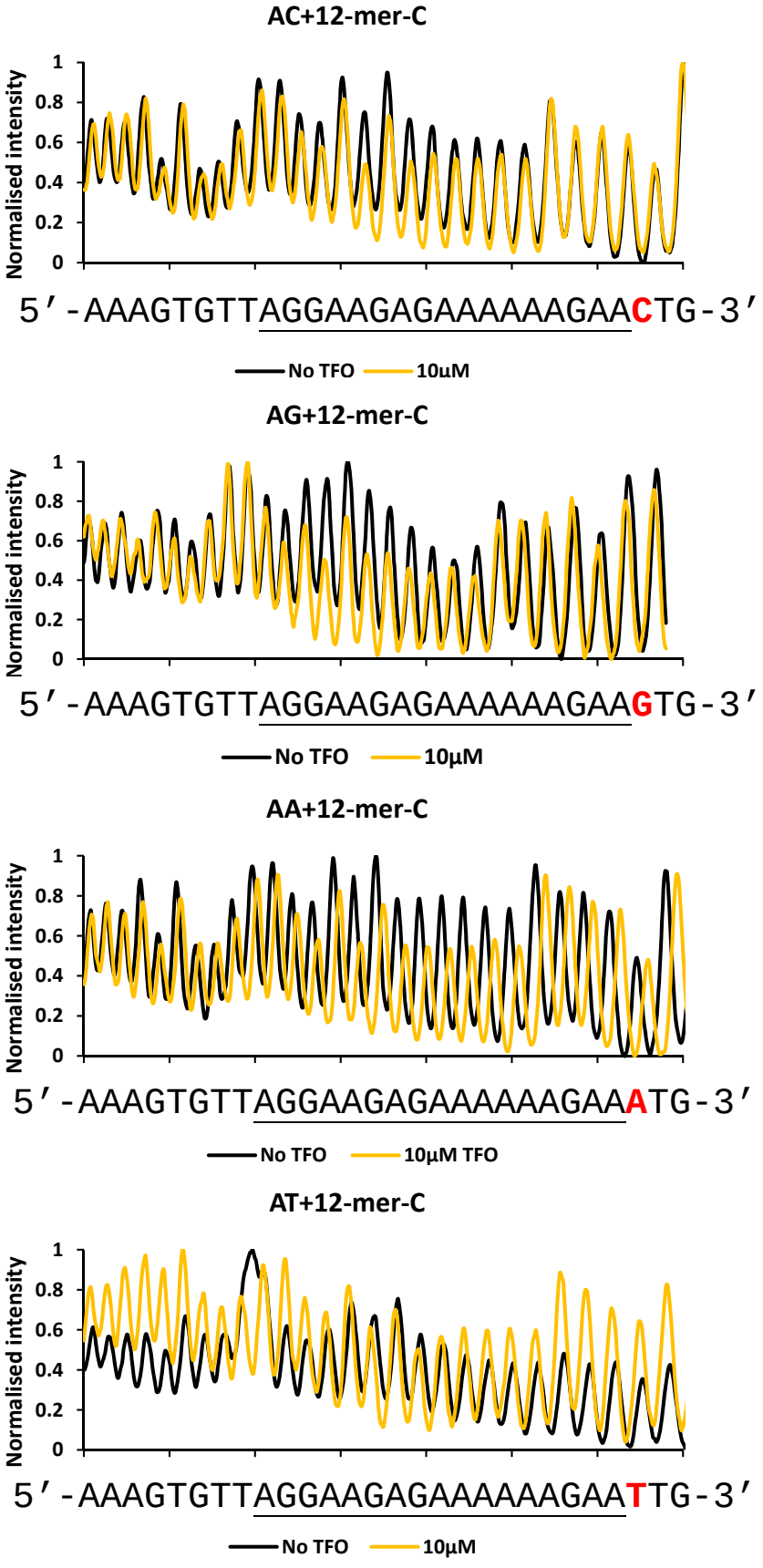

Figure 3.23 Densitometer plots of hydroxyl radical cleavage of the four fragments in the absence (black) and presence (yellow) of 10 μM of the 12-mer-C TFO (taken from the gels shown Figure in 3.22).

3.3.1.4. The effect of flanking bases on the stability of triplex DNA

3.3.1.4.1. 12-mer triplex formation with a 3'-T.AT triplet

The experiments described in the previous sections demonstrate that flanking bases can affect the susceptibility to some enzymes and chemical cleavage agents. However these techniques were not sufficiently sensitive to detect any changes in triplex affinity. We have therefore examined the stability of triplexes that are flanked by different base pairs by thermal melting studies using fluorescently labelled synthetic oligonucleotides. In these experiments the 12-mer third strand TFO is labelled at the 5'-end with dabcyl while the purine strand of the target duplex is labelled at its 5'-end with fluorescein. The sequences of these oligonucleotides are shown in Table 3.1 and were chosen to correspond to the 12-mer target site in the *tyr*T fragments. When the triplex is assembled the fluorophore and quencher are in close proximity and the fluorescence is quenched. On increasing the temperature the triplex melts, separating the fluorophore and quencher, leading to a large increase in fluorescence. These experiments were all performed in 50 mM NaOAC pH 5.0 containing 1 mM $MgCl_2$ and 200 mM NaCl.

For each of the triplexes, both fluorescence melting and annealing profiles were recorded and they show no significant difference between each pairs of duplex targets and TFOs. Therefore the melting profiles will only be presented in this report. Fluorescence melting curves for the four target duplexes (at a concentration of 0.25 μM) in the presence of 5 μM of the 12-mer-T oligonucleotide are presented in Figure 3.24 and T_m values derived from these are presented in Table 3.5. The mean T_m values for the target AC, AA, AG and AT are 40.7 °C, 43.7 °C, 45 °C and 42.3 °C respectively. These are significantly different to each other and appear to show that flanking base pairs can affect the triplex stability. The AG has the highest T_m and AC has the lowest, with a difference of 4.3 °C.

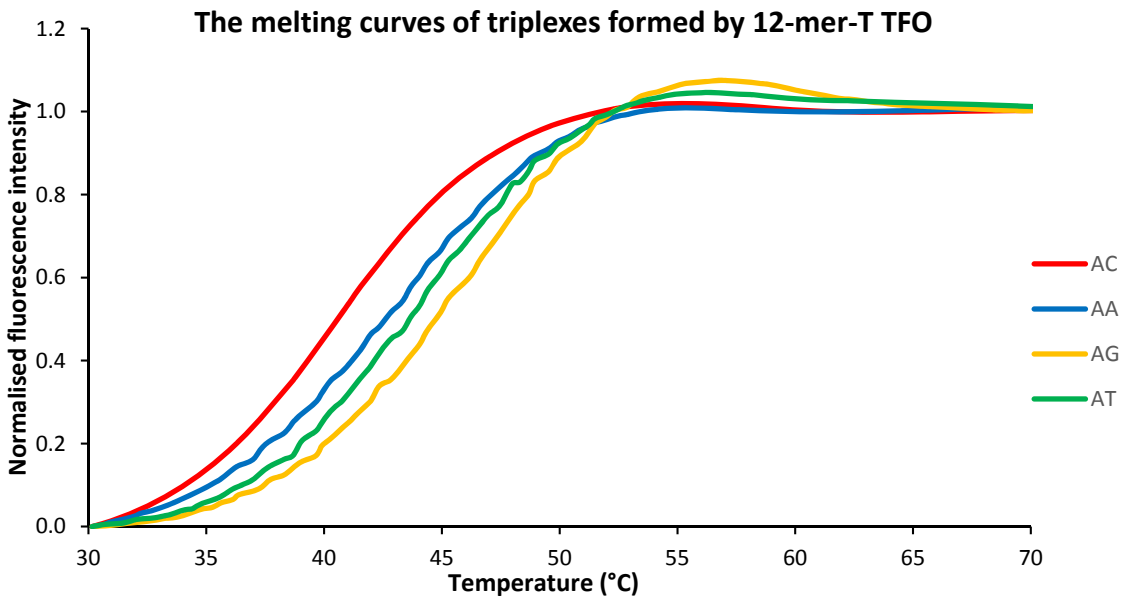

Figure 3.24 Fluorescence melting curves of the 12-mer triplex formed between the dabcyl-labelled 12-mer-T TFO and the fluorescently labelled duplex target sites in which the triplex target site is flanked by each base pair in turn : AC (red), AA (blue), AG (yellow) and AT (green).

3.3.1.4.2. 11-mer triplex formation

The results of similar experiments with the shorter 11-mer TFO on these four target sequences are shown in Figure 3.25. As expected the T_ms of these 11-mer triplexes are lower than those of the 12-mer-T triplexes (Table 3.5). The difference of these is pronounced and is about 2.5-3 °C for AC, AA and AT, but greater for AG (4.8 °C). The AC has the lowest T_m (38.2 °C), which is significantly lower than the T_ms of AA (40.4 °C), AG (40.2 °C) and AT (39.8 °C) that are not significantly different to each other.

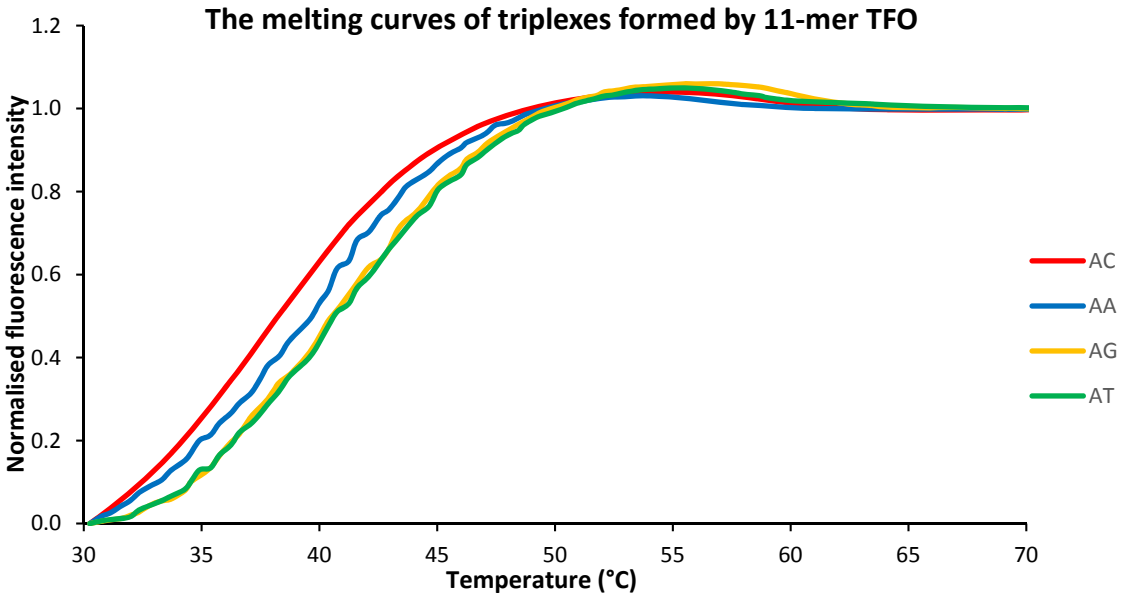

Figure 3.25 Fluorescence melting curves for the triplex formed between the dabcyl-labelled 11-mer TFO and the four target duplexes: AC (red), AA (blue), AG (yellow) and AT (green).

3.3.1.4.3. 12-mer triplex formation with a C.AT mismatch at the 3'-end

Figure 3.26 shows the results of experiments with the same target duplexes, but with the dabcyl-labelled oligonucleotide 12-mer-C, which generates a C.AT triplet mismatch at the 3'-end. The T_m values estimated from these data are shown in Table 3.5. Although these triplexes have slightly different melting temperatures, the differences are much less pronounced than with the 12-mer-T (Figure 3.24). In contrast to the results with 12-mer-T, the triplex formed at AC now has the highest T_m (42.8 °C), though this is similar to those with AA (42.1 °C) and AG (41.8 °C), but higher than AT, which has the lowest T_m (40.7 °C). Comparing the T_m of the 12-mer-C triplexes (Figure 3.26) with those formed with 12-mer-T (Figure 3.24) it can be seen that the T_m of AA, AG and AT decrease by 1.6, 3.2 and 1.6 °C respectively on changing the T.AT triplex to C.AT. Interestingly the T_m of AC increases by 2.1 °C. Despite having the same canonical triplets, triplexes formed with 12-mer-C provide higher T_ms (Table 3.5) than those with 11-mer. The difference of these is between 1-2 °C for AA, AG and AT, but is much greater for AC (4.6 °C).

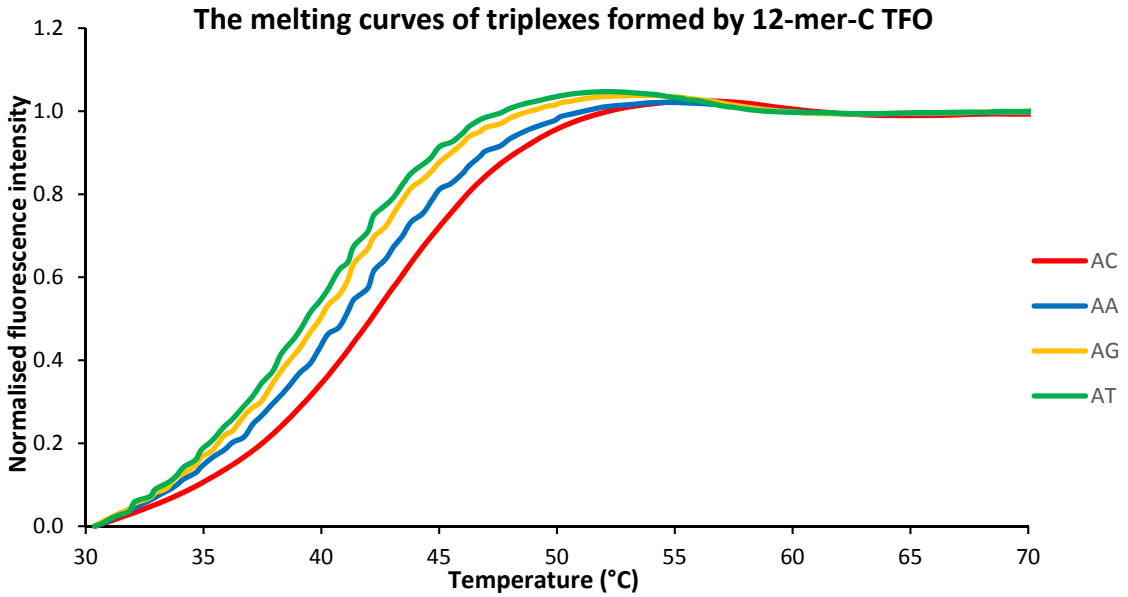

Figure 3.26 Fluorescence melting curves for the 12-mer triplex formed between the dabcyl-labelled 12-mer-C TFO and the fluorescently labelled duplex target sites in which the triplex target site is flanked by each base pair in turn: AC (red), AA (blue), AG (yellow) and AT (green).

***tyr*T derivative**	**T_m Values (°C) (mean±SD)**		
	12-mer-T	**11-mer**	**12-mer-C**
AC	40.7±0.4	38.2±0.5	42.8±0.2
AG	45.0±0.3	40.2±0.2	41.8±0.2
AA	43.7±0.3	40.4±0.2	42.1±0.4
AT	42.3±0.2	39.8±0.3	40.7±0.2

Table 3.5 T_m values estimated from the maxima in the first derivatives of the melting profile of triplexes formed between fluorescently labelled duplex targets AC, AG, AA and AT with either dabcyl-labelled 12-mer-T, 11-mer or 12-mer-T TFO.

3.3.2. The effects of 3'-flanking bases on a triplex with a 3'-C^+.GC triplet.

3.3.2.1. The formation of 12-mer triplex with 12-mer-C TFO

All the results presented above concern triplexes that have a 3'-terminal T.AT triplet (or a C.AT mismatch). In order to assess how this terminal triplet affects the properties of the triplex we changed the base at the 3'-end of the oligopurine tract from adenine to guanine, in fragments with the four different 3'-flanking bases. This generated fragments GA, GC, GT and GG. These form a 12-mer triplex with oligo 12-mer-C (5'-CTCTTTTTTCTC-3'), that is the same as that with 12-mer-T, but ends in a C^+.GC triplet instead of T.AT. By comparison with the previous results this will enable us to examine how the base pair at the 3'-end of the target site affects the triplex affinity and the associated enhancements. Footprinting experiments were performed with these four new variants of the *tyr*T sequence. 12-mer-C produces a complex with 12 canonical triplets with these targets, and the results with this oligo were compared with 12-mer-T, which produces an 11-mer triplex followed by a T.GC triplet mismatch. The 11-mer TFO was also included in these studies.

DNase I footprints for the interaction of 12-mer-C with the four *tyr*T sequence variants are shown in Figures 3.27. These were performed under the same conditions as the experiments described previously. The gels show concentration dependent footprints with all four variants, which persists to concentrations of about 0.2 μM. This is lower than the triplexes with the terminal T.AT triplet, for which the footprints persist to about 1 μM. This stronger binding is consistent with the known greater stability of C^+.GC than T.AT. The footprints are also accompanied by enhanced cleavage at the 3'-end of the target site, at the triplex-duplex junction. For all these variants, the DNase I footprints are larger than the actual target site and persist for about 3 bases above the 5'-end; attenuated cleavage is also observed below (3'-) the target site below the enhancement at the triplex-duplex junctions. The intensity of the enhanced bands is similar to those with AC, AG, AA and AT for which GC was the greatest (Table 3.6). Quantitative analyses of the concentration dependence of these enhancements are presented in Figures 3.28 and the calculated C_{50} values are presented in Table 3.6 and show that GC and GT seem to give the lowest value though these are not significantly different.

5′-…CAACCAXCTCTTTTTTCTCTTCCTAACACTT…-3′
3′-…GTTGGTXGAGAAAAAAAGAGAAGGATTGTGAA…-5′
3′-CTCTTTTTTCTC-5′ (12-mer-C TFO)

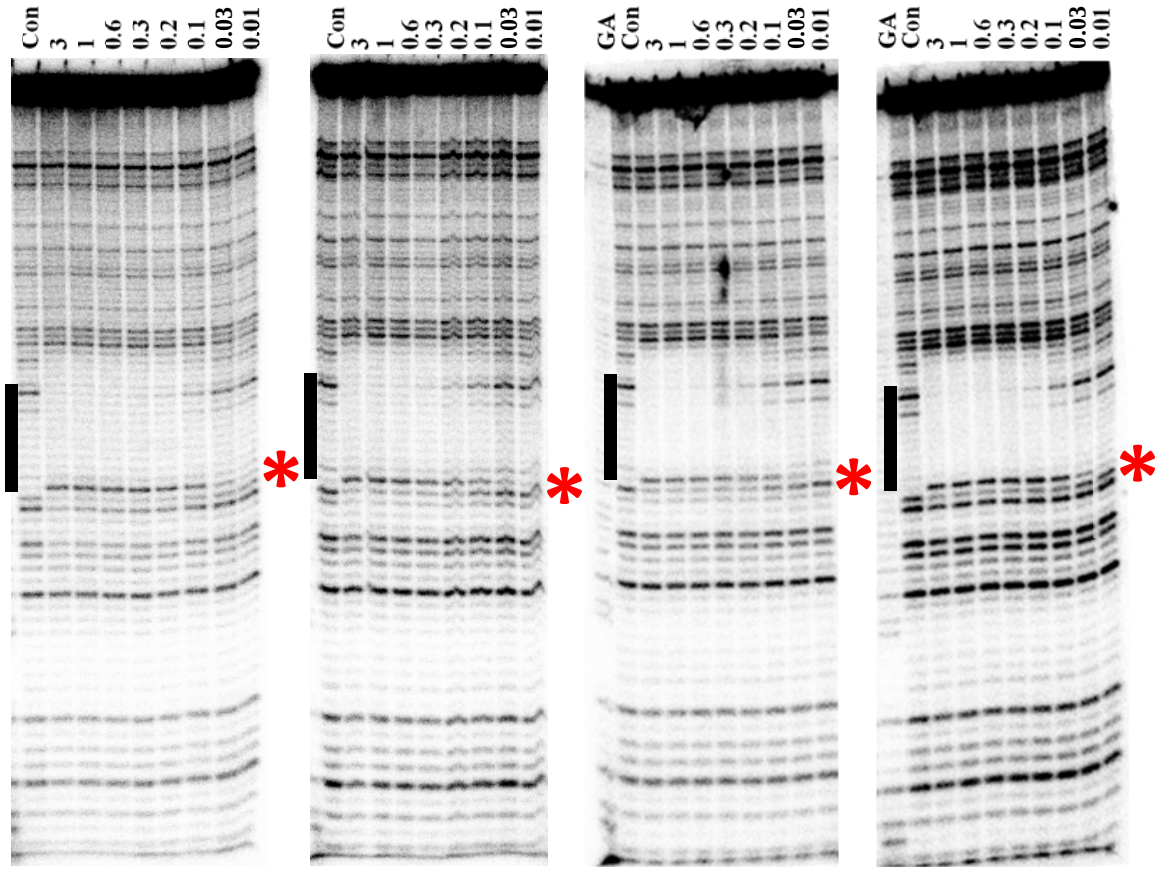

Figure 3.27 DNase I cleavage patterns of the four *tyr*T fragments in the presence of the 12-mer-C TFO. X is C, G, A and T in turn. These experiments were performed in 50 mM NaOAc at pH 5.0 in the presence of 1 mM $MgCl_2$ and equilibrated for 2 hours at room temperature before digesting with the enzyme. TFO concentrations (μM) are shown at the top of each gel lane. The tracks labelled "GA" and "con" are Maxam-Gilbert markers specific for purines and the cleavage patterns in the absence of TFOs respectively. The filled boxes indicate the location of the triplex target sites and the red asterisks show the positions of enhanced DNase I cleavage.

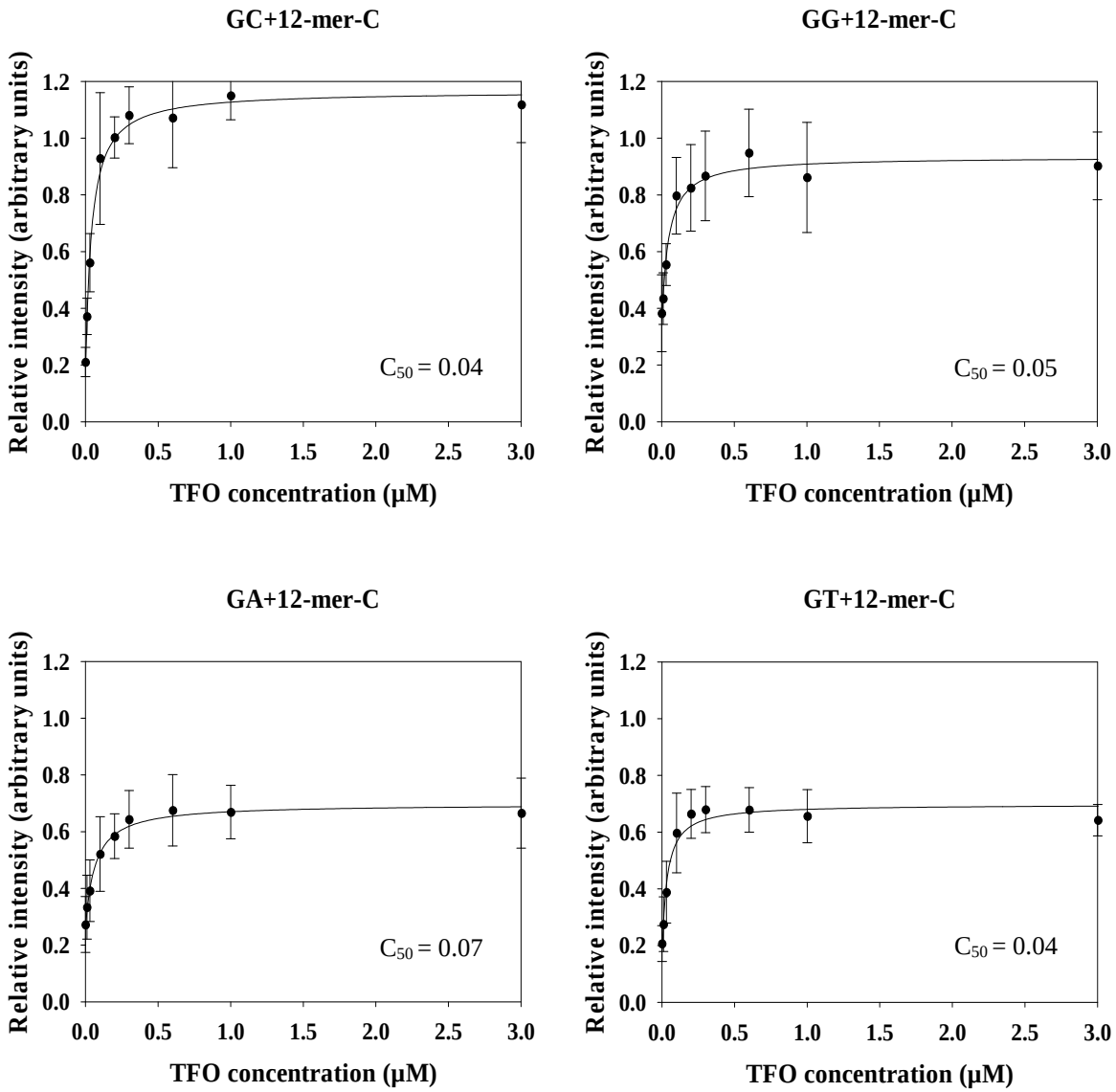

Figure 3.28 Footprinting plots showing the relative intensity of the enhanced band (arbitrary units) as a function of TFO concentration (µM). These were obtained from the DNase I footprinting gels of with 12-mer-C, which are shown in Figure 3.27. GC (top left), GG (top right), GA (bottom left) and GT (bottom right). The calculated C_{50} values, which correspond to the TFO concentrations at which the relative intensity is half the maximum, are shown in Table 3.6. The curves correspond to a simple binding equation that was fitted to the data.

*tyr*T derivatives	12-mer-C TFO	
	Enhanced band intensities (Relative arbitrary unit)	**C_{50} values (μM)**
GC	1.12±0.13	0.04±0.01
GG	0.80±0.07	0.05±0.02
GA	0.67±0.12	0.07±0.01
GT	0.64±0.06	0.04±0.02

Table 3.6 The intensities of enhanced bands at the highest TFO concentration (relative arbitrary unit) and C_{50} values (μM) and Enhanced band intensities (relative arbitrary unit) obtained from the DNase I footprinting plots of triplexes formed between 12-mer-C TFO and GC, GG, GA and GT respectively.

Cleavage by other agents was also conducted for these triplexes. The reaction with DEPC is shown in Figure 3.29. Although the bands within the oligopurine tract show reduced intensity in the presence of the TFO, no cleavage enhancements are evident with any of these fragments. Interestingly, the DEPC modification patterns of the free DNA controls (con) of these *tyr*T variants differ from those found in sequences with a 3'-terminal A due to the replacement of adenine by guanine.

The results of modification experiments with $KMnO_4$ are shown in Figure 3.30. As seen with the triplexes ending in T.AT there are no TFO-induced changes in the cleavage pattern with the 12-mer-C TFO. This is especially noteworthy for GT, which contains an additional thymine at the triplex-duplex junction.

Similarly none of the four duplex targets show TFO-induced changes in the micrococcal nuclease (Figure 3.31) or the hydroxyl radical (Figure 3.32) cleavage patterns. Again the decreased hydroxyl cleavage within the binding sites are evident in all four variant sequences (Figure 3.33).

5′-…CAACCAXCTCTTTTTTCTCTTCCTAACACTT…-3′
3′-…GTTGGTXGAGAAAAAAGAGAAGGATTGTGAA…-5′
3′-CTCTTTTTTCTC-5′ (12-mer-C TFO)

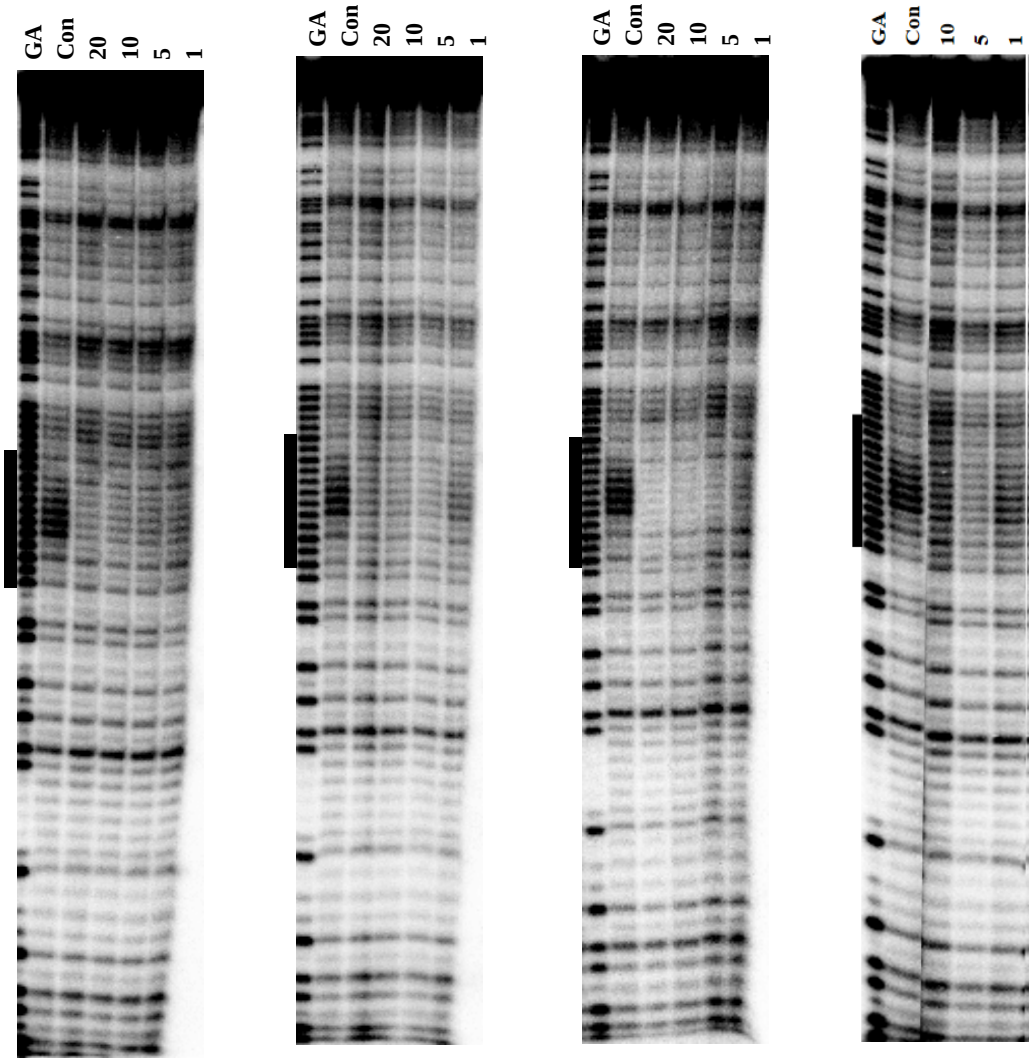

GC **GG** **GA** **GT**

Figure 3.29 DEPC cleavage patterns of the four *tyr*T sequences, GC, GG, GA, and GT, in the presence of the 12-mer-C TFO. These experiments were performed in 50 mM NaOAc at pH 5.0 in the presence of 1 mM $MgCl_2$ and equilibrated for 2 hours at room temperature, before adding DEPC. TFO concentrations (µM) are shown at the top of each gel lane. The tracks labelled "GA" and "con" are Maxam-Gilbert markers specific for purines and the cleavage patterns in the absence of TFOs respectively. The filled boxes indicate the location of the triplex target sites. The 20 µM lane for GT was cropped out as it was an abnormal cleavage.

5′-…CAACCAXCTCTTTTTTCTCTTCCTAACACTT…-3′
3′-…GTTGGTXGAGAAAAAAGAGAAGGATTGTGAA…-5′
3′-CTCTTTTTTCTC-5′ (12-mer-C TFO)

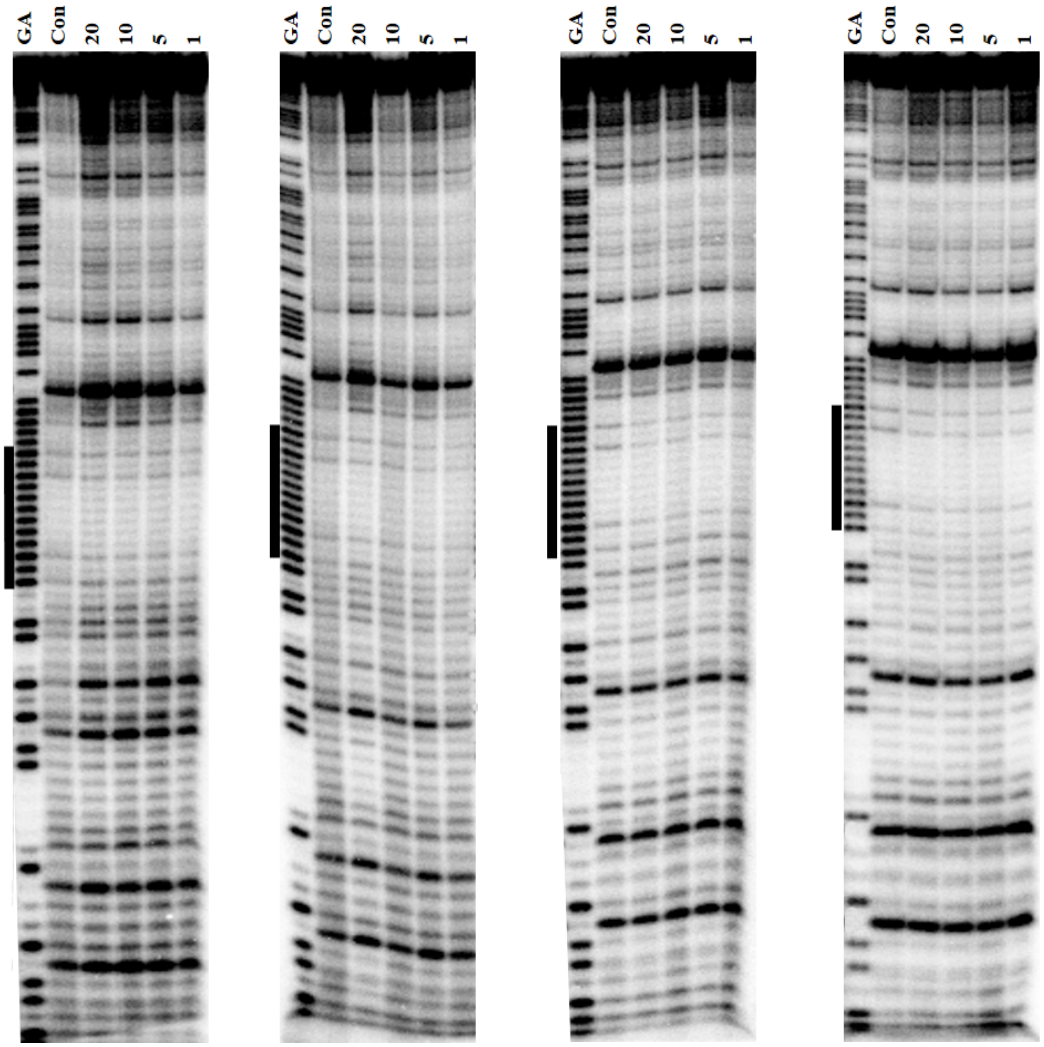

GC **GG** **GA** **GT**

Figure 3.30 $KMnO_4$ cleavage patterns of the four *tyr*T DNA fragments, GC, GG, GA, and GT in the presence of the 12-mer-C TFO. These experiments were performed in 50 mM NaOAc at pH 5.0 in the presence of 1 mM $MgCl_2$ and equilibrated for 2 hours at room temperature before the addition of $KMnO_4$. The TFO concentrations (μM) are shown at the top of each gel lane. The tracks labelled "GA" and "con" are Maxam-Gilbert markers specific for purines and the cleavage patterns in the absence of TFOs respectively. The filled boxes indicate the location of the triplex target sites.

5′-…CAACCAXCTCTTTTTTCTCTTCCTAACACTT…-3′
3′-…GTTGGTXGAGAAAAAAGAGAAGGATTGTGAA…-5′
3′-CTCTTTTTTCTC-5′ (12-mer-C TFO)

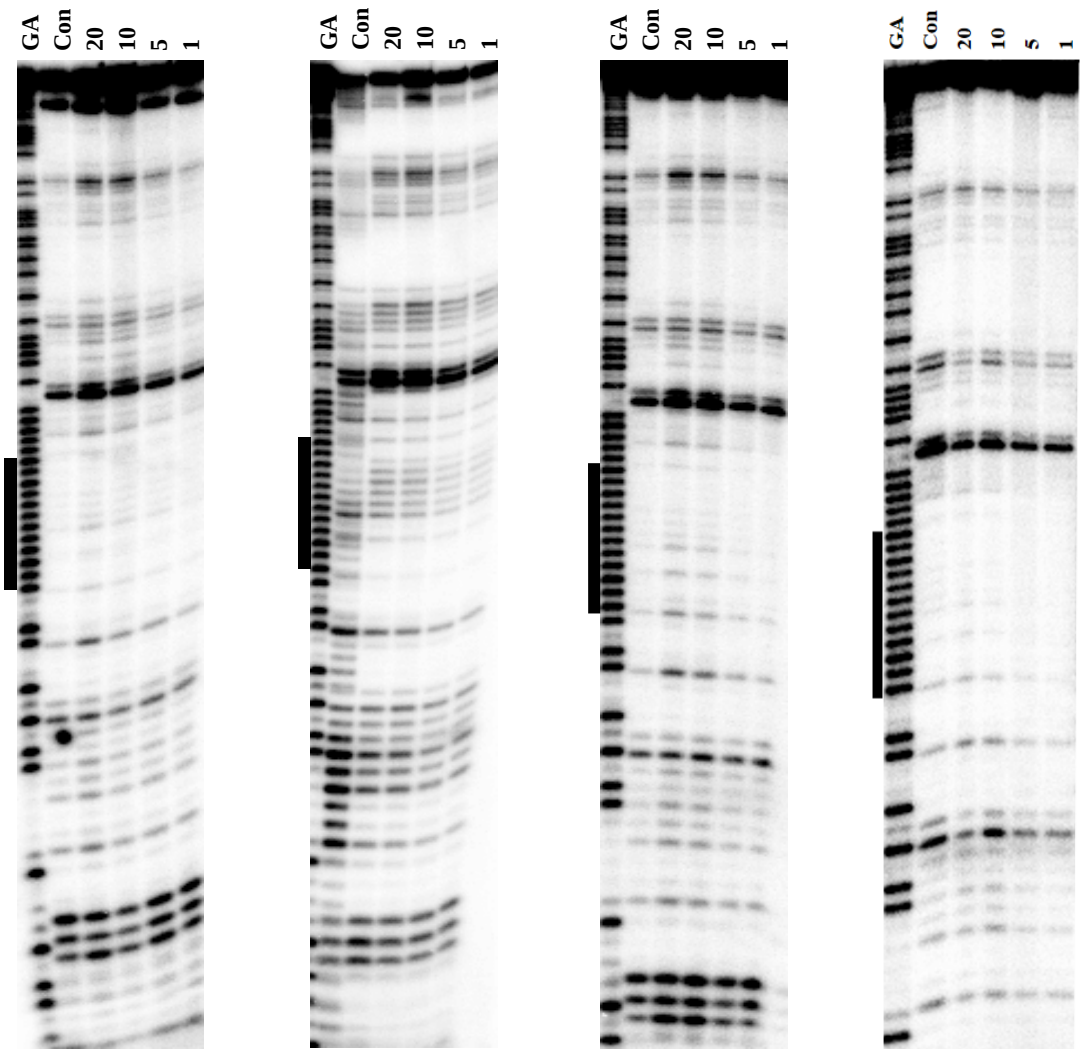

Figure 3.31 Micrococcal nuclease cleavage patterns of the four *tyr*T DNA fragments; GC, GG, GA, and GT in the presence of the 12-mer-C TFO. These experiments were performed in 50 mM NaOAc at pH 5.0 in the presence of 1 mM $MgCl_2$ and equilibrated for 2 hours at room temperature before addition of the enzyme. The TFO concentrations (μM) are shown at the top of each gel lane. The tracks labelled "GA" and "con" are Maxam-Gilbert markers specific for purines and the cleavage patterns in the absence of TFOs respectively. The filled boxes indicate the location of the triplex target sites.

5′-…CAACCAXCTCTTTTTTCTCTTCCTAACACTT…-3′
3′-…GTTGGTXGAGAAAAAAGAGAAGGATTGTGAA…-5′
3′-CTCTTTTTTCTC-5′ (12-mer-C TFO)

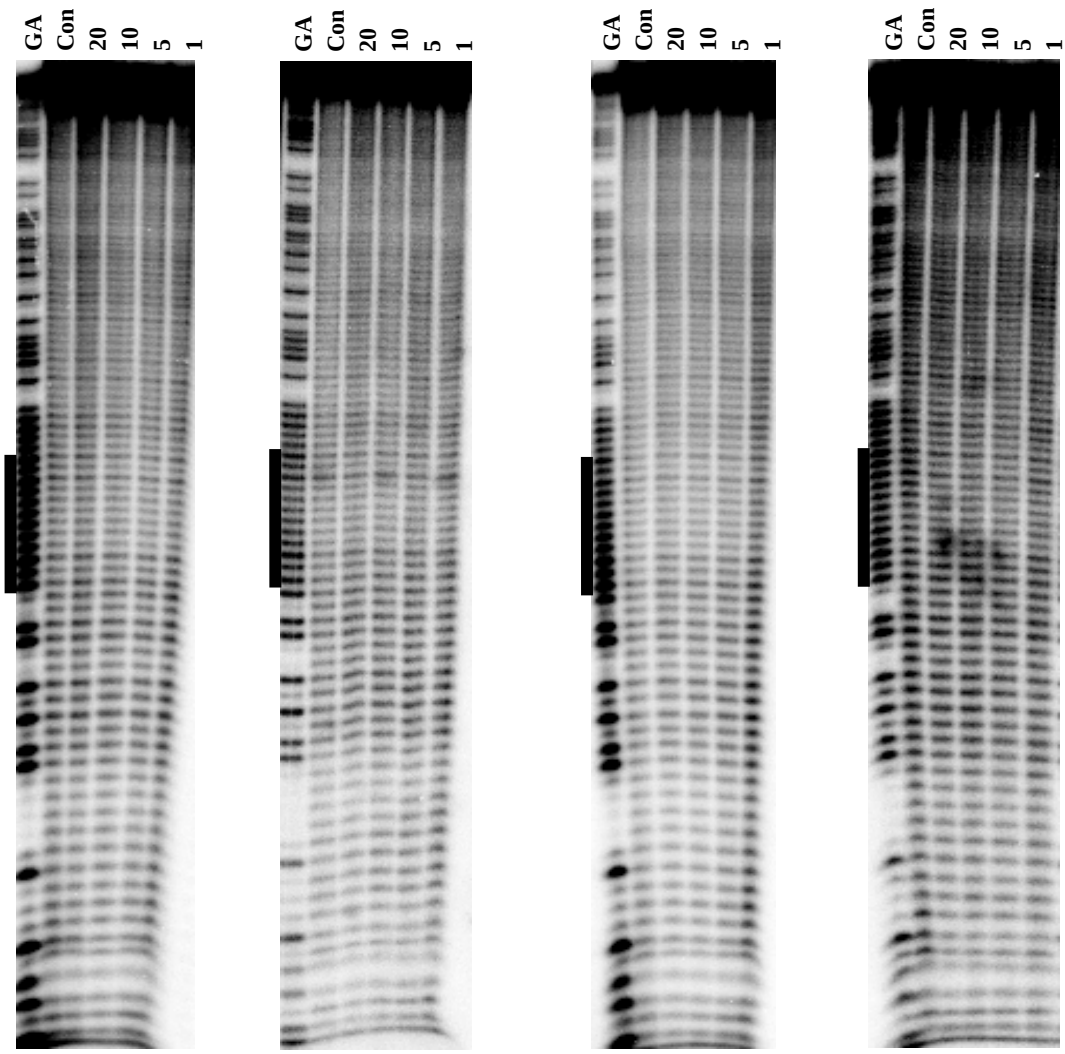

GC **GG** **GA** **GT**

Figure 3.32 Hydroxyl radical cleavage patterns of the four *tyr*T fragment GC, GG, GA, and GT in the presence of the 12-mer-C TFO. These experiments were performed in 50 mM NaOAc at pH 5.0 in the presence of 1 mM $MgCl_2$ and equilibrated for 2 hours at room temperature before adding the hydroxyl radical mixture. The TFO concentrations (μM) are shown at the top of each gel lane. Tracks labelled "GA" and "con" are Maxam-Gilbert markers specific for purines and the cleavage patterns in the absence of TFOs respectively. The filled boxes indicate the location of the triplex target sites.

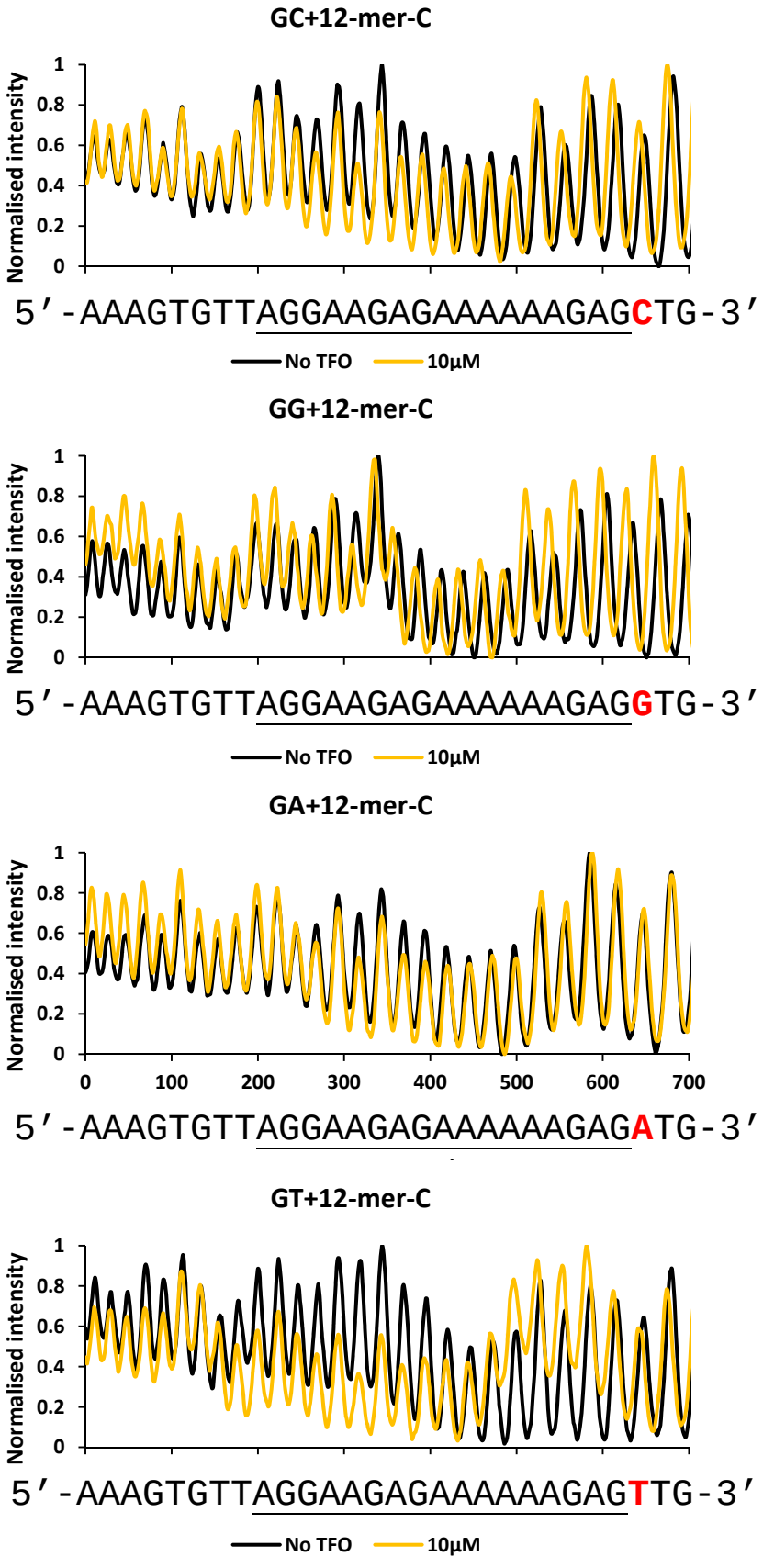

Figure 3.33 Densitometer plots of hydroxyl radical cleavage of the four fragments in the absence (black) and presence (yellow) of 10 μM of the 12-mer-C TFO (taken from the gels shown Figure in 3.32).

3.3.2.2. The formation of 11-mer triplex

We also investigated the interaction of the 11-mer TFO with the target sites that end in a 3'-G. This triplex is identical to that formed between this TFO and the targets ending in A, though the immediate 3'-flanking base is G instead of A. The results of the DNase I footprinting experiments are shown in Figures 3.34 showing concentration dependent footprints that persist to a concentration of about 1 μM. This concentration is about 10 times higher than that required to produce DNase I footprints with 12-mer-C at this target sequence. These footprints are accompanied by enhanced cleavage, which as expected, is located at a band one position higher than with 12-mer-C. Footprinting plots derived from these data are shown in Figure 3.35 and the C_{50} values derived from these data are presented in Table 3.7. The values for each of the duplexes are not significantly different from each other. Interestingly these are almost ten-fold higher than those with 12-mer-C as a results of missing a 3'-C^+.GC. The results of footprinting experiments with DEPC, $KMnO_4$, Micrococcal nuclease and hydroxyl radical are presented in Figures 3.36-3.40. Unsurprisingly, these are similar to those generated with 12-mer-C.

5′-…CAACCAXCTCTTTTTTCTCTTCCTAACACTT…-3′
3′-…GTTGGTXGAGAAAAAAGAGAAGGATTGTGAA…-5′
3′-TCTTTTTTCTC-5′ (11-mer TFO)

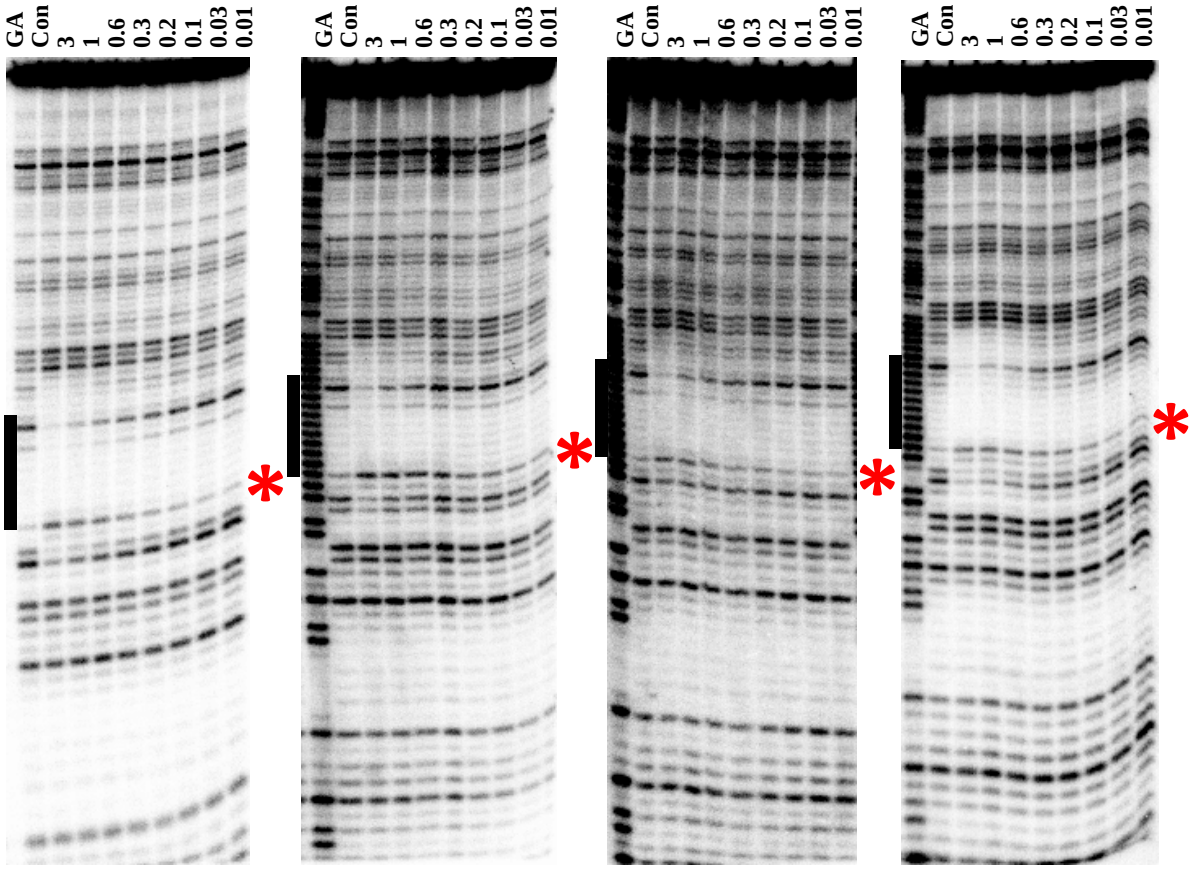

Figure 3.34 DNase I cleavage patterns of the four *tyr*T fragments in the presence of the 11-mer TFO. X is C, G, A and T in turn. These experiments were performed in 50 mM NaOAc at pH 5.0 in the presence of 1 mM $MgCl_2$ and were equilibrated for 2 hours at room temperature before adding the enzyme. TFO concentrations (μM) are shown at the top of each gel lane. The tracks labelled "GA" and "con" are Maxam-Gilbert markers specific for purines and the cleavage patterns in the absence of TFO respectively. The filled boxes indicate the location of the triplex target sites and the red asterisks show the positions of enhanced DNase I cleavage.

.

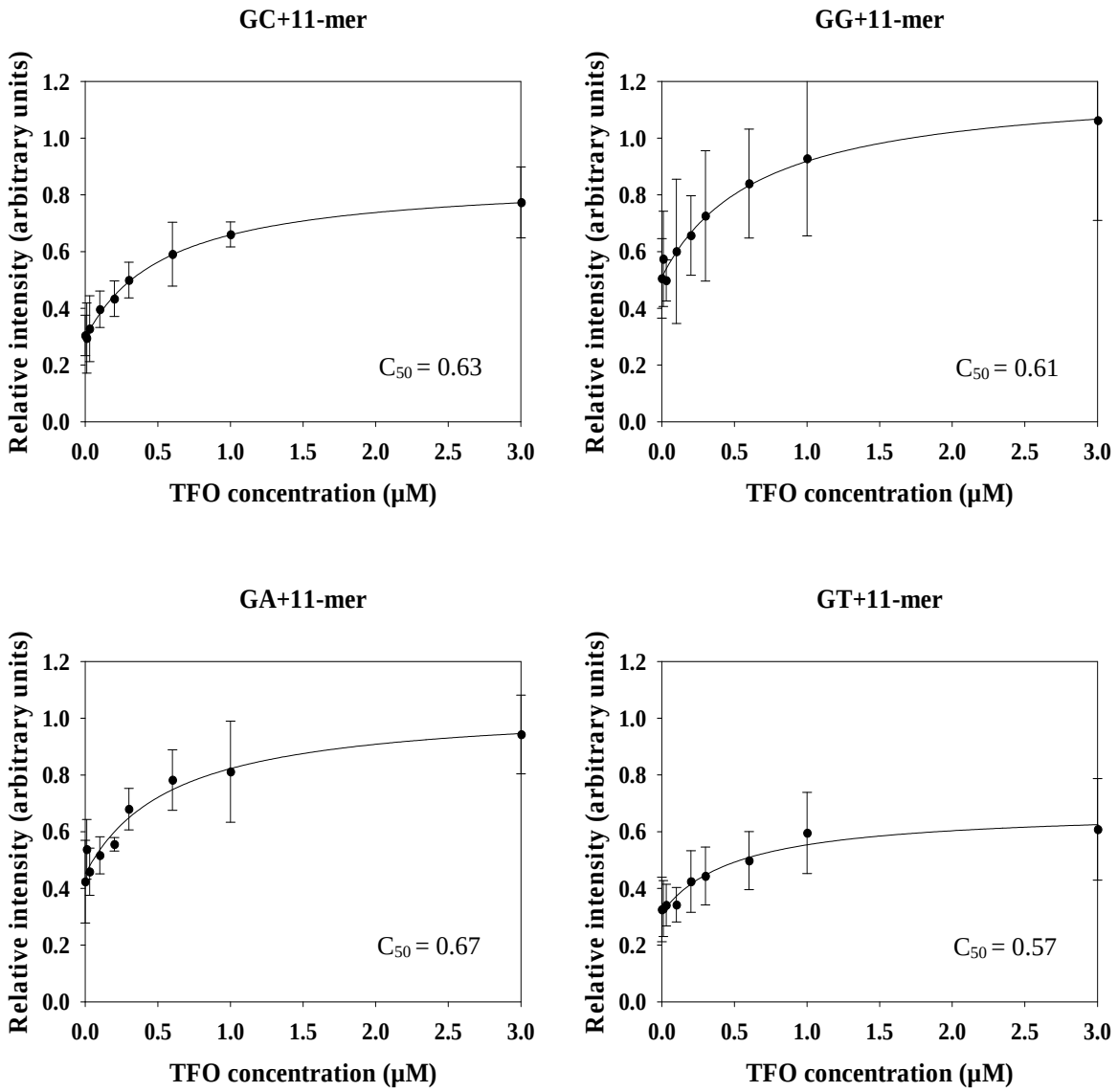

Figure 3.35 Footprinting plots showing the relative intensities of the enhanced band (arbitrary units) as a function of TFO concentration (μM). These were obtained from the DNase I footprinting gels of the 11-mer TFO as shown in Figures 3.34. GC (top left), GG (top right), GA (bottom left) and GT (bottom right). The C_{50} values, which correspond to the TFO concentrations at which the relative intensity is half the maximum, are obtained and shown in Table 3.7. The curves correspond to a simple binding equation that was fitted to the data.

***tyr*T derivative**	**11-mer TFO**	
	Enhanced band intensities (relative arbitrary unit)	**C_{50} values (μM)**
GC	0.83±0.05	0.63±0.04
GG	1.19±0.16	0.61±0.30
GA	0.94±0.14	0.67±0.43
GT	0.74±0.09	0.57±0.33

Table 3.7 The intensities of enhanced bands at the highest TFO concentration (relative arbitrary unit) and C_{50} values (μM) obtained from the DNase I footprinting plots of triplexes formed between 11-mer TFOs and GC, GG, GA and GT respectively.

5′-…CAACCAGCTCTTTTTTCTCTTCCTAACACTT…-3′
3′-…GTTGGTXGAGAAAAAAGAGAAGGATTGTGAA…-5′
3′-TCTTTTTTCTC-5′ (11-mer TFO)

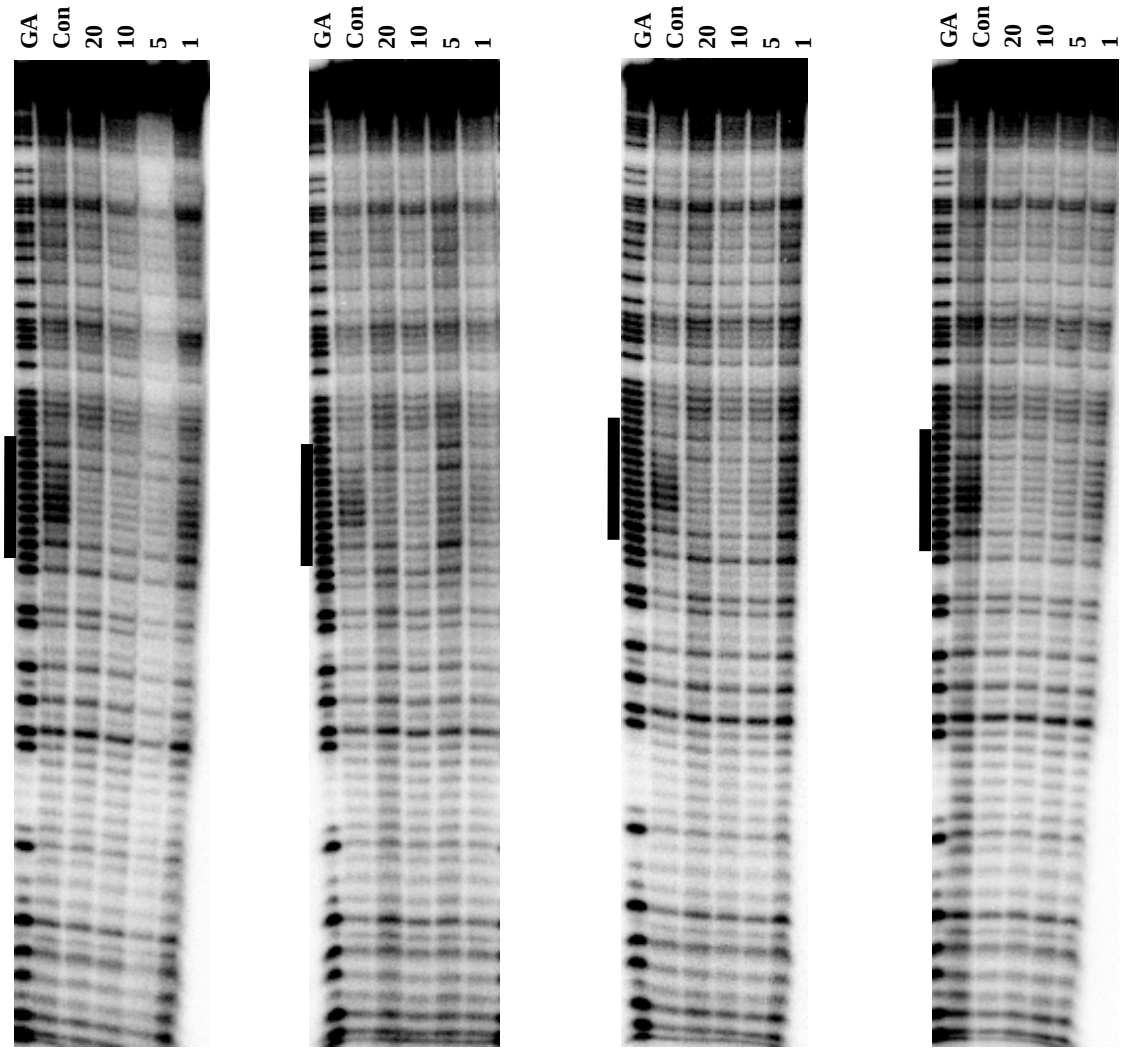

GC **GG** **GA** **GT**

Figure 3.36 DEPC cleavage patterns of the four *tyr*T sequences, GC, GG, GA, and GT in the presence of the 11-mer TFO. These experiments were performed in 50 mM NaOAc at pH 5.0 in the presence of 1 mM $MgCl_2$ and equilibrated for 2 hours at room temperature before adding the DEPC. TFO concentrations (μM) are shown at the top of each gel lane. The tracks labelled "GA" and "con" are Maxam-Gilbert markers specific for purines and the cleavage patterns in the absence of TFO respectively. The filled boxes indicate the locations of the triplex target sites.

5′-…CAACCAGCTCTTTTTTCTCTTCCTAACACTT…-3′
3′-…GTTGGTXGAGAAAAAAGAGAAGGATTGTGAA…-5′
3′-TCTTTTTTCTC-5′ (11-mer TFO)

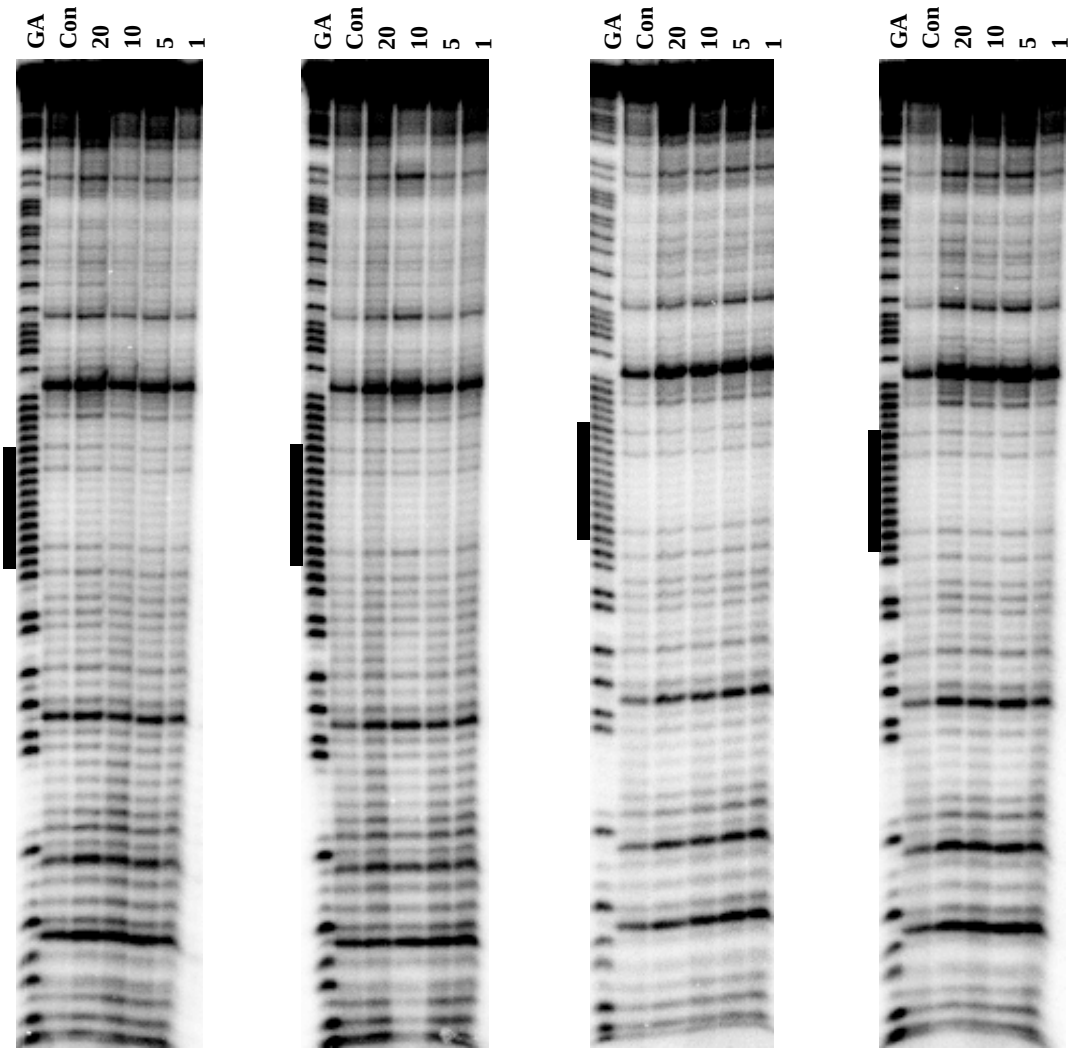

Figure 3.37 $KMnO_4$ cleavage patterns of the four *tyr*T sequences, GC, GG, GA, and GT in the presence of the 11-mer TFO. These experiments were performed in 50 mM NaOAc at pH 5.0 in the presence of 1 mM $MgCl_2$ and equilibrated for 2 hours at room temperature before adding the $KMnO_4$. TFO concentrations (μM) are shown at the top of each gel lane. The tracks labelled "GA" and "con" are Maxam-Gilbert markers specific for purines and the cleavage patterns in the absence of TFOs respectively. The filled boxes indicate the location of the triplex target sites.

5′-…CAACCAGCTCTTTTTTCTCTTCCTAACACTT…-3′
3′-…GTTGGTXGAGAAAAAAGAGAAGGATTGTGAA…-5′
3′-TCTTTTTTCTC-5′ (11-mer TFO)

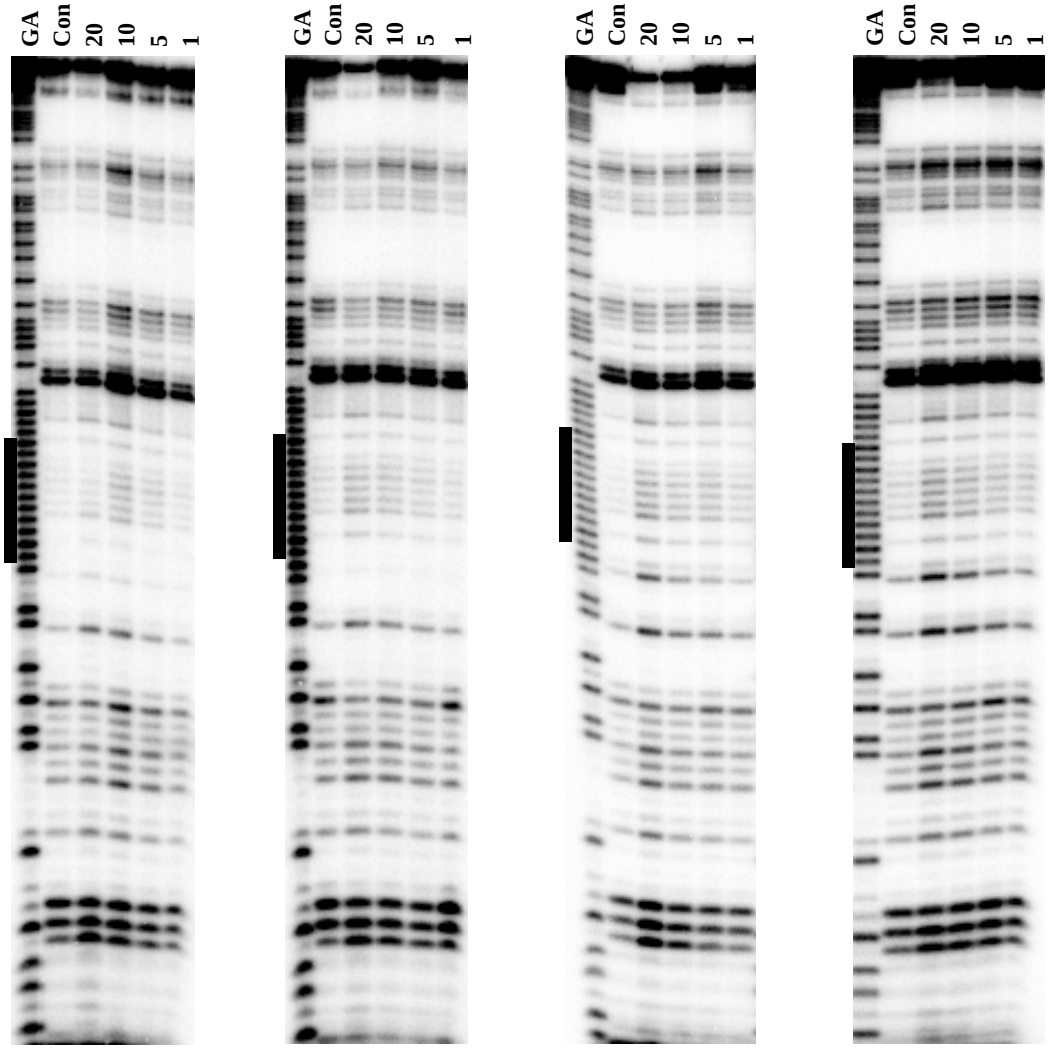

Figure 3.38 Micrococcal nuclease cleavage patterns of the four *tyr*T sequences, GC, GG, GA, and GT in the presence of the 11-mer TFO. These experiments were performed in 50 mM NaOAc at pH 5.0 in the presence of 1 mM $MgCl_2$ and equilibrated for 2 hours at room temperature before adding the enzyme. TFO concentrations (μM) are shown at the top of each gel lane and the tracks labelled "GA" and "con" are Maxam-Gilbert markers specific for purines and the cleavage patterns in the absence of TFOs respectively. The filled boxes indicate the location of the triplex target sites.

5′-…CAACCAGCTCTTTTTTCTCTTCCTAACACTT…-3′
3′-…GTTGGTXGAGAAAAAAGAGAAGGATTGTGAA…-5′
3′-TCTTTTTTCTC-5′ (11-mer TFO)

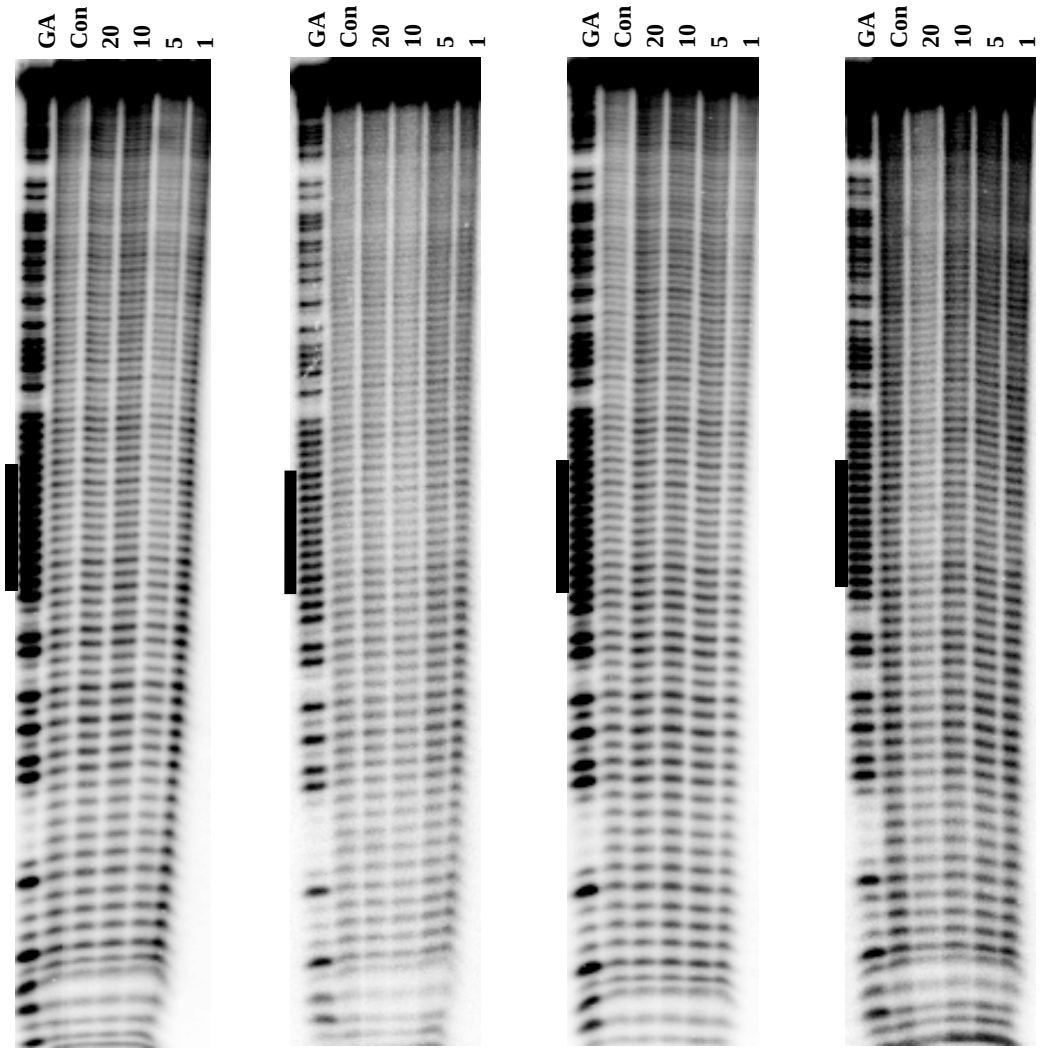

GC **GG** **GA** **GT**

Figure 3.39 Hydroxyl radical cleavage patterns of the four *tyr*T sequences, GC, GG, GA, and GT in the presence of the 11-mer TFO. These experiments were performed in 50 mM NaOAc at pH 5.0 in the presence of 1 mM $MgCl_2$ and equilibrated for 2 hours at room temperature before adding the hydroxyl radical mixture. TFO concentrations (μM) are shown at the top of each gel lane. Tracks labelled "GA" and "con" are Maxam-Gilbert markers specific for purines and the cleavage patterns in the absence of TFO respectively. The filled boxes indicated the location of the triplex target sites.

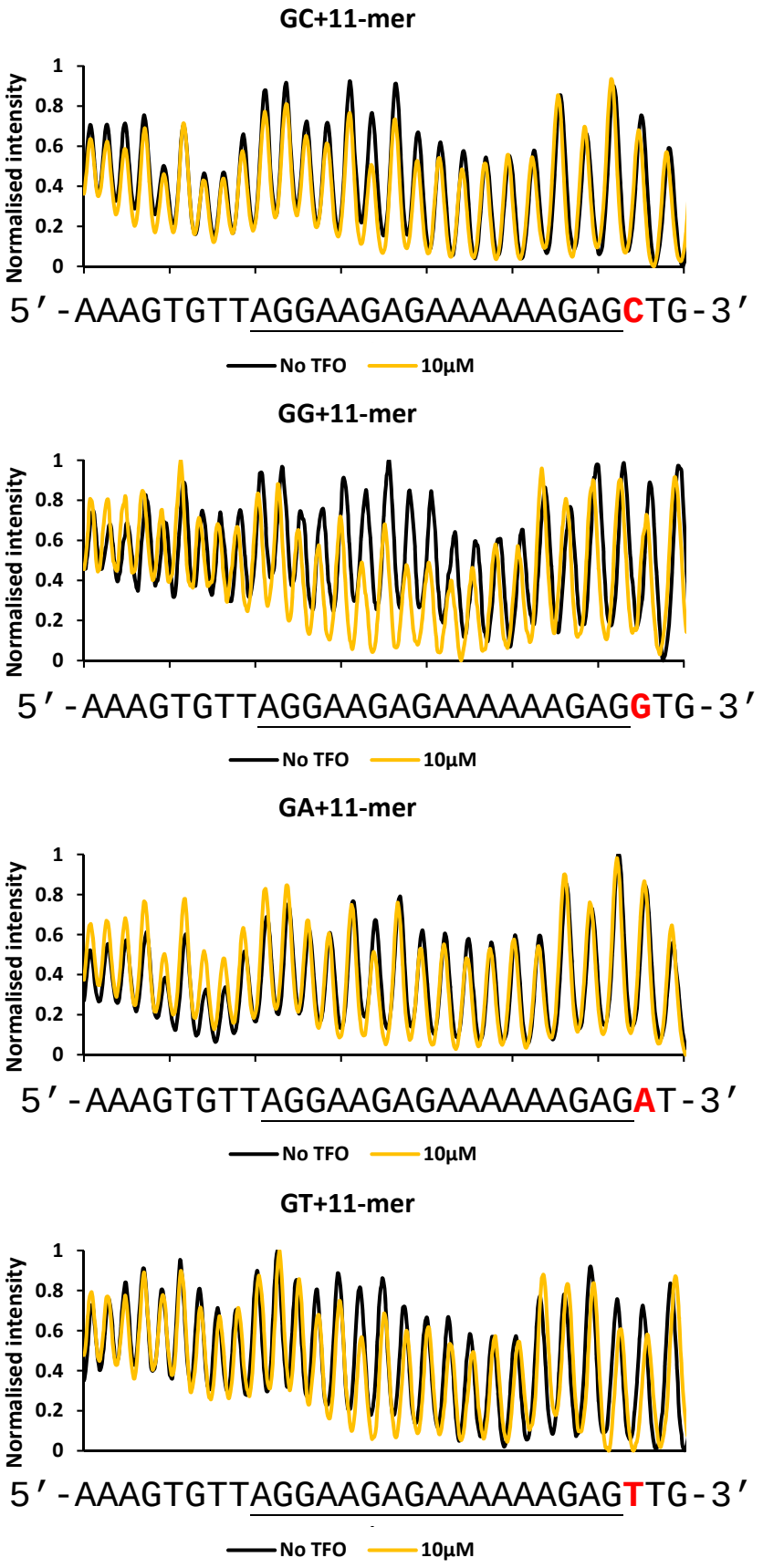

Figure 3.40 Densitometer plots of hydroxyl radical cleavage of the four fragments in the absence (black) and presence (yellow) of 10 μM of the 11-mer TFO (taken from the gels shown Figure in 3.39).

3.3.2.3. The formation of a 12-mer triplex with a 3’-end mismatch

We also examined the interaction of the 12-mer-T TFO with these target sites that contain a 3’-terminal guanine. This should generate a triplex with 11 canonical triplets with a 3’-terminal T.GC mismatch. DNase I footprints for this interaction are shown in Figure 3.41. Although the 12-mer-T TFO produces footprints these are only apparent at the highest concentrations (3 μM). This is almost 10 times higher than the concentrations required to produce footprints with 12-mer-C. These footprints are also accompanied by weak enhancements, which are one base higher than those seen with 12-mer-C; but at the same position as with 11-mer. These enhancements are in the same positions as those found in the triplexes formed by 12-mer-C and 11-mer with the AC, AG, AA and AC variants. The footprinting plots generated from these cleavage patterns are shown in Figure 3.42 and the calculated C_{50} values are presented in Table 3.8. These confirm there are no significant differences in the affinity of the 12-mer-T TFO with each of these duplex targets, thought these C_{50} values are almost ten-fold higher than those with 12-mer-C. The values are very similar to those with 11-mer, as expected, as they contain the same number of canonical triplets.

The results of similar footprinting experiments with DEPC, $KMnO_4$, micrococcal nuclease and hydroxyl radicals are shown in Figures 3.43, 3.44, 3.45 ,and 3.46 and 3.47 respectively. These show no significant changes in the cleavage patterns in the presence of this TFO.

5′-…CAACCAXCTCTTTTTTCTCTTCCTAACACTT…-3′
3′-…GTTGGTXGAGAAAAAAGAGAAGGATTGTGAA…-5′
3′-TTCTTTTTTCTC-5′ (12-mer-T TFO)

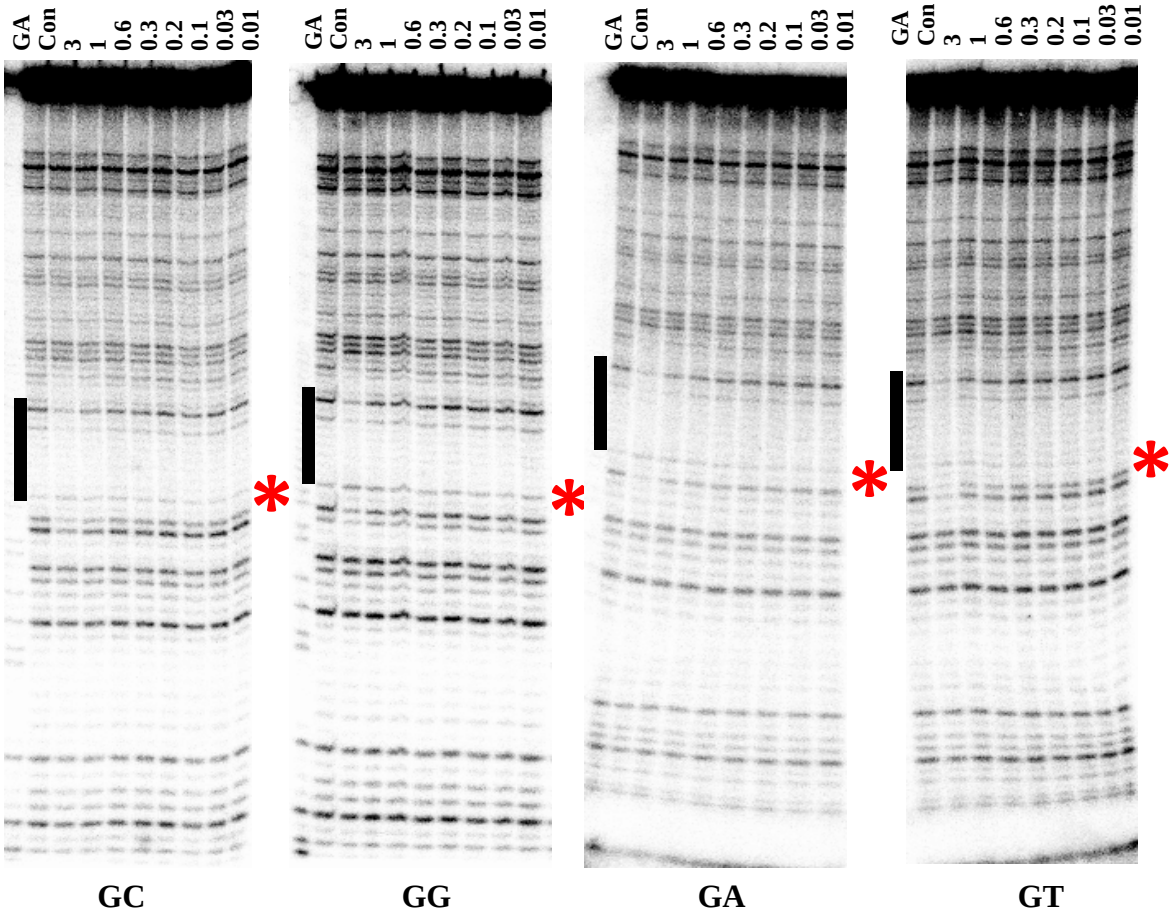

Figure 3.41 DNase I cleavage patterns of the *tyr*T fragments GC, GG, GA and GT in the presence of the 12-mer-T TFO. These experiments were performed in 50 mM NaOAc at pH 5.0 in the presence of 1 mM $MgCl_2$ and equilibrated for 2 hours at room temperature before adding the enzyme. TFO concentrations (μM) are shown at the top of each gel lane. The tracks labelled "GA" and "con" are Maxam-Gilbert markers specific for purines and the cleavage patterns in the absence of TFOs respectively. The filled boxes indicate the location of the triplex target sites and the red asterisks show the position of enhanced DNase I cleavage.

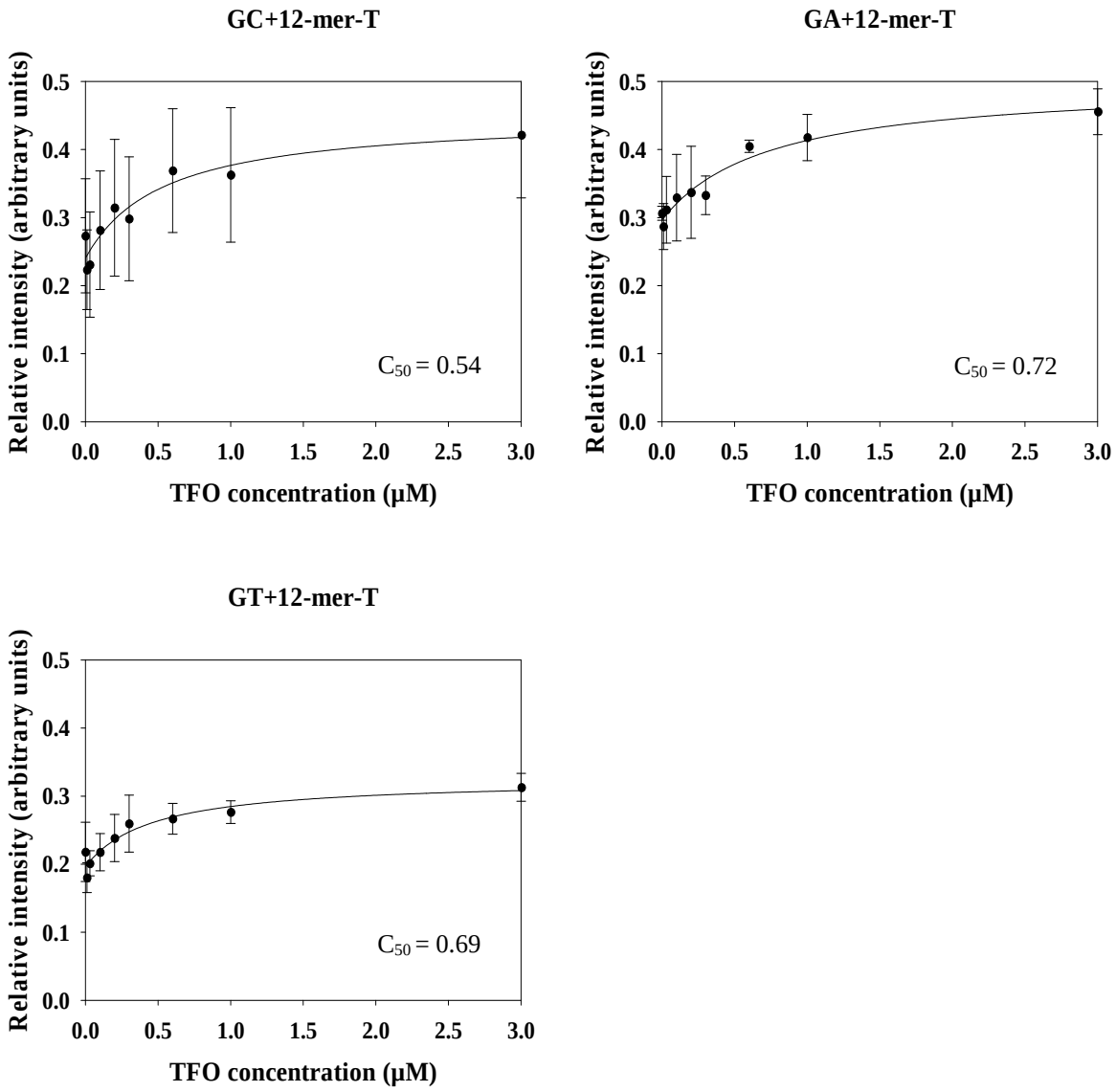

Figure 3.42 Footprinting plots showing the relative intensity of the enhanced band (arbitrary units) as a function of TFO concentration (µM). These were obtained from the DNase I footprinting gels with the 12-mer-T TFO that are shown in Figures 3.41. GC (top left), GA (top right) and GT (bottom left). The C_{50} values, which correspond to the TFO concentrations at which the relative intensity is half the maximum, are obtained and shown in Table 3.8. The curves correspond to a simple binding equation that was fitted to the data.

***tyr*T derivatives**	**12-mer-T TFO**	
	Enhanced band intensities (relative arbitrary unit)	**C_{50} values (μM)**
GC	0.42±0.09	0.54±0.37
GG	N/A	N/A
GA	0.49±0.02	0.72±0.12
GT	0.31±0.02	0.69±0.63

Table 3.8 The intensities of enhanced bands at the highest TFO concentration (relative arbitrary unit) and C_{50} values (μM) and enhanced band intensities (relative arbitrary unit) obtained from the DNase I footprinting plots of triplexes formed between 12-mer-T and GC, GG, GA and GT respectively.

5′-…CAACCAXCTCTTTTTTCTCTTCCTAACACTT…-3′
3′-…GTTGGTXGAGAAAAAAGAGAAGGATTGTGAA…-5′
3′-TTCTTTTTTCTC-5′ (12-mer-T TFO)

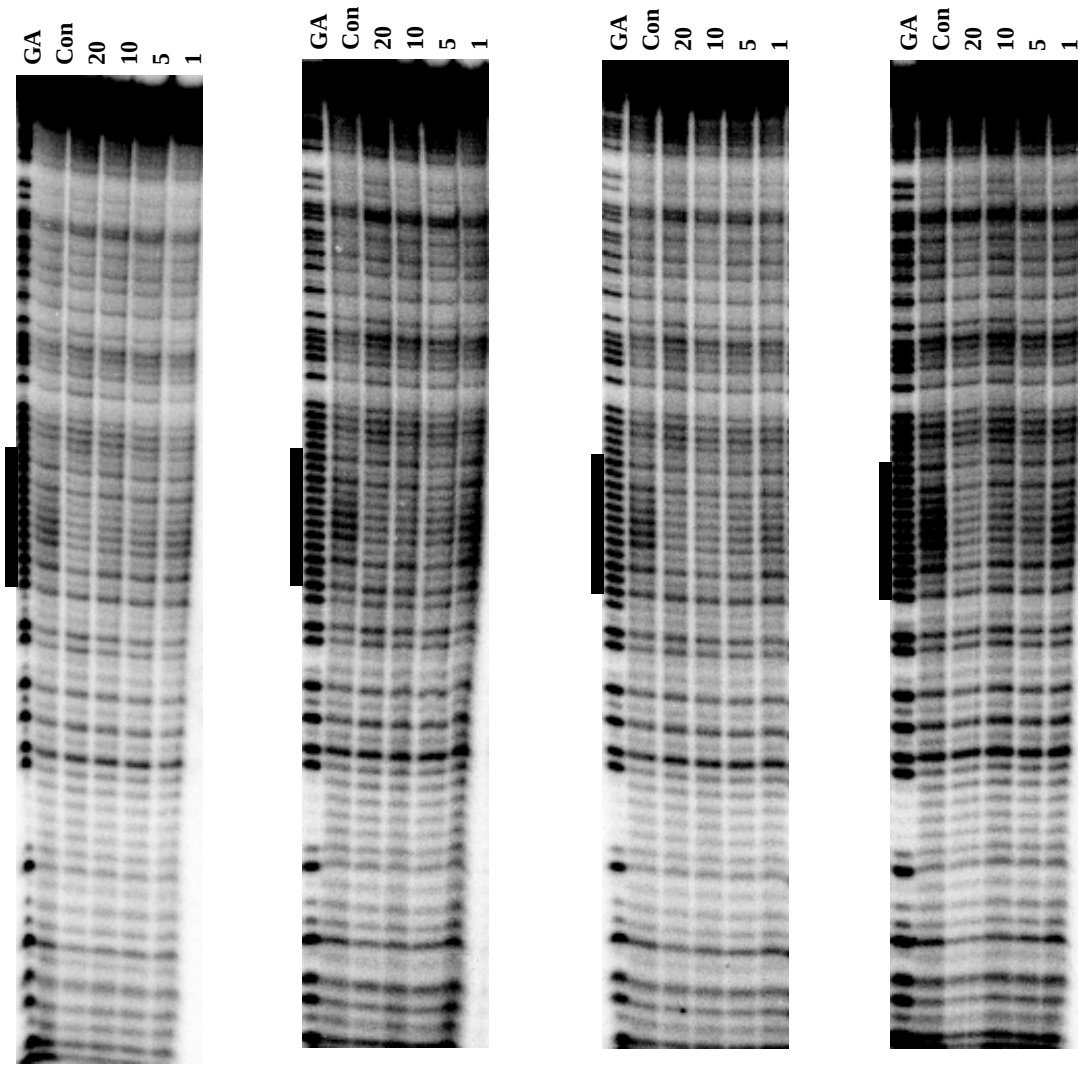

GC **GG** **GA** **GT**

Figure 3.43 DEPC cleavage patterns of four modified *tyr*T fragments (GC, GG, GA and GT) in the presence of the 12-mer-T TFO. These experiments were performed in 50 mM NaOAc at pH 5.0 in the presence of 1 mM $MgCl_2$ and equilibrated for 2 hours at room temperature before adding DEPC. The TFO concentrations (μM) are shown at the top of each gel lane. The tracks labelled "GA" and "con" are Maxam-Gilbert markers specific for purines and the cleavage patterns in the absence of TFOs respectively. The filled boxes indicate the location of the triplex target sites.

5′-…CAACCAXCTCTTTTTTCTCTTCCTAACACTT…-3′
3′-…GTTGGTXGAGAAAAAAGAGAAGGATTGTGAA…-5′
3′-TTCTTTTTTCTC-5′ (12-mer-T TFO)

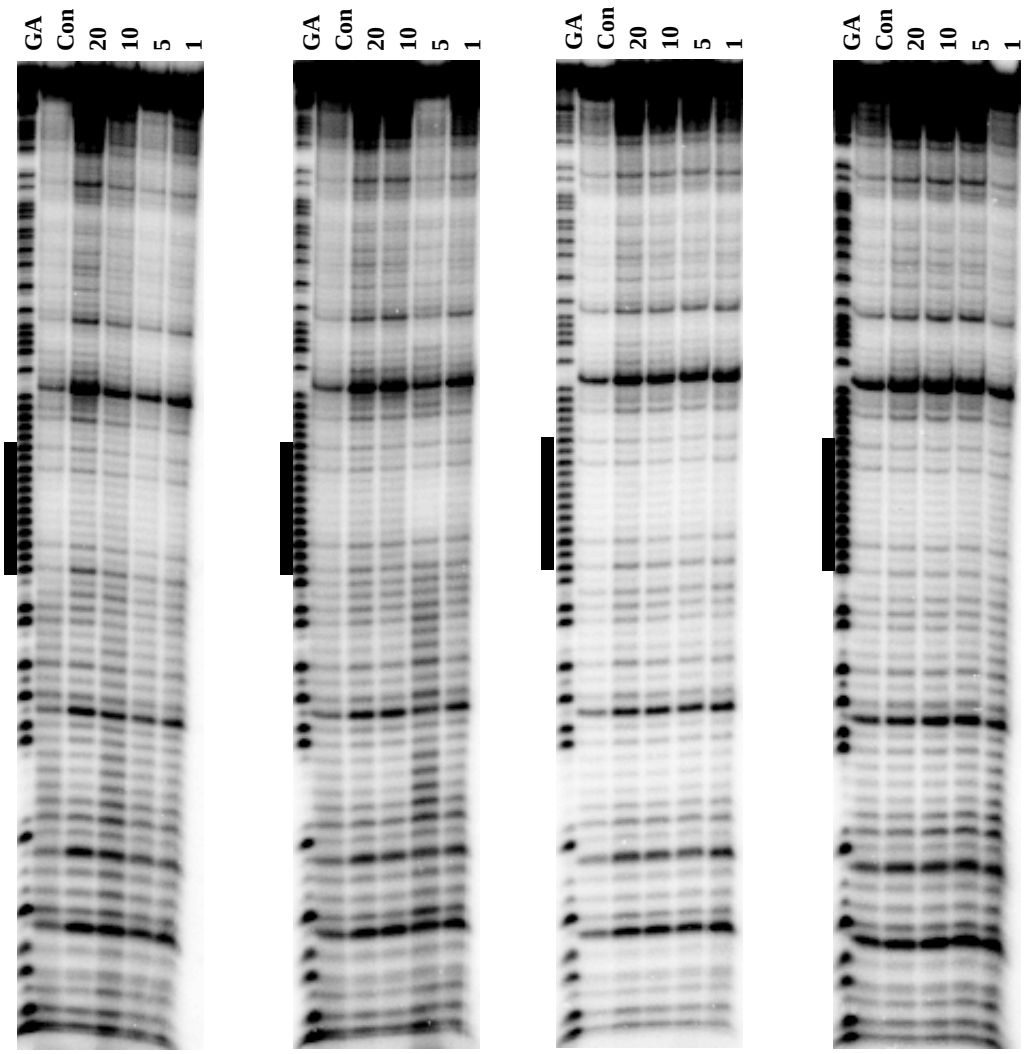

GC **GG** **GA** **GT**

Figure 3.44 $KMnO_4$ cleavage patterns of the modified *tyr*T fragments GC, GG, GA, and GT in the presence of the 12-mer-T TFO. These experiments were performed in 50 mM NaOAc at pH 5.0 in the presence of 1 mM $MgCl_2$ and equilibrated for 2 hours at room temperature before adding the $KMnO_4$. The TFO concentrations (μM) are shown at the top of each gel lane. The tracks labelled "GA" and "con" are Maxam-Gilbert markers specific for purines and the cleavage patterns in the absence of TFOs respectively. The filled boxes indicate the location of the triplex targets.

5′-…CAACCAXCTCTTTTTTCTCTTCCTAACACTT…-3′
3′-…GTTGGTXGAGAAAAAAGAGAAGGATTGTGAA…-5′
3′-TTCTTTTTTCTC-5′ (12-mer-T TFO)

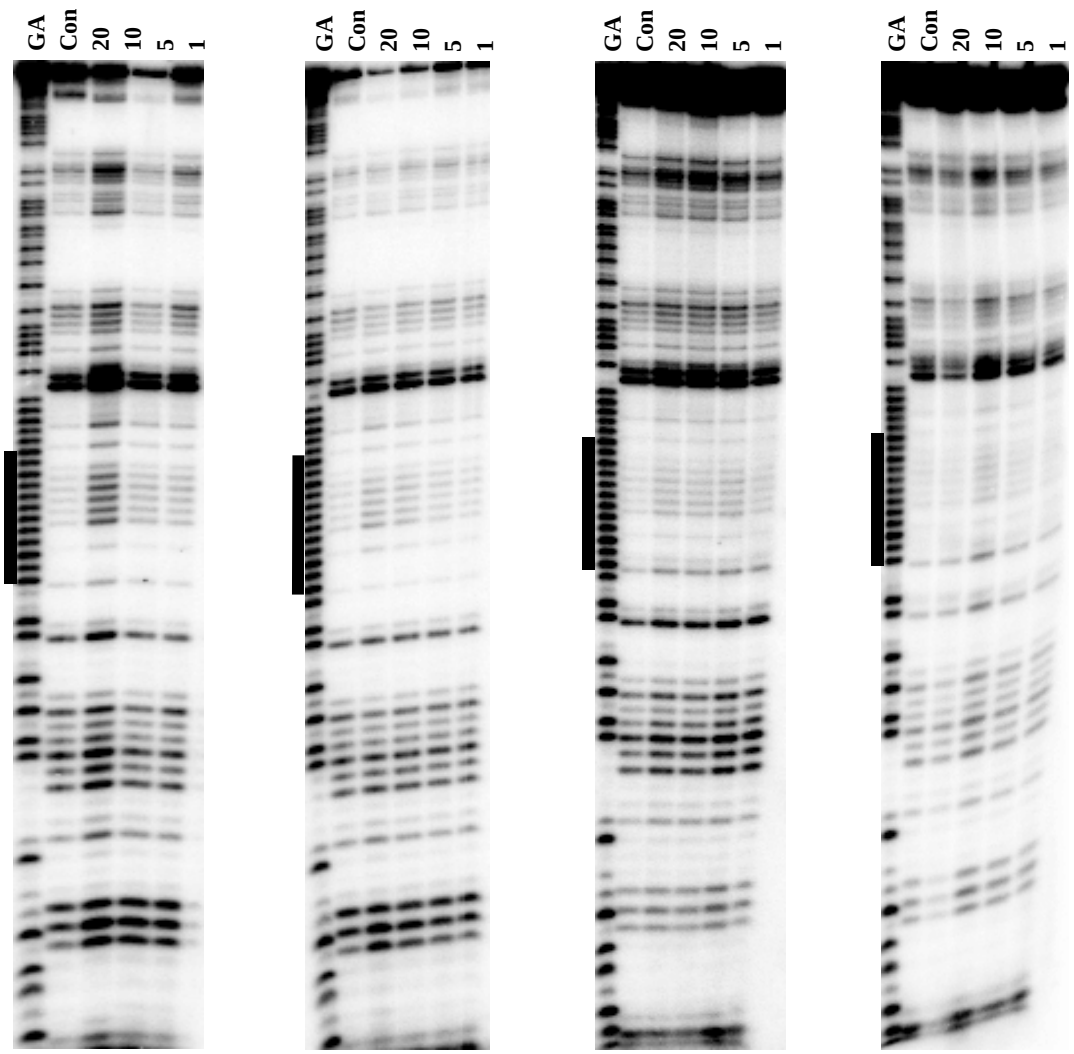

GC **GG** **GA** **GT**

Figure 3.45 Micrococcal nuclease cleavage patterns of the four *tyr*T DNA fragments GC, GG, GA, and GT in the presence of the 12-mer-T TFO. These experiments were performed in 50 mM NaOAc at pH 5.0 in the presence of 1 mM $MgCl_2$ and equilibrated for 2 hours at room temperature before adding the enzyme. The TFO concentrations (μM) are shown at the top of each gel lane. The tracks labelled "GA" and "con" are Maxam-Gilbert markers specific for purines and the cleavage patterns in the absence of TFOs respectively. The filled boxes indicate the location of the triplex targets.

5′-…CAACCAXCTCTTTTTTCTCTTCCTAACACTT…-3′
3′-…GTTGGTXGAGAAAAAAGAGAAGGATTGTGAA…-5′
3′-TTCTTTTTTCTC-5′ (12-mer-T TFO)

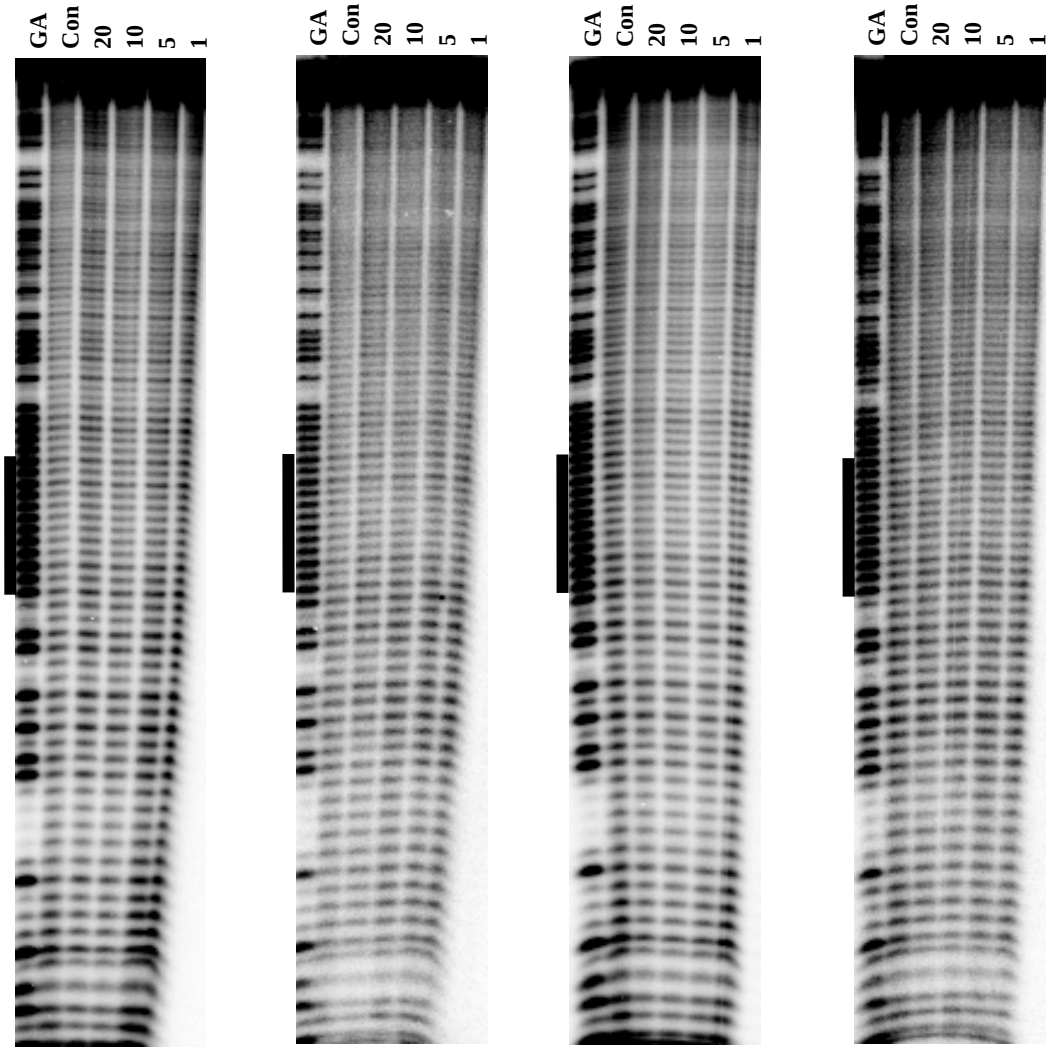

GC **GG** **GA** **GT**

Figure 3.46 Hydroxyl radical cleavage patterns of the four *tyr*T fragments GC, GG, GA, and GT in the presence of the 12-mer-T TFO. These experiments were performed in 50 mM NaOAc at pH 5.0 in the presence of 1 mM $MgCl_2$ and equilibrated for 2 hours at room temperature before adding the hydroxyl radical mix. The TFO concentrations (μM) are shown at the top of each gel lane. The tracks labelled "GA" and "con" are Maxam-Gilbert markers specific for purines and the cleavage patterns in the absence of TFOs respectively. The filled boxes indicate the location of the triplex targets.

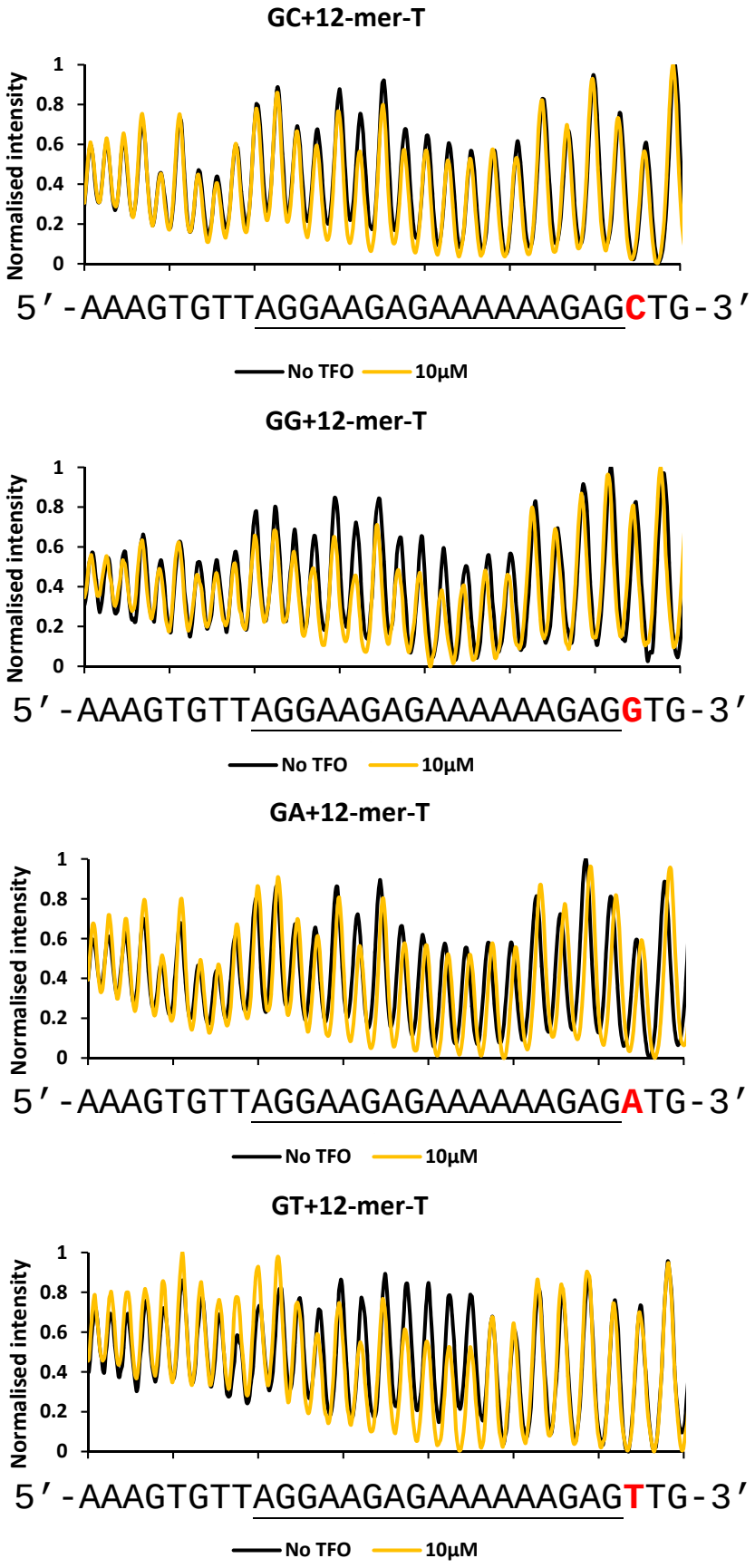

Figure 3.47 Densitometer plots of hydroxyl radical cleavage of the four fragments in the absence (black) and presence (yellow) of 10 μM of the 12-mer-T TFO (taken from the gels shown Figure in 3.46).

3.3.2.4. The effect of flanking bases on the stability of triplex DNA

3.3.2.4.1. 12-mer triplex formation with a 3'-C^+.GC triplet

We also examined the stability of these triplexes with a 3'-C^+.GC triplet by fluorescence melting studies, as described above for the triplexes with a 3'-terminal T.AT (section 3.3.1.4.1). New fluorescently labelled targets were prepared with guanine as the base at the 3'-end of the polypurine tract, flanked by each base in turn. The melting curves of triplexes formed by 5'-dabcyl-labelled 12-mer-C and these four targets are presented in Figure 3.48. The T_m values of these triplexes are presented in Table 3.9. Sequence GT has the highest T_m (49.7 °C), which is not significantly different from GC (49.3 °C), GA (48.7 °C) and GG (48.6 °C). As expected these T_m values are higher than those formed with the four targets with a 3'-terminal T.AT triplet (*i.e.* AC, AA, AG and AT). This is attributed to the greater stability of the C+.GC triplet.

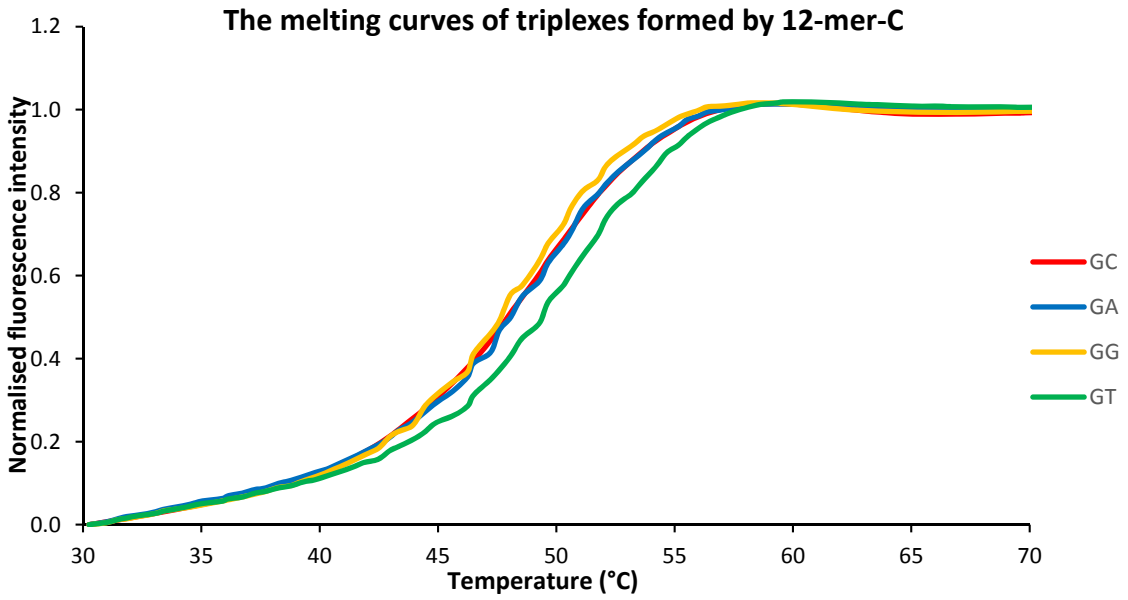

Figure 3.48 Fluorescence melting curves of the 12-mer triplex formed between the dabcyl-labelled 12-mer-C TFO and the fluorescently-labelled duplex target sites in which the triplex target is flanked by each base pair in turn: GC (red), GA (blue), GG (yellow) and GT (green).

3.3.2.4.2. 11-mer triplex formation

The results of similar experiments with the shorter 11-mer TFO on these four target sequences are shown in Figure 3.49. As expected the T_ms of these 11-mer triplexes are lower than those of the 12-mer-C triplexes, and there are only small differences between the T_ms of the different complexes. GC has the lowest T_m (39.7 °C), compared with GT (41.0 °C), GG (40.4 °C) and GA (40.9 °C). As expected the T_m values of these 11-mer triplexes are between 8-10 °C lower than those of their 12-mer counterparts (Figure 3.48 and Table 3.9). Intriguingly this is a much greater reduction than that of the 11-mer triplexes with AC, AA, AG and AT (around 3-5 °C, Figure 3.25 and Table 3.5) compared to their complete 12-mer triplexes (Figure 3.24). Surprisingly these 11-mer triplexes are higher than their 12-mer counterparts with a T.GC triplet mismatch at the 3'-end.

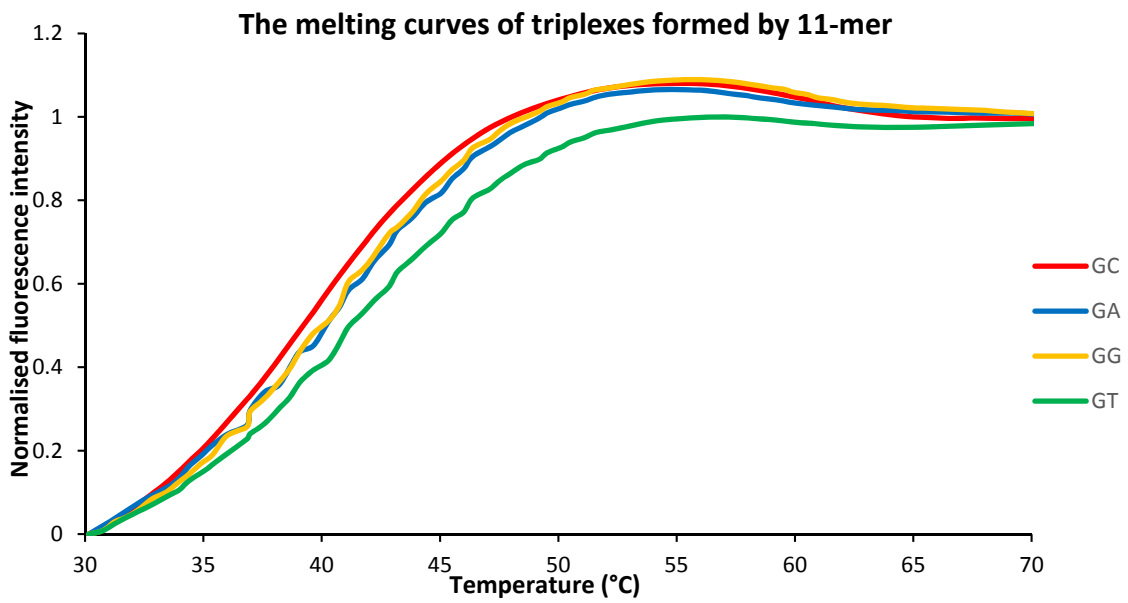

Figure 3.49 Fluorescence melting curves of the triplexes formed between the dabcyl-labelled 11-mer TFO and the fluorescently-labelled duplex targets in which the duplex target sites is flanked by each base pair in turn; GC (red), GA (blue), GG (yellow) and GT (green).

3.3.2.4.3. 12-mer triplex formation with a T.GC mismatch at the 3'-end

We also targeted the sequences that contain a G at the 3'-end of the oligopurine tract with the 12-mer-T, which should form 11 contiguous canonical triplets with a 3'-terminal T.GC mismatch and the results are presented in Figure 3.50. It can be seen that there is no significant differences between these melting curves. GC (red) has the lowest T_m (36.4 °C) which is lower than GA (38.5 °C), GG (37.6 °C) and GT (38.4 °C). Comparing the T_m of these triplexes with the ones in the previous section (Figure 3.48, with the 12-mer triplexes at these targets), it can be seen that, as expected, the terminal mismatch causes a large decrease in stability and these T_ms are about 10 °C lower (Table 3.9). Surprisingly this reduction is much greater than with the complexes containing a terminal C.AT (Figure 3.26) which are only about 2-3 °C lower than the fully matched 12-mer triplex counterparts (Figure 3.24 and Table 3.5).

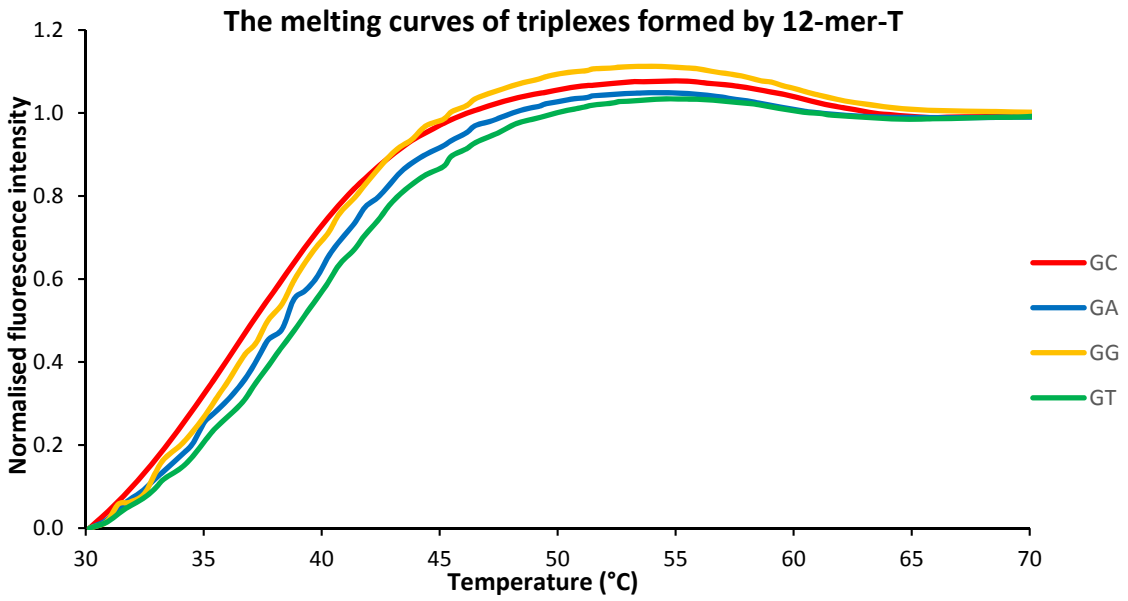

Figure 3.50 Fluorescence melting curves of the 12-mer triplexes formed between the dabcyl-labelled 12-mer-T TFO and the fluorescently labelled duplex targets sites in which the triplex target site is flanked by each base pair in turn GC (red), GA (blue), GG (yellow) and GT (green).

*tyr*T derivatives	T_m Values (mean±SD)		
	12-mer-C	11-mer	12-mer-T
GC	49.3±0.1	39.7±0.36	36.4±0.2
GG	48.6±0.1	40.4±0.32	37.6±0.3
GA	48.7±0.1	40.9±0.06	38.5±0.2
GT	49.7±0.04	41.0±0.04	38.4±0.4

Table 3.9. T_m values estimated from the maxima in the first derivatives of the melting profile of triplexes formed between fluorescently labelled duplex targets GC, GG, GA and GT with either dabcyl-labelled 12-mer-C, 11-mer or 12-mer-T TFO.

3.4. Summary

The target duplexes with a changing of bases at the 3'-end of the polypurine tract were used to examine their effects on parallel triplex formation and enhancements. These include fragments with 3'-adenine flanked with each of the bases in turn generating AC, AG, AA and AT, and fragments with 3'-guanine flanked with the same bases mentioned previously producing GC, GG, GA and GT. Each of these fragments was targeted with these TFOs including 12-mer-T, 11-mer and 12-mer-C to form parallel triplexes with different lengths or different 3'-end triplet identities. The results of DNase I footprinting experiments for fragments AC, AG, AA and AT with the above three TFOs reveal that these TFOs produce concentration dependent footprints for all four fragments which persist to about 1 µM with 12-mer-T and 3 µM with the others. The footprints extend three bases above (5'-) and few bases below (3'-) the TFO binding sites with all four fragments except with 12-mer-T TFO that this 3'-end extension is only present with fragments AA and AG, but not with AC and AT. The footprints are always followed by enhanced DNase I cleavage at the 3'-end of the TFO binding site, at the triplex-duplex junction; the intensity of which is highest with the original sequence AC and lowest with AA. As expected the position of enhancements is one base higher with 11-mer and 12-mer-C than with the 12-mer-T, though there is no enhancement for sequence AG and AA with 12-mer-C. The footprints of these four fragments with the three TFOs are also evident with DEPC reaction, but not with $KMnO_4$, Micrococcal nuclease and hydroxyl radicals. These footprints are also accompanied by 3'-enhancements at the triplex-duplex junction for sequence AC, AG and AA with 11-mer TFO, and sequence AC, AA and AT with 12-mer-C, though there is no enhancement for all fragments with 12-mer-T. The C_{50} values of these fragments are lowest with 12-mer-T (~0.2-

0.4 μM), and highest with 11-mer and 12-mer-C (~0.8-0.9 μM) except the value for fragment AC with 12-mer-C which is comparable to those with 12-mer-T. There is no significant difference of the C_{50} values between the fragments with the same TFO. The T_m values of these four fragments are the highest with 12-mer-T TFO (~40-45 °C), and the lowest with 11-mer (~38-40 °C); the values with 12-mer-C (~40-42 °C) are slightly higher than with 11-mer TFO. Surprisingly, the value for sequence AC with 12-mer-C (42.8 °C) are higher than those triplexes formed by 11-mer (38.2 °C) and 12-mer-T (40.7 °C) with the same fragment.

The DNase I footprints of fragments GC, GG, GA and GT with these TFOs are similar with those the above fragments, though they persist to a much lower concentration with 12-mer-C TFO (0.2 μM or about 10 times lower) otherwise persist to 3 μM with 12-mer-T and 11-mer. These again extend three bases above and a few bases below (5'- and 3'-) the TFO binding site, and are accompanied by enhanced DNase I cleavage at the 3'-end triplex-duplex junction (at the same position with triplexes containing 3'-T.AT triplet). The intensities of these are strongest for sequence GC with 12-mer-C, and sequence GG with 11-mer, though no enhancements observed for sequence GG with 12-mer-T. The footprints with DEPC reaction show no associated enhanced bands for all four fragments with these three TFOs. The C_{50} values of these fragments with 12-mer-C TFO (0.04-0.07 μM) are about 10 times lower than any other parallel triplexes ever studied here, though they are not significantly different between each of the four fragments. The values with 11-mer and 12-mer-T TFOs are about in the same ranges (~0.5-0.7 μM); these are slightly lower than those triplexes formed by the previous fragments with 11-mer (~0.8-0.9 μM), but higher than with the 12-mer-T (~0.2-0.4 μM). Similarly, The T_m values of these fragments with 12-mer-C are the highest compared to other parallel triplexes studied here, though they are not significantly different among each fragments. The values with 12-mer-T are the lowest, and the values with 11-mer are comparable to those triplexes formed by the previous four fragments with the same TFO. Again there is no footprints and enhancements for these fragments with the three TFOs with other cleavage agents (*i.e.* KMnO4, Micrococcal nuclease and Hydroxyl radicals).

3.5. Discussion

It is evident that all three TFOs (*i.e.* 12-mer-T, 12-mer-C and 11-mer) selectively and specifically recognize their target sites in all *tyr*T variants (*i.e.* AC, AG, AA and AT) and form triplexes that generate clear DNase I footprints. A larger footprint than the actual binding site is always observed at both ends of purine tract in all variants, which is thought to be due to the size of the DNase I enzyme that is larger than the TFO binding site. This therefore hinders the entrance of other enzymes to the site and leaves the site uncut. However, this overestimation is unclear with triplexes formed between 12-mer-T, and AA and AT mutants. The interaction of these three TFOs with all four variants is always accompanied by an enhanced cleavage at the 3'-end of oligopurine tract, at the triplex-duplex junction. This may be because the TFOs induce a local duplex DNA conformational changes that allow the duplex to become more susceptible to be recognized and digested by DNase I. Fox and Waring (1984) reported that the interaction of actinomycin or distamycin with *tyr*T fragments led to enhanced cleavage of bases in the regions that flanked to their binding site. This suggested that the binding of ligands to duplex DNA brings about either a local winding or unwinding of minor groove which thereby becomes more susceptible to the access and digestion by DNase I. The flanking sequence, that is strongly cleaved by DNase I, is in A/T-rich tracts for actinomycin and in GC regions for distamycin (Fox and Waring, 1984). Moreover, Waterloh and Fox (1991) reported that the enhancements observed upon the binding between actinomycin and its targets (*i.e.* $(AT)_5GC(AT)_5$, $(TA)_5GC(TA)_5$, T_9GCA_9, A_9GCT_9) generally extend over longer duplex A/T regions flanking the target site and these can be seen on both sides of the (symmetrical) target site. However, enhancements over longer regions may not due to DNA structural changes but can be attributed to the ratio of DNase I and available free DNA. In the presence of actinomycin, the relative concentration of DNase I increases at the other sites outside the target and therefore increases the cleavage (Ward et al., 1988).

In our studies, in which all four bases were located in turn at the 3'-end of the homopurine strand in a position flanking the triplex, enhanced DNase I cleavage was observed in almost every case. This indicates that there is no sequence-dependence for the presence of enhanced cleavage generated by triplex formation with these three TFOs. Moreover, the enhancements at the 3'-end of oligopurine tract are restricted to just one base in all three TFOs therefore they must be due to the structural changes that increase enzyme accessibility to the site and perform its cleavage function. Visual inspection and quantification of the intensity of the enhanced cleavage produced by the 12-mer-T shows that the variant of *tyr*T flanked with cytosine at the 3'-end of the binding site generates a

more intense band compared to the other three variants (Figure 3.3 and Table 3.2). This suggests that flanking cytosine, forming an ApC dinucleotide step, might be the most vulnerable site and needed to undergo the conformational changes to facilitate 12-mer-T TFO binding. Likewise, a study by Travers (Travers, 2004) comparing the sequence-dependent flexibility of dinucleotide steps AA/TT, AT, GA/TC, AC/GT, TA, TG/CA, GC, CG and GG/CC stated that the AA/TT, AT and GA/TC are more restricted to conformational changes than those the AC/GT, TA and TG/CA. Thus, the presence of the TFO generates a conformational change at ApC step which leads to an increase in DNase I recognition and digestion. The reasons for the enhanced cleavage for the variants flanked with A and T, which generate AA and AT flanking sequence respectively, might be similar to those reported by Drew and Travers (Drew and Travers, 1984) and Fox and Waring (Fox and Waring, 1984) which revealed that the low cleavage efficiency of AA, AT and TT steps in duplex DNA is due to the fact that their minor groove is narrower than the average. Therefore, the presence of the TFO may induce a wider groove, which eventually facilitates DNase I recognition and more efficient digestion. This is clearly evident from all of the resulted footprinting gels.

In order to compare the extent of the structural changes at each of the flanking bases, the fractional increase in cleavage relative to the control needs to be measured. However, the cleavage in the control is too low to measure, and it is therefore not possible to assess the relative fractional cleavage enhancements. For this reason, the intensities of the enhancements at the highest TFO concentration were quantified and normalized with the bands outside the TFO binding site as an estimation of the cleavage enhancements. The enhancement is only found at the 3'-end of the labelled purine strand and not on the pyrimidine strand. The reasons for this might be due to the bound TFO or the changes in the orientation of the phosphate at this position that prevents the strand from DNase I cleavage. The enhanced cleavage sites for the triplexes formed by 12-mer-C and 11-mer are at AA sites for all the fragments (*i.e.* AAC, AAG, AAA and AAT) and are therefore in the same adjacent sequence environment as those produced by the 12-mer-T with the AA mutant. Differ to the 11-mer the 12-mer-C has the flanking cytosine at its 3'-end. The calculated C_{50} values from the footprinting plots provide an estimate for K_d, the dissociation constant for the TFO-DNA interaction. The data presented here confirm that the affinity of the triplexes formed with the 12-mer-T and all four *tyr*T variants is higher than those formed by the 12-mer-C and the 11-mer. This is simply because the 12-mer-T contains one more base at its 3'-end that contributes to a longer triplex formation.

In addition to the DNase I footprinting experiments, several other cleavage agents were also used to detect the structural changes of these triplexes (*i.e.* DEPC, $KMnO_4$, micrococcal nuclease and hydroxyl radicals). The reaction of DEPC with these fragments is attenuated in the presence of all three TFOs, though unlike with DNase I this protection is not complete even at the highest TFO concentration (*i.e.* 20 μM). This may be attributed to the size and cleavage mechanisms of DEPC that differ from the DNase I; it is relatively smaller and not dependent on the DNA's grooves, but to the stacking patterns of base adenine. The reaction with these fragments in the absence of the TFOs is enhanced at the TFO binding site especially in As containing region and at a few bases at the 3'-end of the binding site of fragments AA and AT. This emphasizes the base preference of DEPC for which adenine is preferred over other three bases (Kahl and Paule, 2009, Jeppesen and Nielsen, 1988). Surpringly, there are DEPC cleavage enhancements with fragments AC, AA and AG, but not with AT in the presence of the 11-mer TFO and with fragments AC, AA and AT, but not with AG in the presence of the 12-mer-C. These are all located at the same base position which corresponds to the terminal 3'-adenine. The most intensed enhancement is seen for fragment AA with both TFOs and no such enhancements is seen with 12-mer-T TFO. These suggest that the target duplexes must be distorted by the TFO leading to a change with the stacking pattern of the 3'-adenine which favours the reaction with DEPC. This distortion is also determined by the duplex flanking bases; flanking cytosine and adenine always contribute to the conformational changes however flanking guanine and thymine only affect with 11-mer and 12-mer-C TFOs respectively. Unlike with the two TFOs the 12-mer-T, generating triplexes with 12 canonical triplets, does not play a role in changes of adenine stacking pattern even with fragment AA generating flanking base AT at the 3'-end of the triplexes; this flanking AT renders enhancements with the 12-mer-C TFO. The cleavage of the four fragments with KMnO4, micrococcal nuclease and hydroxyl radicals shows no 3'-enhancements in the presence of all three TFOs. This suggests that there is no subtle conformational changes with the bases around the 3'-end triplex-duplex site that favour the recognition by these agents. It is worth noting that micrococcal nuclease, which cleaves single strand pT and pA (Drew, 1984), does not recognize 3'-adenine as with DEPC. This is due to the differences between cleavage mechanisms of the two cleavage agents. The combination of cleavage agents used in our studies is therefore essential to provide details of the DNA conformation.

Thermal stabilities determined by fluorescence melting studies is generally highest with triplexes formed with 12-mer-T as they contain longer canical triplets (i.e. 12-mer) except that with fragment AC in the presence of 12-mer-C which is 2.1 °C higher than with this TFO. This may be due to the interaction of a 3'-terminal cytosine of the 12-mer-C with

a 3'-terminal AT base pair generating a terminal 3'-C.AT triplet and other stabilizing forces occurred between the 3'-C.AT and the flanking cytosine. Pei and colleageus (Pei *et al.*, 1991) reported that this triplet has a weak stability, though they did not consider the effects of bases flanking this triplet. We discovered similar results, but with other three bases flanking the 3'-C.AT (i.e. G, A and T in fragments AG, AA and AT respectively). The formation of a 3'-C.AT is further supported by comparing the stability of triplexes formed with 11-mer and those with 12-mer-C TFO. The laters are slightly stable than the former as they have additional 3'-C.AT, otherwise comparable stabilities should be observed as they both have the same number of triplets (11-mer).

The interaction of the 12-mer-C TFO with all four of these sequence variants (GC, GG, GA and GT) is also always accompanied by enhanced cleavage at the 3'-end of oligopurine tract, at the triplex-duplex junction. This is at the same position as the previous findings and shows that there is no sequence-dependence for enhanced cleavage of triplex formed by this TFO. Intriguingly, the introduction of guanine as the last base at the 3'-end of the purine tract instead of adenine leads to reduced cleavage of the bases next to the triplex-duplex junction, outside the target site. This may be attributed to the conformational flexibility of the dinucleotide steps at the 3'-end (*i.e.* GC, GG, GA, GT) of the purine tract which may be less restricted than the AA/TT, AT as reported by Travers (2004) and El Hassan *et al.* (1996). In a presence of 12-mer-C, their conformational changes are therefore more pronounced than the previous target sites (*i.e.* AC, AG, AA, AT). This consequently attracts increased DNase I access to the sites and perform its cleavage function more effectively. As the structural changes favour the DNase I function the enzyme will be concentrated at the site and leave the neighbouring base region with relatively lower enzyme concentration. Consequently, the bases close to the triplex-duplex junction are cut less than usual. This agrees with the enzyme redistribution mechanisms explained by Ward *et al.* (1988). Although the 12-mer-T has the same sequence length as the 12-mer-C, replacement of the last base at the 3'-end of the purine tract from cytosine to thymine generates base mismatch (i.e. T.GC triplet). This considerably destabilizes the formation of the triplex which can be seen from the weak footprints though at the high concentration of TFO. A study comparing the melting temperature (T_m) of triplets C.GC and T.GC located in the middle of the 13-mer triplex shows that the triplex containing T.GC mismatch produces 13 ^oC less in T_m than the C.GC one. A terminal triplet mismatch also destabilizes triplex though less than the central one (Mergny et al., 1991). Despite binding at the same site and producing enhancement at the same base position as the 12-mer-T, the 11-mer always gives additional enhancements at a position one base lower than the usual one (at the same site as 12-mer-C). Though these are at very low intensity. This suggests that the conformational

changes at the triplex-duplex junction could transmit its effect to the adjacent base within the purine tract but not the flanking bases outside the target site. This finding is also evident from the previous study. The disappearance of this additional enhancement in 12-mer-T may be attributed to the mismatch T.GC triplet hampering the conformational transmission.

The C_{50} values with the 12-mer-C TFO are about 10-fold lower than for 12-mer-T with its target site (i.e. AC, AG, AA and AT). This is due to substitution of the last base from adenine to guanine at the 3'-end of oligopurine tract that generates a C^+.GC triplet in place of T.AT. This is consistent with the previous studies showing that C^+.GC is more stable than the T.AT at pH 5.0. Once comparing the C_{50} values of the 12-mer-C with its target and of the 12-mer-T and the 11-mer with the same target, they are also 10-fold lower than the latter two. This is attributed to the longer sequence and the additional C^+.GC triplet of the triplex formed by 12-mer-C. The introduction of a T.GC triplet confirms that a single mismatch at the 3'-end can destabilize the triplex, though it is less pronounced than the mismatch at the central triplex. This mismatch slightly reduces its C_{50} values relative to the 12-mer-T with its target site (i.e. AC, AG, AA and AT) and brings about the values close to the 11-mer. This is consistent with a study by Mergny et al. (1991) mentioned above. The C_{50} values of the 11-mer with its target are slightly lower than the 11-mer with the previous study, though they are not significantly different.

Unlike with the previous fragments (i.e. AC, AG, AA and AT) none of the three TFOs induces enhanced reaction with DEPC in these four fragments (i.e. GC, GG, GC and GT) even at the highest TFO concentration (20 μM). This may be the result of replacing 3'-adenine to guanine which unfavours a modification by DEPC and leaves this base position uncut. The cleavage agent with a high specificity to guanine is therefore needed to probe conformational changes at this base position, especially with triplexes formed with 11-mer and 12-mer-T TFOs which showed DEPC cleavage enhancements in the previous fragments. The cleavage patterns of these fragments in the control experiments showed that the bands at the 3'-end of the target site containing base guanine are not reactive to DEPC confirming that this cleavage agent is not reactive to guanine; though the cleavage of the same region in the fragments with 3'-adenine was highly reactive to this agent. Similarly, no changes with cleavage patterns and enhancement were detected by other footprinting agents as a result of these triplexes formation.

The thermal stabilities of triplexes formed between these fragments and 12-mer-C TFO are unsurprisingly higher than the rest of the triplexes examined in this study as a result of a 3'-terminal C^+.GC triplet. The cation of this triplet is believed to reduce electrostatic repulsion between negatively charged phosphate backbones and therefore stabilize the

structure, though this can have destabilizing effect if a number of the ions are clustered around the same region. The result of a replacement of a 3'-T.AT (in the previous 12-mer triplexes) with C^+.GC triplet (these triplexes) supports the above statement as the former has the lower T_ms than the latter (3-5 °C lowers in AG and AA and 7-9 °C with AC and AT). The stabilities of triplexes with 11-mer TFO again confirm that the absence of a 3'-C^+.GC triplet reduces the stability much more drastic than the absence of a 3'-T.AT as the former renders the reduction of T_ms as much as 10 times while the latter lower to about only 2-3 °C compared to their 12-mer canonical triplexes. We expected to see a similar stabilizing effect of a 3'-T.GC as that observed with a 3'-C.AT, though the results are not surprising; this triplet mismatch has a destabilizing effect rather than stabilizing the structure. Chandler and Fox (1996) reported the formation of a weak T.GC triplet in GA containing triplexes, though this is oriented in an opposite direction against the purine target site. This orientation of T.GC might be a factor that destabilizes the rest of parallel triplets. The stabilities of all triplexes formed between these four fragments and the three TFOs are not dependent on the flanking bases as there are no significant differences of thermal stabilities in each fragments.

CHAPTER 4 THE EFFECTS OF BASE VARIATIONS AT THE 3'-END OF AN ANTI-PARALLEL DNA TRIPLEX

4.1. Introduction

The previous chapter investigated the effects of bases flanking the TFO's binding sites on the formation of parallel triplexes. We were also interested to see how these factors affect the formation of antiparallel triplexes. Antiparallel triplexes also require a polypurine tract as a site for TFO binding. These TFOs are GA-containing oligonucleotide, instead of CT, and are oriented in the opposite direction to the duplex purine strand (Beal and Dervan., 1991). The binding of the TFO is stabilised by divalent cations, particularly Mn^{2+} and high ionic strength (*i.e.* Na^{+}) (Chandler and Fox, 1996). This interaction is generally less stable than their parallel counterparts (Fox, 2000). Interestingly, this structure was demonstrated to occur naturally at physiological conditions in a sequence containing long GA repeats (H-DNA) (Lyamichev *et al*., 1986, Mirkin *et al*., 1987). It is therefore considered to be a promising structure to use in cellular contexts (Mirkin *et al*., 1987). A number of studies have reported the *in vitro* and *in vivo* formation of this triplex (Lacoste *et al*., 1997), though there have been no systematic studies on the effects of the sequences flanking the binding site on the antiparallel triplex formation. Using the same sets of *tyr*T fragments that were used in Chapter 3, the formation of 12-mer antiparallel triplexes with a 3'-A.AT triplet flanked by each base pair in turn was studied with 12-mer-A TFO (5'-AAGAAAAAAGAG). Likewise the 12-mer triplexes ending with a 3'G.GC triplet were studied with the 12-mer-G TFO (5'-GAGAAAAAAGAG). These were expected to provide insights on the formation of 12-mer antiparallel triplexes and their effects on the enhancements and affinity. The results are also compared with the parallel ones with 12-mer-T, 11-mer and 12-mer-C TFOs (Chapter 3). Since longer TFOs generate higher triplex stability (Arimondo *et al*., 1998), the formation of similar 17-mer triplexes was also examined using a 17-mer-A TFO (5'-AAGAAAAAAGAGAAGGA), forming a 3'-A.AT triplet, flanked by each base pair in turn. Similar complexes with a 3'-G.GC triplet used the 17-mer-G TFO (5'-GAGAAAAAAGAGAAGGA). The only difference between these longer triplexes and the12-mer TFOs is the addition of a further five triplets at the 5'-end of the TFO. The effects of 3'-mismatched triplets were also investigated. To probe these interactions, a combination of techniques was used, similar to those employed in chapter 3 and includes footprinting experiments with DNase I, Micrococcal nuclease, hydroxyl radicals, DEPC and $KMnO_4$. Melting experiments with fluorescently-labelled molecular beacon oligonucleotides, using the LightCycler are also used to measure triplex stability (Darby *et al*., 2002). These GA-containing TFOs had a quencher attached at their 3'-end (instead of 5'-end for the parallel

triplexes) using the same duplex targets (*i.e.* with the fluorophore attached to the 5'-end of the polypurine strand).

4.2. Experimental design

4.2.1. DNA fragments

For these studies the DNA fragments, which are identical with those in Chapter 3, were used. These includes fragments with 3'-adenine containing each of the flanking base pairs in turn (*i.e.* AC, AG, AA and AT), and fragments with 3'-guanine with the same patterns of flanking base pairs (*i.e.* GC, GG, GA and GT).

4.2.2. Footprinting assays of antiparallel triplex formation

The radiolabelled AC, AG, AA and AT fragments were incubated with different concentrations of 5'-AAGAAAAAAGAGAAGGA (17-mer-A), 5'-GAGAAAAAAGAGAAGGA (17-mer-G) and 5'-AAGAAAAAAGAG (12-mer-A) to form 17-mer, 17-mer with a 3'-end triplet mismatch and 12-mer, antiparallel triplexes respectively. The reactions were performed in 10 mM Tris-HCl at pH 7.0 in the presence of 10 mM $MnCl_2$ and 50 mM NaCl. All other details are the same as described in Chapter 3 (section 3.2.3). Similar experiments were also performed with DNA fragments GC, GG, GA and GT. These were targeted with 5'-GAGAAAAAAGAGAAGGA (17-mer-G), 5'-AAGAAAAAAGAGAAGGA (17-mer-A) and 5'-GAGAAAAAAGAG (12-mer-G) to form 17-mer, 17-mer with a 3'-end triplet mismatch and 12-mer antiparallel triplexes respectively.

4.2.3. Fluorescence melting studies with antiparallel triplexes

For the determination of antiparallel triplex thermal stability, similar experiments with those described in Chapter 3 (section 3.2.4) were performed using the following 3'-end dabcyl-labelled TFOs and 5'-end fluorophore-labelled target duplex strands. T_ms were estimated from these as previously described.

TFOs used in these studies
Dabcyl-labelled purine TFOs
5’-AAGAAAAAAGAGAAGGA-**Q**-3’ (17-mer-A)
5’-GAGAAAAAAGAGAAGGA-**Q**-3’ (17-mer-G)

A

Target duplexes used to form 17-mer antiparallel triplexes with 3’-A.AT triplet	
Unlabelled-pyrimidine rich strands	5’-fluorophore-labelled purine rich strands
5’-CAACCAGTTCTTTTTTCTCTTCCT-3’	5’-**F**-AGGAAGAGAAAAAAGA**AC**TGGTTG-3’
5’-CAACCACTTCTTTTTTCTCTTCCT-3’	5’-**F**-AGGAAGAGAAAAAAGA**AG**TGGTTG-3’

B

Target duplexes used to form 17-mer antiparallel triplexes with 3’-G.GC triplet	
Unlabelled-pyrimidine rich strands	5’-fluorophore-labelled purine rich strands
5’- CAACCAGCTCTTTTTTCTCTTCCT-3’	5’-**F**-AGGAAGAGAAAAAAGA**GC**TGGTTG-3’
5’- CAACCACCTCTTTTTTCTCTTCCT-3’	5’-**F**-AGGAAGAGAAAAAAGA**GG**TGGTTG-3’

C

Table 4.1 Oligonucleotide sequences used in antiparallel triplex melting studies. The TFOs shown in **(A)** are the same length (17-mer), but have different bases at the 5’-end. 17-mer-A has a 5’-adenine while 17-mer-G has a 5’-guanosine. Both are labelled with dabcyl at the 3’-end. The sequences shown in **(B)** are used to form target duplexes that end with 3’-AC and AG dinucleotides (underlined). The purine-rich strands with different 3’-end flanking bases (in red) are on the right panel; the unlabelled complementary strands are presented on the left. The sequences shown in (**C)** are used to form target duplexes with 3’-end GC and GG dinucleotides (underlined). The purine-rich strands with different 3’-end flanking bases (in red) are shown in the right panel and the unlabelled complementary strands are presented on the left. These purine target strands were all labelled with fluorophore at their 5’-end.

4.3. Results

4.3.1. The effects of flanking base changes at the 3'-end of the target site

4.3.1.1. The 17-mer triplex formed with 17-mer-A

To investigate the effects of flanking bases at the 3'-end of the target site on antiparallel triplex formation and to compare the results of these with those parallel counterparts (in chapter 3), we first incubated fragments AA, AT, AG and AC with 12-mer-A TFO in 10 mM Tris-HCl at pH 7.0 containing 10 mM $MnCl_2$ and 50 mM NaCl. We expected that this TFO would bind polypurine strand in an antiparallel orientation and generate triplexes containing A.AT and G.GC triplets and would cover the same sequence as the parallel 12-mers studied in chapter 3. The results of DNase I footprinting experiments with these TFOs are shown in Figure 4.1. There is no cleavage protection is seen for all the fragments, even at high TFO concentration (*i.e.* 20 μM). This might be attributed to the low stability of antiparallel triplexes that prevents the formation of the structure in these conditions. To investigate this further the experiments were repeated with the longer 17-mer-A TFO. This TFO binds at the same site as the 12-mer-A and generates triplexes with the same 3'-end flanking sequences, but with five more triplets towards the 5'-end of the binding site. DNase I footprinting experiments with this TFO are presented in Figures 4.2. As expected, this 17-mer TFO generates footprints with all four DNA fragments. The footprints are concentration dependent and extend above (5'-), but not below (3'-), the TFO binding site. These footprints are not as clear as those with parallel counterparts (12-mer or 11-mer), even at the highest TFO concentration (3 μM). All the footprints are accompanied by enhanced DNase I cleavage, which is evident as a number of bands above (5'-) the TFO binding site (red asterisks), rather than a single band at the 3'-end of the triplex-duplex junction as seen with the parallel triplexes. These enhancements could arise from either structural changes in the DNA or as a result of redistribution of the enzyme onto free sites. The latter seemed less likely as the enhancements are localised to the region immediately above the TFO binding sites, while cleavage in the rest of the fragments unaffected. These footprints were used to generate footprinting plots, which are presented in Figure 4.3. The calculated C_{50} values are shown in Table 4.2 and reveal that there is no significant difference in the C_{50} values for each of the target fragments. These values are in the same range as those obtained with the shorter (12-mer) parallel triplexes.

5′-…CAACCAXTTCTTTTTTCTCTTCCTAACACTT…-3′
3′-…GTTGGTXAAGAAAAAAGAGAAGGATTGTGAA…-5′
5′-AAGAAAAAAGAG-3′ (12-mer-A TFO)

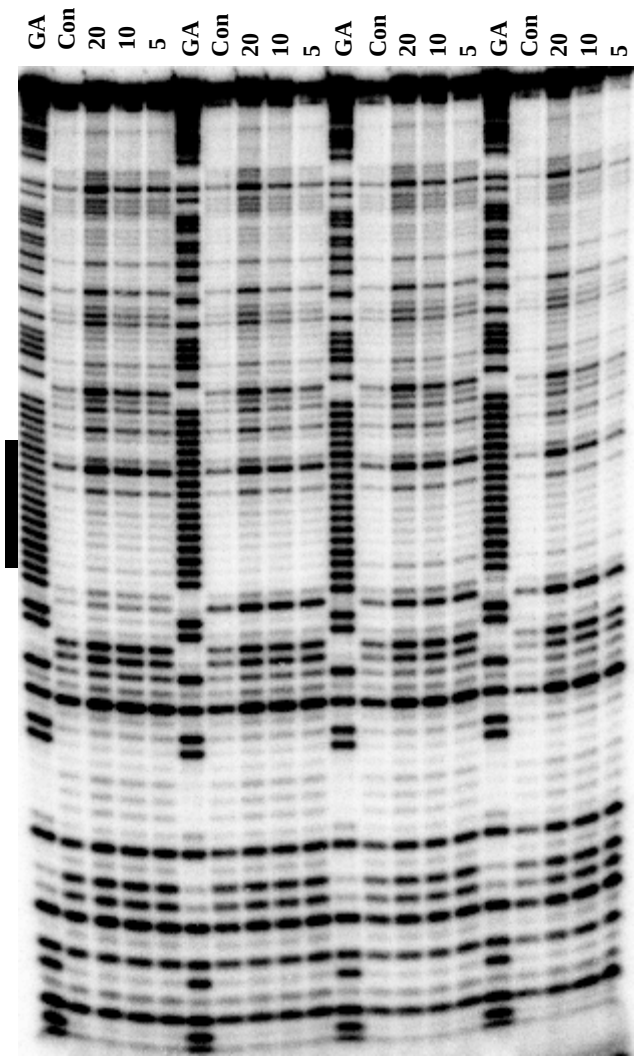

Figure 4.1 DNase I cleavage patterns of the four DNA fragments (AA, AT, AG and AC) containing different bases (X) at the 3'-end of the homopurine seqeunce (underlined) in the presence of different concentration of the 12-mer-A TFO. These experiments were performed in 10 mM Tris-HCl at pH 7.0 in the presence of 10 mM $MnCl_2$ and 50 mM NaCl and were equilibrated for 2 hours at room temperature before digesting with DNase I. TFO concentrations (μM) are shown at the top of each gel lane. The tracks labelled "GA" and "con" are Maxam-Gilbert markers specific for purines and the cleavage pattern in the absence of TFOs respectively. The filled box indicates the location of the triplex target site.

5′-…CAACCAXTTCTTTTTTCTCTTCCTAACACTT…-3′
3′-…GTTGGTXAAGAAAAAAGAGAAGGATTGTGAA…-5′
5′-AAGAAAAAAGAGAAGGA-3′(17-mer-A)

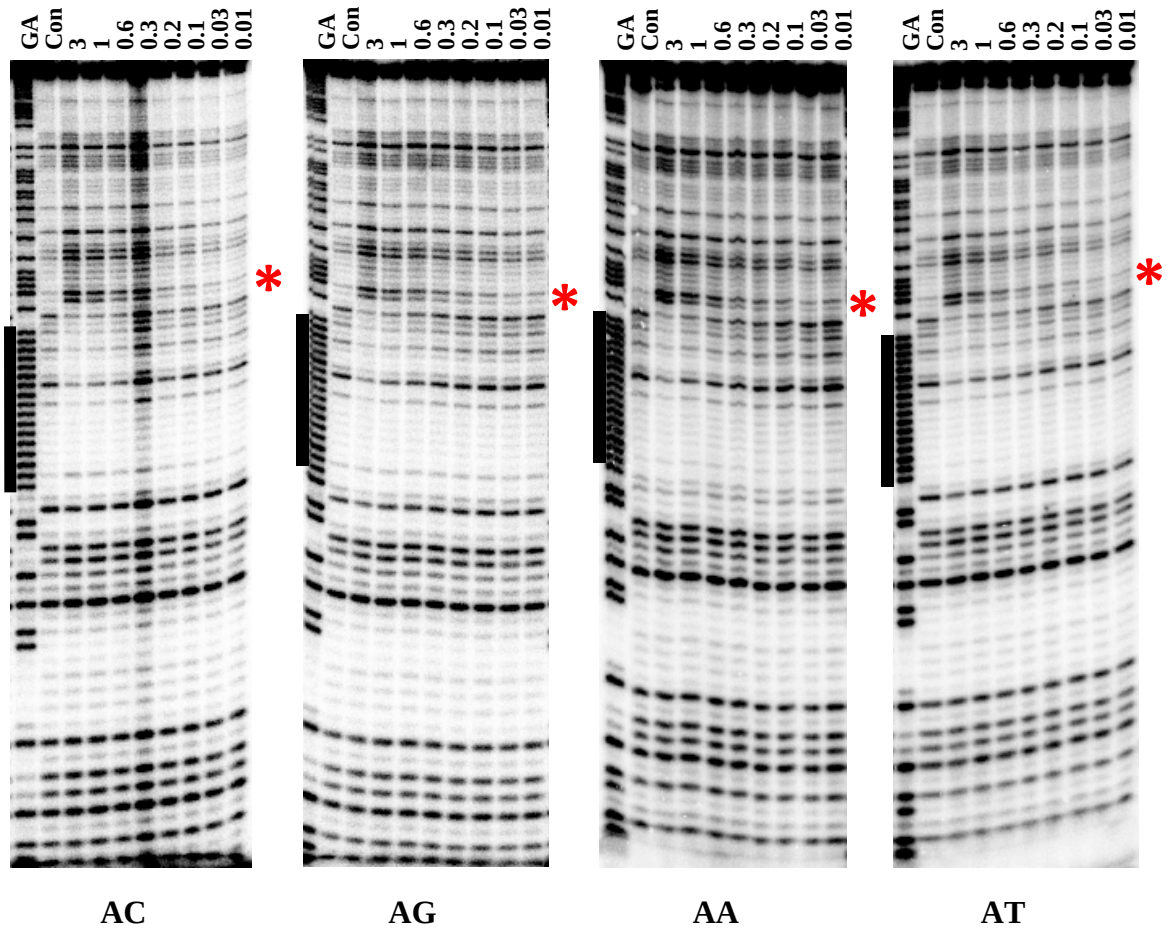

Figure 4.2 DNase I cleavage patterns of the four *tyr*T fragments in the presence of the 17-mer-A TFO. X is C, G, A and T in turn. These experiments were performed in 10 mM Tris-HCl at pH 7.0 in the presence of 10 mM $MnCl_2$ and 50 mM NaCl and equilibrated for 2 hours at room temperature before digesting with DNase I. TFO concentrations (μM) are shown at the top of each gel lane. Tracks labelled "GA" and "con" are Maxam-Gilbert markers specific for purines and the cleavage patterns in the absence of TFO respectively. The filled boxes indicate the location of the triplex target sites and the red asterisks show the position of enhanced DNase I cleavage at the 5'-end of the TFO binding site.

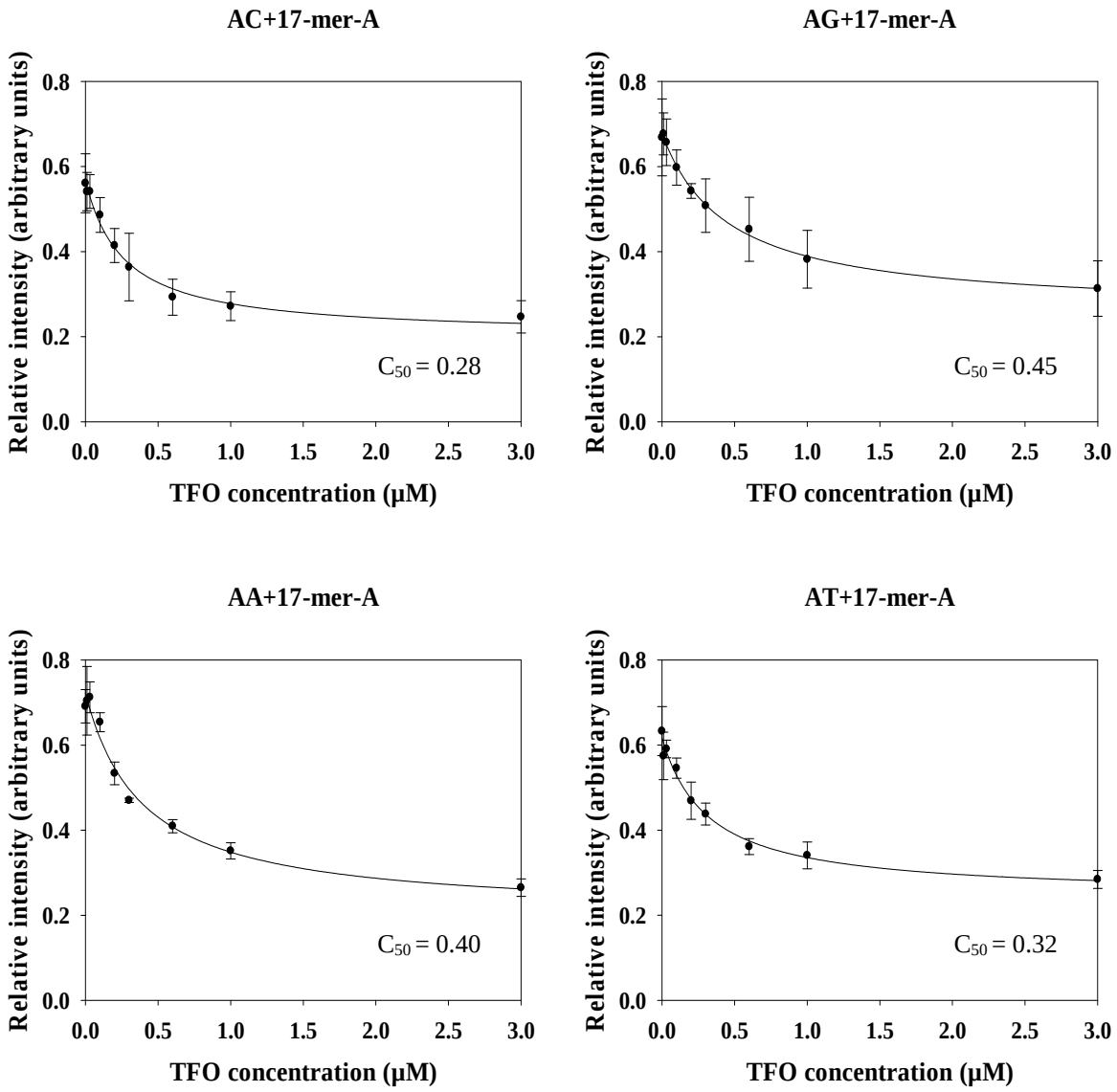

Figure 4.3 Footprinting plots showing the intensities of the footprints (arbitrary units) as a function of TFO concentration (μM). These were obtained from the DNase I footprinting gels of the triplex formed between 17-mer-A TFO and the four *tyr*T sequences as shown in Figure 4.2. The C_{50} values, which correspond to the TFO concentration at which the relative intensity is half the maximum, are shown in Table 4.2. The curves correspond to a simple binding equation that was fitted to the data.

***tyr*T derivatives**	**17-mer-A TFO**
	C_{50} values (µM)
AC	0.28±0.09
AG	0.45±0.09
AA	0.40±0.09
AT	0.32±0.01

Table 4.2 The C_{50} values (µM) obtained from the DNase I footprinting plots of triplexes formed between 17-mer-A and the four *tyr*T fragments (AC, AG, AA and AT).

These triplexes were also probed with DEPC, $KMnO_4$, micrococcal nuclease and hydroxyl radicals as described for the parallel triplexes in Chapter 3. The results of footprinting experiments with DEPC are shown in Figure 4.4. As noted in Chapter 3 the higher reactivity in the control lanes is evident around the As in the TFO binding site. These show reduced cleavage at the binding site in the presence of the 17-mer-A TFO. Again there is no TFO-induced enhanced cleavage at any position in all four fragments.

Figure 4.5 shows the results of $KMnO_4$ reactions with these four fragments in the presence of the 17-mer-A TFO. The patterns are similar to those with the parallel triplexes and the 12-mer-T TFO and show high reactivity at the TT dinucleotide at above (5'-) the TFO's binding site , though in this case there appear to be two enhanced bands. However, these are fainter than those with 12-mer-T. Again there is no TFO-induced changes in $KMnO_4$ reaction, even in AT sequence.

Figure 4.6 presents the results of footprinting experiments with micrococcal nuclease on these four fragments. The control cleavage patterns of these fragments are identical to those shown in chapter 3 and reveal good cleavage at a site above (5'-) the binding site. The enzyme cuts fragments with higher TFO concentrations (*i.e.* 20, 10, 5 µM) at a very low efficiency as it digests the TFO at the same time. Again there are no TFO-induced changes in the cleavage patterns of these four fragments, even in AA and AT.

Cleavage with hydroxyl radicals of these fragments has similar patterns with those obtained in parallel tiplexes (chapter 3). The fragments were cleaved equally which is evident on the gels as bands with equal intensity (Figure 4.7). There is no TFO-induced enhancements observed using this agent.T

5′-…CAACCAXTTCTTTTTTCTCTTCCTAACACTT…-3′
3′-…GTTGGTXAAGAAAAAAGAGAAGGATTGTGAA…-5′
5′-AAGAAAAAAGAGAAGGA-3′(17-mer-A)

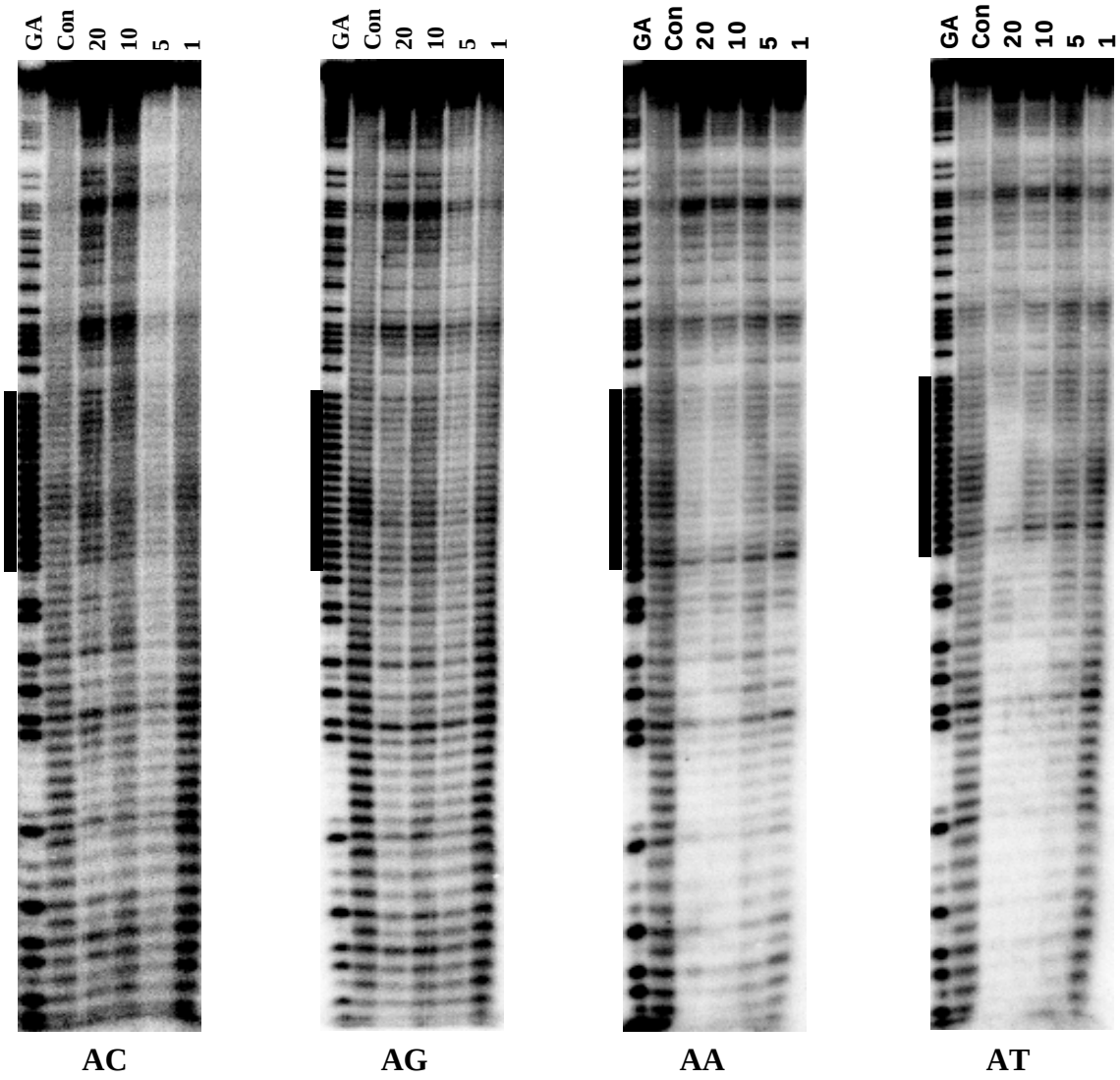

Figure 4.4 DEPC cleavage patterns of the four *tyr*T fragments in the presence of the 17-mer-A TFO. X is C, G, A and T in turn. These experiments were performed in 10 mM Tris-HCl at pH 7.0 in the presence of 10 mM $MnCl_2$ and 50 mM NaCl and were equilibrated for 2 hours at room temperature before reacting with DEPC. TFO concentrations (μM) are shown at the top of each gel lane and the tracks labelled "GA" and "con" are Maxam-Gilbert markers specific for purines and the cleavage patterns in the absence of TFO respectively. The filled boxes indicate the location of the triplex target sites.

5′-…CAACCAXTTCTTTTTTCTCTTCCTAACACTT…-3′
3′-…GTTGGTXAAGAAAAAAGAGAAGGATTGTGAA…-5′
5′-AAGAAAAAAGAGAAGGA-3′(17-mer-A)

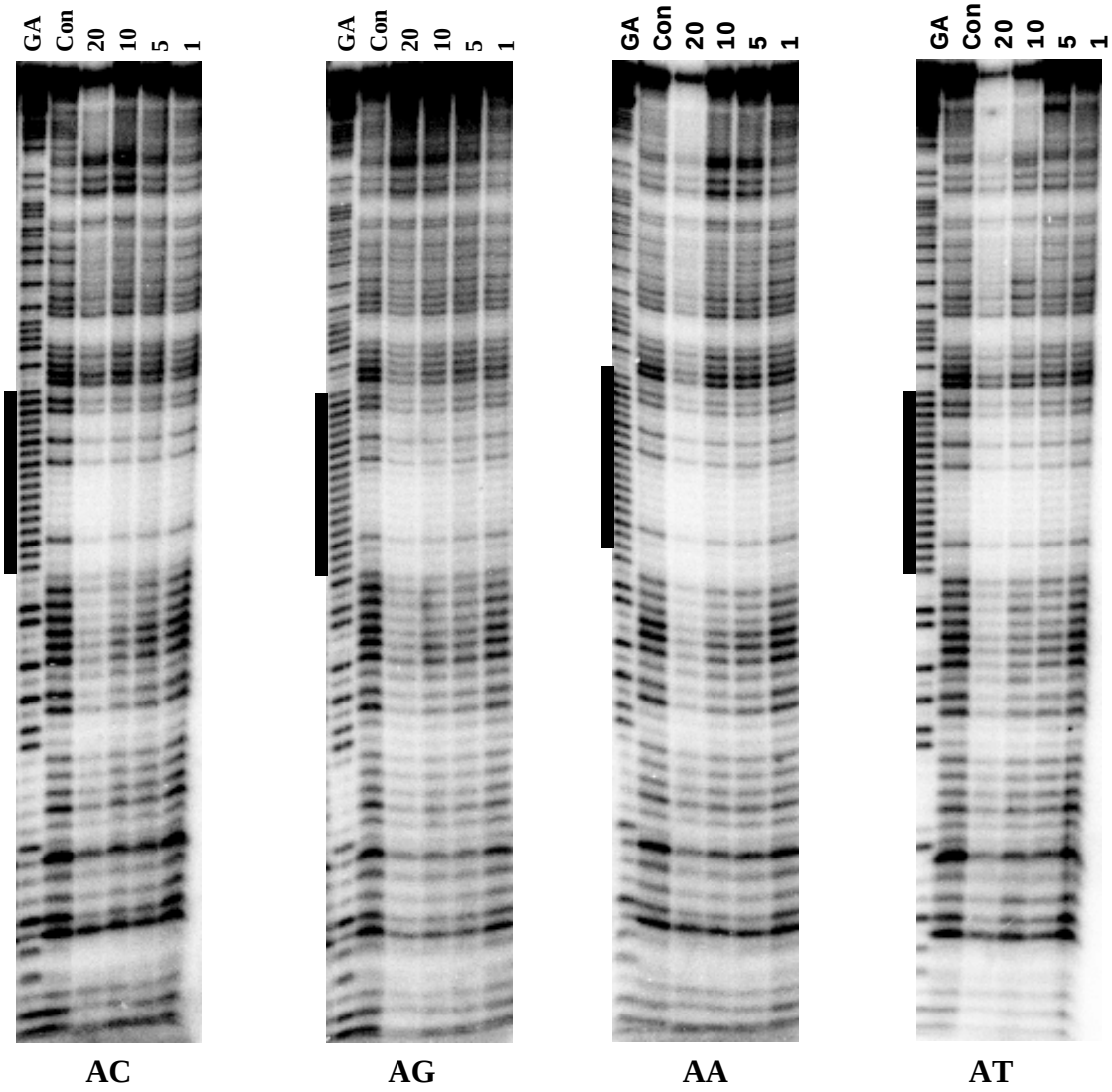

Figure 4.5 $KMnO_4$ cleavage patterns of the four *tyr*T DNA fragments in the presence of the 17-mer-A TFO. X is C, G, A and T in turn. These experiments were performed in 10 mM Tris-HCl at pH 7.0 in the presence of 10 mM $MnCl_2$ and 50 mM NaCl and were equilibrated for 2 hours at room temperature before reacting with $KMnO_4$. TFO concentrations (μM) are shown at the top of each gel lane. Tracks labelled "GA" and "con" are Maxam-Gilbert markers for specific for purines and the cleavage pattern in the absence of TFOs respectively. The filled boxes indicate the location of the triplex target sites.

5′-…CAACCAXTTCTTTTTTCTCTTCCTAACACTT…-3′
3′-…GTTGGTXAAGAAAAAAGAGAAGGATTGTGAA…-5′
5′-AAGAAAAAAGAGAAGGA-3′(17-mer-A)

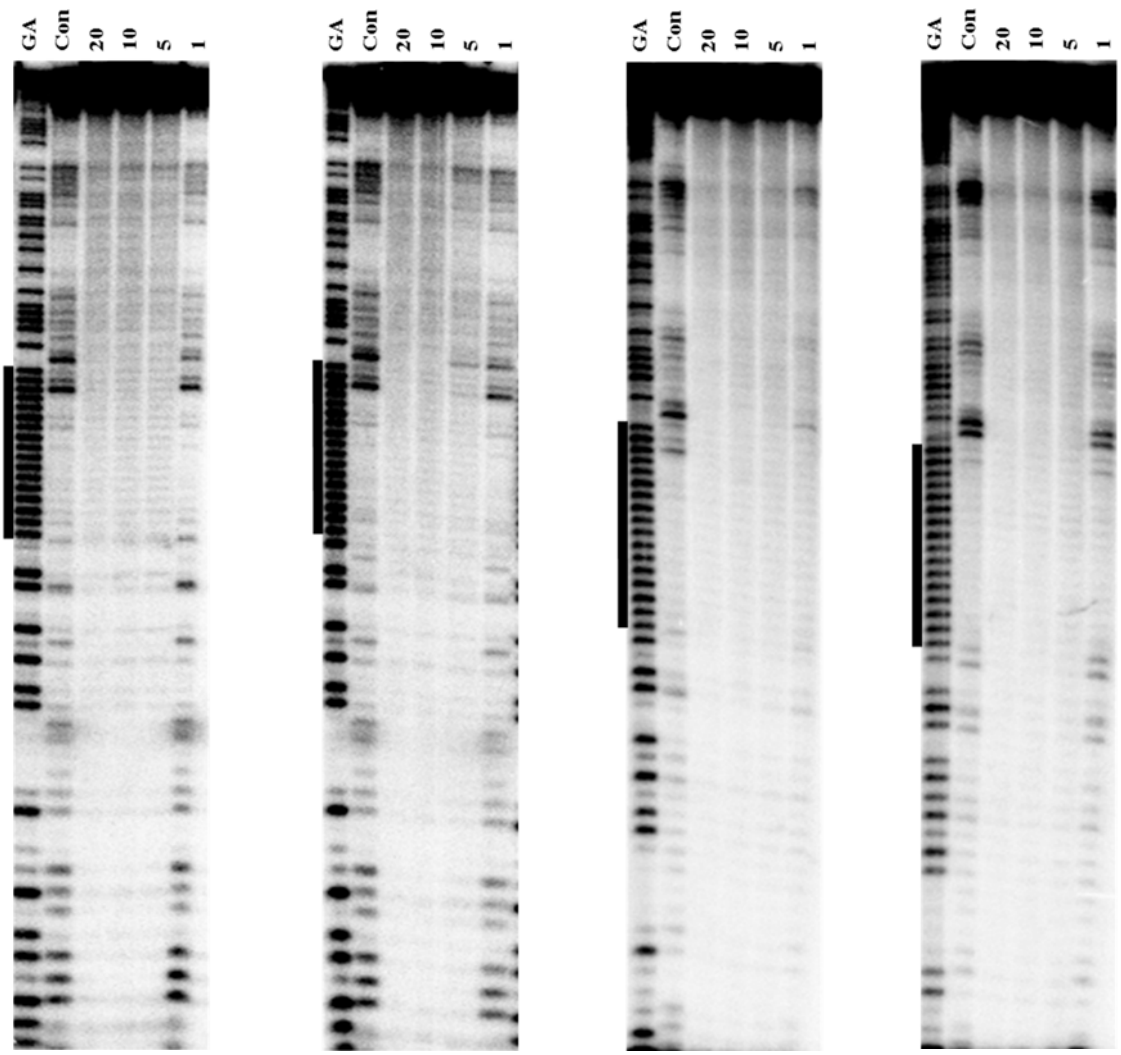

AC **AG** **AA** **AT**

Figure 4.6 Micrococcal nuclease cleavage of the four *tyr*T fragments in the presence of the 17-mer-A TFO. X is a C, G, A and T in turn. These experiments were performed in 10 mM Tris-HCl at pH 7.0 in the presence of 10 mM $MnCl_2$ and 50 mM NaCl and were equilibrated for 2 hours at room temperature before digesting with the enzyme. TFO concentrations (μM) are shown at the top of each gel lane. The tracks labelled "GA" and "con" are Maxam-Gilbert markers specific for purines and the cleavage patterns in the absence of TFOs respectively. The filled boxes indicate the location of the triplex target sites.

5′-…CAACCAXTTCTTTTTTCTCTTCCTAACACTT…-3′
3′-…GTTGGTXAAGAAAAAAGAGAAGGATTGTGAA…-5′
5′-AAGAAAAAAGAGAAGGA-3′(17-mer-A)

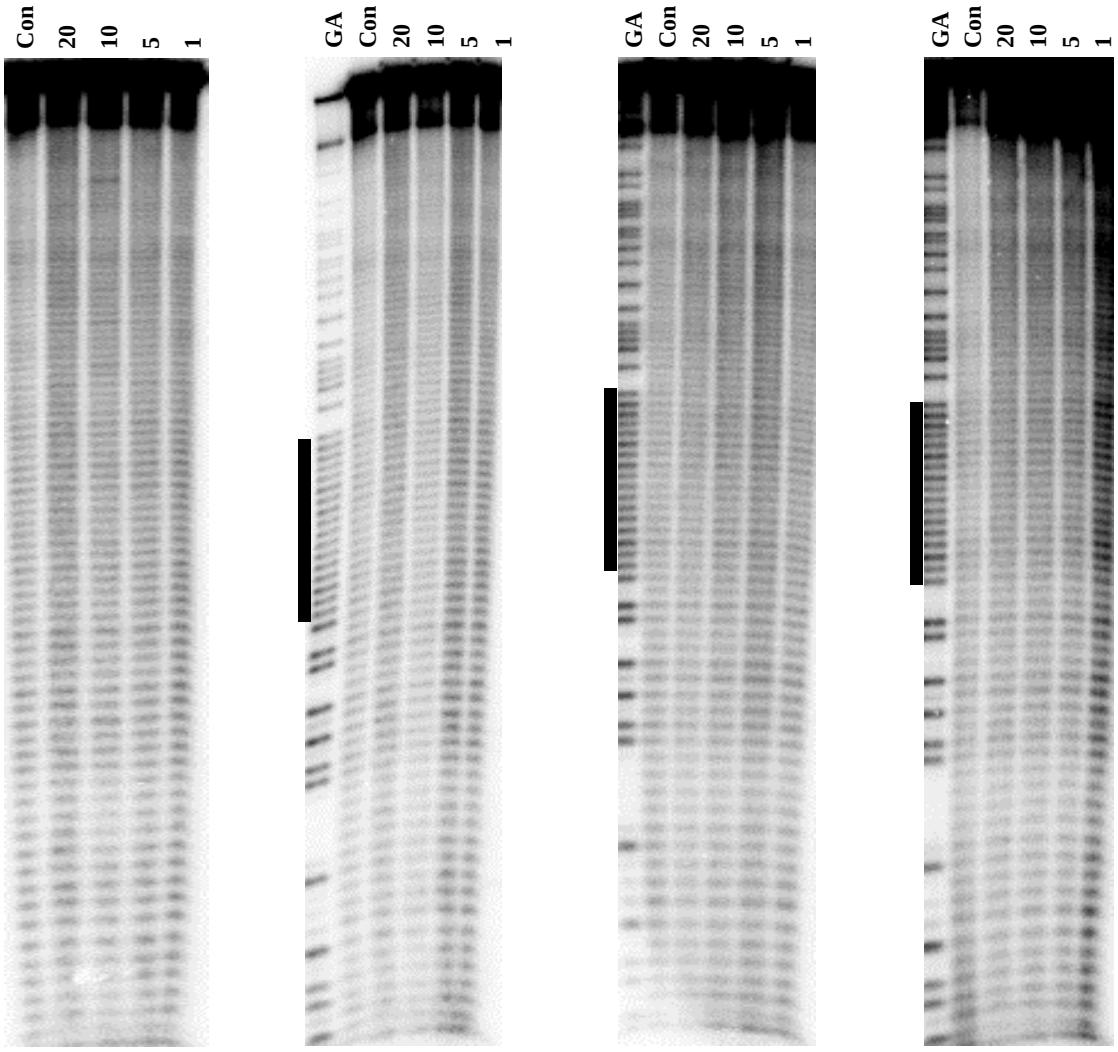

Figure 4.7 Hydroxyl radical cleavage of the four *tyr*T fragments in the presence of the 17-mer-A TFO. X is C, G, A and T in turn. These experiments were performed in 10 mM Tris-HCl at pH 7.0 in the presence of 10 mM $MnCl_2$ and 50 mM NaCl and were equilibrated for 2 hours at room temperature before digesting with the hydroxyl radical mixture. TFO concentrations (μM) are shown at the top of each gel lane. The tracks labelled "GA" and "con" are Maxam-Gilbert markers specific for purines and the cleavage patterns in the absence of TFOs respectively. The filled boxes indicate the location of the triplex target sites.

4.3.1.2. The 17-mer triplex with 17-mer-G TFO, generating a 3'-end mismatch

In addition to these antiparallel triplexes with 17 canonical triplets, we were interested to see how the presence of a 3'-end triplet mismatch affects triplex formation in each of these sequences. Similar experiments were therefore performed with the 17-mer-G TFO, which differs from 17-mer-A by the replacement of the 3'-A with G; this generates triplexes with 16 canonical G.GA and A.AT triplets and a 3'-terminal G.AT triplet mismatch. These experiments were inspired by the results of DEPC reaction of these fragments with the parallel TFOs, which showed enhanced DEPC reaction of some fragments with 12-mer-C, but not with 12-mer-T (Chapter 3). DNase I footprinting experiments with the 17-mer-G TFO are presented in Figure 4.7. Interestingly, this TFO generates clearer footprints in some fragments (*i.e.* AC and AT) despite producing triplexes with fewer canonical triplets. These persist to TFO concentration as low as 0.1 μM with AC, and around 0.6 μM in AT. In contrast, the footprints of fragments AG and AA are as similar as those with 17-mer-A, which are less clear even at a high TFO concentration (3 μM). These footprints again extend above (5'-end) the TFO binding site. In all four fragments, the footprints are accompanied by enhanced DNase I cleavage at a number of bands above (5'-end) the binding site. Quantitative analysis of the concentration dependence of these footprints is shown in Figure 4.8 and the calculated C_{50} values are presented in Table 4.3. Surprisingly, the value of AC is much lower than the other three fragments and it is about 10 times lower than AA and AG, and about 3 times compared with AT. There is no significant difference between the values with AG, AA and AT.

5′-…CAACCAXTTCTTTTTTCTCTTCCTAACACTT…-3′
3′-…GTTGGTXAAGAAAAAAGAGAAGGATTGTGAA…-5′
5′-GAGAAAAAAGAGAAGGA-3′(17-mer-G)

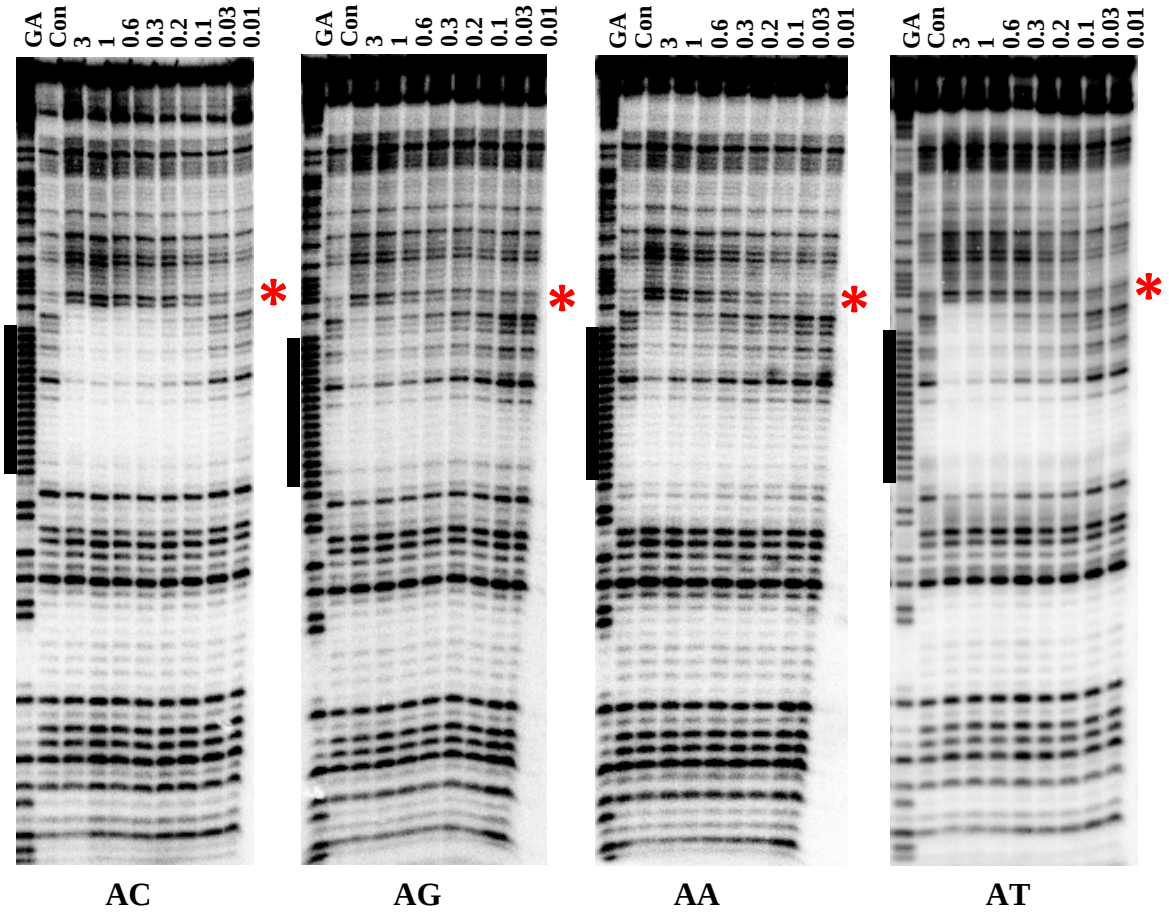

Figure 4.8 DNase I cleavage patterns of the four *tyr*T fragments in the presence of the 17-mer-G TFO. X is C, G, A and T in turn. These experiments were performed in 10 mM Tris-HCl at pH 7.0 in the presence of 10 mM $MnCl_2$ and 50 mM NaCl and were equilibrated for 2 hours at room temperature before digesting with DNase I. TFO concentrations (μM) are shown at the top of each gel lane. Tracks labelled "GA" and "con" are Maxam-Gilbert markers specific for purines and the cleavage patterns in the absence of TFO respectively. The filled boxes indicate the location of the triplex target sites and the red asterisks show the position of enhanced DNase I cleavage at the 5'-end of the TFO binding site.

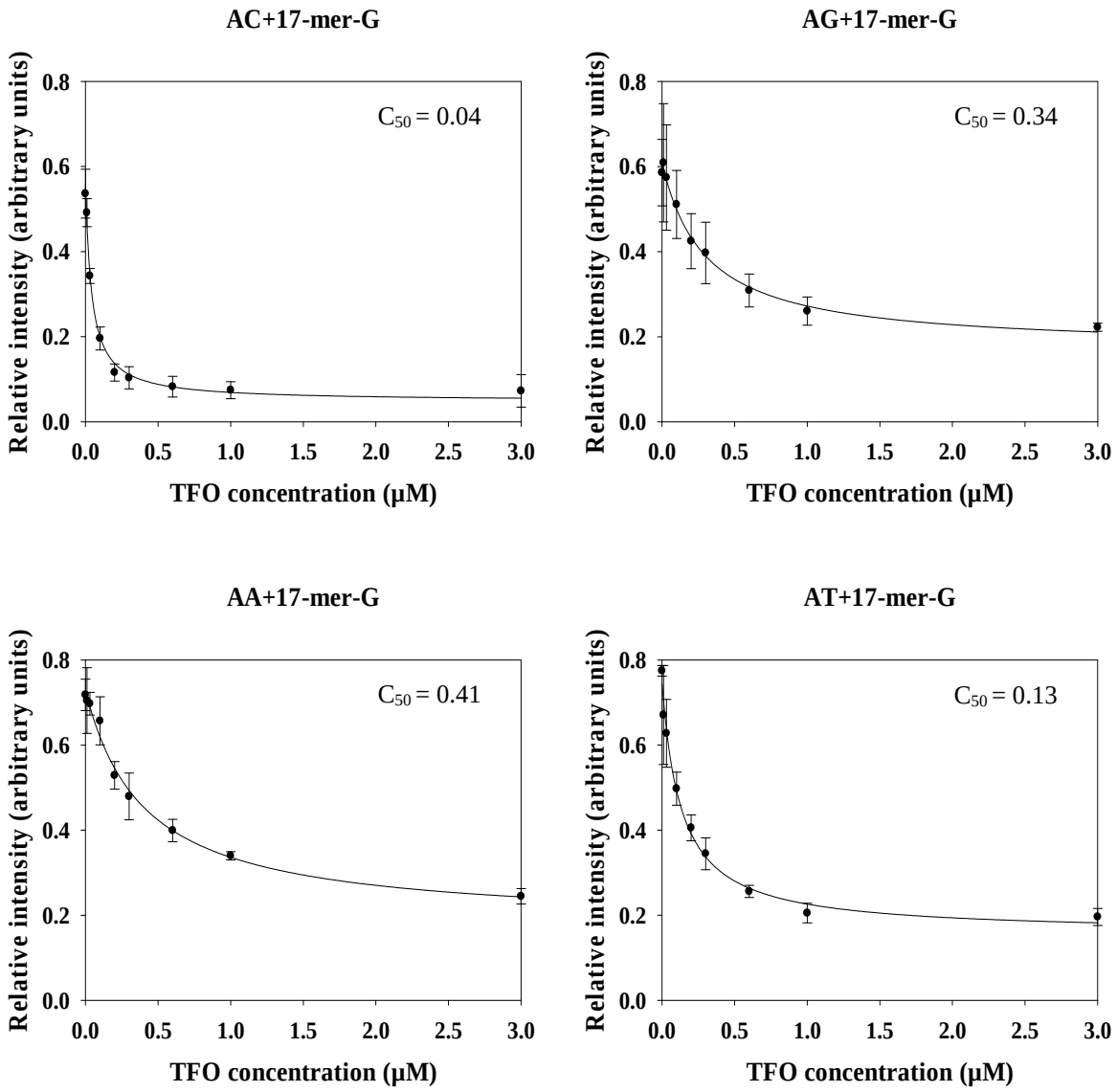

Figure 4.9 Footprinting plots showing the intensities of the footprints (arbitrary units) as a function of TFO concentration (µM). These were obtained from the DNase I footprinting gels of the triplex formed between 17-mer-G TFO and the four *tyr*T sequences shown in Figure 4.8. The C_{50} values, which correspond to the TFO concentration at which the relative intensity is half the maximum, are shown in Table 4.3. The curves correspond to a simple binding equation that was fitted to the data.

***tyr*T derivative**	**17-mer-G**
	C_{50} values (µM)
AC	0.04±0.01
AG	0.34±0.17
AA	0.41±0.14
AT	0.13±0.02

Table 4.3 The C_{50} values (µM) obtained from the DNase I footprinting plots of triplex formed between 17-mer-G and the four *tyr*T fragments (AC, AG, AA and AT).

Cleavage by other agents was also performed with these triplexes. The results of footprinting experiments with DEPC are presented in Figure 4.10. Again, the cleavage in controls of all four fragments is greatest around the As in the TFO binding site, and at a few bases at the 3'-end of the binding site in fragments AA and AT. Similar to the results with the 17-mer-A TFO, the cleavage patterns of all four fragments show reduced intensity in the presence of the 17-mer-G TFO. However, these are not accompanied by any DEPC enhanced cleavage.

The reaction of $KMnO_4$ with these four sequences in the presence of 17-mer-G TFO is presented in Figure 4.11. As noted with the 17-mer-A TFO, there are no TFO-induced changes in the cleavage patterns. Similarly the results of footprinting experiments with micrococcal nuclease also show that this TFO does not affect the cleavage patterns of the four fragments (Figure 4.12).

Figure 4.13 shows hydroxyl radical footprinting reactions with these four fragments in the presence of 17-mer-G TFO. As observed in the previous studies there are no significant TFO-induced changes in the cleavage pattern. Although there is some reduction in the band intensity within the binding site (Figure 4.14) the cleavage pattern is unaltered.

5′-…CAACCAXTTCTTTTTTCTCTTCCTAACACTT…-3′
3′-…GTTGGTXAAGAAAAAAGAGAAGGATTGTGAA…-5′
5′-GAGAAAAAAGAGAAGGA-3′(17-mer-G)

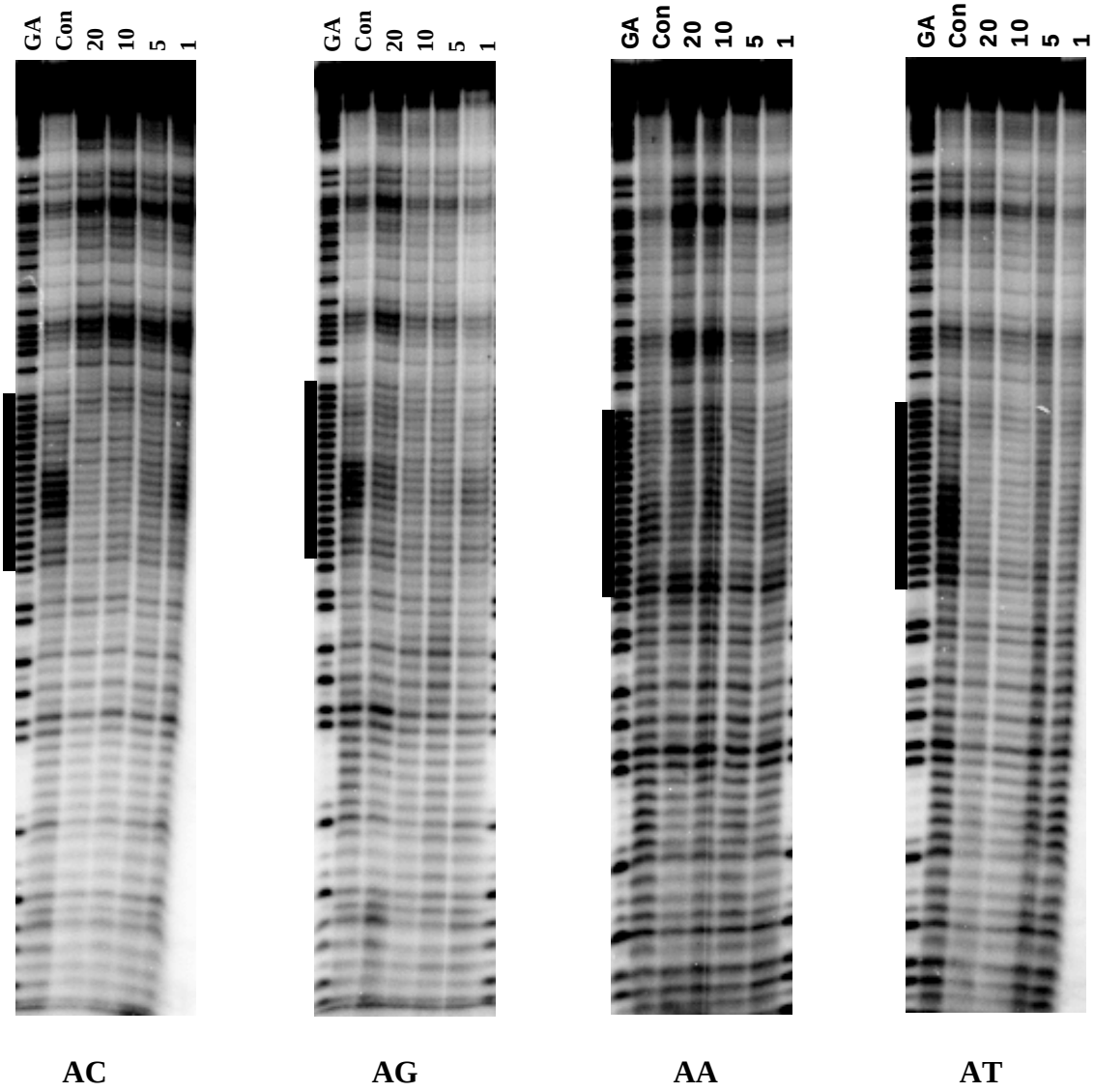

Figure 4.10 DEPC cleavage patterns of the four *tyr*T fragments in the presence of the 17-mer-G TFO. X is C, G, A and T in turn. These experiments were performed in 10 mM Tris-HCl at pH 7.0 in the presence of 10 mM $MnCl_2$ and 50 mM NaCl and were equilibrated for 2 hours at room temperature before reacting with DEPC. TFO concentrations (μM) are shown at the top of each gel lane and the tracks labelled "GA" and "con" are Maxam-Gilbert markers specific for purines and the cleavage patterns in the absence of TFO respectively. The filled boxes indicate the location of the triplex target sites.

5′-…CAACCAXTTCTTTTTTCTCTTCCTAACACTT…-3′
3′-…GTTGGTXAAGAAAAAAGAGAAGGATTGTGAA…-5′
5′-GAGAAAAAAGAGAAGGA-3′(17-mer-G)

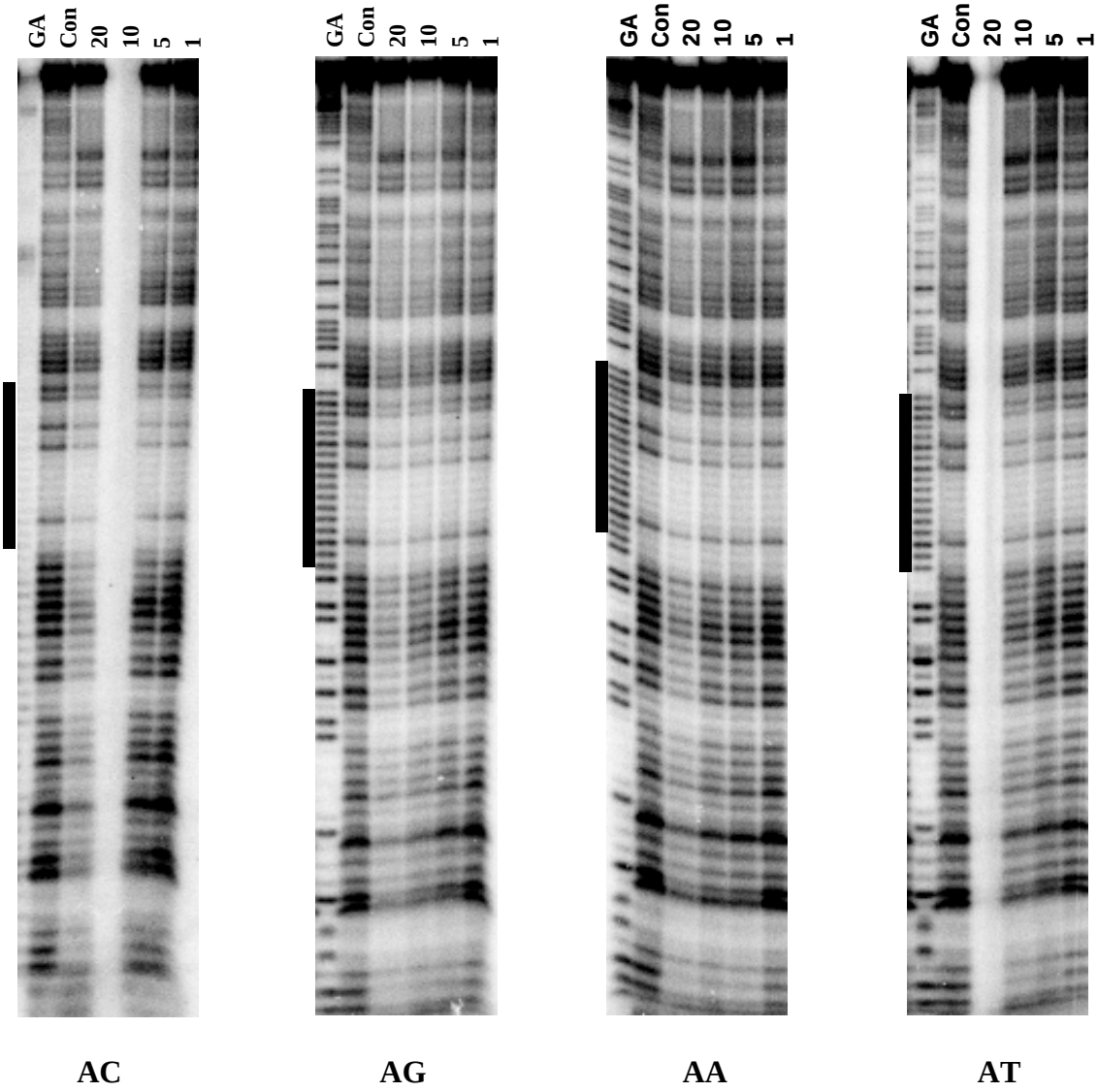

Figure 4.11 $KMnO_4$ cleavage patterns of the four *tyr*T DNA fragments in the presence of the 17-mer-G TFO. X is C, G, A and T in turn. These experiments were performed in 10 mM Tris-HCl at pH 7.0 in the presence of 10 mM $MnCl_2$ and 50 mM NaCl and were equilibrated for 2 hours at room temperature before reacting with $KMnO_4$. TFO concentrations (μM) are shown at the top of each gel lane. Tracks labelled "GA" and "con" are Maxam-Gilbert markers for specific for purines and the cleavage pattern in the absence of TFOs respectively. The filled boxes indicate the location of the triplex target sites.

5′-…CAACCAXTTCTTTTTTCTCTTCCTAACACTT…-3′
3′-…GTTGGTXAAGAAAAAAGAGAAGGATTGTGAA…-5′
5′-GAGAAAAAAGAGAAGGA-3′(17-mer-G)

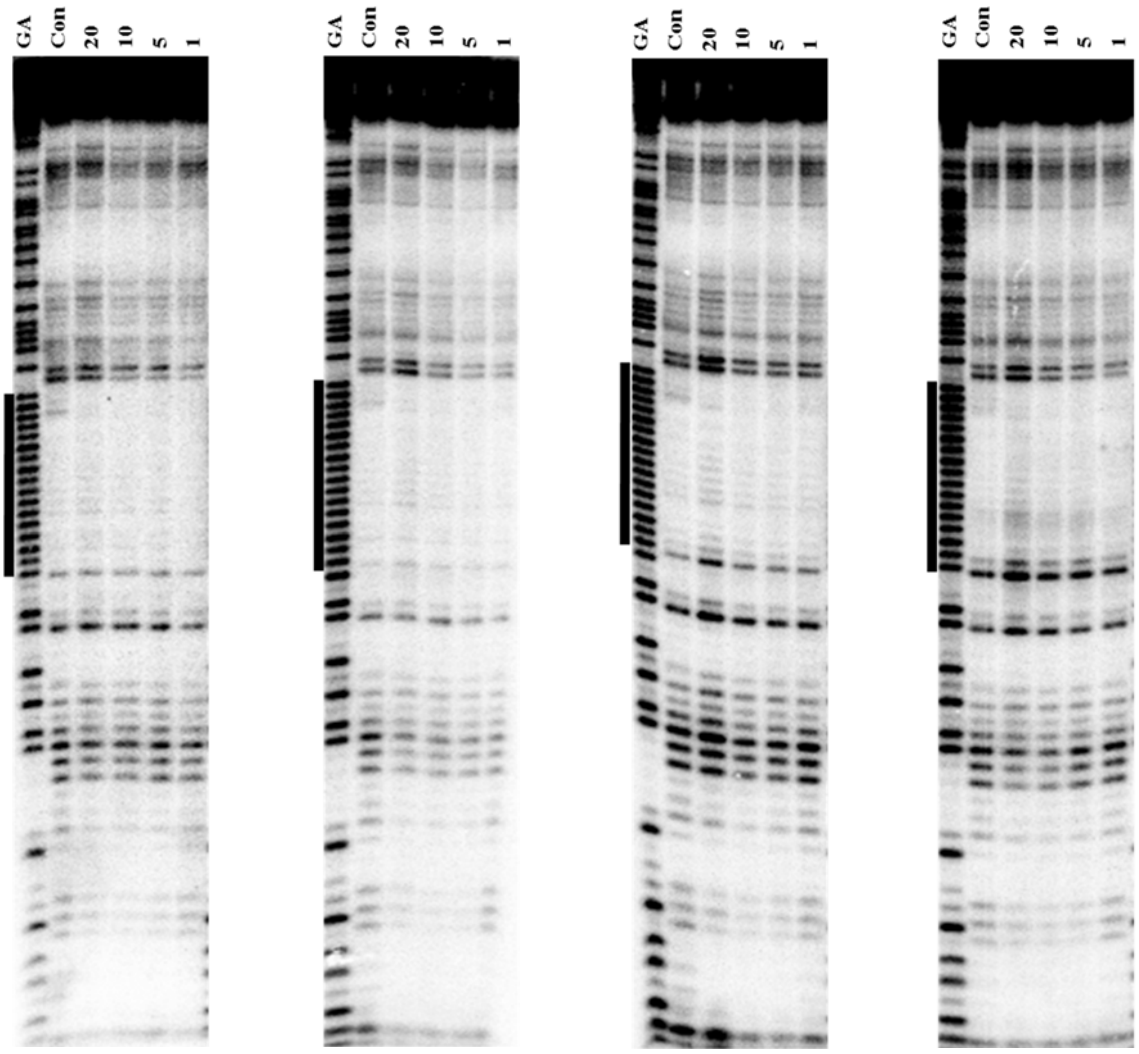

Figure 4.12 Micrococcal nuclease of the four *tyr*T fragments in the presence of the 17-mer-G TFO. X is a C, G, A and T in turn. These experiments were performed in 10 mM Tris-HCl at pH 7.0 in the presence of 10 mM $MnCl_2$ and 50 mM NaCl and were equilibrated for 2 hours at room temperature before digesting with the enzyme. TFO concentrations (μM) are shown at the top of each gel lane. The tracks labelled "GA" and "con" are Maxam-Gilbert markers specific for purines and the cleavage patterns in the absence of TFOs respectively. The filled boxes indicate the location of the triplex target sites.

5′-…CAACCAXTTCTTTTTTCTCTTCCTAACACTT…-3′
3′-…GTTGGTXAAGAAAAAAGAGAAGGATTGTGAA…-5′
5′-GAGAAAAAAGAGAAGGA-3′(17-mer-G)

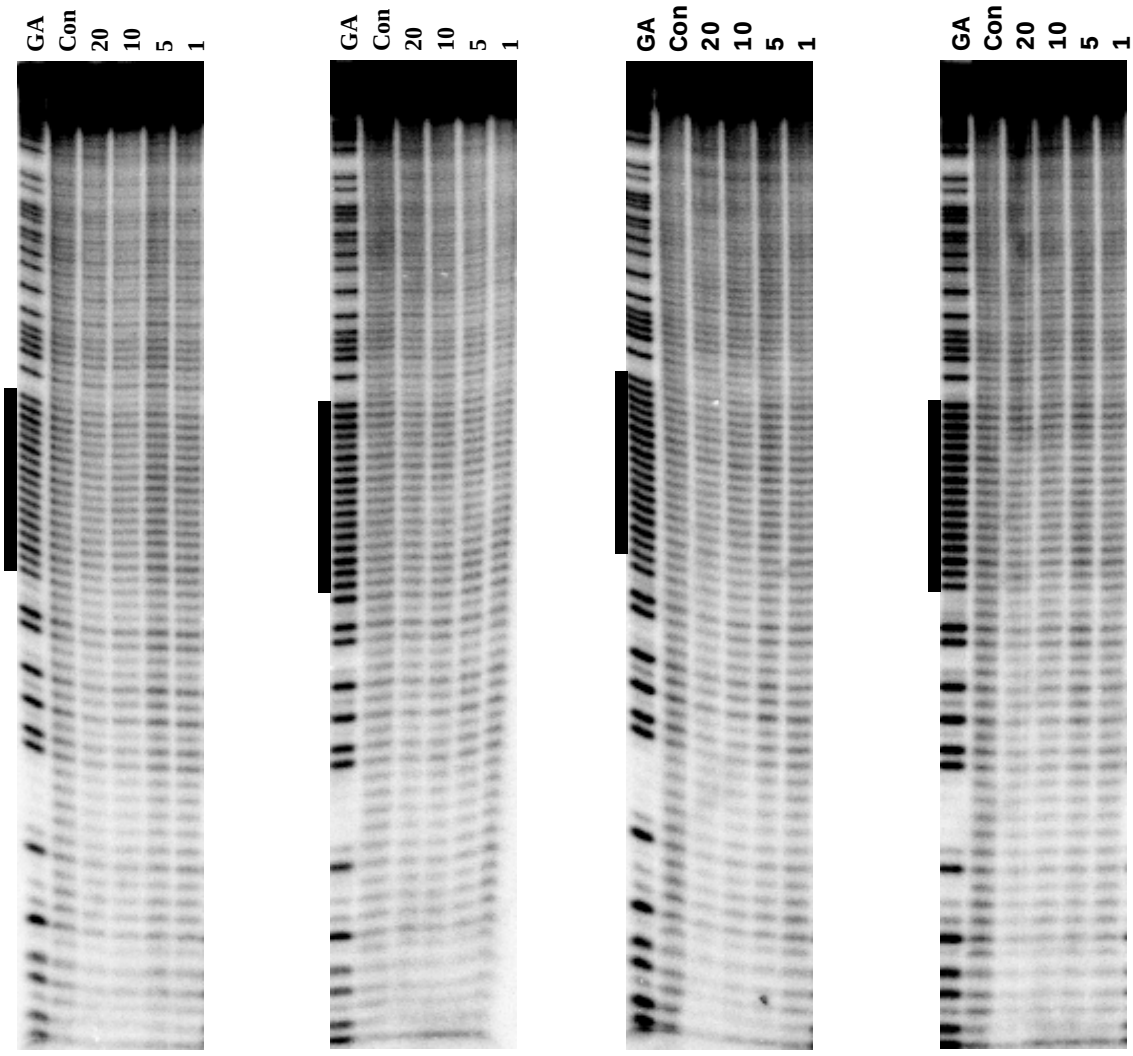

AC **AG** **AA** **AT**

Figure 4.13 Hydroxyl radical cleavage of the four *tyr*T fragments in the presence of the 17-mer-G TFO. X is C, G, A and T in turn. These experiments were performed in 10 mM Tris-HCl at pH 7.0 in the presence of 10 mM $MnCl_2$ and 50 mM NaCl and were equilibrated for 2 hours at room temperature before digesting with the hydroxyl radical mixture. TFO concentrations (μM) are shown at the top of each gel lane. The tracks labelled "GA" and "con" are Maxam-Gilbert markers specific for purines and the cleavage patterns in the absence of TFOs respectively. The filled boxes indicate the location of the triplex target sites.

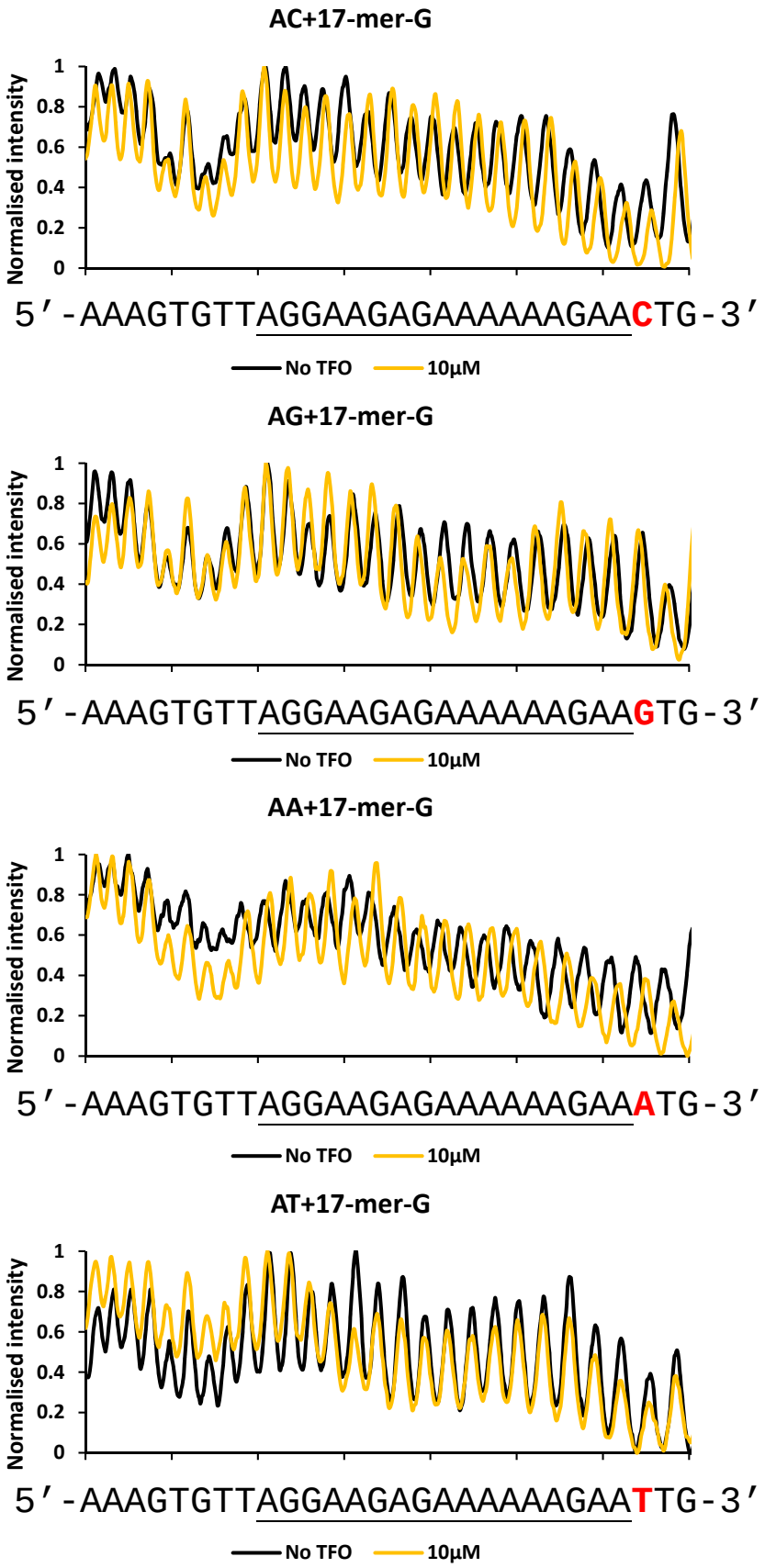

Figure 4.14 Densitometer plots of hydroxyl radical cleavage of the four fragments in the absence (black) and presence (yellow) of 10 μM of the 17-mer-G TFO (taken from the gels shown in Figure 4.13).

4.3.2. The effects of 3'-flanking bases on a triplex with a 3'-G.GC triplet.

4.3.2.1. The formation of 17-mer triplex with 17-mer-G TFO

The results in Chapter 3 with parallel triplexes showed that a 12-mer TFO with a 3'-C^+.GC triplet bound about 10 times better than the one with a 3'-T.AT (chapter 3, section 3.3.2.1). With this result in mind, we expected that antiparallel triplexes with a terminal G.GC would bind better than those with a terminal A.AT. We therefore examined the interaction of the 12-mer-G TFO with the four DNA fragments, to examine whether it bound better than 12-mer-A. The DNase I footprinting experiments with this TFO are presented in Figure 4.15. Similar to those with 3'-A.AT, no protection is seen in either of the four fragments. We therefore extended these studies with the longer 17-mer-G TFO. This TFO binds to the same site generating triplexes with a terminal G.GC triplet, as with 12-mer-G, but with 5 more triplets at the 5'-end of the polypurine target site. These results are shown in Figure 4.16. Again the longer TFO (17-mer-G) generates clear footprints with all four fragments. The footprints extend above (5'-), but not below (3'-end) the target site and persist to concentrations of about 0.2 μM. This is about 10 times lower than the triplexes with a 3'-A.AT triplet, for which the footprints persist to about 3 μM. All the footprints are accompanied by enhanced DNase I cleavage above (5'-) the binding site. Quantitative analysis of the concentration dependence of these footprints are presented in Figure 4.17 and the calculated C_{50} values are shown in Table 4.4. These show no significant difference between the four fragments though they are about 10 times lower than the values of triplexes with a 3'-A.AT triplet (Table 4.2).

5′-…CAACCAGCTCTTTTTTCTCTTCCTAACACTT…-3′
3′-…GTTGGTXGAGAAAAAAGAGAAGGATTGTGAA…-5′
5′-GAGAAAAAAGAG-3′ (12-mer-G TFO)

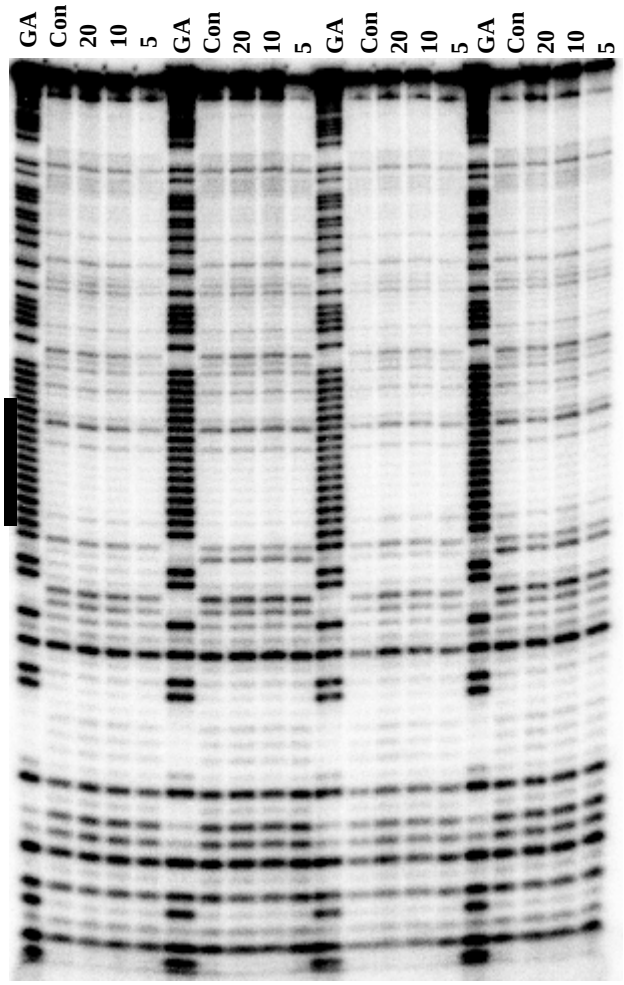

Figure 4.15 DNase I cleavage patterns of four DNA fragments (GA, GT, GG and GC) containing different bases (X) at the 3'-end of the homopurine stretch (underlined) in the presence of different concentration of the 12-mer-G TFO. These experiments were performed in 10 mM Tris-HCl at pH 7.0 in the presence of 10 mM $MnCl_2$ and 50 mM NaCl and were equilibrated for 2 hours at room temperature before digesting with DNase I. TFO concentrations (μM) are shown at the top of each gel lane. The tracks labelled "GA" and "con" are Maxam-Gilbert markers specific for purines and the cleavage pattern in the absence of TFOs respectively. The filled box indicates the location of the triplex target site.

5′-…CAACCAXCTCTTTTTTCTCTTCCTAACACTT…-3′
3′-…GTTGGTXGAGAAAAAAGAGAAGGATTGTGAA…-5′
5′-GAGAAAAAAGAGAAGGA-3′(17-mer-G)

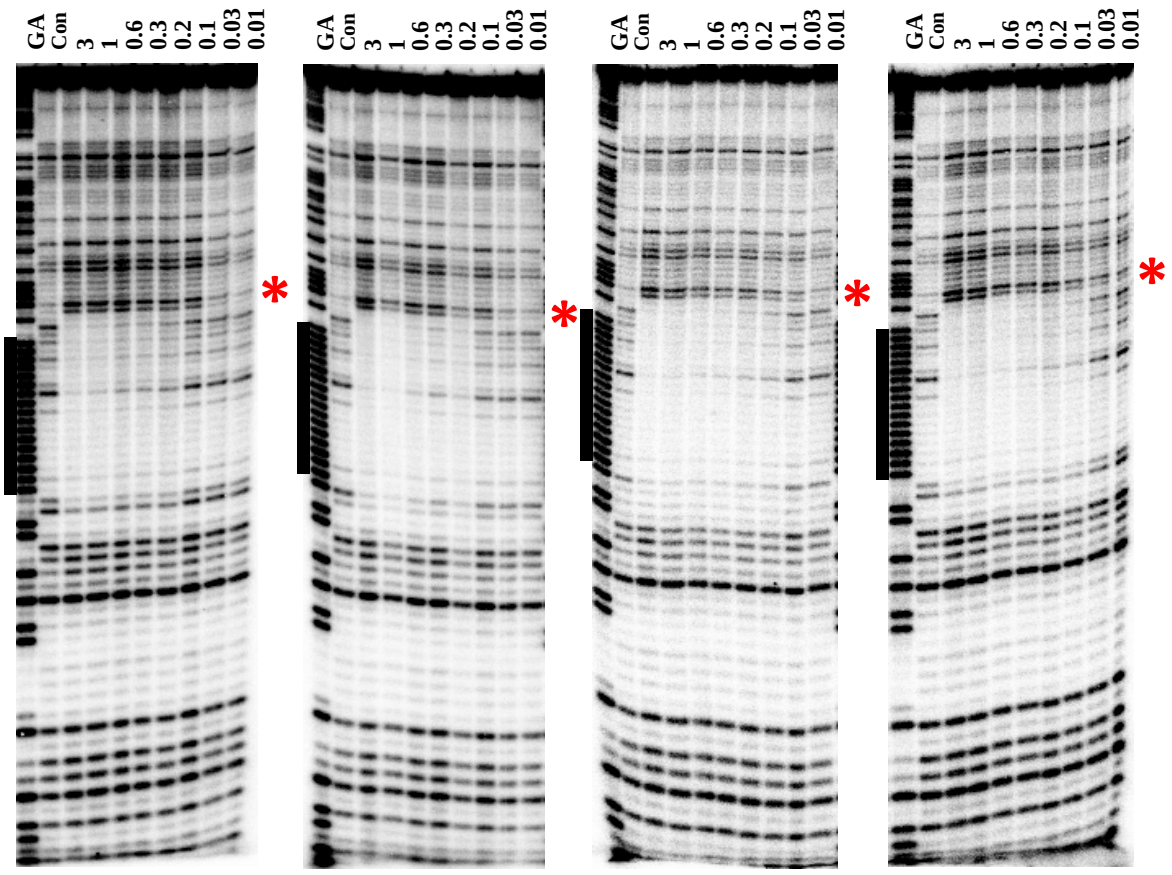

Figure 4.16 DNase I cleavage patterns of the four *tyr*T fragments in the presence of the 17-mer-G TFO. X is C, G, A and T in turn. These experiments were performed in 10 mM Tris-HCl at pH 7.0 in the presence of 10 mM $MnCl_2$ and 50 mM NaCl and were equilibrated for 2 hours at room temperature before digesting with DNase I. TFO concentrations (μM) are shown at the top of each gel lane. Tracks labelled “GA” and “con” are Maxam-Gilbert markers specific for purines and the cleavage patterns in the absence of TFO respectively. The filled boxes indicate the location of the triplex target sites and the red asterisks show the position of enhanced DNase I cleavage at the 5’-end of the TFO binding site.

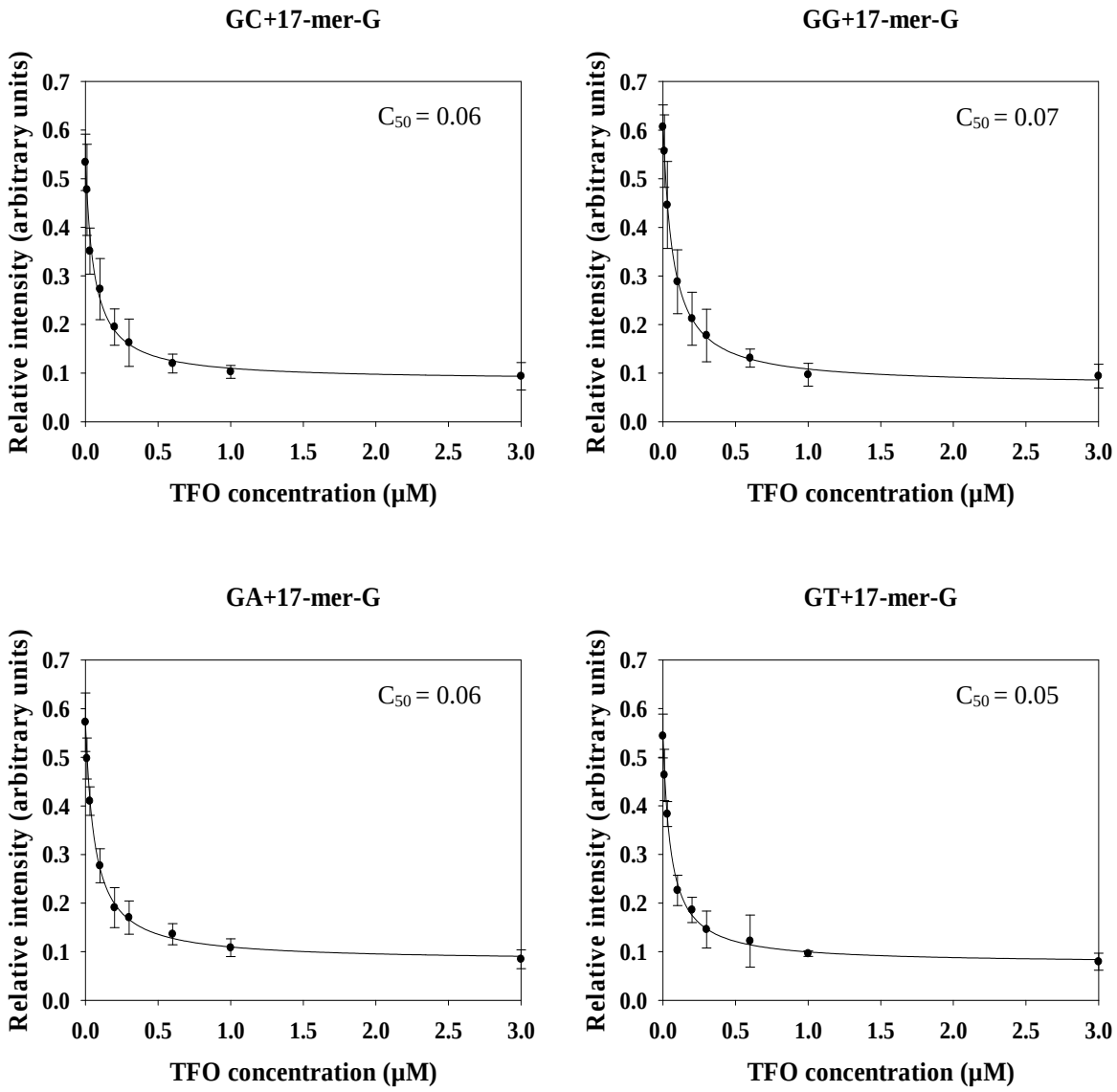

Figure 4.17 Footprinting plots showing the intensities of the footprints (arbitrary units) as a function of TFO concentration (μM). These were obtained from the DNase I footprinting gels of the triplex formed between 17-mer-G TFO and the four *tyr*T sequences as shown in Figure 4.16. The C_{50} values, which correspond to the TFO concentration at which the relative intensity is half the maximum, are shown in Table 4.4. The curves correspond to a simple binding equation that was fitted to the data.

***tyr*T derivative**	**17-mer-G**
	C_{50} values (µM)
GC	0.06±0.02
GG	0.07±0.02
GA	0.06±0.03
GT	0.05±0.01

Table 4.4 The C_{50} values (µM) obtained from the DNase I footprinting plots for the triplex formed with the 17-mer-G and the four *tyr*T fragments (GC, GG, GA and GT).

The results of footprinting experiments with DEPC are shown in Figure 4.18. Reductions in band intensity are seen within the target sites for all four fragments, but there are no TFO-induced enhancements in reaction with DEPC.

Figure 4.19 presents the results of $KMnO_4$ reactions with these four fragments in the presence of 17-mer-G TFO. Again the TT dinucleotide at above (5'-) the TFO's binding site of all fragments is highly reactive to $KMnO_4$. However there are no TFO-induced changes in this reaction, even in the fragment AT.

Figure 4.20 shows the results of footprinting experiments with micrococcal nuclease on these four fragments. Once again there is very low cleavage efficiency at the higher TFO concentrations (*i.e.* 20, 10, 5 µM). Similarly, there are no TFO-induced cleavage enhancements with these four fragments, even in AA and AT.

Figure 4.21 shows the results of hydroxyl radical cleavage with these four fragments. There is no TFO-induced cleavage enhancements with fragments.

5′-…CAACCAXCTCTTTTTTCTCTTCCTAACACTT…-3′
3′-…GTTGGTXGAGAAAAAAGAGAAGGATTGTGAA…-5′
5′-GAGAAAAAAGAGAAGGA-3′(17-mer-G)

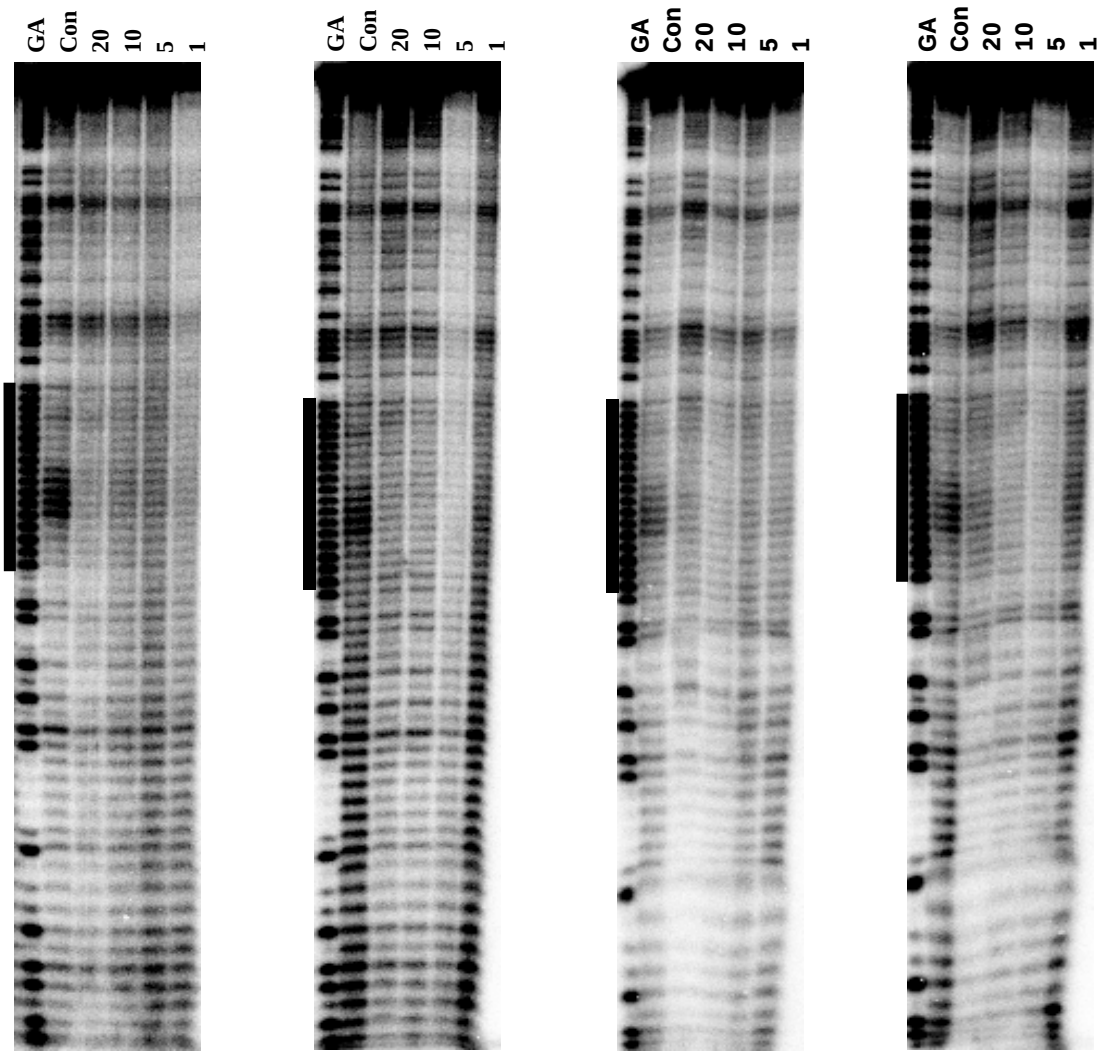

GC GG GA GT

Figure 4.18 DEPC cleavage patterns of the four *tyr*T fragments in the presence of the 17-mer-G TFO. X is C, G, A and T in turn. These experiments were performed in 10 mM Tris-HCl at pH 7.0 in the presence of 10 mM $MnCl_2$ and 50 mM NaCl and were equilibrated for 2 hours at room temperature before reacting with DEPC. TFO concentrations (μM) are shown at the top of each gel lane and the tracks labelled "GA" and "con" are Maxam-Gilbert markers specific for purines and the cleavage patterns in the absence of TFO respectively. The filled boxes indicate the location of the triplex target sites.

5′-…CAACCAXCTCTTTTTTCTCTTCCTAACACTT…-3′
3′-…GTTGGTXGAGAAAAAAGAGAAGGATTGTGAA…-5′
5′-GAGAAAAAAGAGAAGGA-3′(17-mer-G)

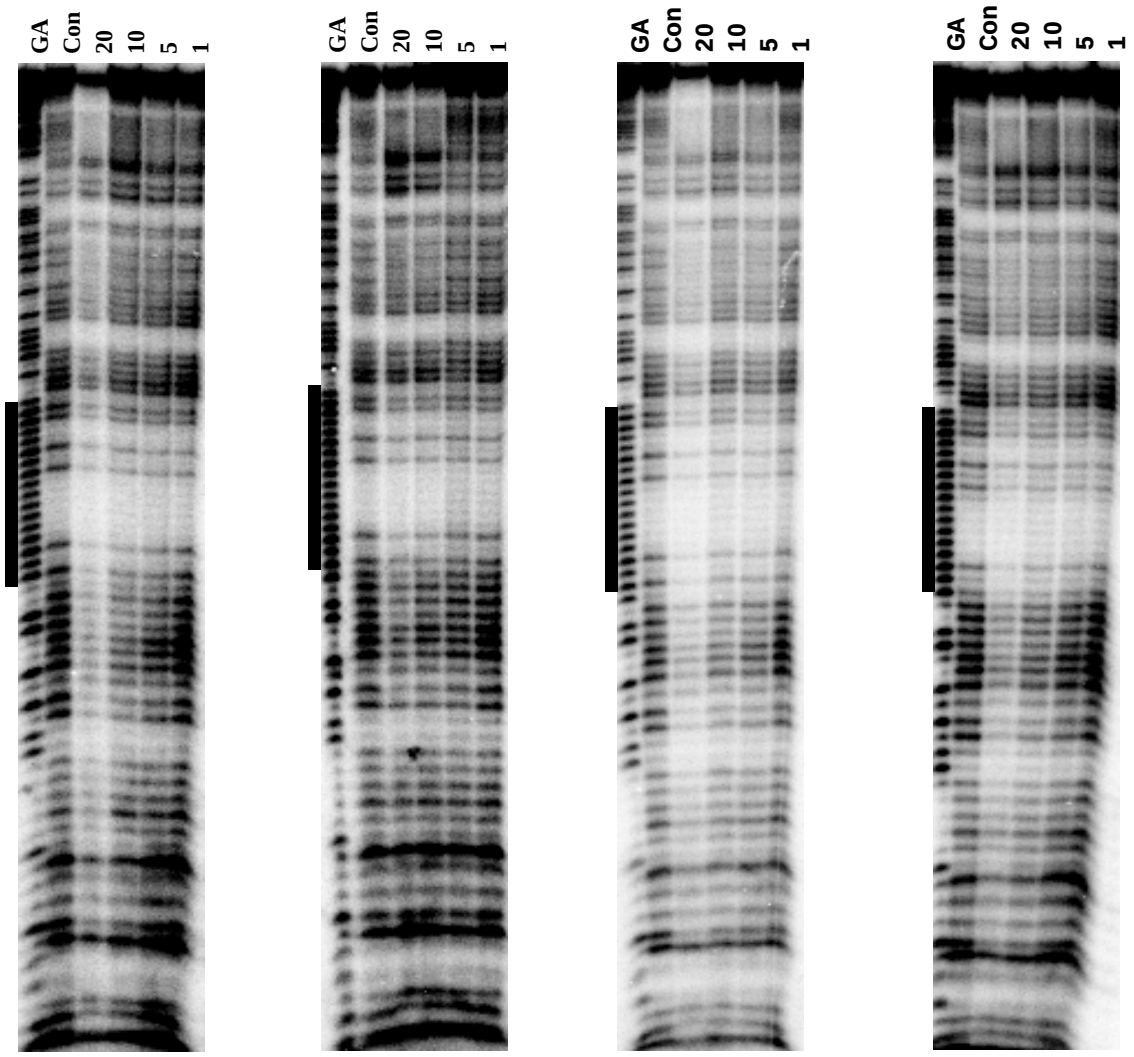

GC GG GA GT

Figure 4.19 $KMnO_4$ cleavage patterns of the four *tyr*T DNA fragments in the presence of the 17-mer-G TFO. X is C, G, A and T in turn. These experiments were performed in 10 mM Tris-HCl at pH 7.0 in the presence of 10 mM $MnCl_2$ and 50 mM NaCl and were equilibrated for 2 hours at room temperature before reacting with $KMnO_4$. TFO concentrations (μM) are shown at the top of each gel lane. Tracks labelled "GA" and "con" are Maxam-Gilbert markers for specific for purines and the cleavage pattern in the absence of TFOs respectively. The filled boxes indicate the location of the triplex target sites.

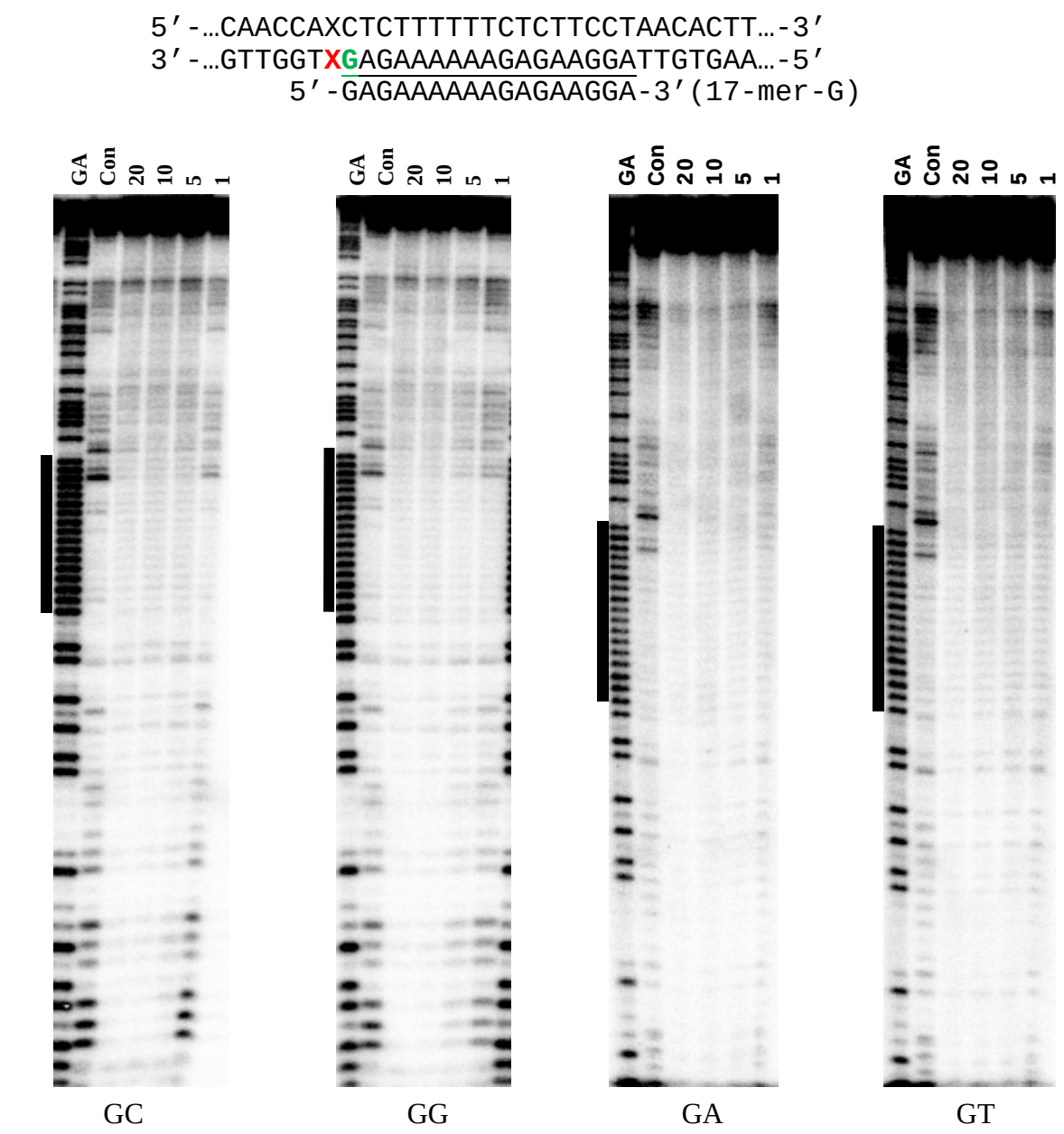

Figure 4.20 Micrococcal nuclease cleavage of the four *tyr*T fragments in the presence of the 17-mer-G TFO. X is a C, G, A and T in turn. These experiments were performed in 10 mM Tris-HCl at pH 7.0 in the presence of 10 mM $MnCl_2$ and 50 mM NaCl and were equilibrated for 2 hours at room temperature before digesting with the enzyme. TFO concentrations (μM) are shown at the top of each gel lane. The tracks labelled "GA" and "con" are Maxam-Gilbert markers specific for purines and the cleavage patterns in the absence of TFOs respectively. The filled boxes indicate the location of the triplex target sites.

5′-…CAACCAXCTCTTTTTTCTCTTCCTAACACTT…-3′
3′-…GTTGGTXGAGAAAAAAGAGAAGGATTGTGAA…-5′
5′-GAGAAAAAAGAGAAGGA-3′(17-mer-G)

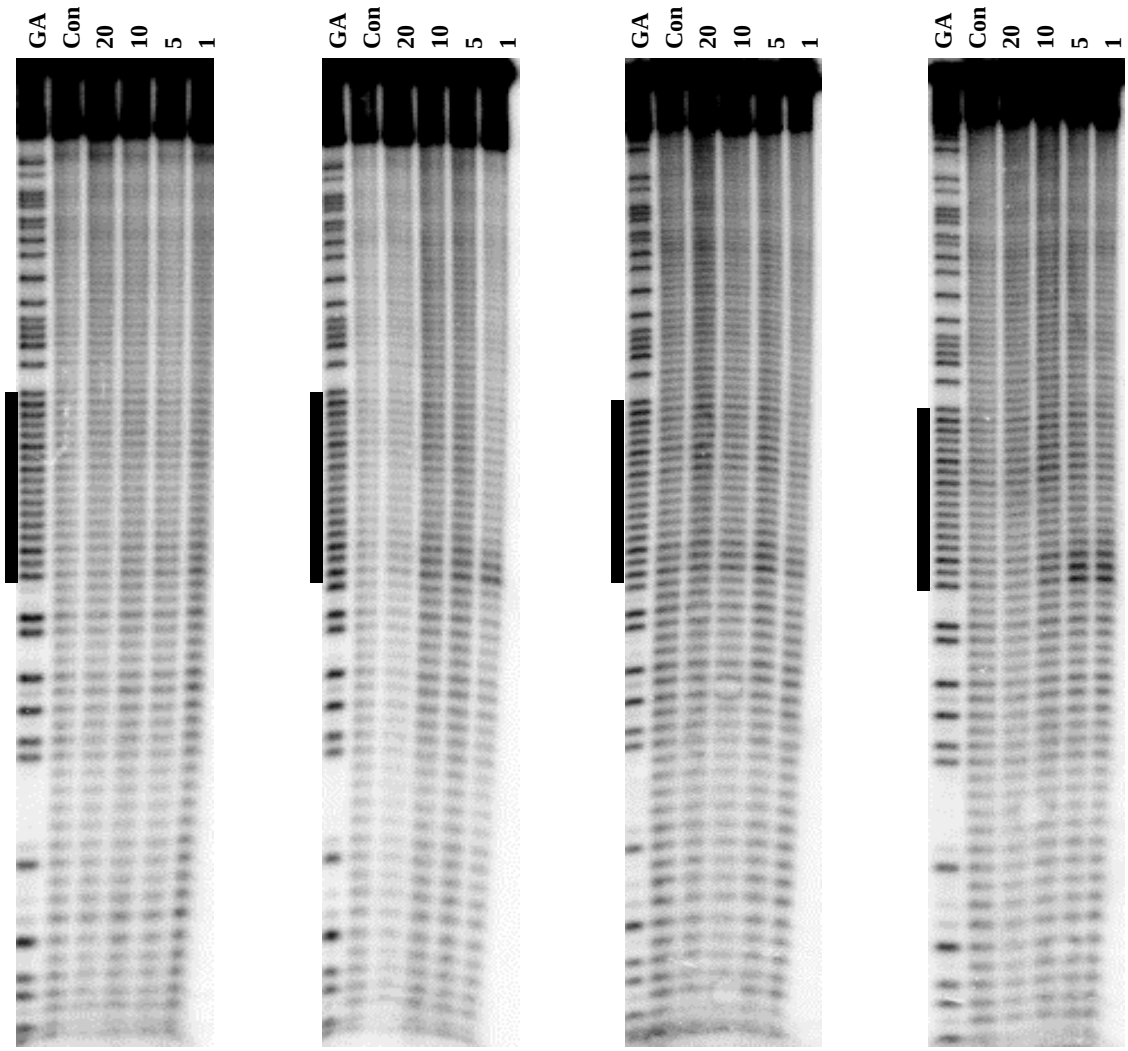

Figure 4.21 Hydroxyl radical cleavage of the four *tyr*T fragments in the presence of the 17-mer-G TFO. X is C, G, A and T in turn. These experiments were performed in 10 mM Tris-HCl at pH 7.0 in the presence of 10 mM $MnCl_2$ and 50 mM NaCl and were equilibrated for 2 hours at room temperature before digesting with the hydroxyl radical mixture. TFO concentrations (μM) are shown at the top of each gel lane. The tracks labelled "GA" and "con" are Maxam-Gilbert markers specific for purines and the cleavage patterns in the absence of TFOs respectively. The filled boxes indicate the location of the triplex target sites.

4.3.2.2. The 17-mer triplex with 17-mer-A TFO, generating a 3’ A.GC mismatch

DNase I footprinting results of triplexes with a 3’G.AT triplet mismatch (section 4.3.1.2) were surprising, showing substantially strong footprints with some fragments (*i.e.* AC and AT). We therefore explored whether a 3’-A.GC triplet mismatch would have the same effect on triplex formation. The four fragments were incubated with the 17-mer-A TFO, generating triplexes containing 16 canonical G.GA and A.AT triplets and a 3’-terminal A.GC triplet mismatch. The DNase I footprinting results are presented in Figure 4.22. As expected, this TFO does not bind very well and the footprints are very faint even at the highest TFO concentration (3 μM). Again, these extend beyond the 5’-, but not 3’-end of the TFO binding site. These are also accompanied by enhanced DNase I cleavage in a number of bands above (5’-end) the binding site. Quantitative analyses of these footprints are shown in Figure 4.23 and the calculated C_{50} values are presented in Table 4.5. These show no significant differences between the values of each of the fragments, which are unsurprisingly much higher than those triplexes with the fully matched 17-mer-G TFO.

5′-…CAACCAXCTCTTTTTTCTCTTCCTAACACTT…-3′
3′-…GTTGGTXGAGAAAAAAGAGAAGGATTGTGAA…-5′
5′-AAGAAAAAAGAGAAGGA-3′(17-mer-A)

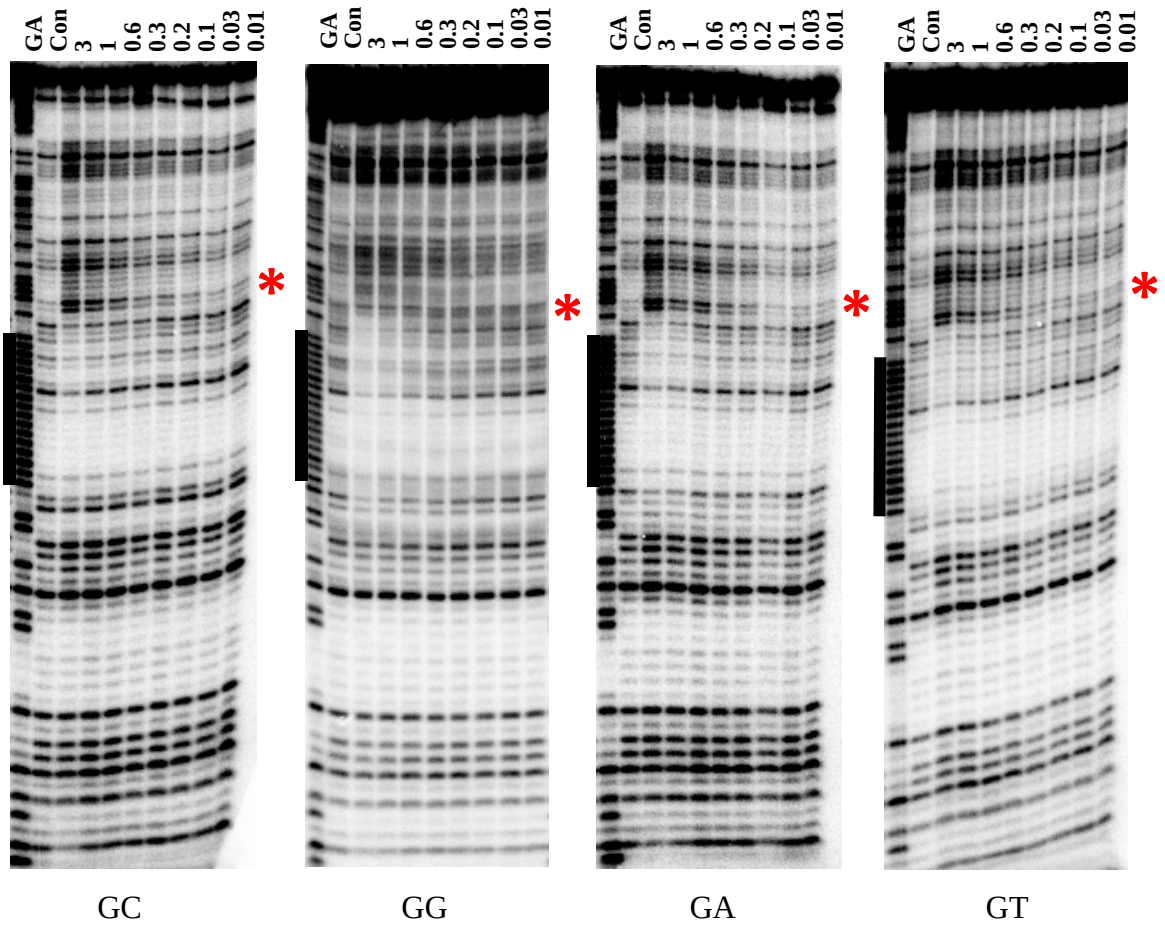

Figure 4.22 DNase I cleavage patterns of the four *tyr*T fragments in the presence of the 17-mer-A TFO. X is C, G, A and T in turn. These experiments were performed in 10 mM Tris-HCl at pH 7.0 in the presence of 10 mM $MnCl_2$ and 50 mM NaCl and were equilibrated for 2 hours at room temperature before digesting with DNase I. TFO concentrations (μM) are shown at the top of each gel lane. Tracks labelled “GA” and “con” are Maxam-Gilbert markers specific for purines and the cleavage patterns in the absence of TFO respectively. The filled boxes indicate the location of the triplex target sites and the red asterisks show the position of enhanced DNase I cleavage at the 5’-end of the TFO binding site.

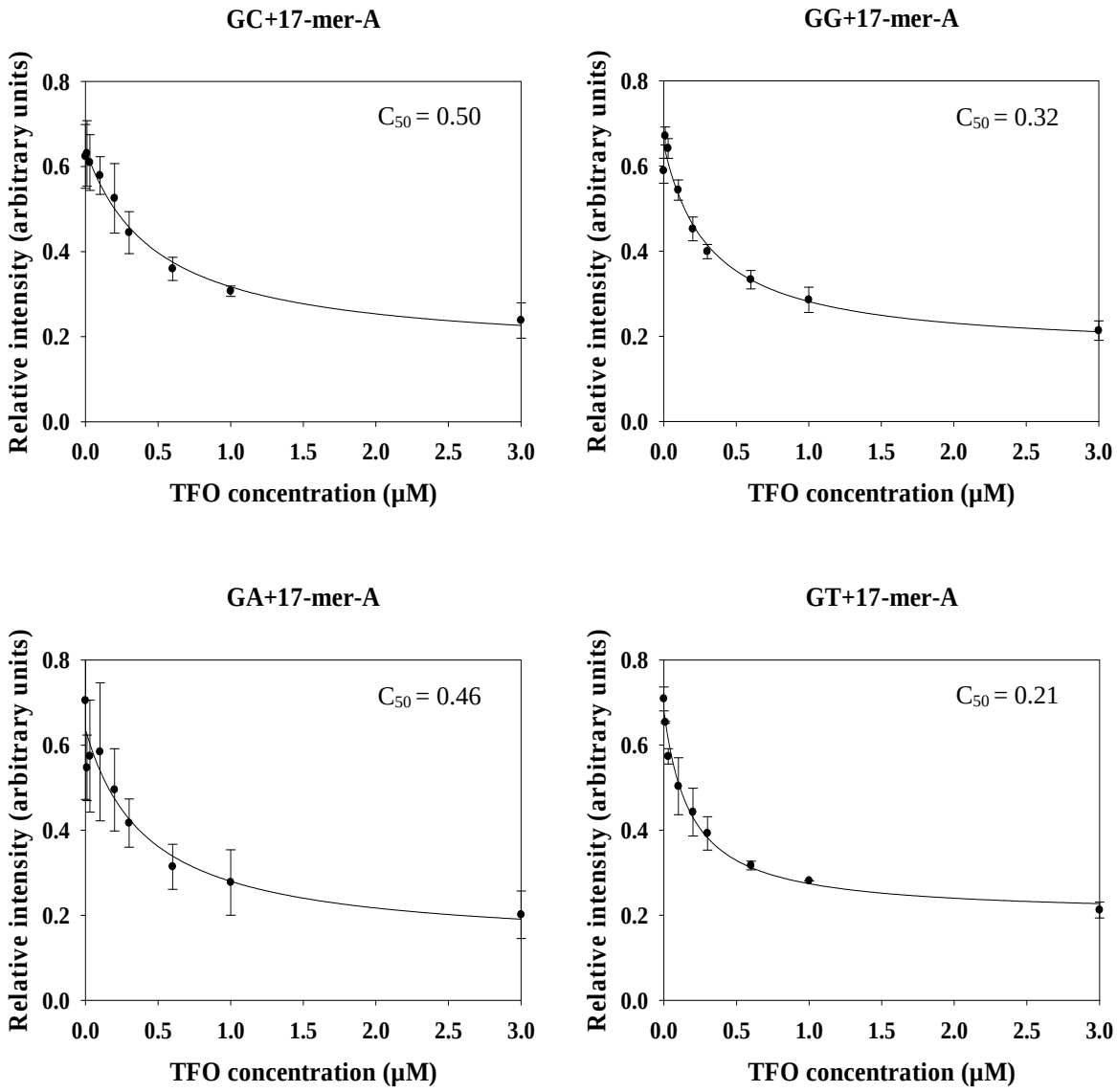

Figure 4.23 Footprinting plots showing the intensities of the footprints (arbitrary units) as a function of TFO concentration (μM). These were obtained from the DNase I footprinting gels of the triplex formed between 17-mer-A TFO and the four *tyr*T sequences as shown in Figure 4.22. The C_{50} values, which correspond to the TFO concentration at which the relative intensity is half the maximum, are shown in Table 4.5. The curves correspond to a simple binding equation that was fitted to the data.

***tyr*T derivative**	**17-mer-A**
	C_{50} values (µM)
GC	0.50±0.07
GG	0.32±0.01
GA	0.46±0.15
GT	0.21±0.17

Table 4.5 C_{50} values (µM) obtained from the DNase I footprinting plots of the triplex formed between 17-mer-A and the four *tyr*T fragments (GC, GG, GA and GT).

The reactions with DEPC and $KMnO_4$ were again performed for these triplexes, and the results are presented in Figure 4.24 and 4.25 respectively. The cleavage patterns of these fragments with 17-mer-A TFO are identical to those triplexes with 17-mer-G TFO; there are no TFO-induced enhanced reaction with both cleavage agents.

Figure 4.26 shows the results of footprinting experiments with micrococcal nuclease using these fragments. There are no TFO-induced changes in the cleavage patterns of the four fragments. Similarly, none of these fragments show TFO-induced enhanced cleavage with hydroxyl radicals as shown in Figure 4.27 and 4.28.

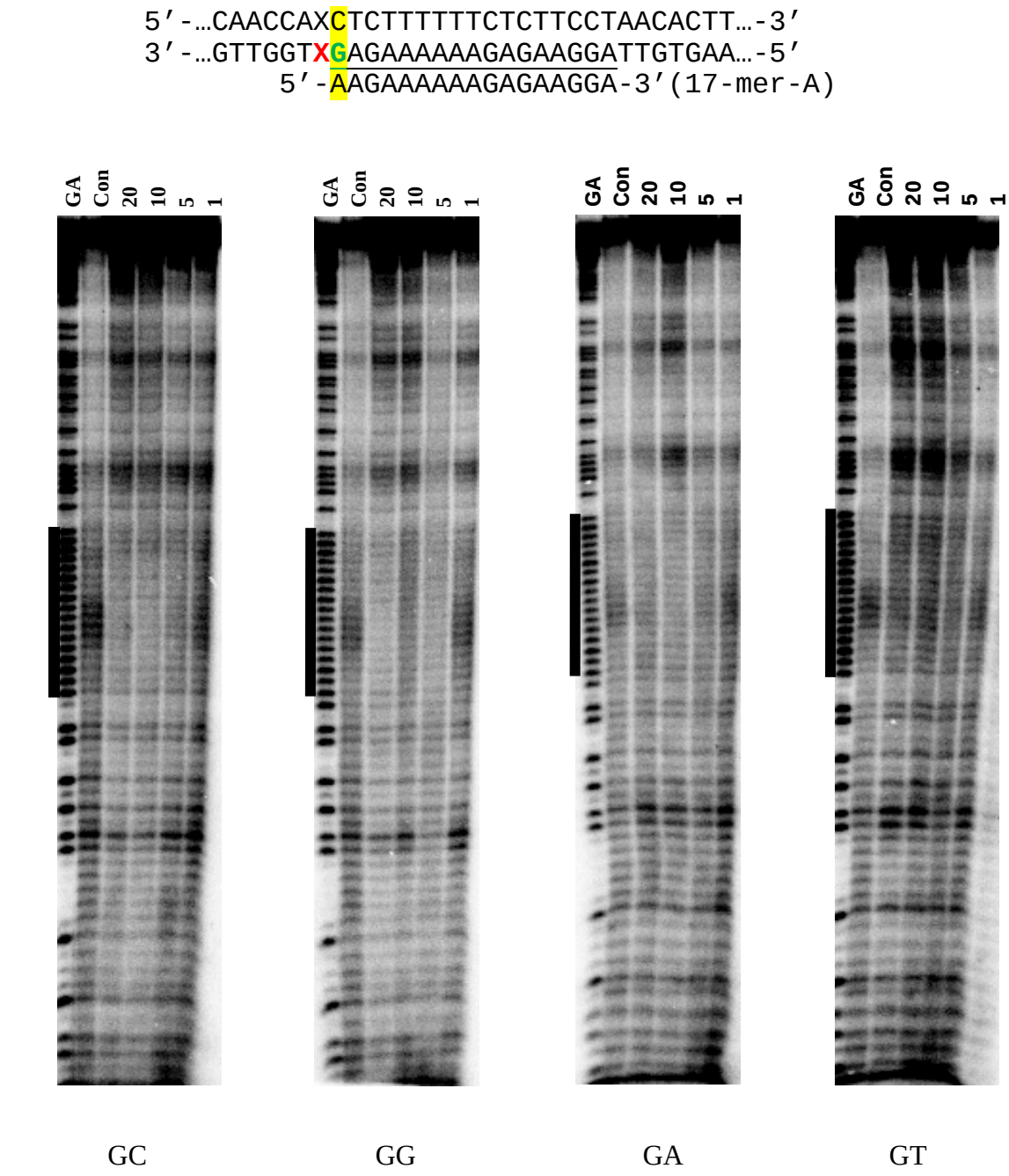

Figure 4.24 DEPC cleavage patterns of the four *tyr*T fragments in the presence of the 17-mer-A TFO. X is C, G, A and T in turn. These experiments were performed in 10 mM Tris-HCl at pH 7.0 in the presence of 10 mM $MnCl_2$ and 50 mM NaCl and were equilibrated for 2 hours at room temperature before reacting with DEPC. TFO concentrations (μM) are shown at the top of each gel lane and the tracks labelled "GA" and "con" are Maxam-Gilbert markers specific for purines and the cleavage patterns in the absence of TFO respectively. The filled boxes indicate the location of the triplex target sites.

```
5′-…CAACCAXCTCTTTTTTCTCTTCCTAACACTT…-3′
3′-…GTTGGTXGAGAAAAAAGAGAAGGATTGTGAA…-5′
        5′-AAGAAAAAAGAGAAGGA-3′(17-mer-A)
```

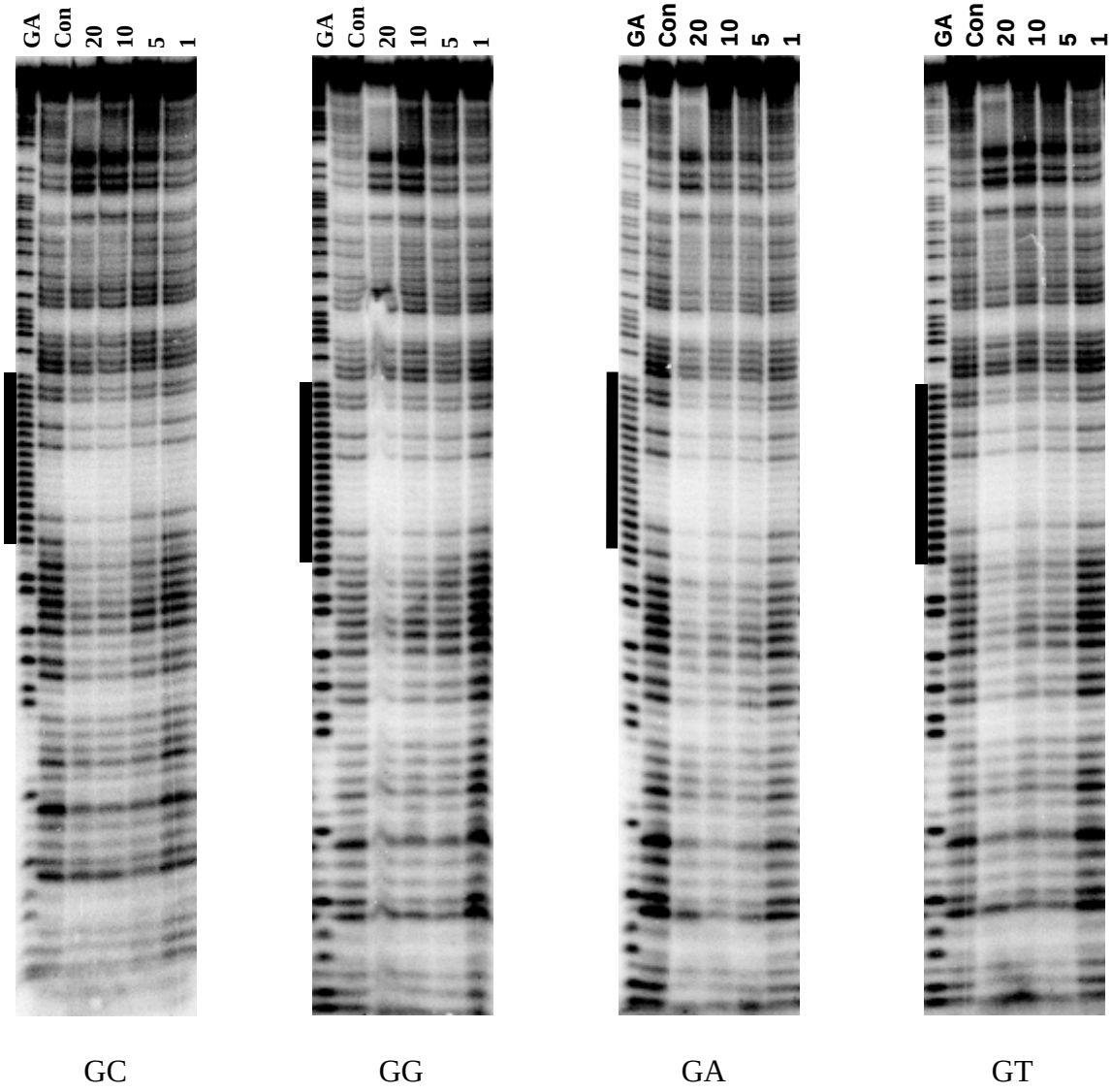

Figure 4.25 $KMnO_4$ cleavage patterns of the four *tyr*T DNA fragments in the presence of the 17-mer-A TFO. X is C, G, A and T in turn. These experiments were performed in 10 mM Tris-HCl at pH 7.0 in the presence of 10 mM $MnCl_2$ and 50 mM NaCl and were equilibrated for 2 hours at room temperature before reacting with $KMnO_4$. TFO concentrations (μM) are shown at the top of each gel lane. Tracks labelled "GA" and "con" are Maxam-Gilbert markers for specific for purines and the cleavage pattern in the absence of TFOs respectively. The filled boxes indicate the location of the triplex target sites.

5′-…CAACCAXCTCTTTTTTCTCTTCCTAACACTT…-3′
3′-…GTTGGTXGAGAAAAAAGAGAAGGATTGTGAA…-5′
5′-AAGAAAAAAGAGAAGGA-3′(17-mer-A)

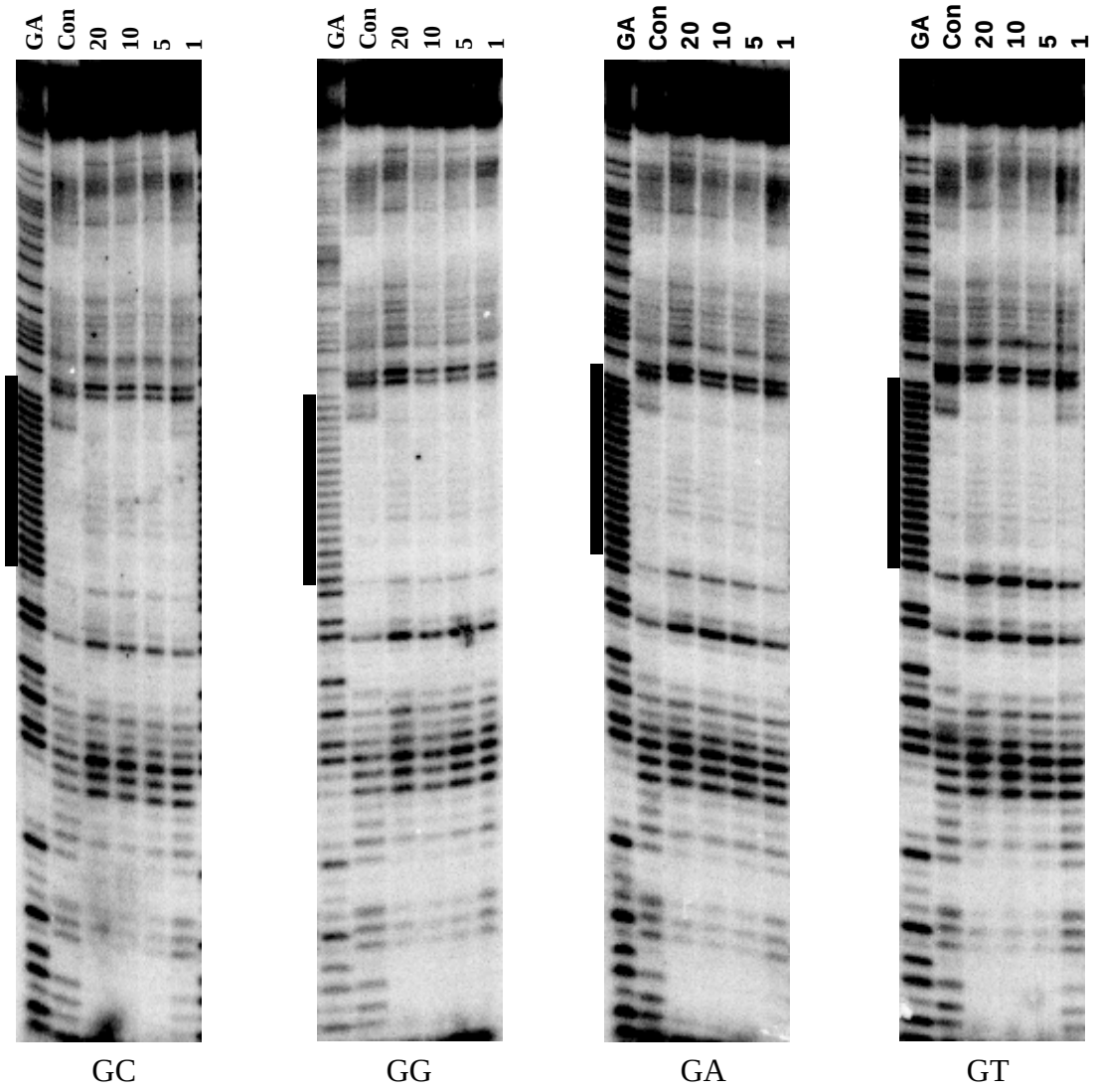

Figure 4.26 Micrococcal nuclease digestion of the four *tyr*T fragments in the presence of the 17-mer-A TFO. X is a C, G, A and T in turn. These experiments were performed in 10 mM Tris-HCl at pH 7.0 in the presence of 10 mM $MnCl_2$ and 50 mM NaCl and were equilibrated for 2 hours at room temperature before digesting with the enzyme. TFO concentrations (μM) are shown at the top of each gel lane. The tracks labelled "GA" and "con" are Maxam-Gilbert markers specific for purines and the cleavage patterns in the absence of TFOs respectively. The filled boxes indicate the location of the triplex target sites.

5′-…CAACCAXCTCTTTTTTCTCTTCCTAACACTT…-3′
3′-…GTTGGTXGAGAAAAAAGAGAAGGATTGTGAA…-5′
5′-AAGAAAAAAGAGAAGGA-3′(17-mer-A)

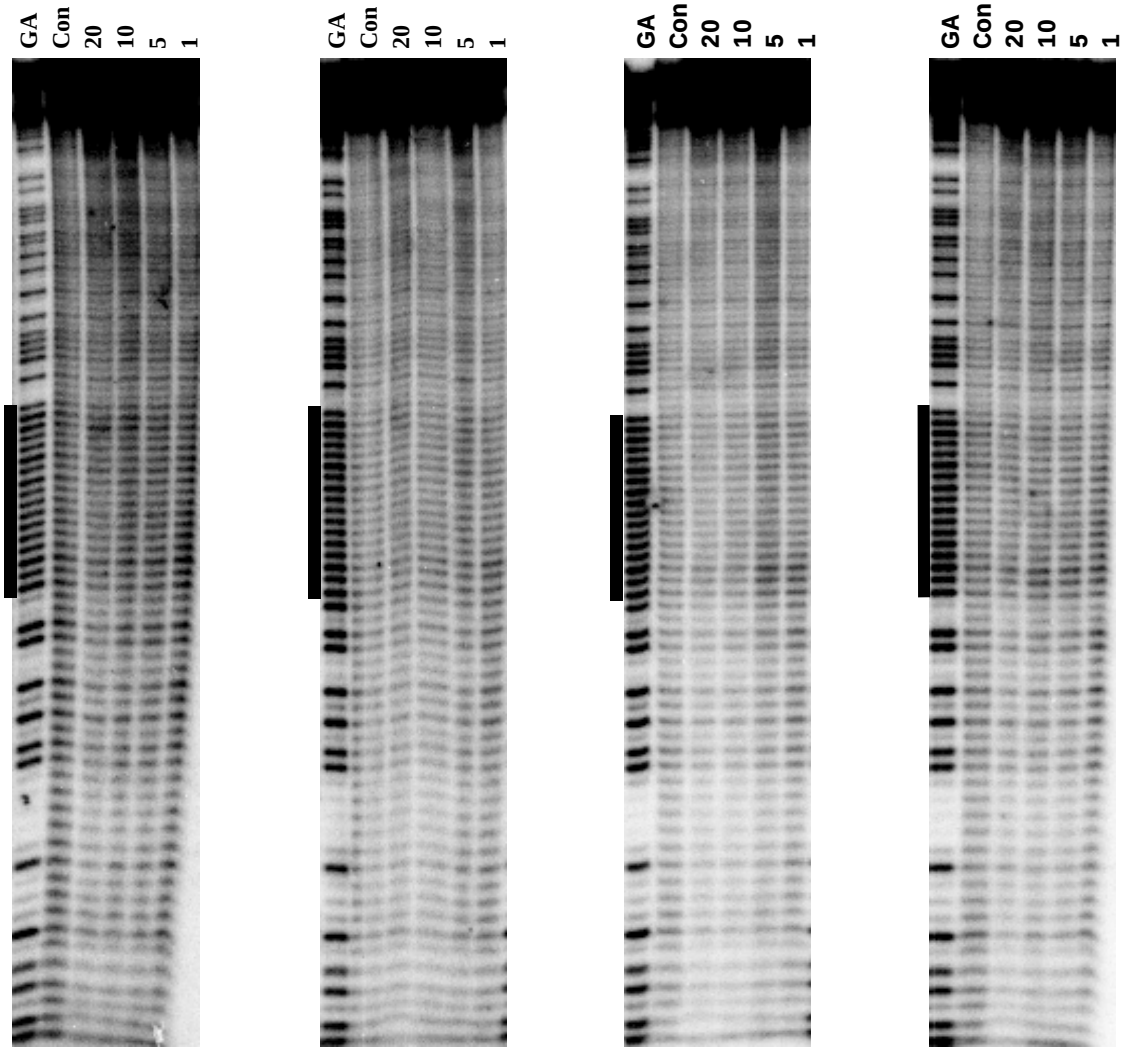

GC GG GA GT

Figure 4.27 Hydroxyl radical cleavage of the four *tyr*T fragments in the presence of the 17-mer-A TFO. X is C, G, A and T in turn. These experiments were performed in 10 mM Tris-HCl at pH 7.0 in the presence of 10 mM $MnCl_2$ and 50 mM NaCl and were equilibrated for 2 hours at room temperature before digesting with the hydroxyl radical mixture. TFO concentrations (μM) are shown at the top of each gel lane. The tracks labelled "GA" and "con" are Maxam-Gilbert markers specific for purines and the cleavage patterns in the absence of TFOs respectively. The filled boxes indicate the location of the triplex target sites.

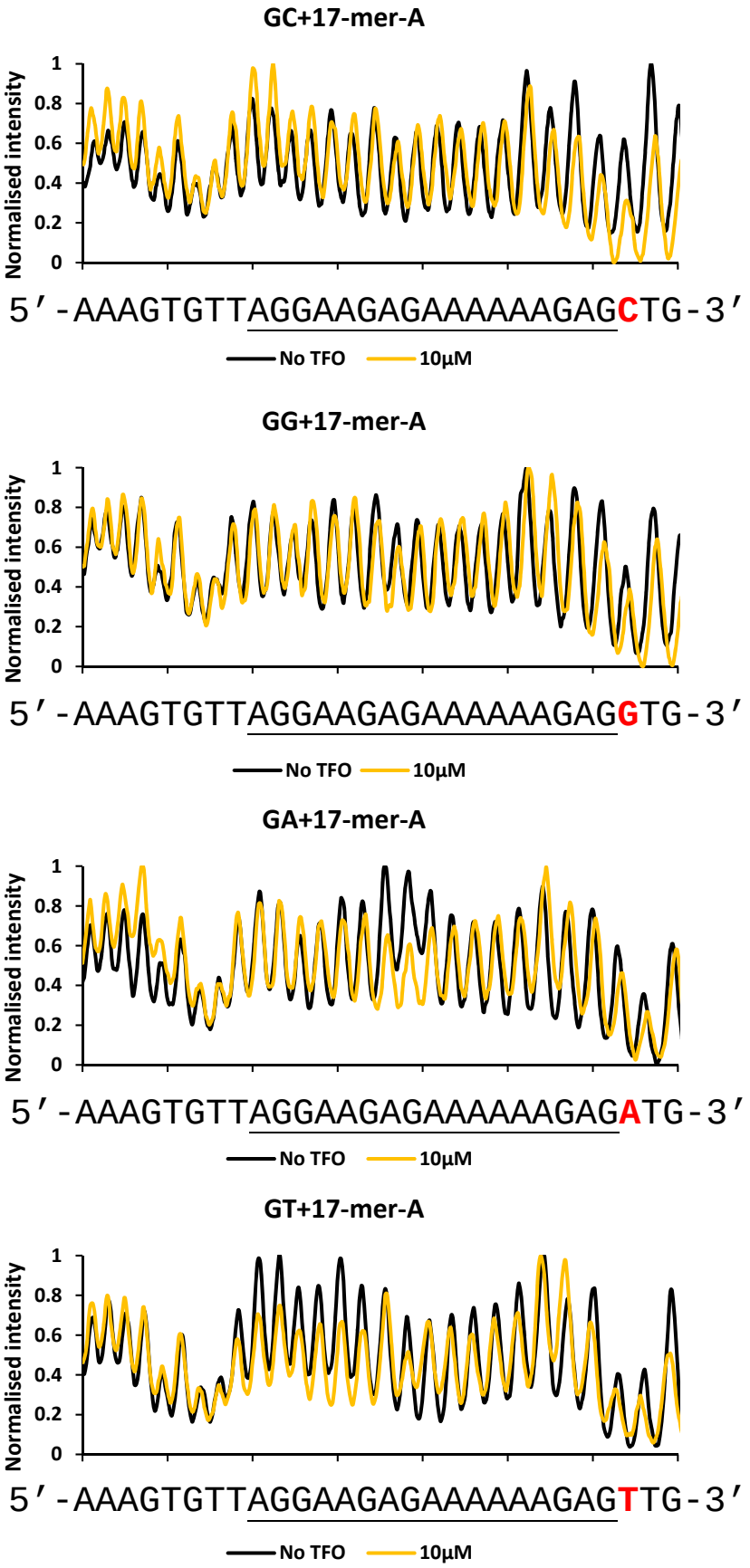

Figure 4.28 Densitometer traces of hydroxyl radical cleavage of triplexes formed by the four fragments in the absence (black) and presence (yellow) of 10 μM 17-mer-A TFO (shown in Figure 4.27).

4.3.2.3. The effect of flanking bases on the stability of antiparallel triplex DNA

4.3.2.3.1. 17-mer antiparallel triplex formation with a 3'-G.GC triplet

Similar with Chapter 3, the stability of antiparallel triplexes were also examined by fluorescence melting studies. In these studies the 17-mer polypurine tract of the target duplex is labelled at the 5'-end with fluorescein, while the TFOs are labelled at the 3'-end with dabcyl. The sequences of these oligonucleotides and TFOs are shown in Table 4.1 and are corresponding to the target site in the *tyr*T fragments and the TFOs used in footprinting experiments. The formation of these triplexes suppresses fluorescence signal, whereas the dissociation of the complexes increases the signal.

First, we examined the stability of triplexes with a 3'-G.GC triplet as they showed highest affinity determined by footprinting experiments. Figure 4.29 shows fluorescence melting curves for triplexes formed between fragment GC (at a concentration of 0.25 μM) and 17-mer-G TFO at various concentrations (*i.e.* 9, 5, 3, 1 and 0.25 μM) generating triplexes with 3'-G.GC triplet. At 30 °C Fluorescence intensities are reduced compared to the higher degrees with the TFO concentrations of 9, 5 and 3 μM, though these are at the same or higher level with the concentrations of 1 and 0.25 μM. The T_ms of these triplexes are estimated from the maxima of the first derivatives of the melting profiles, though these are very broad and shallow; the T_ms are presented in Table 4.6. The increase of TFO concentrations (*i.e.* to 30, 25, 20, 15 and 10 μM) has no effects on the maxima and raises the T_ms to some extent; the values are unchanged after the concentration of 20 μM (Table 4.6). However, this widens the differences between fluorescence intensities at 30 °C and those with higher temperatures (Figure 4.30). These experiments were performed in 50 mM NaOAC at pH 5.0 containing 10 mM $MnCl_2$ and 200 mM NaCl. The replacement of $MnCl_2$ with $MgCl_2$ disrupts the formation of triplexes as seen in Figure 4.31.

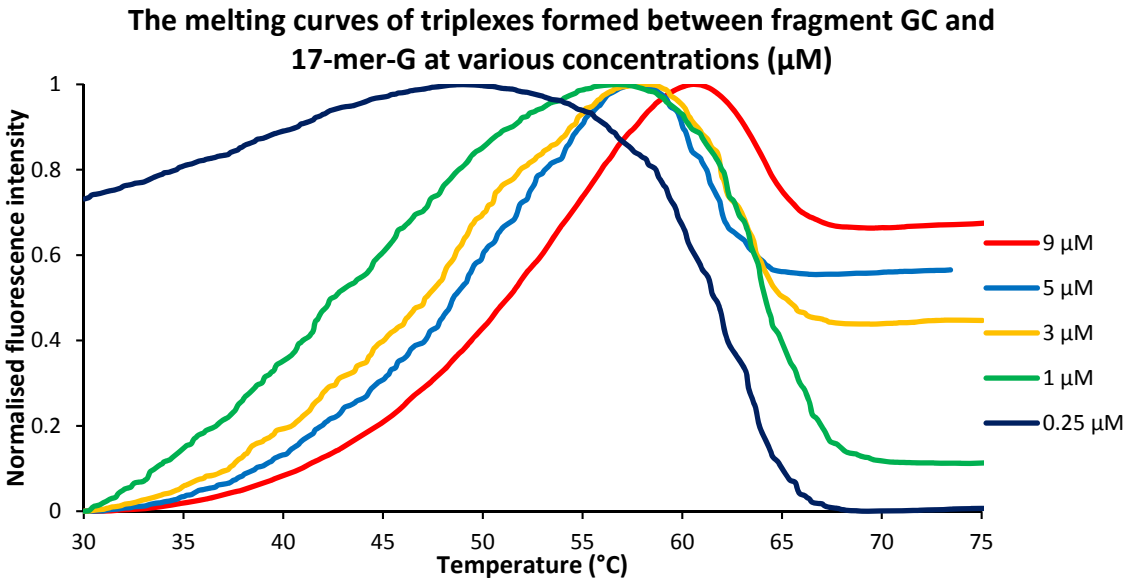

Figure 4.29 Fluorescence melting curves of the 17-mer antiparallel triplex formed between the fluorescently-labelled duplex target flanked by cytosine (*i.e.* fragment GC) and the dabcyl-labelled 17-mer-G TFO at various concentrations: 9 µM (red), 5 µM (blue), 3 µM (yellow), 1 µM (green) and 0.25 µM (black). This is performed in 50 mM NaOAC at pH 5.0 containing 10 mM $MnCl_2$ and 200 mM NaCl.

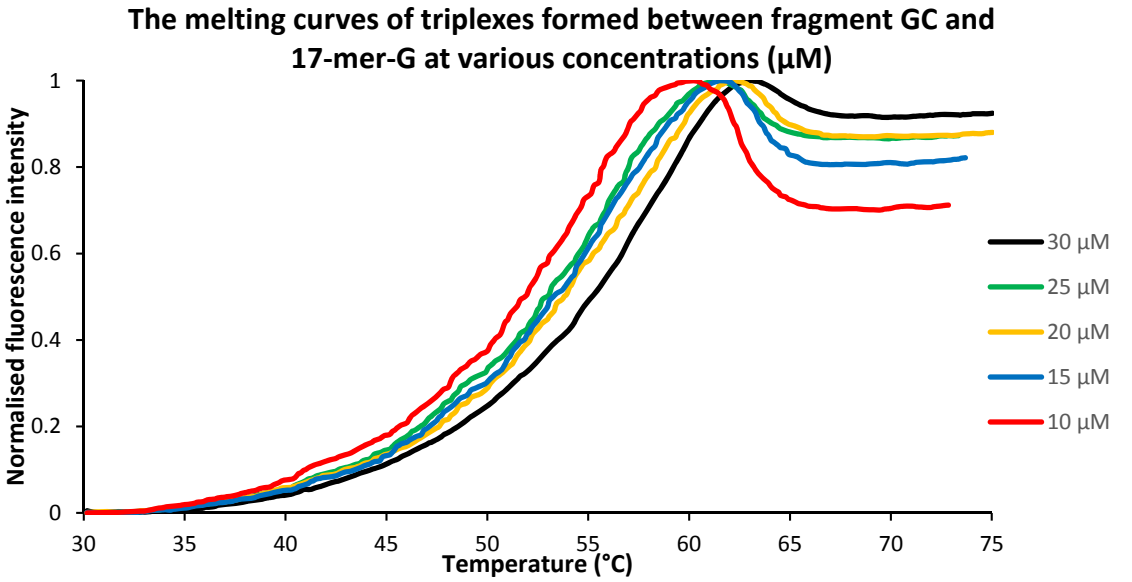

Figure 4.30 Fluorescence melting curves of the 17-mer antiparallel triplex formed between the fluorescently-labelled duplex target flanked by cytosine (*i.e.* fragment GC) and the dabcyl-labelled 17-mer-G TFO at various concentrations: 30 µM (black), 25 µM (green), 20 µM (yellow), 15 µM (blue) and 10 µM (red). This is performed in 50 mM NaOAC at pH 5.0 containing 10 mM $MgCl_2$ and 200 mM NaCl.

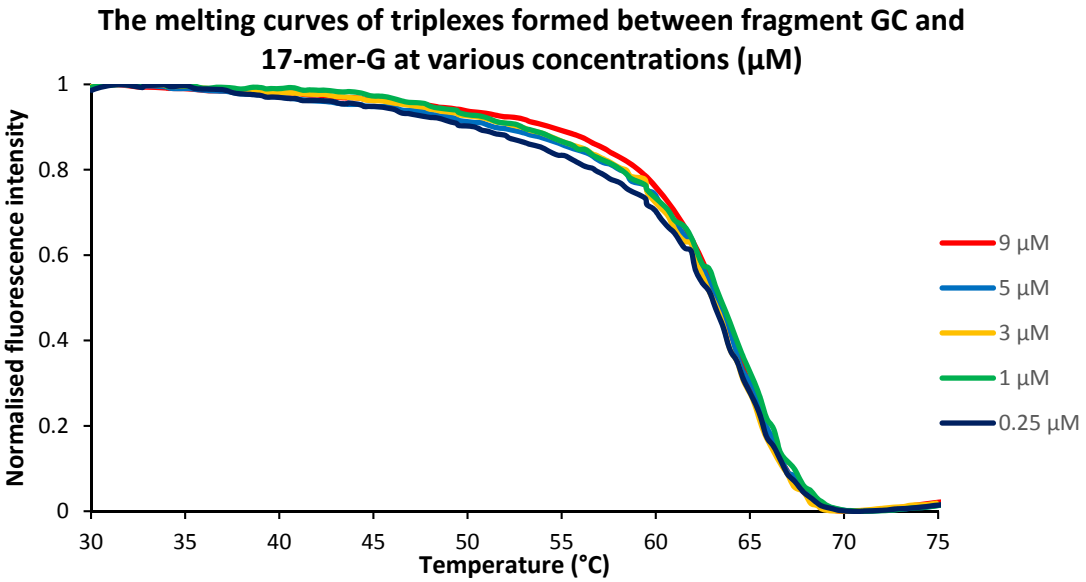

Figure 4.31 Fluorescence melting curves of the 17-mer antiparallel triplex formed between the fluorescently-labelled duplex target flanked by cytosine (*i.e.* fragment GC) and the dabcyl-labelled 17-mer-G TFO at various concentrations: 9 µM (red), 5 µM (blue), 3 µM (yellow), 1 µM (green) and 0.25 µM (black). This is performed in 50 mM NaOAC at pH 5.0 containing 10 mM $MgCl_2$ and 200 mM NaCl.

T_m values of triplexes formed between fragment GC and 17-mer-G TFO			
Concentrations of the TFO (µM)	T_ms (°C)	Concentrations of the TFO (µM)	T_ms (°C)
30	58.6	9	55.2
25	58.2	5	52.6
20	58.2	3	49.2
15	57.2	1	42.9
10	55.8	0.25	38.5

Table 4.6. T_m values estimated from the maxima in the first derivatives of the melting profile of triplexes formed between fluorescently labelled duplex target GC with 17-mer-G TFO.

4.4. Summary

The effects of the 3'-end base pair and the sequence flanking the polypurine tract on the formation of antiparallel triplexes were examined using a variety of techniques; these include footprinting experiments with various cleavage agents and fluorescence melting studies.

The DNase I footprinting experiments revealed footprints with all eight fragments with both 17-mer-A and 17-mer-G TFOs, though they persist to different TFO concentrations. In the presence of 17-mer-A, the footprints of all fragments persist to the same concentration which is about 3 μM; these are similar to those triplexes formed by sequence AG and AA with 17-mer-G TFO. The footprints of fragments AC, AT, and fragments containing 3'-G (*i.e.* GC, GG, GA and GT) with 17-mer-G persist to a much lower TFO concentration. These are about 0.1 μM with sequence AC, GA and GT, 0.2 μM with fragment GC and GG, and 0.6 μM with sequence AT. All footprints extend three bases above (5'-), but not below (3'-end) the TFO binding site. The C_{50} values of these eight fragments with 17-mer-A TFO are between 0.2-0.5 μM which is in the same range for fragment AA and AG with 17-mer-G TFO. Surprisingly, the value of fragment AC with 17-mer-G TFO are comparable to those values of triplexes formed by fragments GC, GG, GA and GT with the same TFO (~0.05-0.06 μM) despite containing a triplet mismatch. These values are about 10 times lower than those with 17-mer-A. The value of fragment AT with 17-mer-G is slightly higher than that of sequence AC with the same TFO, though it is still lower than those with 17-mer-A. All above footprints are accompanied by enhanced cleavage with a number of bands above (5'-) the TFO binding site. Again the footprints are evident with DEPC reaction, but not with $KMnO_4$, micrococcal nuclease and hydroxyl radicals; no TFO-induced enhancement is seen with these agents. The fluorescence melting experiments for fragment GC and 17-mer-G TFO obtain the estimates of concentration dependent T_ms, though these are seized after the TFO concentration of 20 μM. The melting profiles of this triplex are broader and shallower than the parallel counterparts, as a result it is very difficult to estimate accurate T_ms.

4.5. Discussion

Unlike parallel triplexes with CT-containing TFOs, the formation of antiparallel triplexes with the 12-mer GA-containing oligonucleotides was unsuccessful even with TFO concentrations as high as 20 μM. However, the addition of five nucleotides to the TFO (17-mer-A and 17-mer-G), interacting with a longer region of the oligopurine tract enabled the formation of triplexes at TFO concentrations similar to those required with their parallel

counterparts. However, these were performed in a different reaction buffer, containing Tris-HCl at pH 7.0 in the presence of $MnCl_2$ and NaCl, at a pH more similar to the cellular environment. For this reason the formation of antiparallel triplexes is in principle more likely to have applications in biological contexts than their parallel counterparts. Although Van Dyke and Cheng (1994) reported the formation of antiparallel triplexes with 12-mer TFOs, they used GT containing TFOs in a buffer containing HEPES.Na^+ at pH 8.2 in the presence of $MgCl_2$. We also attempted the footprinting reactions in the presence of Mg^{2+} instead of Mn^{2+} but were unable to detect triplex formation. This is consistent with previous observations (Chandler & Fox) that manganese imparts greater stability to triplexes than magnesium. In contrast, Keppler and colleagues (Keppler *et al.*, 2001) found that the formation of some 17-mer GT-containing antiparallel triplexes was unsuccessful without the addition of stabilizing ligands. As expected the DNase I footprints with 17-mer-A are larger than its actual binding site, extending for several bases above (5') the end of the oligopurine target site. The footprints of these interactions were always followed by enhanced DNase I cleavage of a number of bands in the region flanking the 5'-end of the oligopurine strand, in a region around the sequence GCTGTAAAGT. This finding is similar to the results of a study performed by Waterloh and Fox (1991) which reported the enhancements observed by actinomycin binding to the targets $(AT)_5GC(AT)_5$, $(TA)_5GC(TA)_5$, T_9GCA_9 and A_9GCT_9 generally extend over longer duplex A/T regions flanking the target site. In contrast to this study, our result shows no enhancement on the 3'-side of the binding site and also contrasts with the results with the parallel TFOs, which only produced a single enhancement at the 3'-end of the target. It is worth noting that in some instances observed DNase I enhancements can be attributed to changes in the ratio of DNase I and free DNA, which results in a general increase in cleavage in all regions to which the ligand is not bound (Ward *et al.*, 1988). The enhancements found in our studies are highly localised and are proximal to the TFO binding site, suggesting that they most likely reflect changes in the local DNA structure.

The C_{50} values of these four fragments with 17-mer-A are not significantly different to each other which suggests that the affinity of these triplexes is independent of the flanking bases. The values are also unexpectedly similar to those with 17-mer-G TFO and sequences AG and AA, which each contain a terminal 3'-G.AT triplet mismatch. This might suggest that 5'-G of the TFO is able to form a hydrogen bond with the 3'-AT base pair of the target generating an antiparallel G.TA, thereby stabilising the structure, though it is still odd that this is the same affinity as the fully matched 17-mer triplex. Surprisingly, the affinity of 17-mer-G for sequences AC and AT was not only higher than to fragment AG and AA but also than with those triplexes with 17-mer-A containing complete 17 canonical triplets. In addition to the possible formation of an antiparallel G.TA triplet, there must also be other

stabilizing forces from the presence of flanking pyrimidine bases (*i.e.* between AC and AT with 17-mer-G) that contribute to a further increase in affinity.

Malvy *et al.* (1994) demonstrated that a stable antiparallel triplex can be formed between GGGGAGGGGGAGG and an oligopurine tract in the c-pim-1 proto-oncogene. Our replacement of 3'-adenine with guanine in fragments GC, GG, GA and GT was therefore expected to facilitate the stable triplex formation with 12-mer-G TFO, though this is not sufficient to promote triplex formation. This is probably due to the base composition of our TFO which had 33% G, compared with 84% G in Malvy's study. The longer 17-mer-G TFO was therefore used to form triplexes with these four fragments. The DNase I footprinting experiments showed the same footprints and enhancements as the results with 17-mer-A, though the C_{50} values for 17-merG are much lower. The increased affinity of these triplexes is mainly due to the presence of a G.GC triplet (rather than A.AT) at the 3'-end of the target site, but the C_{50} values do not depend on the flanking bases. A similar result was also observed with the formation of antiparallel triplexes between $A_6G_6.C_6T_6$ target and Acr-G_5T_5 TFO in which a G.GC triplet showed higher affinity than a T.AT (Fox, 1994). However, the TFOs used in this study were linked with an acridine molecule. Another study by Chandler and Fox (1996) also demonstrated that triplexes containing central G.GA are much more stable than those with central A.AT, though G-rich oligonucleotide increases the propensity of forming other competing structures (e.g. G-quadruplexes). The replacement of this triplet with its mismatch, as seen in triplexes formed by 17-mer-A with these fragments, generating triplexes with a 3'-A.GC triplet mismatch, therefore reduces the affinity. The footprints of the triplexes with the 3'-A.GC triplet mismatch show similar C_{50} values to those formed by the previous fragments with 17-mer-A TFO.

As enhanced DNase I cleavage appears with these antiparallel TFOs at several band above (5') the TFO binding site, we used a range of other cleavage agents (DEPC, micrococcal nuclease, $KMnO_4$ and hydroxyl radicals) to probe for changes in the local DNA structure. DEPC reacts with complete or partially unstacked adenine in distorted or melted region of DNA (Kahl and Paule, 2009). We therefore looked for enhanced reactivity at adenines in the region of the DNase I enhancements (*i.e.* GCTGTAAAGT), though none was observed. There could be a number of reasons; either the TFOs did not induce any structural changes in this region or any changes might not favour reaction with DEPC. Similarly micrococcal nuclease and $KMnO_4$ were tested as structural probes, but the results with these two agents also showed no enhanced cleavage within the region of enhanced DNase I cleavage; even at position containing A/T bases (*i.e.* GCTGTAAAGT). No changes were observed in the hydroxyl radical cleavage pattern.

Although the C_{50} value suggests a high binding affinity between fragment GC and 17-mer-G TFO, its melting profiles performed in NaOAC at pH 5.0 in the presence of $MnCl_2$ are characterised as broad and shallow peaks making these not ideal to obtain accurate T_ms. On the contrary, these are narrow and deep with parallel counterparts. In the presence of $MgCl_2$ the formation of this triplex is completely disrupted suggesting that this divalent cation (*i.e.* Mg^{2+}) is unfavourable for GA containing triplex formation. Keppler and colleagues (Keppler *et al.*, 2001) also reported the failure of 17-mer GA-containing triplex formation in the presence of $MgCl_2$ and this can be rescued by the replacement with $MnCl_2$. The increase of the TFO concentrations contributes to the rising of T_ms up to the concentration of 20 μM; the T_ms are barely changed after this point. This may be due to the amount of TFO reaches the saturated point, therefore the addition of the TFO beyond this point has little effect on T_ms. The formation of this triplex in $NaHPO_4$ at pH 7.0 in the presence of $MnCl_2$ and $MgCl_2$ were also performed, though these conditions do not afford the formation of the triplex (results not shown). This is in contrary with the report by Darby and colleagues (Darby *et al.*, 2002) in which $NaHPO_4$ was recommended to use for fluorescence studies of triplex forming at pH 7.0. Unlike DNase I footprinting experiment, Tris-HCl is not appropriate for use in melting studies as its pH changes upon changing temperature cycles.

Altogether, the results suggest that the DNase I enhancements observed in all antiparallel triplexes examined here are most due to the TFO-induced enhancements as they are highly localised at only one side of the target site, but not another. Although the formation of antiparallel triplexes was observed in all eight fragments with the two 17-mer TFOs, the triplexes with a 3'-G.GC triplet are the most stable compared to the ones with a 3'-A.AT triplet and a 3'-end triplet mismatch. However, the complexes with a 3'-G.AT triplet mismatch flanked with 3'-pyrimidines (*i.e.* the triplexes formed by fragments AC and AT with 17-mer-G TFO) are as stable as those with a 3'-G.GC. The fluorescence melting studies of the most stable triplex obtain the broad and shallow melting profiles which do not improve with the increase of the TFO concentrations; though this stabilizes the structure to a certain concentration and has no stabilising effect once reaching saturated point.

CHAPTER 5 GENERAL CONCLUSION

5.1. TFO-induced enhancements

To examine the effects of sequences at the 3'-end of a purine target site on triplex formation and properties, two sets of variant *tyr*T fragments have been prepared. Fragments AC, AG, AA and AT have the same adenine at the 3'-end of the purine strand of the target, but with each of the flanking bases in turn. Fragments GC, GG, GA and GT are similar, but with the replacement of 3'-terminal adenine with guanine. Each of these fragments was targeted with both parallel TFOs (*i.e.* 12-mer-T, 11-mer and 12-mer-C) and antiparallel TFOs (*i.e.* 12-mer-A, 12-mer-G, 17-mer-A and 17-mer-G) to generate parallel and antiparallel triplexes respectively. With these TFOs further details about the effects of the length and the 3'-end triplet mismatches on the two categories of triplexes were obtained. Footprinting with various agents including DNase I, micrococcal nuclease, DEPC, $KMnO_4$ and hydroxyl radicals was used in this study to examine TFO's binding site and to probe for any TFO-induced enhancements. For all the parallel triplexes the DNase I footprints are clear at the highest concentration (*i.e.* 3 μM) and these always extend beyond the actual TFO target site by about 3 bases above its 5'-end. This is thought to be due to the size of the enzyme, for which the active site cannot approach any closer to the bound TFO. Most of these footprints are accompanied by enhanced cleavage at the 3'-end of the target except for those formed on fragments AG and AA with 12-mer-C TFO, generating a 3'-C.AT triplet and on fragment GG with 12-mer-T, generating a 3'-T.GC. This enhancement is only found at the 3'-end of the purine strand and is usually attributed to the bound TFO causing changes in the orientation of the phosphate at this position. These enhancements are only found at the triplex-duplex junction and they must result from an induced local DNA conformational change that favours DNase I recognition and digestion. An enzyme redistribution mechanism would affect the cleavage of many bands that are not protected by the TFO, and so is not a sufficient explanation for this localised effect. The enhancements are always observed at the triplex-duplex junction and so are one base higher for the 11-mer than the 12-mer-T and the 12-mer-C with their complete targets (*i.e.* fragments with 3'-adenine and fragments with 3'-guanine respectively). However these enhancements are seen at two bands for triplexes formed by fragments AC and AT with 12-mer-C TFO generating a 3'-C.AT triplet; one is at the same position as those with 11-mer and another one is at the same position with 12-mer-T. The reason for the enhancement at a higher position might be similar to those with 11-mer as this is a duplex-triplex junction where the enhanced cleavage is always observed. However the enhancement at a lower position could possibly due to a combinatorial effect of a 3'-C.AT mismatch and flanking pyrimidines. The enhancement

seen with fragment AC is more intense than the others (*i.e.* AG, AA and AT), presumably because its flanking ApC step is more flexible to the conformational change upon TFO binding (Travers, 2004). This could increase DNase I recognition and cleavage. For variants flanked with A and T, generating AA and AT flanking sequences, the enhancements may be due to the widening of the AA and AT minor groove upon TFO binding (Drew and Travers, 1984; Fox and Waring, 1984). As the 11-mer forms a triplex with an AA flanking sequence in all variants, the immediate sequence context is similar to the triplex formed by 12-mer-T and fragment AA. Fragment GC with 12-mer-C also provides the strongest enhancements compared to the others (*i.e.* GG, GA and GT), in the same way that AC produces the greatest enhancement with the other series. This may be because the dinucleotide steps at the 3'-end (*i.e.* GC, GG, GA and GT) are sensitive to conformational changes which consequently accommodate DNase I cleavage. Interestingly, reduced cleavage is always found at the bases next to (below) the triplex-duplex junction which is attributed to the redistribution mechanisms of the enzyme around the triplex junction. The enzymes are more concentrated at the triplex-duplex junction and less at the adjacent bases therefore the bases next to the junction are less cut. Though the 11-mer produces enhancements at the same position as the 12-mer-T and their pattern is similar to the 11-mer with fragments AA, AG, AA and AT, it always produce additional enhancements below its usual position. This suggests that there is a conformational transmission from the triplex-duplex junction to the neighbouring bases within the purine tract only, not outside the flanking region. Using DEPC to probe the structural changes at the triplex-duplex junction showed that the 11-mer TFO altered the stacking patterns of the adjacent bases for fragments AC, AG and AA, but not with fragment AT. Similar results were also observed with 12-mer-C with fragments AC, AA and AT, but not with AG. These DEPC enhancements are in the same position as those observed with 12-mer-T and its complete targets (*i.e.* AC, AG, AA and AT). There were no changes in cleavage patterns and enhancements for all the other cleavage agents (*i.e.* Micrococcal nuclease, $KMnO_4$ and hydroxyl radicals).

Unlike the parallel triplexes mentioned above, 12-mer antiparallel TFOs (*i.e.* 12-mer-A and 12-mer-G) did not promote antiparallel triplex formation with any of the fragments as these generate less stable triplexes than their parallel counterparts of similar length. However the binding was improved by increasing the TFO's length from a 12-mer to a 17-mer (*i.e.* 17-mer-A and 17-mer-G) as the longer TFO typically increases the triplex's stability. DNase I footprints of these two TFOs (*i.e.* 17-mer-A and 17-mer-G) with all eight fragments are similar to those observed with the parallel ones; they bind to the same target site but generate a triplex that is five triplets longer towards the 5'-end of the binding site. These are concentration dependent and are clearest at the highest TFO concentration. The footprints

also extend above the 5'-end, but not the 3'-end the TFO's binding site. These triplexes contain G.GC and A.AT triplets instead of C^+.GC and T.AT, and the TFOs are oriented in an opposite direction to the polypurine tract. DNase I cleavage enhancements are also evident with these triplexes but are located at a number of bands above (5'-) the TFO's binding site, instead of the single band at the 3'-end observed with the parallel counterparts. This is also thought to be due to structural changes in the DNA as the enhancements are localised to the region immediately above the binding sites, and are not seen in the rest of the fragments. Again, there was no change in cleavage patterns and enhancements with other cleavage agents (*i.e.* DEPC, Micrococcal nuclease, $KMnO_4$ and hydroxyl radicals)

5.2. Triplex binding affinity

As well as examining the TFO's binding sites and enhancements, the footprinting technique can also provide an estimate of the binding affinity. The footprinting C_{50} value provides a good estimate of the dissociation constant of the TFO, so long as the concentration of the target duplex is much lower than the dissociation constant (Hampshire *et al.*, 2007). This corresponds to the reaction condition used in this work, for which the concentration of duplex target is nanomolar compared to the micromolar TFO dissociation constants. The DNase I footprinting studies of fragments with 3'-adenine reveal that all three parallel TFOs generate concentration-dependent footprints with these fragments, but with different binding affinities. C_{50} values were obtained from quantitative analyses of the concentration-dependent enhancements. The 12-mer-T bound the targets tighter (C_{50}~0.2-0.4 μM) than 11-mer (C_{50}~0.8-0.9) and 12-mer-C (C_{50}~0.4-0.8) as it generates triplexes with more canonical triplets (*i.e.* 12, compared to 11 with the 11-mer and 12-mer-C). Despite having the same length as the 12-mer-T, the 12-mer-C bound the targets with lower affinity as it generates triplexes with only 11 canonical triplets and a 3'-C.AT mismatch. The replacement of 3'-adenine with guanine in fragments GC, GG, GA and GT increases the affinity of triplexes formed with 12-mer-C by about 10-fold (C_{50}~0.04-0.07 μM) compared to the other parallel triplexes studied here. This is because the C^+.GC triplet is known to be more stable than T.AT at low pH, and this further reduces the charge repulsion between the three negative strands. The affinities of triplexes formed between the 11-mer TFO and these fragments are slightly higher (C_{50}~0.6-0.7 μM) than with the previous four (C_{50}~0.8-0.9) as a result of the 3'-flanking guanine instead of adenine. There is no substantial difference between the triplexes with 3'-C.AT and 3'-T.GC mismatches as they both contain 11 canonical triplets and a triplet mismatch.

Unlike the parallel TFOs, the 12-mer GA-containing TFOs were unable to induce antiparallel triplex formation with all eight fragments, though footprints were restored by

increasing the length of the TFOs to 17 nucleotides. The affinities of complexes formed between fragments that end with 3'-adenine (*i.e.* AC, AG, AA and AT) and 17-mer-A TFO (C_{50}~0.3-0.5 μM) are comparable to those formed with 12-mer-T on the same targets, despite containing more canonical triplets (17-mer). This is because antiparallel triplexes are known to be less stable than their equivalent parallel counterparts. With the 17-mer-G TFO, fragments AG and AA generated triplexes that contain 16-mer canonical triplets and a 3'-G.AT triplet. These display similar affinities to those in the presence of 17-mer-A (C_{50}~0.3-0.4 μM). Interestingly, fragments AC and AT generated triplexes with higher affinity (C_{50}~0.04-0.1 μM) despite having the same numbers of canonical triplets and a triplet mismatch. This might reflect the role of the flanking pyrimidines (*i.e.* cytosine and thymine), which increase the affinity of these two triplexes. As expected the formation of triplexes between fragments with a 3'-guanine (*i.e.* GC, GG, GA and GT) and 17-mer-G increases the affinity by about 10 times (C_{50}~0.05-0.07 μM) compared to those formed between the previous four fragments and the 17-mer-A TFO. This is attributed to the presence of a 3'-G.GC triplet instead of an A.AT; this has a similar effect as replacing T.AT with C^+.GC in parallel triplex formation. The interaction of these fragments with the 17-mer-A TFO generates triplexes that have much lower affinity than the previous ones as they contain fewer canonical triplets and a 3'-A.GC triplet mismatch.

5.3. Triplex thermal stability

The stability of parallel triplexes was examined further by thermal melting studies using 5'-end fluorescently labelled oligonucleotides that correspond to the 12-mer target site in the *tyr*T fragments and 5'-end dabcyl labelled TFOs. When the triplex is formed the fluorescence is quenched and on melting the complex the fluorescence increases. Both the fluorescence melting and annealing profiles were recorded and the T_m values were obtained. The T_ms of triplexes formed between 12-mer-T and the four fragments with 3'-adenine and each of flanking bases in turn (*i.e.* AC, AG, AA and AT) are significantly different to each other. Fragment AG showed the highest T_m (45 °C) and AC displayed the lowest (40.7 °C). This is a 4.3 °C difference with a single flanking base pair difference. As expected, lower T_ms were observed with the 11-mer TFO (~38-40 °C) compared to the 12-mer-T (~40-45 °C) with the same fragments as the result of a shorter length. With this TFO, fragment AC produced the lowest T_m (38.2 °C) whereas fragments AG, AA and AT have comparable T_ms. 12-mer-C bound to the four fragments at the same site as the 12-mer-T, but produced triplexes that only contain 11 canonical triplets and a C.AT triplet mismatch and each of the flanking bases in turn. The T_ms of these are not much different between each of the fragments, though they are slightly higher than those with the 11-mer. The substantial

difference is observed with fragment AC; for which the T_m of the12-mer-C is 4.6 °C higher than that with the 11-mer. The T_ms with 12-mer-C are lower than those with 12-mer-T, except with fragment AC that surprisingly has a 2.1 °C higher T_m despite having fewer canonical triplets and a triplet mismatch. Fragments GC, GG, GA and GT were also targeted with the 12-mer-C TFOs, generating triplexes with a 3'-C^+.GC triplet. The T_ms of these (~48-49 °C) are unsurprisingly the highest relative to others studied here, though there are no significantly different between each of the fragments. These are about 8-10 and 10-15 °C higher than those with 11-mer and 12-mer-T TFOs respectively. The T_ms of the 11-mer with these fragments are comparable to those with the previous ones and again there is no significant difference between the T_ms for each of these fragments. Comparing triplexes with 3'-C.AT and the ones with 3'-T.GC triplet mismatch, the former surprisingly are about 3-5 °C higher than the latter. The representative melting curves of antiparallel triplexes formed between fragment GC and 17-mer-G TFO are very shallow and broad, the estimation of the T_m is therefore very difficult and unreliable.

APPENDIX 1

Schematic representation of pUC18 (bottom panel) and a wild type *tyr*T(43-59) sequence (top panel). The pUC18 plasmid map showing its beta-galactosidase gene (*lacZ*), multiple cloning sites (MCS), ampicillin resistance gene (Ap^R) and origin of replication (Ori). The wild type *tyr*T(43-50) sequence with the cytosine (highlighted in yellow) flanking the 3'-end of the polypurine tract (underlined) is position between the the EcoRI and AvaI sites generating AC plasmid. The letter A refers to the last adenine at the 3'-end of polypurine tract (highlighted in green) and C refers to 3'-end cytosine flanking the polypurine tract (highlighted in yellow).

APPENDIX 2

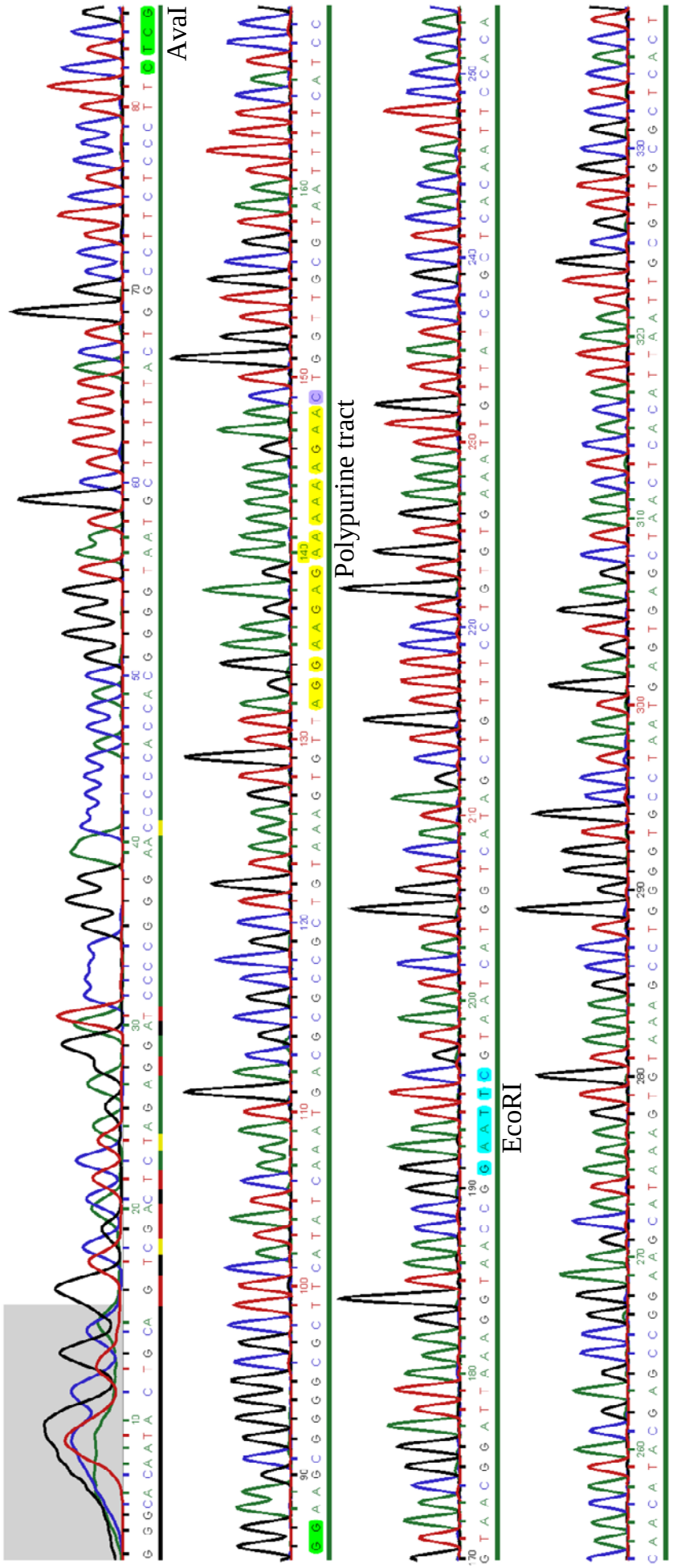

Sequencing electropherogram of *tyr*T(43-59) derivative (AC). The EcoRI site is highlighted in blue and the AvaI site is highlighted in green. The 17-mer polypurine tract is highlighted in yellow with the 3'-flanking cytosine highlighted in purple.

APPENDIX 3

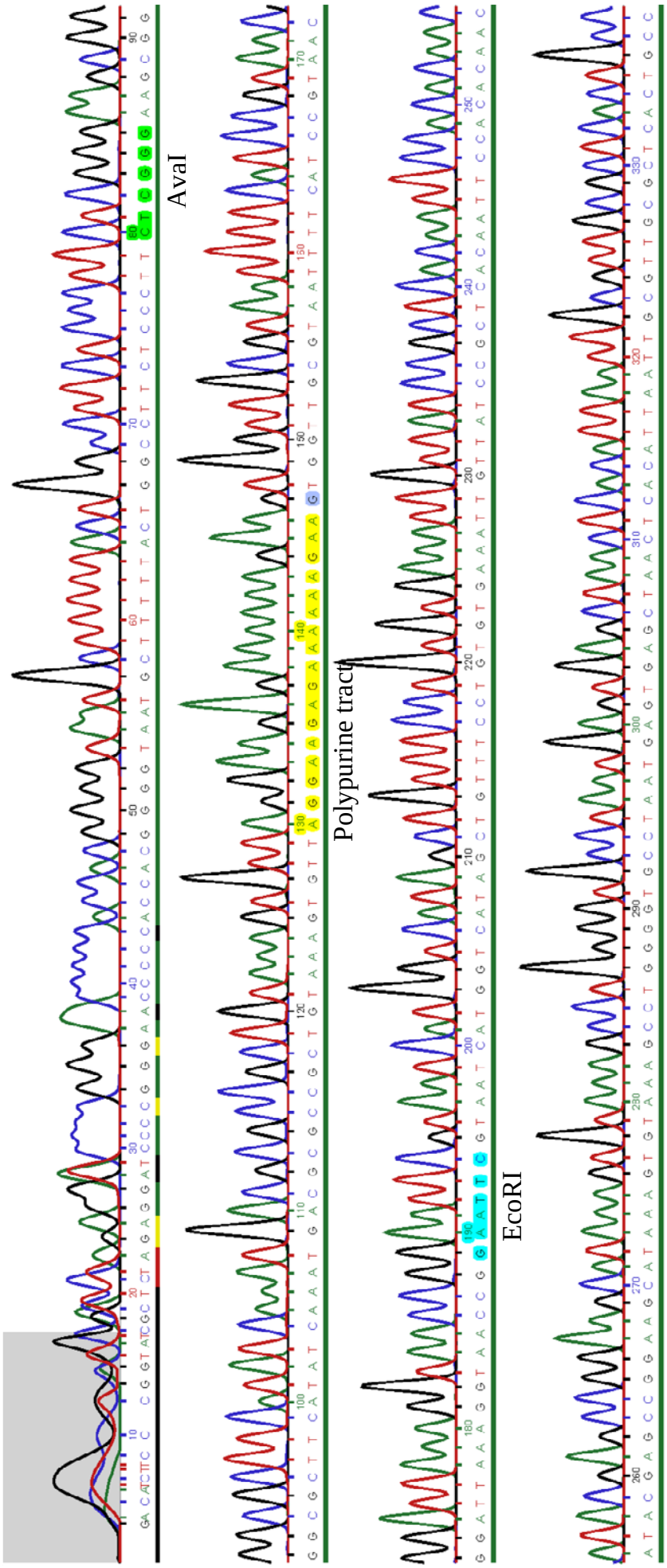

Sequencing electropherogram of *tyr*T(43-59) derivative (AG). The EcoRI site is highlighted in blue and the AvaI site is highlighted in green. The 17-mer polypurine tract is highlighted in yellow with the 3'-flanking guanine highlighted in purple.

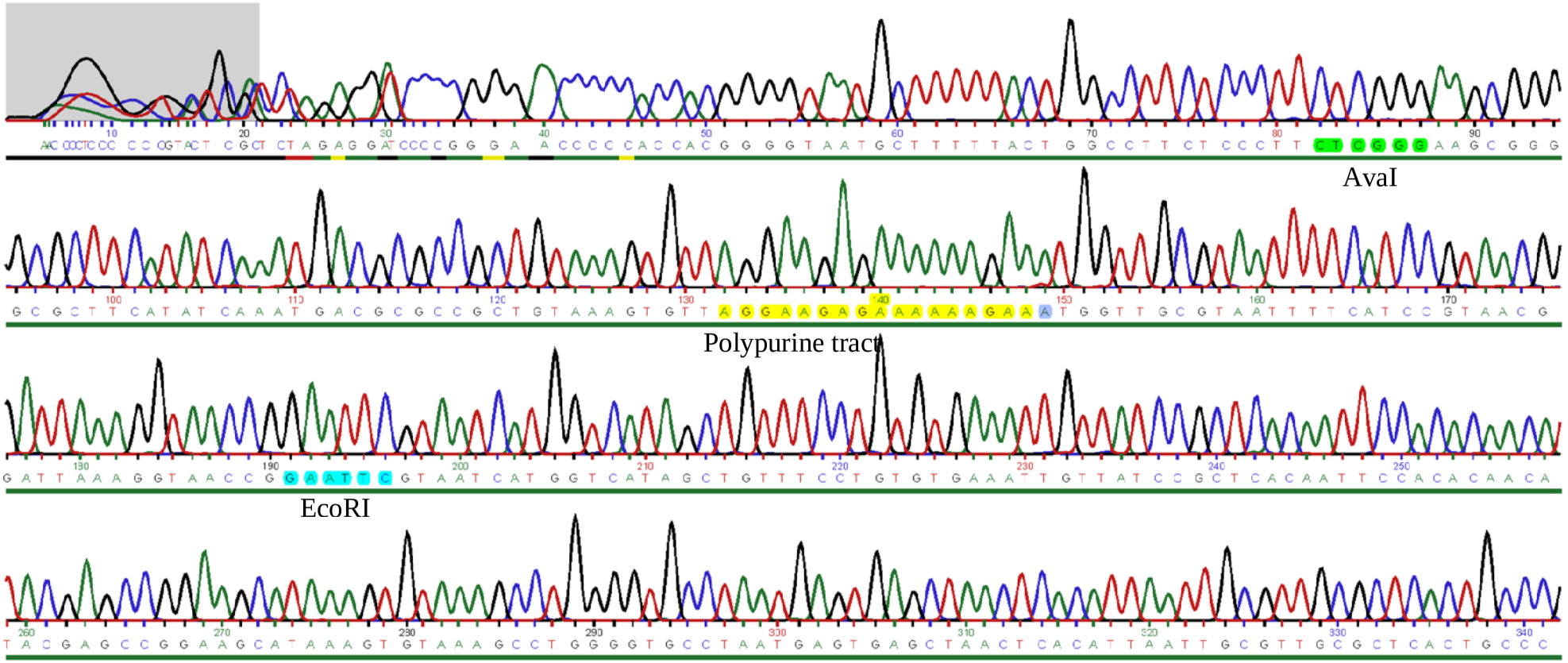

Sequencing electropherogram of *tyr*T(43-59) derivative (AA). The EcoRI site is highlighted in blue and the AvaI site is highlighted in green. The 17-mer polypurine tract is highlighted in yellow with the 3'-flanking adenine is highlighted in purple.

APPENDIX 5

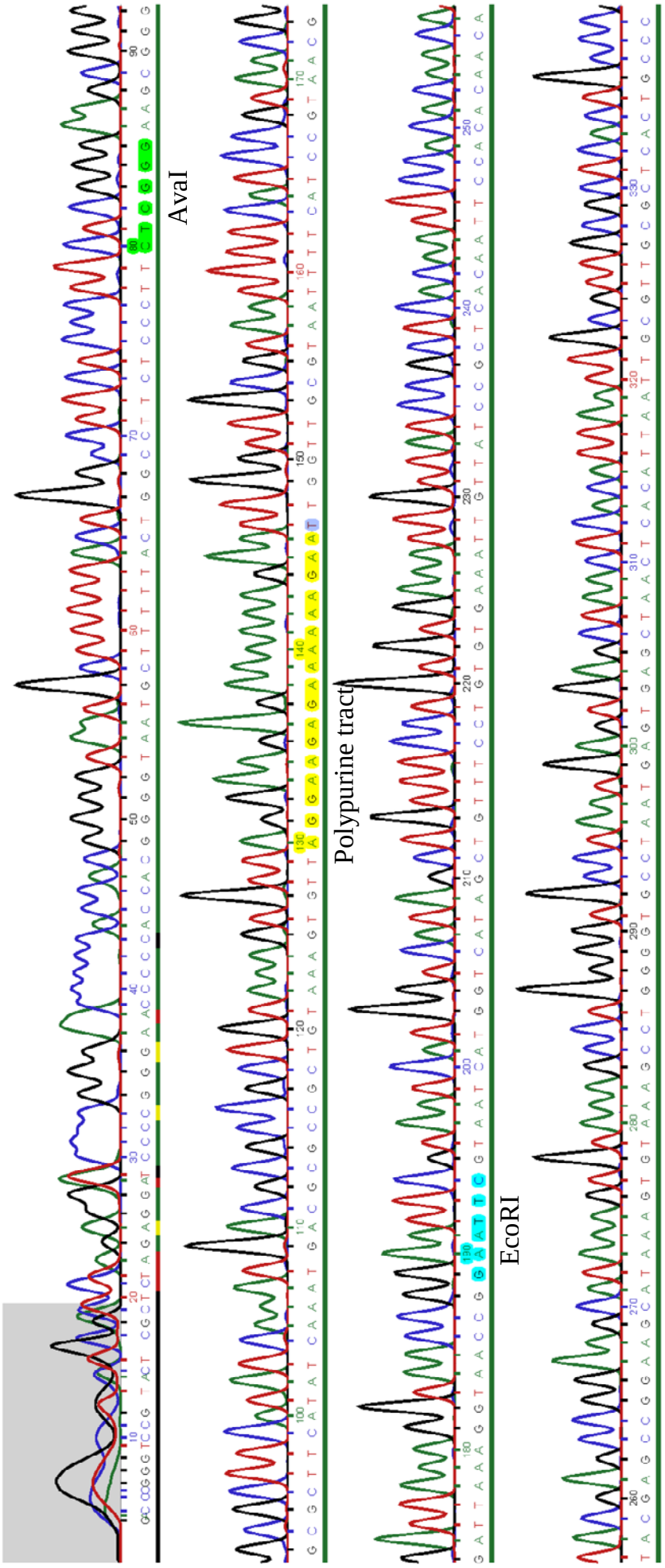

Sequencing electropherogram of *tyr*T(43-59) derivative (AT). The EcoRI site is highlighted in blue and the AvaI site is highlighted in green. The 17-mer polypurine tract is highlighted in yellow with the 3'-flanking thymine is highlighted in purple.

APPENDIX 6

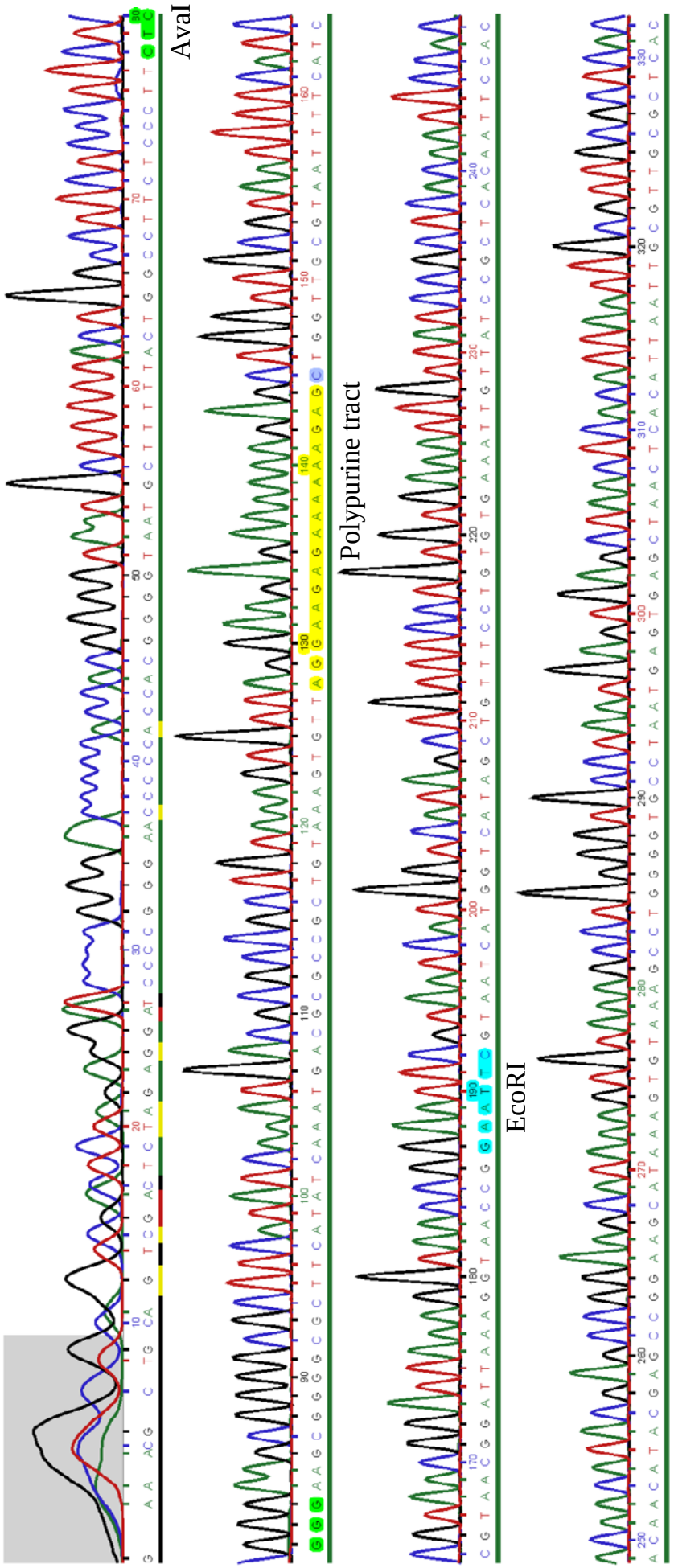

Sequencing electropherogram of *tyr*T(43-59) derivative (GC). The guanine at the 3'-end of the polypurine target site is boxed. The EcoRI site is highlighted in blue and the AvaI site is highlighted in green. The 17-mer polypurine tract is highlighted in yellow with the 3'-flanking cytosine is highlighted in purple.

APPENDIX 7

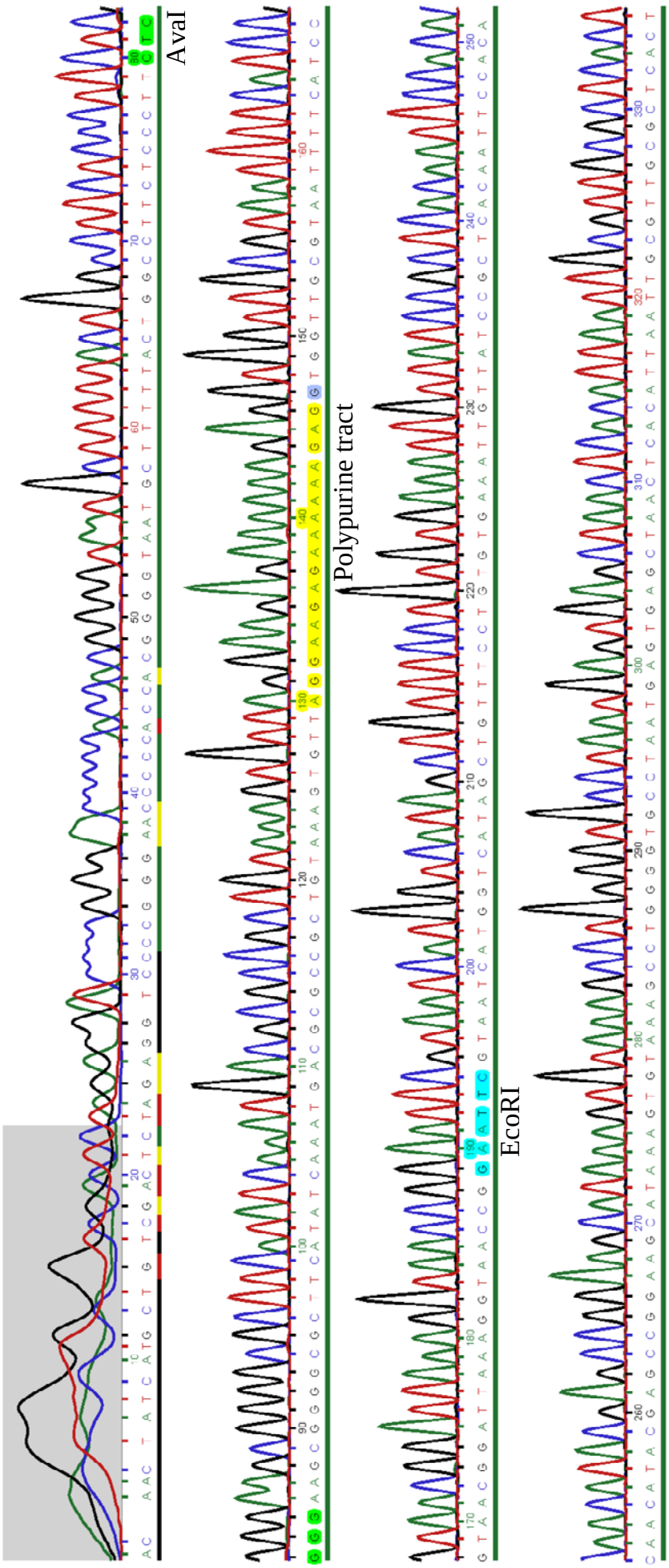

Sequencing electropherogram of *tyr*T(43-59) derivative (GG). The guanine at the 3'-end of the polypurine target site is boxed. The EcoRI site is highlighted in blue and the AvaI site is highlighted in green. The 17-mer polypurine tract is highlighted in yellow with the 3'-flanking guanine is highlighted in purple.

APPENDIX 8

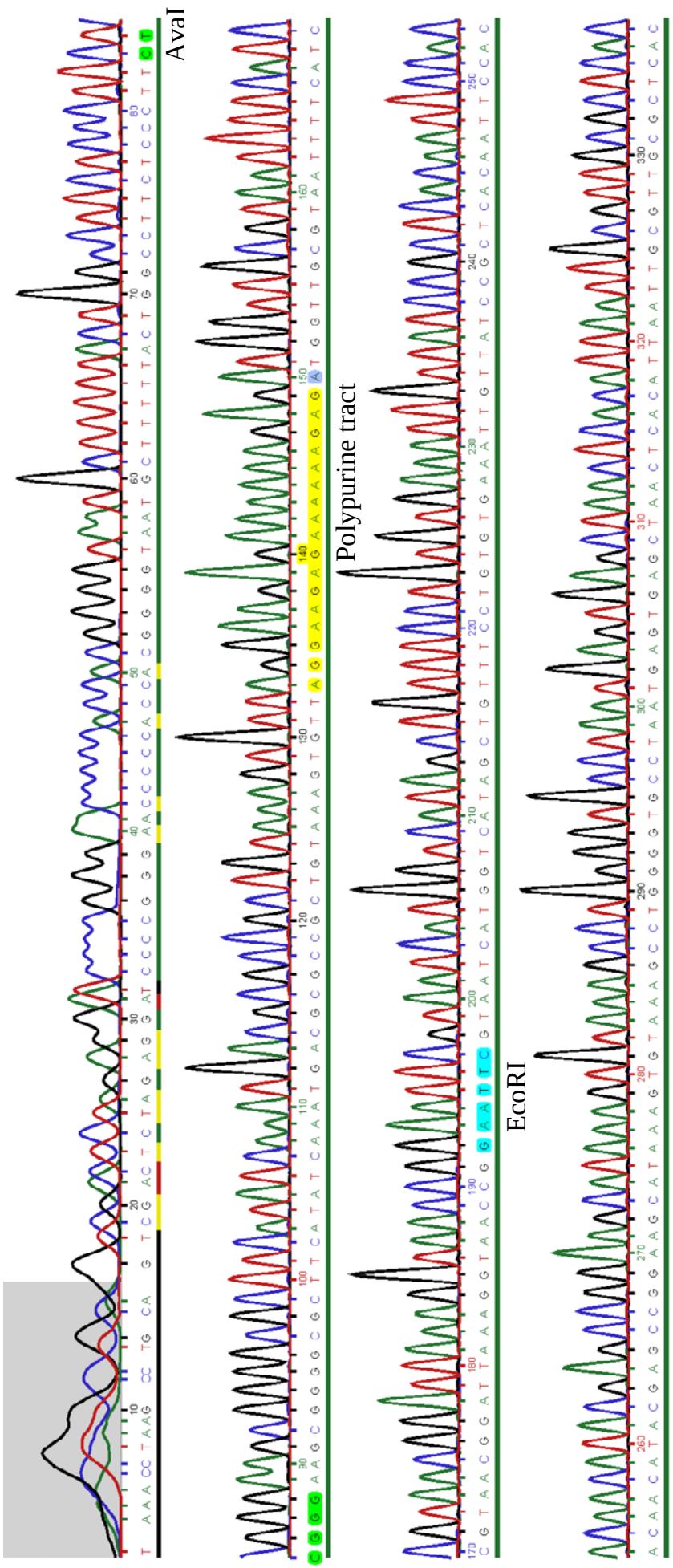

Sequencing electropherogram of *tyr*T(43-59) derivative (GA). The guanine at the 3'-end of the polypurine target site is boxed. The EcoRI site is highlighted in blue and the AvaI site is highlighted in green. The 17-mer polypurine tract is highlighted in yellow with the 3'-flanking adenine is highlighted in purple.

APPENDIX 9

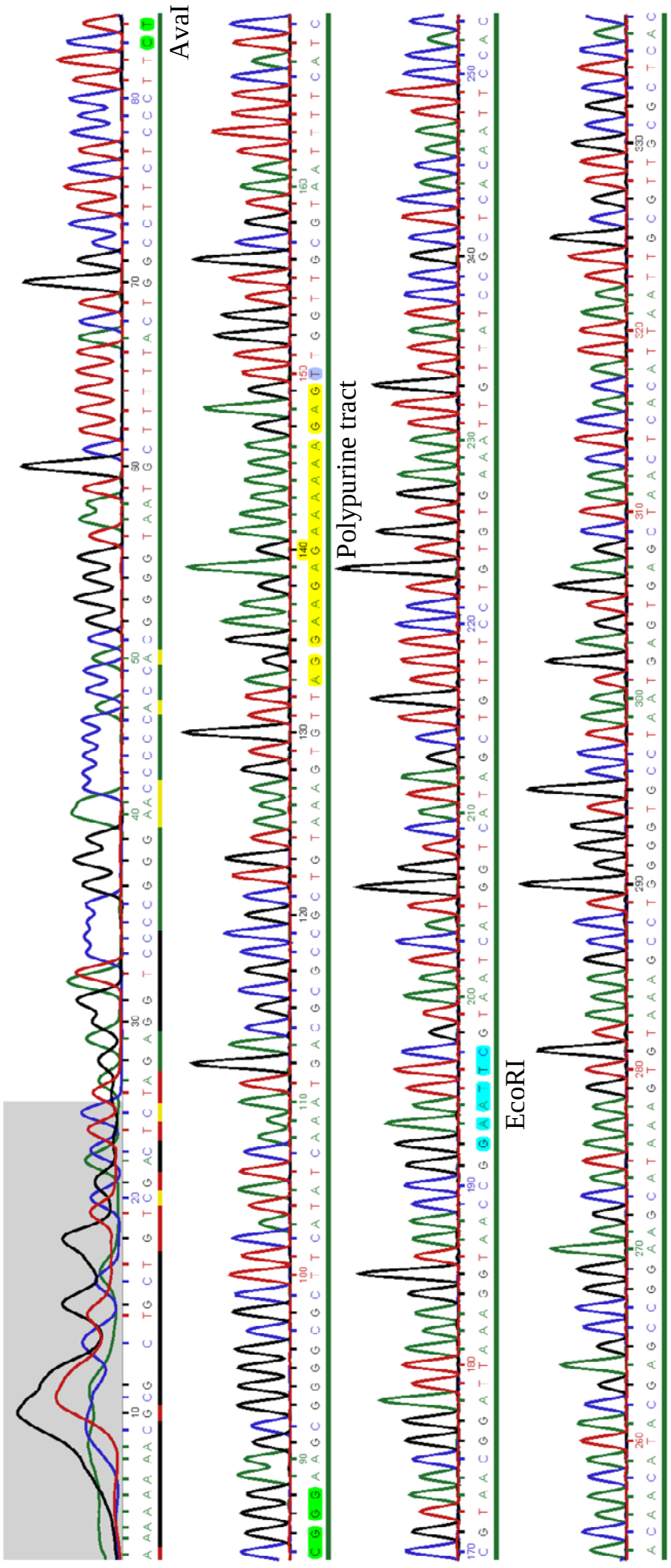

Sequencing electropherogram of *tyr*T(43-59) derivative (GT). The guanine at the 3'-end of the polypurine target site is boxed. The EcoRI site is highlighted in blue and the AvaI site is highlighted in green. The 17-mer polypurine tract is highlighted in yellow with the 3'-flanking thymine is highlighted in purpl

References

Abu-Daya, A., Brown, P. M.and Fox, K. R. (1995). DNA sequence preferences of several AT-selective minor groove binding ligands. *Nucleic Acids Research,* 23 (17)**,** 3385-3392.

Alunni-Fabbroni, M., Manzini, G., Quadrifoglio, F.and Xodo, L. E. (1996). Guanine-rich oligonucleotides targeted to a critical R . Y site located in the Ki-ras promoter. The effect of competing self-structures on triplex formation. *Eur J Biochem,* 238 (1)**,** 143-51.

Arimondo, P. B., Barcelo, F., Sun, J. S., Maurizot, J. C., Garestier, T.and Helene, C. (1998). Triple helix formation by (G,A)-containing oligonucleotides: asymmetric sequence effect. *Biochemistry,* 37 (47)**,** 16627-35.

Asensio, J. L., Brown, T.and Lane, A. N. (1999). Solution conformation of a parallel DNA triple helix with 5' and 3' triplex-duplex junctions. *Structure,* 7 (1)**,** 1-11.

Barre, F. X., Ait-Si-Ali, S., Giovannangeli, C., Luis, R., Robin, P., Pritchard, L. L., Helene, C.and Harel-Bellan, A. (2000). Unambiguous demonstration of triple-helix-directed gene modification. *Proc Natl Acad Sci U S A,* 97 (7)**,** 3084-8.

Barre, F. X., Giovannangeli, C., Helene, C.and Harel-Bellan, A. (1999). Covalent crosslinks introduced via a triple helix-forming oligonucleotide coupled to psoralen are inefficiently repaired. *Nucleic Acids Res,* 27 (3)**,** 743-9.

Basye, J., Trent, J. O., Gao, D.and Ebbinghaus, S. W. (2001). Triplex formation by morpholino oligodeoxyribonucleotides in the HER-2/neu promoter requires the pyrimidine motif. *Nucleic Acids Res,* 29 (23)**,** 4873-80.

Bates, P. J., Laughton, C. A., Jenkins, T. C., Capaldi, D. C., Roselt, P. D., Reese, C. B.and Neidle, S. (1996). Efficient triple helix formation by oligodeoxyribonucleotides containing alpha- or beta-2-amino-5-(2-deoxy-D-ribofuranosyl) pyridine residues. *Nucleic Acids Res,* 24 (21)**,** 4176-84.

Bates, P. J., Macaulay, V. M., Mclean, M. J., Jenkins, T. C., Reszka, A. P., Laughton, C. A.and Neidle, S. (1995). Characteristics of triplex-directed photoadduct formation by psoralen-linked oligodeoxynucleotides. *Nucleic Acids Res,* 23 (21)**,** 4283-9.

Baudoin, O., Marchand, C., Teulade-Fichou, M.-P., Vigneron, J.-P., Sun, J.-S., Garestier, T., Hélène, C.and Lehn, J.-M. (1998). Stabilization of DNA Triple Helices by Crescent-Shaped Dibenzophenanthrolines. *Chemistry – A European Journal,* 4 (8)**,** 1504-1508.

Berg, J. M., Tymoczdo, J. L.and Stryer, L. (2002). *Biochemistry*.

Bernal-Mendez, E.and Leumann, C. J. (2001). Conformational diversity versus nucleic acid triplex stability, a combinatorial study. *J Biol Chem,* 276 (38)**,** 35320-7.

Besch, R., Giovannangeli, C., Kammerbauer, C.and Degitz, K. (2002). Specific Inhibition of ICAM-1 Expression Mediated by Gene Targeting with Triplex-forming Oligonucleotides. *Journal of Biological Chemistry,* 277 (36)**,** 32473-32479.

Bijapur, J., Bergqvist, S., Brown, T., Keppler, M. D.and Fox, K. R. (1999). 5-(1-propargylamino)-2′-deoxyuridine (UP): A novel thymidine analogue for generating DNA triplexes with increased stability. *Nucleic Acids Research,* 27 (8)**,** 1802-1809.

Birg, F., Praseuth, D., Zerial, A., Thuong, N. T., Asseline, U., Le Doan, T.and Helene, C. (1990). Inhibition of simian virus 40 DNA replication in CV-1 cells by an oligodeoxynucleotide covalently linked to an intercalating agent. *Nucleic Acids Res,* 18 (10)**,** 2901-8.

Boer, D. R., Canals, A.and Coll, M. (2009). DNA-binding drugs caught in action: the latest 3D pictures of drug-DNA complexes. *Dalton Transactions,* (3)**,** 399-414.

Brown, P. M., Drabble, A.and Fox, K. R. (1996). Effect of a triplex-binding ligand on triple helix formation at a site within a natural DNA fragment. *Biochem J,* 314 (Pt 2) 427-32.

Brown, P. M.and Fox, K. R. (1999). DNA triple-helix formation on nucleosome core particles. *European Journal of Biochemistry,* 261 (1)**,** 301-310.

Brunar, H.and Dervan, P. B. (1996). Sequence composition effects on the stabilities of triple helix formation by oligonucleotides containing N7-deoxyguanosine. *Nucleic Acids Res,* 24 (11)**,** 1987-91.

Brunet, E., Alberti, P., Perrouault, L., Babu, R., Wengel, J.and Giovannangeli, C. (2005). Exploring cellular activity of locked nucleic acid-modified triplex-forming oligonucleotides and defining its molecular basis. *J Biol Chem,* 280 (20)**,** 20076-85.

Burge, S., Parkinson, G. N., Hazel, P., Todd, A. K.and Neidle, S. (2006). Quadruplex DNA: sequence, topology and structure. *Nucleic Acids Research,* 34 (19)**,** 5402-5415.

Callahan, D. E., Trapane, T. L., Miller, P. S., Ts'o, P. O.and Kan, L. S. (1991). Comparative circular dichroism and fluorescence studies of oligodeoxyribonucleotide and oligodeoxyribonucleoside methylphosphonate pyrimidine strands in duplex and triplex formation. *Biochemistry,* 30 (6)**,** 1650-5.

Carbone, G. M., Mcguffie, E., Napoli, S., Flanagan, C. E., Dembech, C., Negri, U., Arcamone, F., Capobianco, M. L.and Catapano, C. V. (2004). DNA binding and antigene activity of a daunomycin-

conjugated triplex-forming oligonucleotide targeting the P2 promoter of the human c-myc gene. *Nucleic Acids Res,* 32 (8)**,** 2396-410.

Carbone, G. M., Mcguffie, E. M., Collier, A.and Catapano, C. V. (2003). Selective inhibition of transcription of the Ets2 gene in prostate cancer cells by a triplex-forming oligonucleotide. *Nucleic Acids Res,* 31 (3)**,** 833-43.

Cardew, A. S., Brown, T.and Fox, K. R. (2012). Secondary binding sites for heavily modified triplex forming oligonucleotides. *Nucleic Acids Research,* 40 (8)**,** 3753-3762.

Cardew, A. S.and Fox, K. R. (2010). DNase I Footprinting. *In:* Fox, K. R. (ed.) *Drug-DNA Interaction Protocols.* Humana Press.

Cassidy, S. A., Slickers, P., Trent, J. O., Capaldi, D. C., Roselt, P. D., Reese, C. B., Neidle, S.and Fox, K. R. (1997). Recognition of GC base pairs by triplex forming oligonucleotides containing nucleosides derived from 2-aminopyridine. *Nucleic Acids Res,* 25 (24)**,** 4891-8.

Cassidy, S. A., Strekowski, L.and Fox, K. R. (1996). DNA sequence specificity of a naphthylquinoline triple helix-binding ligand. *Nucleic Acids Res,* 24 (21)**,** 4133-8.

Cassidy, S. A., Strekowski, L., Wilson, W. D.and Fox, K. R. (1994). Effect of a Triplex-Binding Ligand on Parallel and Antiparallel DNA Triple Helixes Using Short Unmodified and Acridine-Linked Oligonucleotides. *Biochemistry,* 33 (51)**,** 15338-15347.

Chandler, S. P., Strekowski, L., Wilson, W. D.and Fox, K. R. (1995). Footprinting Studies on Ligands which Stabilize DNA Triplexes: Effects on Stringency within a Parallel Triple Helix. *Biochemistry,* 34 (21)**,** 7234-7242.

Chen, D. L.and Mclaughlin, L. W. (2000). Use of pK(a) differences to enhance the formation of base triplets involving C-G and G-C base pairs. *J Org Chem,* 65 (22)**,** 7468-74.

Cheng, A.-J.and Dyke, M. W. V. (1994). Oligodeoxyribonucleotide length and sequence effects on intermolecular purine—purine—pyrimidine triple-helix formation. *Nucleic Acids Research,* 22 (22)**,** 4742-4747.

Cheng, K., Ye, Z., Guntaka, R. V.and Mahato, R. I. (2006). Enhanced hepatic uptake and bioactivity of type alpha1(I) collagen gene promoter-specific triplex-forming oligonucleotides after conjugation with cholesterol. *J Pharmacol Exp Ther,* 317 (2)**,** 797-805.

Cherny, D. I., Malkov, V. A., Volodin, A. A.and Frank-Kamenetskii, M. D. (1993). Electron Microscopy Visualization of Oligonucleotide Binding to Duplex DNA via Triplex Formation. *Journal of Molecular Biology,* 230 (2)**,** 379-383.

Chin, T. M., Lin, S. B., Lee, S. Y., Chang, M. L., Cheng, A. Y., Chang, F. C., Pasternack, L., Huang, D. H.and Kan, L. S. (2000). "Paper-clip" type triple helix formation by 5'-d-(TC)3Ta(CT)3Cb(AG)3 (a and b = 0-4) as a function of loop size with and without the pseudoisocytosine base in the Hoogsteen strand. *Biochemistry,* 39 (40)**,** 12457-64.

Christensen, L. A., Conti, C. J., Fischer, S. M.and Vasquez, K. M. (2004). Mutation frequencies in murine keratinocytes as a function of carcinogenic status. *Mol Carcinog,* 40 (2)**,** 122-33.

Collier, D. A., Mergny, J. L., Thuong, N. T.and Helene, C. (1991). Site-specific intercalation at the triplex-duplex junction induces a conformational change which is detectable by hypersensitivity to diethylpyrocarbonate. *Nucleic Acids Res,* 19 (15)**,** 4219-24.

Cons, B. M. G.and Fox, K. R. (1990). The GC-selective ligand mithramycin alters the structure of (AT)n sequences flanking its binding sites. *FEBS Letters,* 264 (1)**,** 100-104.

Darby, R. a. J., Sollogoub, M., Mckeen, C., Brown, L., Risitano, A., Brown, N., Barton, C., Brown, T.and Fox, K. R. (2002). High throughput measurement of duplex, triplex and quadruplex melting curves using molecular beacons and a LightCycler. *Nucleic Acids Research,* 30 (9)**,** e39.

Datta, H. J., Chan, P. P., Vasquez, K. M., Gupta, R. C.and Glazer, P. M. (2001). Triplex-induced recombination in human cell-free extracts. Dependence on XPA and HsRad51. *J Biol Chem,* 276 (21)**,** 18018-23.

Day, H. A., Pavlou, P.and Waller, Z. a. E. (2014). i-Motif DNA: Structure, stability and targeting with ligands. *Bioorganic & Medicinal Chemistry,* 22 (16)**,** 4407-4418.

Debart, F., Meyer, A., Vasseur, J.-J.and Rayner, B. (1998). Anomeric inversion (from β to α) in methylphosphonate oligonucleosides enhances their affinity for DNA and RNA. *Nucleic Acids Research,* 26 (20)**,** 4551-4556.

Ding, Y., Kwok, C. K., Tang, Y., Bevilacqua, P. C.and Assmann, S. M. (2015). Genome-wide profiling of in vivo RNA structure at single-nucleotide resolution using structure-seq. *Nat. Protocols,* 10 (7)**,** 1050-1066.

Diviacco, S., Rapozzi, V., Xodo, L., Helene, C., Quadrifoglio, F.and Giovannangeli, C. (2001). Site-directed inhibition of DNA replication by triple helix formation. *FASEB J,* 15 (14)**,** 2660-8.

Dobbelstein, M. (2003). Viruses in therapy--royal road or dead end? *Virus Res,* 92 (2)**,** 219-21.

Drew, H. R. (1984). Structural specificities of five commonly used DNA nucleases. *Journal of Molecular Biology,* 176 (4)**,** 535-557.

Drew, H. R.and Travers, A. A. (1984). DNA structural variations in the E. coli tyrT promoter. *Cell,* 37 (2)**,** 491-502.

Duca, M., Vekhoff, P., Oussedik, K., Halby, L.and Arimondo, P. B. (2008). The triple helix: 50 years later, the outcome. *Nucleic Acids Res,* 36 (16)**,** 5123-38.

Durland, R. H., Rao, T. S., Revankar, G. R., Tinsley, J. H., Myrick, M. A., Seth, D. M., Rayford, J., Singh, P.and Jayaraman, K. (1994). Binding of T and T analogs to CG base pairs in antiparallel triplexes. *Nucleic Acids Res,* 22 (15)**,** 3233-40.

Ebbinghaus, S. W., Fortinberry, H.and Gamper, H. B., Jr. (1999). Inhibition of transcription elongation in the HER-2/neu coding sequence by triplex-directed covalent modification of the template strand. *Biochemistry,* 38 (2)**,** 619-28.

El Hassan, M. A.and Calladine, C. R. (1996). Propeller-Twisting of Base-pairs and the Conformational Mobility of Dinucleotide Steps in DNA. *Journal of Molecular Biology,* 259 (1)**,** 95-103.

Eldrup, A. B., Dahl, O.and Nielsen, P. E. (1997). A novel peptide nucleic acid monomer for recognition of thymine in triple-helix structures. *Journal of the American Chemical Society,* 119 (45)**,** 11116-11117.

Escude, C., Giovannangeli, C., Sun, J. S., Lloyd, D. H., Chen, J. K., Gryaznov, S. M., Garestier, T.and Helene, C. (1996). Stable triple helices formed by oligonucleotide N3'-->P5' phosphoramidates inhibit transcription elongation. *Proc Natl Acad Sci U S A,* 93 (9)**,** 4365-9.

Escude, C., Nguyen, C. H., Kukreti, S., Janin, Y., Sun, J. S., Bisagni, E., Garestier, T.and Helene, C. (1998). Rational design of a triple helix-specific intercalating ligand. *Proc Natl Acad Sci U S A,* 95 (7)**,** 3591-6.

Escude, C., Nguyen, C. H., Mergny, J.-L., Sun, J.-S., Bisagni, E., Garestier, T.and Helene, C. (1995). Selective Stabilization of DNA Triple Helixes by Benzopyridoindole Derivatives. *Journal of the American Chemical Society,* 117 (41)**,** 10212-10219.

Faruqi, A. F., Datta, H. J., Carroll, D., Seidman, M. M.and Glazer, P. M. (2000). Triple-helix formation induces recombination in mammalian cells via a nucleotide excision repair-dependent pathway. *Mol Cell Biol,* 20 (3)**,** 990-1000.

Faruqi, A. F., Egholm, M.and Glazer, P. M. (1998). Peptide nucleic acid-targeted mutagenesis of a chromosomal gene in mouse cells. *Proc Natl Acad Sci U S A,* 95 (4)**,** 1398-403.

Felsenfeld, G.and Rich, A. (1957). Studies on the formation of two- and three-stranded polyribonucleotides. *Biochim Biophys Acta,* 26 (3)**,** 457-68.

Fox, K. R. (1994). Formation of DNA triple helices incorporating blocks of G.GC and T.AT triplets using short acridine-linked oligonucleotides. *Nucleic Acids Res,* 22 (11)**,** 2016-21.

Fox, K. R. (1997). DNase I Footprinting. *In:* Fox, K. R. (ed.) *Drug-DNA Interaction Protocols.* Totowa, NJ: Springer New York.

Fox, K. R. (2000). Targeting DNA with triplexes. *Curr Med Chem,* 7 (1)**,** 17-37.

Fox, K. R.and Grigg, G. W. (1988). Diethylpyrocarbonate and permanganate provide evidence for an unusual DNA conformation induced by binding of the antitumour antibiotics bleomycin and phleomycin. *Nucleic Acids Research,* 16 (5)**,** 2063-2075.

Fox, K. R.and Waring, M. J. (1984). DNA structural variations produced by actinomycin and distamycin as revealed by DNAase I footprinting. *Nucleic Acids Research,* 12 (24)**,** 9271-9285.

Fox, K. R.and Waring, M. J. (1986). Nucleotide sequence binding preferences of nogalamycin investigated by DNase I footprinting. *Biochemistry,* 25 (15)**,** 4349-4356.

Fox, K. R.and Waring, M. J. (1987). The use of micrococcal nuclease as a probe for drug-binding sites on DNA. *Biochimica et Biophysica Acta (BBA) - Gene Structure and Expression,* 909 (2)**,** 145-155.

Fox, K. R., Waring, M. J., Brown, J. R.and Neidle, S. (1986). DNA sequence preferences for the anti-cancer drug mitoxanthrone and related anthraquinones revealed by DNase I footprinting. *FEBS Letters,* 202 (2)**,** 289-294.

François, J. C., Saison-Behmoaras, T., Barbier, C., Chassignol, M., Thuong, N. T.and Hélène, C. (1989). Sequence-specific recognition and cleavage of duplex DNA via triple-helix formation by oligonucleotides covalently linked to a phenanthroline-copper chelate. *Proceedings of the National Academy of Sciences,* 86 (24)**,** 9702-9706.

Frantz, B.and O'halloran, T. V. (1990). DNA distortion accompanies transcriptional activation by the metal-responsive gene-regulatory protein MerR. *Biochemistry,* 29 (20)**,** 4747-4751.

Furlong, J. C.and Lilley, D. M. J. (1986). Highly selective chemical modification of cruciform loops by diethyl pyrocarbonate. *Nucleic Acids Research,* 14 (10)**,** 3995-4007.

Galas, D. J.and Schmitz, A. (1978). DNAase footprinting a simple method for the detection of protein-DNA binding specificity. *Nucleic Acids Research,* 5 (9)**,** 3157-3170.

Gamper, H. B., Jr., Kutyavin, I. V., Rhinehart, R. L., Lokhov, S. G., Reed, M. W.and Meyer, R. B. (1997). Modulation of Cm/T, G/A, and G/T triplex stability by conjugate groups in the presence and absence of KCl. *Biochemistry,* 36 (48)**,** 14816-26.

Gasparro, F. P., Havre, P. A., Olack, G. A., Gunther, E. J.and Glazer, P. M. (1994). Site-specific targeting of psoralen photoadducts with a triple helix-forming oligonucleotide: characterization of psoralen monoadduct and crosslink formation. *Nucleic Acids Res,* 22 (14)**,** 2845-52.

Giovannangeli, C.and Helene, C. (1997). Progress in developments of triplex-based strategies. *Antisense Nucleic Acid Drug Dev,* 7 (4)**,** 413-21.

Giovannangeli, C., Perrouault, L., Escude, C., Gryaznov, S.and Helene, C. (1996). Efficient inhibition of transcription elongation in vitro by oligonucleotide phosphoramidates targeted to proviral HIV DNA. *J Mol Biol,* 261 (3)**,** 386-98.

Giovannangeli, C., Thuong, N. T.and Helene, C. (1992). Oligodeoxynucleotide-directed photo-induced cross-linking of HIV proviral DNA via triple-helix formation. *Nucleic Acids Res,* 20 (16)**,** 4275-81.

Goodisman, J.and Dabrowiak, J. C. (1992). Structural changes and enhancements in DNase I footprinting experiments. *Biochemistry,* 31 (4)**,** 1058-1064.

Gowers, D. M.and Fox, K. R. (1998). Triple helix formation at (AT)n adjacent to an oligopurine tract. *Nucleic Acids Research,* 26 (16)**,** 3626-3633.

Gowers, D. M.and Fox, K. R. (1999). Towards mixed sequence recognition by triple helix formation. *Nucleic Acids Res,* 27 (7)**,** 1569-77.

Grigoriev, M., Praseuth, D., Robin, P., Hemar, A., Saison-Behmoaras, T., Dautry-Varsat, A., Thuong, N. T., Helene, C.and Harel-Bellan, A. (1992). A triple helix-forming oligonucleotide-intercalator conjugate acts as a transcriptional repressor via inhibition of NF kappa B binding to interleukin-2 receptor alpha-regulatory sequence. *J Biol Chem,* 267 (5)**,** 3389-95.

Gryaznov, S. M.and Winter, H. (1998). RNA mimetics: oligoribonucleotide N3'-->P5' phosphoramidates. *Nucleic Acids Res,* 26 (18)**,** 4160-7.

Guieysse, A. L., Praseuth, D., Francois, J. C.and Helene, C. (1995). Inhibition of replication initiation by triple helix-forming oligonucleotides. *Biochem Biophys Res Commun,* 217 (1)**,** 186-94.

Hacia, J. G., Dervan, P. B.and Wold, B. J. (1994). Inhibition of Klenow fragment DNA polymerase on double-helical templates by oligonucleotide-directed triple-helix formation. *Biochemistry,* 33 (20)**,** 6192-200.

Hacia, J. G., Wold, B. J.and Dervan, P. B. (1994). Phosphorothioate oligonucleotide-directed triple helix formation. *Biochemistry,* 33 (18)**,** 5367-9.

Hahn, S., Buratowski, S., Sharp, P. A.and Guarente, L. (1989). Yeast TATA-binding protein TFIID binds to TATA elements with both consensus and nonconsensus DNA sequences. *Proceedings of the National Academy of Sciences,* 86 (15)**,** 5718-5722.

Hampshire, A. J., Rusling, D. A., Broughton-Head, V. J.and Fox, K. R. (2007). Footprinting: a method for determining the sequence selectivity, affinity and kinetics of DNA-binding ligands. *Methods (San Diego, Calif.),* 42 (2)**,** 128-140.

Haq, I., Ladbury, J. E., Chowdhry, B. Z.and Jenkins, T. C. (1996). Molecular Anchoring of Duplex and Triplex DNA by Disubstituted Anthracene-9,10-diones: Calorimetric, UV Melting, and Competition Dialysis Studies. *Journal of the American Chemical Society,* 118 (44)**,** 10693-10701.

Hari, Y., Obika, S., Inohara, H., Ikejiri, M., Une, D.and Imanishi, T. (2005). Synthesis and triplex-forming ability of 2',4'-BNAs bearing imidazoles as a nucleobase. *Chem Pharm Bull (Tokyo),* 53 (7)**,** 843-6.

Hari, Y., Obika, S., Sekiguchi, M.and Imanishi, T. (2003). Selective recognition of CG interruption by 2′,4′-BNA having 1-isoquinolone as a nucleobase in a pyrimidine motif triplex formation. *Tetrahedron,* 59 (27)**,** 5123-5128.

Herbert, A.and Rich, A. (1999). Left-handed Z-DNA: structure and function. *Genetica,* 106 (1-2)**,** 37-47.

Hermiston, T. W.and Kuhn, I. (2002). Armed therapeutic viruses: strategies and challenges to arming oncolytic viruses with therapeutic genes. *Cancer Gene Ther,* 9 (12)**,** 1022-35.

Herr, W. (1985). Diethyl pyrocarbonate: a chemical probe for secondary structure in negatively supercoiled DNA. *Proceedings of the National Academy of Sciences,* 82 (23)**,** 8009-8013.

Hewett, P. W., Daft, E. L., Laughton, C. A., Ahmad, S., Ahmed, A.and Murray, J. C. (2006). Selective inhibition of the human tie-1 promoter with triplex-forming oligonucleotides targeted to Ets binding sites. *Mol Med,* 12 (1-3)**,** 8-16.

Hojland, T., Kumar, S., Babu, B. R., Umemoto, T., Albaek, N., Sharma, P. K., Nielsen, P.and Wengel, J. (2007). LNA (locked nucleic acid) and analogs as triplex-forming oligonucleotides. *Org Biomol Chem,* 5 (15)**,** 2375-9.

Hunziker, J., Priestley, E. S., Brunar, H.and Dervan, P. B. (1995). Design of an N7-Glycosylated Purine Nucleoside for Recognition of GC Base Pairs by Triple Helix Formation. *Journal of the American Chemical Society,* 117 (9)**,** 2661-2662.

Jain, A., Wang, G.and Vasquez, K. M. (2008). DNA triple helices: Biological consequences and therapeutic potential. *Biochimie,* 90 (8)**,** 1117-1130.

James, P. L., Brown, T.and Fox, K. R. (2003). Thermodynamic and kinetic stability of intermolecular triple helices containing different proportions of C+*GC and T*AT triplets. *Nucleic Acids Res,* 31 (19)**,** 5598-606.

Jeppesen, C.and Nielsen, P. E. (1988). Detection of intercalation-induced changes in DNA structure by reaction with diethyl pyrocarbonate or potassium permanganate Evidence against the induction of Hoogsteen base pairing by echinomycin. *FEBS Letters,* 231 (1)**,** 172-176.

Jetter, M. C.and Hobbs, F. W. (1993). 7,8-Dihydro-8-oxoadenine as a replacement for cytosine in the third strand of triple helices. Triplex formation without hypochromicity. *Biochemistry,* 32 (13)**,** 3249-54.

Jiang, H., Zacharias, W.and Amirhaeri, S. (1991). Potassium permanganate as a in situ probe for B-Z and Z-Z junctions. *Nucleic Acids Research,* 19 (24)**,** 6943-6948.

Johannsen, M. W., Gerrard, S. R., Melvin, T.and Brown, T. (2014). Triplex-mediated analysis of cytosine methylation at CpA sites in DNA. *Chemical Communications,* 50 (5)**,** 551-553.

Kahl, B.and Paule, M. (2009). The Use of Diethyl Pyrocarbonate and Potassium Permanganate as Probes for Strand Separation and Structural Distortions in DNA. *In:* Leblanc, B.andMoss, T. (eds.) *DNA-Protein Interactions.* Humana Press.

Kainz, M.and Roberts, J. (1992). Structure of transcription elongation complexes in vivo. *Science,* 255 (5046)**,** 838-841.

Kan, Y., Armitage, B.and Schuster, G. B. (1997). Selective stabilization of triplex DNA by anthraquinone sulfonamide derivatives. *Biochemistry,* 36 (6)**,** 1461-6.

Karympalis, V., Kalopita, K., Zarros, A.and Carageorgiou, H. (2004). Regulation of gene expression via triple helical formations. *Biochemistry (Mosc),* 69 (8)**,** 855-60.

Keppler, M. D.and Fox, K. R. (1997). Relative stability of triplexes containing different numbers of T·AT and C+·GC triplets. *Nucleic Acids Research,* 25 (22)**,** 4644-4649.

Keppler, M. D., Read, M. A., Perry, P. J., Trent, J. O., Jenkins, T. C., Reszka, A. P., Neidle, S.and Fox, K. R. (1999). Stabilization of DNA triple helices by a series of mono- and disubstituted amidoanthraquinones. *Eur J Biochem,* 263 (3)**,** 817-25.

Kibler-Herzog, L., Kell, B., Zon, G., Shinozuka, K., Mizan, S.and Wilson, W. D. (1990). Sequence dependent effects in methylphosphonate deoxyribonucleotide double and triple helical complexes. *Nucleic Acids Res,* 18 (12)**,** 3545-55.

Kibler-Herzog, L., Zon, G., Whittier, G., Mizan, S.and Wilson, W. D. (1993). Stabilities of duplexes and triplexes of dA19 + dT19 with alternating methylphosphonate and phosphodiester linkages. *Anticancer Drug Des,* 8 (1)**,** 65-79.

Kiessling, L. L., Griffin, L. C.and Dervan, P. B. (1992). Flanking sequence effects within the pyrimidine triple-helix motif characterized by affinity cleaving. *Biochemistry,* 31 (10)**,** 2829-34.

Klysik, J., Kinsey, B. M., Hua, P., Glass, G. A.and Orson, F. M. (1997). A 15-base acridine-conjugated oligodeoxynucleotide forms triplex DNA with its IL-2R alpha promoter target with greatly improved avidity. *Bioconjug Chem,* 8 (3)**,** 318-26.

Kochetkova, M., Iversen, P. O., Lopez, A. F.and Shannon, M. F. (1997). Deoxyribonucleic acid triplex formation inhibits granulocyte macrophage colony-stimulating factor gene expression and suppresses growth in juvenile myelomonocytic leukemic cells. *J Clin Invest,* 99 (12)**,** 3000-8.

Koh, J. S.and Dervan, P. B. (1992). Design of a nonnatural deoxyribonucleoside for recognition of GC base pairs by oligonucleotide-directed triple helix formation. *Journal of the American Chemical Society,* 114 (4)**,** 1470-1478.

Koolman, J. and Roehm, K.H. (2005). Color Atlas of Biochemistry. 84-87.

Kypr, J., Kejnovská, I., Renčiuk, D.and Vorlíčková, M. (2009). Circular dichroism and conformational polymorphism of DNA. *Nucleic Acids Research,* 37 (6)**,** 1713-1725.

Lacoste, J., Francois, J. C.and Helene, C. (1997). Triple helix formation with purine-rich phosphorothioate-containing oligonucleotides covalently linked to an acridine derivative. *Nucleic Acids Res,* 25 (10)**,** 1991-8.

Lacroix, L., Arimondo, P. B., Takasugi, M., Helene, C.and Mergny, J. L. (2000). Pyrimidine morpholino oligonucleotides form a stable triple helix in the absence of magnesium ions. *Biochem Biophys Res Commun,* 270 (2)**,** 363-9.

Latimer, L. J., Hampel, K.and Lee, J. S. (1989). Synthetic repeating sequence DNAs containing phosphorothioates: nuclease sensitivity and triplex formation. *Nucleic Acids Res,* 17 (4)**,** 1549-61.

Leung, C. H., Chan, D. S., Ma, V. P.and Ma, D. L. (2013). DNA-binding small molecules as inhibitors of transcription factors. *Med Res Rev,* 33 (4)**,** 823-46.

Liepinsh, E., Leupin, W.and Otting, G. (1994). Hydration of DNA in aqueous solution: NMR evidence for a kinetic destabilization of the minor groove hydration of d-(TTAA)2 versus d-(AATT)2 segments. *Nucleic Acids Research,* 22 (12)**,** 2249-2254.

Lilley, D. M. J. (1983). Dynamic, Sequence-dependent DNA Structure as Exemplified by Cruciform Extrusion from Inverted Repeats in Negatively Supercoiled DNA. *Cold Spring Harbor Symposia on Quantitative Biology,* 47 101-112.

Liu, L. F.and Wang, J. C. (1987). Supercoiling of the DNA template during transcription. *Proceedings of the National Academy of Sciences,* 84 (20)**,** 7024-7027.

Lyamichev, V. I., Mirkin, S. M.and Frank-Kamenetskii, M. D. (1986). Structures of Homopurine-homopyrimidine Tract in Superhelical DNA. *Journal of Biomolecular Structure and Dynamics,* 3 (4)**,** 667-669.

Macaulay, V. M., Bates, P. J., Mclean, M. J., Rowlands, M. G., Jenkins, T. C., Ashworth, A.and Neidle, S. (1995). Inhibition of aromatase expression by a psoralen-linked triplex-forming oligonucleotide targeted to a coding sequence. *FEBS Lett,* 372 (2-3)**,** 222-8.

Maher, L., Wold, B.and Dervan, P. (1989). Inhibition of DNA binding proteins by oligonucleotide-directed triple helix formation. *Science,* 245 (4919)**,** 725-730.

Maher, L. J., 3rd (1996). Prospects for the therapeutic use of antigene oligonucleotides. *Cancer Invest,* 14 (1)**,** 66-82.

Majumdar, A., Khorlin, A., Dyatkina, N., Lin, F. L., Powell, J., Liu, J., Fei, Z., Khripine, Y., Watanabe, K. A., George, J., Glazer, P. M.and Seidman, M. M. (1998). Targeted gene knockout mediated by triple helix forming oligonucleotides. *Nat Genet,* 20 (2)**,** 212-4.

Marchand, C., Bailly, C., Nguyen, C. H., Bisagni, E., Garestier, T., Helene, C.and Waring, M. J. (1996). Stabilization of triple helical DNA by a benzopyridoquinoxaline intercalator. *Biochemistry,* 35 (15)**,** 5022-32.

Marchand, P., Resch, K.and Radeke, H. H. (2000). Selective inhibition of monocyte chemoattractant protein-1 gene expression in human embryonal kidney cells by specific triple helix-forming oligonucleotides. *J Immunol,* 164 (4)**,** 2070-6.

Marfurt, J.and Leumann, C. (1998). Evidence for C−H···O Hydrogen Bond Assisted Recognition of a Pyrimidine Base in the Parallel DNA Triple-Helical Motif. *Angewandte Chemie International Edition,* 37 (1-2)**,** 175-177.

Mergny, J. L., Duval-Valentin, G., Nguyen, C. H., Perrouault, L., Faucon, B., Rougee, M., Montenay-Garestier, T., Bisagni, E.and Helene, C. (1992). Triple helix-specific ligands. *Science,* 256 (5064)**,** 1681-4.

Mergny, J. L., Sun, J. S., Rougee, M., Montenay-Garestier, T., Barcelo, F., Chomilier, J.and Helene, C. (1991). Sequence specificity in triple helix formation: experimental and theoretical studies of the effect of mismatches on triplex stability. *Biochemistry,* 30 (40)**,** 9791-9798.

Michel, T., Debart, F., Vasseur, J. J., Geinguenaud, F.and Taillandier, E. (2003). FTIR and UV spectroscopy studies of triplex formation between alpha-oligonucleotides with non-ionic phoshoramidate linkages and DNA targets. *J Biomol Struct Dyn,* 21 (3)**,** 435-45.

Miller, J. C., Holmes, M. C., Wang, J., Guschin, D. Y., Lee, Y. L., Rupniewski, I., Beausejour, C. M., Waite, A. J., Wang, N. S., Kim, K. A., Gregory, P. D., Pabo, C. O.and Rebar, E. J. (2007). An improved zinc-finger nuclease architecture for highly specific genome editing. *Nat Biotechnol,* 25 (7)**,** 778-85.

Miller, P. S.and Cushman, C. D. (1993). Triplex formation by oligodeoxyribonucleotides involving the formation of X.U.A triads. *Biochemistry,* 32 (12)**,** 2999-3004.

Mirkin, S. M., Lyamichev, V. I., Drushlyak, K. N., Dobrynin, V. N., Filippov, S. A.and Frank-Kamenetskii, M. D. (1987). DNA H form requires a homopurine-homopyrimidine mirror repeat. *Nature,* 330 (6147)**,** 495-497.

Moser, H.and Dervan, P. (1987). Sequence-specific cleavage of double helical DNA by triple helix formation. *Science,* 238 (4827)**,** 645-650.

Mouscadet, J. F., Ketterle, C., Goulaouic, H., Carteau, S., Subra, F., Le Bret, M.and Auclair, C. (1994). Triple helix formation with short oligonucleotide-intercalator conjugates matching the HIV-1 U3 LTR end sequence. *Biochemistry,* 33 (14)**,** 4187-96.

Nagatsugi, F., Sasaki, S., Seidmen, M. M.and Miller, P. S. (2002). Mutagenesis targeted by triple-helix forming oligonucleotides containing a reactive nucleoside analogue. *Nucleic Acids Res Suppl,* (2)**,** 31-2.

Napoli, S., Negri, U., Arcamone, F., Capobianco, M. L., Carbone, G. M.and Catapano, C. V. (2006). Growth inhibition and apoptosis induced by daunomycin-conjugated triplex-forming oligonucleotides targeting the c-myc gene in prostate cancer cells. *Nucleic Acids Research,* 34 (2)**,** 734-744.

Obika, S., Hari, Y., Sekiguchi, M.and Imanishi, T. (2001). A 2',4'-Bridged Nucleic Acid Containing 2-Pyridone as a Nucleobase: Efficient Recognition of a C small middle dotG Interruption by Triplex Formation with a Pyrimidine Motif Part of this work was supported by a Grant-in-Aid for Scientific Research (B) (No. 12557201) from the Japan Society for the Promotion of Science. *Angew Chem Int Ed Engl,* 40 (11)**,** 2079-2081.

Ohlsen, K. L.and Gralla, J. D. (1992). Melting during steady-state transcription of the rrnB P1 promoter in vivo and in vitro. *Journal of Bacteriology,* 174 (19)**,** 6071-6075.

Ono, A., Ts'o, P. O. P.and Kan, L. S. (1991). Triplex formation of oligonucleotides containing 2'-O-methylpseudoisocytidine in substitution for 2'-deoxycytidine. *Journal of the American Chemical Society,* 113 (10)**,** 4032-4033.

Ono, A., Ts'o, P. O. P.and Kan, L. S. (1992). Triplex formation of an oligonucleotide containing 2'-O-methylpseudoisocytidine with a DNA duplex at neutral pH. *The Journal of Organic Chemistry,* 57 (11)**,** 3225-3230.

Orphanides, G.and Maxwell, A. (1994). Evidence for a conformational change in the DNA gyrase–DNA complex from hydroxyl radical footprinting. *Nucleic Acids Research,* 22 (9)**,** 1567-1575.

Orson, F. M., Klysik, J., Bergstrom, D. E., Ward, B., Glass, G. A., Hua, P.and Kinsey, B. M. (1999). Triple helix formation: binding avidity of acridine-conjugated AG motif third strands containing natural, modified and surrogate bases opposed to pyrimidine interruptions in a polypurine target. *Nucleic Acids Res,* 27 (3)**,** 810-6.

Petersen, M.and Wengel, J. (2003). LNA: a versatile tool for therapeutics and genomics. *Trends Biotechnol,* 21 (2)**,** 74-81.

Povsic, T. J.and Dervan, P. B. (1989). Triple helix formation by oligonucleotides on DNA extended to the physiological pH range. *Journal of the American Chemical Society,* 111 (8)**,** 3059-3061.

Powers, T.and Noller, H. F. (1995). Hydroxyl radical footprinting of ribosomal proteins on 16S rRNA. *RNA,* 1 (2)**,** 194-209.

Praseuth, D., Guieysse, A. L.and Helene, C. (1999). Triple helix formation and the antigene strategy for sequence-specific control of gene expression. *Biochim Biophys Acta,* 1489 (1)**,** 181-206.

Prevot-Halter, I.and Leumann, C. J. (1999). Selective recognition of a C-G base-pair in the parallel DNA triple-helical binding motif. *Bioorg Med Chem Lett,* 9 (18)**,** 2657-60.

Prigodich, R. V.and Martin, C. T. (1990). Reaction of single-stranded DNA with hydroxyl radical generated by iron(II)-ethylenediaminetetraacetic acid. *Biochemistry,* 29 (35)**,** 8017-8019.

Radhakrishnan, I.and Patel, D. J. (1994). Solution Structure and Hydration Patterns of a Pyrimidine?Purine?Pyrimidine DNA Triplex Containing a Novel T?CG Base-triple. *Journal of Molecular Biology,* 241 (4)**,** 600-619.

Radhakrishnan, I., Patel, D. J., Priestly, E. S., Nash, H. M.and Dervan, P. B. (1993). NMR structural studies on a nonnatural deoxyribonucleoside which mediates recognition of GC base pairs in pyrimidine-purine-pyrimidine DNA triplexes. *Biochemistry,* 32 (41)**,** 11228-34.

Rahman, S. M., Seki, S., Obika, S., Yoshikawa, H., Miyashita, K.and Imanishi, T. (2008). Design, synthesis, and properties of 2',4'-BNA(NC): a bridged nucleic acid analogue. *J Am Chem Soc,* 130 (14)**,** 4886-96.

Ranasinghe, R. T., Rusling, D. A., Powers, V. E., Fox, K. R.and Brown, T. (2005). Recognition of CG inversions in DNA triple helices by methylated 3H-pyrrolo[2,3-d]pyrimidin-2(7H)-one nucleoside analogues. *Chem Commun (Camb),* (20)**,** 2555-7.

Rapozzi, V., Cogoi, S., Spessotto, P., Risso, A., Bonora, G. M., Quadrifoglio, F.and Xodo, L. E. (2002). Antigene effect in K562 cells of a PEG-conjugated triplex-forming oligonucleotide targeted to the bcr/abl oncogene. *Biochemistry,* 41 (2)**,** 502-10.

Renneberg, D.and Leumann, C. J. (2004). Exploring Hoogsteen and reversed-Hoogsteen duplex and triplex formation with tricyclo-DNA purine sequences. *Chembiochem,* 5 (8)**,** 1114-8.

Reynolds, M. A., Arnold, L. J., Jr., Almazan, M. T., Beck, T. A., Hogrefe, R. I., Metzler, M. D., Stoughton, S. R., Tseng, B. Y., Trapane, T. L., Ts'o, P. O.and Et Al. (1994). Triple-strand-forming methylphosphonate oligodeoxynucleotides targeted to mRNA efficiently block protein synthesis. *Proc Natl Acad Sci U S A,* 91 (26)**,** 12433-7.

Rhee, S., Han, Z.-J., Liu, K., Miles, H. T.and Davies, D. R. (1999). Structure of a Triple Helical DNA with a Triplex−Duplex Junction. *Biochemistry,* 38 (51)**,** 16810-16815.

Rhodes, D. (1985). Structural analysis of a triple complex between the histone octamer, a Xenopus gene for 5S RNA and transcription factor IIIA. *The EMBO Journal,* 4 (13A)**,** 3473-3482.

Rogers, F. A., Lloyd, J. A.and Glazer, P. M. (2005). Triplex-forming oligonucleotides as potential tools for modulation of gene expression. *Curr Med Chem Anticancer Agents,* 5 (4)**,** 319-26.

Rogers, F. A., Manoharan, M., Rabinovitch, P., Ward, D. C.and Glazer, P. M. (2004). Peptide conjugates for chromosomal gene targeting by triplex-forming oligonucleotides. *Nucleic Acids Res,* 32 (22)**,** 6595-604.

Rogers, F. A., Vasquez, K. M., Egholm, M.and Glazer, P. M. (2002). Site-directed recombination via bifunctional PNA-DNA conjugates. *Proc Natl Acad Sci U S A,* 99 (26)**,** 16695-700.

Rusling, D. A., Brown, T.and Fox, K. R. (2006). DNA Recognition by Triple Helix Formation. *In:* Waring, M. J. (ed.) *Sequence-specific DNA Binding Agents.* Cambridge: The Royal Society of Chemistry.

Rusling, D. A., Powers, V. E., Ranasinghe, R. T., Wang, Y., Osborne, S. D., Brown, T.and Fox, K. R. (2005). Four base recognition by triplex-forming oligonucleotides at physiological pH. *Nucleic Acids Res,* 33 (9)**,** 3025-32.

Santhakumaran, L. M., Thomas, T.and Thomas, T. J. (2004). Enhanced cellular uptake of a triplex-forming oligonucleotide by nanoparticle formation in the presence of polypropylenimine dendrimers. *Nucleic Acids Res,* 32 (7)**,** 2102-12.

Sasse-Dwight, S.and Gralla, J. D. (1989). KMnO4 as a probe for lac promoter DNA melting and mechanism in vivo. *Journal of Biological Chemistry,* 264 (14)**,** 8074-8081.

Shaw, P.and Stewart, A. F. (2001). Identification of Protein-DNA Contacts with Dimethyl Sulfate. *In:* Moss, T. (ed.) *DNA-Protein Interactions.* Humana Press.

Shlyakhtenko, L. S., Potaman, V. N., Sinden, R. R.and Lyubchenko, Y. L. (1998). Structure and dynamics of supercoil-stabilized DNA cruciforms. *J Mol Biol,* 280 (1)**,** 61-72.

Singleton, C. K., Klysik, J.and Wells, R. D. (1983). Conformational flexibility of junctions between contiguous B- and Z-DNAs in supercoiled plasmids. *Proceedings of the National Academy of Sciences,* 80 (9)**,** 2447-2451.

Singleton, S. F.and Dervan, P. B. (1992). Influence of pH on the equilibrium association constants for oligodeoxyribonucleotide-directed triple helix formation at single DNA sites. *Biochemistry,* 31 (45)**,** 10995-1003.

Song, J., Intody, Z., Li, M.and Wilson, J. H. (2004). Activation of gene expression by triplex-directed psoralen crosslinks. *Gene,* 324 183-90.

Sørensen, J. J., Nielsen, J. T.and Petersen, M. (2004). Solution structure of a dsDNA:LNA triplex. *Nucleic Acids Research,* 32 (20)**,** 6078-6085.

St. Clair, A., Xiang, G.and Mclaughlin, L. W. (1998). Synthesis and Triplex Forming Properties of an Acyclic N7-Glycosylated Guanine Nucleoside. *Nucleosides and Nucleotides,* 17 (5)**,** 925-937.

Steffens, R.and Leumann, C. J. (1999). Synthesis and Thermodynamic and Biophysical Properties of Tricyclo-DNA. *Journal of the American Chemical Society,* 121 (14)**,** 3249-3255.

Stierle, V., Duca, M., Halby, L., Senamaud-Beaufort, C., Capobianco, M. L., Laigle, A., Jolles, B.and Arimondo, P. B. (2008). Targeting MDR1 gene: synthesis and cellular study of modified daunomycin-triplex-forming oligonucleotide conjugates able to inhibit gene expression in resistant cell lines. *Mol Pharmacol,* 73 (5)**,** 1568-77.

Stonehouse, T. J.and Fox, K. R. (1994). DNase I footprinting of triple helix formation at polypurine tracts by acridine-linked oligopyrimidines: stringency, structural changes and interaction with minor groove binding ligands. *Biochim Biophys Acta,* 1218 (3)**,** 322-30.

Strekowski, L., Gulevich, Y., Baranowski, T. C., Parker, A. N., Kiselyov, A. S., Lin, S. Y., Tanious, F. A.and Wilson, W. D. (1996). Synthesis and structure-DNA binding relationship analysis of DNA triple-helix specific intercalators. *J Med Chem,* 39 (20)**,** 3980-3.

Suck, D.and Oefner, C. (1986). Structure of DNase I at 2.0 [angst] resolution suggests a mechanism for binding to and cutting DNA. *Nature,* 321 (6070)**,** 620-625.

Sugimoto, N., Wu, P., Hara, H.and Kawamoto, Y. (2001). pH and Cation Effects on the Properties of Parallel Pyrimidine Motif DNA Triplexes†. *Biochemistry,* 40 (31)**,** 9396-9405.

Sun, B. W., Babu, B. R., Sorensen, M. D., Zakrzewska, K., Wengel, J.and Sun, J. S. (2004). Sequence and pH effects of LNA-containing triple helix-forming oligonucleotides: physical chemistry, biochemistry, and modeling studies. *Biochemistry,* 43 (14)**,** 4160-9.

Sun, J. S., Francois, J. C., Montenay-Garestier, T., Saison-Behmoaras, T., Roig, V., Thuong, N. T.and Helene, C. (1989). Sequence-specific intercalating agents: intercalation at specific sequences on duplex DNA via major groove recognition by oligonucleotide-intercalator conjugates. *Proc Natl Acad Sci U S A,* 86 (23)**,** 9198-202.

Sun, J. S., Giovannangeli, C., Francois, J. C., Kurfurst, R., Montenay-Garestier, T., Asseline, U., Saison-Behmoaras, T., Thuong, N. T.and Helene, C. (1991). Triple-helix formation by alpha oligodeoxynucleotides and alpha oligodeoxynucleotide-intercalator conjugates. *Proc Natl Acad Sci U S A,* 88 (14)**,** 6023-7.

Svinarchuk, F., Nagibneva, I., Cherny, D., Ait-Si-Ali, S., Pritchard, L. L., Robin, P., Malvy, C., Harel-Bellan, A.and Chern, D. (1997). Recruitment of transcription factors to the target site by triplex-forming oligonucleotides. *Nucleic Acids Res,* 25 (17)**,** 3459-64.

Takasugi, M., Guendouz, A., Chassignol, M., Decout, J. L., Lhomme, J., Thuong, N. T.and Helene, C. (1991). Sequence-specific photo-induced cross-linking of the two strands of double-helical DNA by a psoralen covalently linked to a triple helix-forming oligonucleotide. *Proc Natl Acad Sci U S A,* 88 (13)**,** 5602-6.

Tarköy, M.and Leumann, C. (1993). Synthesis and Pairing Properties of Decanucleotides from (3′S,5′R)-2′-Deoxy-3′, 5′-ethanoβ-D-ribofuranosyladenine and -thymine. *Angewandte Chemie International Edition in English,* 32 (10)**,** 1432-1434.

Tarköy, M., Phipps, A. K., Schultze, P.and Feigon, J. (1998). Solution Structure of an Intramolecular DNA Triplex Linked by Hexakis(ethylene glycol) Units: d(AGAGAGAA-(EG)6-TTCTCTCT-(EG)6-TCTCTCTT). *Biochemistry,* 37 (17)**,** 5810-5819.

Tijerina, P., Mohr, S.and Russell, R. (2007). DMS Footprinting of Structured RNAs and RNA-Protein Complexes. *Nature protocols,* 2 (10)**,** 2608-2623.

Tiner Sr, W. J., Potaman, V. N., Sinden, R. R.and Lyubchenko, Y. L. (2001). The structure of intramolecular triplex DNA: atomic force microscopy study1. *Journal of Molecular Biology,* 314 (3)**,** 353-357.

Trapane, T. L., Hogrefe, R. I., Reynolds, M. A., Kan, L. S.and Ts'o, P. O. (1996). Interstrand complex formation of purine oligonucleotides and their nonionic analogs: the model system of d(AG)8 and its complement, d(CT)8. *Biochemistry,* 35 (17)**,** 5495-508.

Travers, A. A. (2004). The structural basis of DNA flexibility. Philosophical Transactions of the Royal Society of London. Series A: Mathematical, Physical and Engineering Sciences, 362 (1820)**,** 1423-1438.

Travers, A. A., Lamond, A. I., Mace, H. a. F.and Berman, M. L. (1983). RNA polymerase interactions with the upstream region of the E. coli tyrT promoter. *Cell,* 35 (1)**,** 265-273.

Tullius, T. D.and Dombroski, B. A. (1986). Hydroxyl radical "footprinting": high-resolution information about DNA-protein contacts and application to lambda repressor and Cro protein. *Proceedings of the National Academy of Sciences,* 83 (15)**,** 5469-5473.

Vasquez, K. M., Marburger, K., Intody, Z.and Wilson, J. H. (2001). Manipulating the mammalian genome by homologous recombination. *Proc Natl Acad Sci U S A,* 98 (15)**,** 8403-10.

Vasquez, K. M.and Wilson, J. H. (1998). Triplex-directed modification of genes and gene activity. *Trends Biochem Sci,* 23 (1)**,** 4-9.

Wang, G., Levy, D. D., Seidman, M. M.and Glazer, P. M. (1995). Targeted mutagenesis in mammalian cells mediated by intracellular triple helix formation. *Mol Cell Biol,* 15 (3)**,** 1759-68.

Wang, G., Seidman, M. M.and Glazer, P. M. (1996). Mutagenesis in mammalian cells induced by triple helix formation and transcription-coupled repair. *Science,* 271 (5250)**,** 802-5.

Ward, B., Rehfuss, R., Goodisman, J.and Dabrowiak, J. C. (1988). Rate enhancements in the DNase I footprinting experiment. *Nucleic Acids Res,* 16 (4)**,** 1359-69.

Washbrook, E.and Fox, K. R. (1994). Comparison of antiparallel A-AT and T-AT triplets within an alternate strand DNA triple helix. *Nucleic Acids Research,* 22 (19)**,** 3977-3982.

Waterloh, K.and Fox, K. R. (1991). The effects of actinomycin on the structure of dAn.dTn and (dA-dT)n regions surrounding its GC binding site. A footprinting study. *Journal of Biological Chemistry,* 266 (10)**,** 6381-6388.

Wittig, B., Dorbic, T.and Rich, A. (1991). Transcription is associated with Z-DNA formation in metabolically active permeabilized mammalian cell nuclei. *Proceedings of the National Academy of Sciences of the United States of America,* 88 (6)**,** 2259-2263.

Xiang, G., Bogacki, R.and Mclaughlin, L. W. (1996). Use of a pyrimidine nucleoside that functions as a bidentate hydrogen bond donor for the recognition of isolated or contiguous G-C base pairs by oligonucleotide-directed triplex formation. *Nucleic Acids Res,* 24 (10)**,** 1963-70.

Xiang, G.and Mclaughlin, L. W. (1998). A cytosine analogue containing a conformationally flexible acyclic linker for triplex formation at sites with contiguous G-C base pairs. *Tetrahedron,* 54 (3–4)**,** 375-392.

Xodo, L. E., Manzini, G.and Quadrifoglio, F. (1990). Spectroscopic and calorimetric investigation on the DNA triplex formed by d(CTCTTCTTTCTTTTCTTTCTTCTC) and d(GAGAAGAAAGA) at acidic pH. *Nucleic Acids Research,* 18 (12)**,** 3557-3564.

Xodo, L. E., Manzini, G., Quadrifoglio, F., Van Der Marel, G. A.and Van Boom, J. H. (1991). Effect of 5-methylcytosine on the stability of triple-stranded DNA--a thermodynamic study. *Nucleic Acids Res,* 19 (20)**,** 5625-31.

Xu, X. S., Glazer, P. M.and Wang, G. (2000). Activation of human gamma-globin gene expression via triplex-forming oligonucleotide (TFO)-directed mutations in the gamma-globin gene 5' flanking region. *Gene,* 242 (1-2)**,** 219-28.

Yang, M., Ghosh, S. S.and Millar, D. P. (1994). Direct Measurement of Thermodynamic and Kinetic Parameters of DNA Triple Helix Formation by Fluorescence Spectroscopy. *Biochemistry,* 33 (51)**,** 15329-15337.

Yang, M., Ren, L.-Q., Huang, M., Kong, R. Y. C.and Fong, W. F. (1998). A DNA Assay Based on Fluorescence Resonance Energy Transfer and DNA Triplex Formation. *Analytical Biochemistry,* 259 (2)**,** 272-274.

Zhou-Sun, B., Sun, J., Gryaznov, S. M., Liquier, J., Garestier, T., Helene, C.and Taillandier, E. (1997). A physico-chemical study of triple helix formation by an oligodeoxythymidylate with N3'--> P5' phosphoramidate linkages. *Nucleic Acids Res,* 25 (9)**,** 1782-7.

Ziemba, A., Derosier, L. C., Methvin, R., Song, C. Y., Clary, E., Kahn, W., Milesi, D., Gorn, V., Reed, M.and Ebbinghaus, S. (2001). Repair of triplex-directed DNA alkylation by nucleotide excision repair. *Nucleic Acids Res,* 29 (21)**,** 4257-63.

Zimmerman, S. B. (1982). The three-dimensional structure of DNA. *Annu Rev Biochem,* 51 395-427.